Structural and functional characterisation of lipoplexes for tumour vaccination

Dissertation zur Erlangung des Grades
„Doktor der Naturwissenschaften“

im Promotionsfach Pharmazie

am Fachbereich Chemie, Pharmazie, Geographie und Geowissenschaften
der Johannes Gutenberg-Universität Mainz

Antje Ziller
geb. in Bad Salzungen
Mainz, 2019

1. Berichterstatter:
2. Berichterstatter:

Tag der mündlichen Prüfung: 14. Juni 2019

D77

You don't finish a thesis,

you stop a thesis.

(Unknown)

Table of contents

List of abbreviations

APC	Antigen-presenting cell
ATP	Adenosine-5'-triphosphate
CNE	Cationic nanoemulsions
C2C12	Mouse myoblast
DAC	Dual asymmetric centrifuge
DC	Dendritic cell
DC-Chol	3ß-[N-(N',N'-dimethylaminoethane)-carbamoyl]cholesterol
DDAB	Didodecyldimethylammonium
DLPC	Dilauroyl-sn-glycero phosphocholine
DLS	Dynamic light scattering
DMEM	Dulbecco's modified eagle medium
DMPC	Dimyristoyl-phosphatidylcholine
DNA	Deoxyribonucleic acid
DODAP	1,2-Dioleoyloxy-3-dimethylamino-propane
DODMA	1,2-Dioleoyl-N,N-dimethyl-3-aminopropane
DOPC	1,2-Dioleoyl-sn-glycero-3-phosphocholine
DOPE	1,2-Dioleoyl-sn-glycero-3-phosphoethanolamine
DOPG	1,2-Dioleoyl-sn-glycero-3-phospho-(1'-rac-glycerol)
DOTAP	1,2-Dioleoyl-3-trimethylammonium-propane
DOTMA	1,2-Di-O-octadecenyl-3-trimethylammonium-propane
(D)PBS	(Dulbecco's) Phosphate-buffered saline
DPOPE	Dipalmitoleoylphosphatidylethanolamine
DRV	Dehydration-rehydration vesicles
DSC	Differential scanning calorimetry
DTT	Dithiothreitol
EDTA	Ethylenediaminetetraacetic acid
ELS	Electrophoretic light scattering
EMEM	Eagle's minimal essential medium
EPC	Egg-Phosphatidylcholine

EPR	Enhanced Permeability and Retention
FBS	Fetal bovine serum
FCS	Fetal calf serum
FDA	Food and Drug Administration
FWHW	Full width at half maximum
GFP	Green fluorescent protein
HEK	Human embryonic kidney
IFN-α	Interferon-alpha
IKK	IκB kinase-β
IMDM	Iscove's modified dulbecco's medium
LNP	Lipid nanoparticle
LPS	Lipopolysaccharide
Luc	Luciferase
LUV	Large unilamellar vesicle
MHC	Major histocompatibility complex
MLV	Multilamellar vesicle
MML	Membrane mimicking liposome
(m)RNA	(Messenger) ribonucleic acid
MVV	Multivesicular vesicle
N/P	Nitrogen/phosphate (+/-) charge ratio
NaCl	Sodium chloride
NGS	Next generation sequencing
OVA	Ovalbumin
PBMC	Peripheral blood mononuclear cell
PC	Phosphatidylcholine
PE	Phosphatidylethanolamine
PE-CF	1,2-dioleoyl-sn-glycero-3-phosphoethanolamine-N-(carboxyfluorescein)
PEG	Polyethylenglycol
PG	Polyglycerol
PGA	Poly-L-glutamic acid
RNase	Ribonuclease
RT	Room temperature
SANS	Small-angle neutron scattering

SAS	Small-angle scattering
SAXS	Small-angle X-ray scattering
SDS	Sodium dodecyl sulfate
siRNA	Small interfering ribonucleic acid
SLD	Scattering length density
SUV	Small unilamellar vesicle
TAA	Tumour-associated antigen
TC	T cell/lymphocyte
TE buffer	Tris/EDTA buffer
TNS	2-(p-toluidino)-6-naphthalenesulfonic acid
TLR	Toll-like receptor
T_g	Glass transition temperature
T_m	Lipid phase transition temperature
XTT	2,3-Bis(2-methoxy-4-nitro-5-sulfophenyl)-2H-tetrazolium-5-carboxanilide

List of tables

List of figures

List of equations

1 Introduction

In the industrialised countries, cancer is one of the biggest challenge mankind must overcome. With 14 million new cases and 8 million cancer-related death in 2014, it has become the second most common death causes worldwide. [1] First-line therapies are chemotherapy, surgery and radiotherapy. Chemotherapy is often painful and tortuous with low response rates. Surgery is limited to tumours which are accessible and radiotherapy often impairs healthy tissue as well. In addition, the high diversity of tumours based on diverse mutation profiles represents a major hurdle in these treatments. That means that tumours often overexpress proteins like receptors in comparison to healthy cells or even express specific proteins on the cell surface. Therefore, a personalised therapy by tumour vaccination seems to offer a chance to combat the high mortality. The specific expression pattern is the target of the immunotherapy as well as of the targeted chemo- and radiotherapy. With the help of modern sequence methods like next generation sequencing (NGS), the specific protein structures of an individual patient can be analysed. The so-called mutanome comprises all the tumour specific properties and is the basis for the production of an individual tumour therapy. After administration into the patient's body, the found protein structures are presented to the immune systems which then recognise these structures as foreign substances. Thereby, an immune response is started so that the body should able to recognise and combat the tumour cells on its own. The rough principle is illustrated in Fig. 1.

First attempts for tumour vaccination as a novel treatment concept were already made in the 19th century by William B. Coley, who injected attenuated bacteria to stimulate the immune system for cancer treatment. [2] Since then, many other approaches to stimulate the immune systems were found in the following decades. Viruses (Hepatitis B), proteins, peptides, deoxyribonucleic acid (DNA), ribonucleic acid (RNA) and recently Messenger-RNA (mRNA) are considered as possible tumour vaccines. In contrast to the usage of proteins or peptides, DNA or mRNA consist of the corresponding nucleic acid structure and do not transport the active substance itself, but the genetic information for the production of the active substance in the human body.

First achievements with mRNA were made in 1990 when Wolff et al.[3] could detect the resulting protein in the skeletal muscle of mice after injection of the corresponding mRNA into the muscle. [3,4] Just a few years later in 1995, Conry et al.[5] investigated a response of the immune system by measuring generated antibodies, also after intramuscular (i.m.) injection of mRNA. [5]

Shortly after this, Boczkowski et al.[6] could determine specific T-cell production after (*in vitro*) vaccination of DCs with mRNA, followed by a measurable antitumoural effect. [6] In the course of time, mRNA incorporated in lipid-based delivery systems and administered locally have shown impressive immune responses for active immunisation. [7] Recently, in mice studies testing immunisation against Zika virus infection, the local administration of mRNA has had a higher immune response in comparison with the use of DNA. [8] Until now, several ways of application (intranodal, intravenous, subcutaneous, intratumoural) were found to show immune response. [9–12]

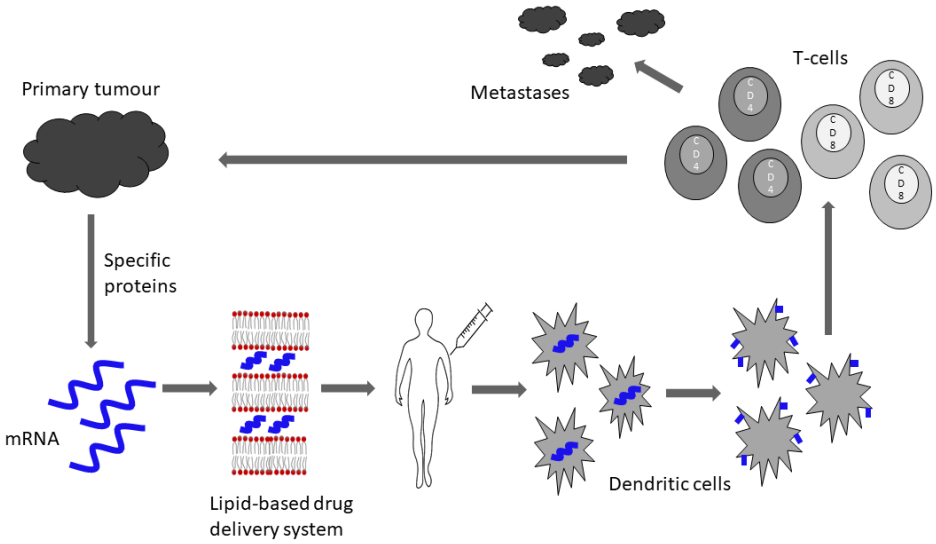

Figure 1: The principle of the individual tumour therapy using mRNA incorporated into a lipid-based drug delivery system

1.1 Nucleic acids for antigen delivery

1.1.1 Nucleic acids

mRNA

The structure of RNA is similar to DNA but differs on some significant issues. While DNA can form a double strand, RNA is single-stranded. The monomer is composed of a phosphate group, a five-carbon sugar and 4 different nitrogen-containing nucleobases. The bases adenine, guanine, cytosine are same in DNA. Instead of thymin, uracil which lacks the 5‘methyl group is the fourth base. The sugar is ribose, which has hydroxyl bonds in 2‘position whereby it is more reactive compared to 2‘deoxyribose of DNA and also not stable under alkaline conditions. Larger grooves also promote instability because enzymes can attack more easily.

Under physiological conditions, the phosphate group of nucleic acids is charged negatively which facilitates complexes with positively charged delivery systems. RNA can appear in different types, like transfer RNA (tRNA), ribosomal (rRNA) or messenger RNA (mRNA). mRNA acts as a working copy of the genetic information provided by the DNA and is needed for the protein synthesis.

As shown in Fig. 2, the structure of mature eukaryotic mRNA can be divided into different parts: the poly-A tail, the 3'untranslated region (3’UTR), the coding region, the 5'untranslated region (5’UTR) and the 5‘cap.

The coding region is the important part for the protein synthesis because it consists of nucleotide triplicates which code for the protein sequence. The 5‘cap is a modified guanosine and promotes protection from 5‘exonucleases. Furthermore, it supports the proper attachment to the ribosome. The 3‘poly-A tail comprises many adenine nucleotides and is important for the stability because it serves as a protection from degradation. Most important is that it promotes the transport out of the nucleus to the cytoplasm. Finally, also the untranslated regions (UTRs) support the stability but also the localisation of mRNA and effects the translation efficiency.

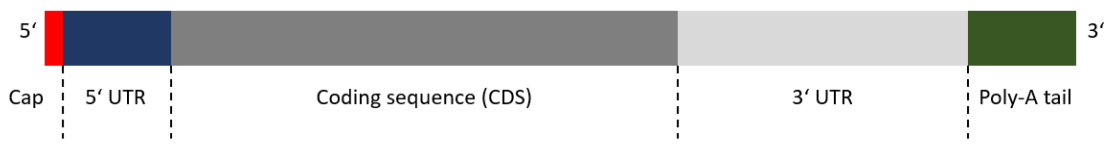

Figure 2: Scheme of mature eukaryotic mRNA

siRNA

Another type of RNA is small interfering RNA (siRNA). It was not used in the experiments but it is mentioned several times in this thesis due to comparative reasons. siRNA consist of short double stranded RNA-molecules (20 to 25 base pairs) with two overhanging nucleotides at both hydroxylated 3'ends. The main function of siRNA is RNA-interference which describes the targeted deactivation of genes. In presence of siRNA, all corresponding mRNA structure in this cell are destroyed which impeded the production of the derived proteins. RNA-interference is a natural mechanism in eukaryotic cells, but is nowadays also used as a therapeutic method to prevent the endogenous production of pathological proteins (gene silencing). [13]

Plasmid DNA

Plasmids consist of small circular, double-stranded DNA molecules which exist normally in bacteria cells but can also be present in eukaryotic organisms. They are located separately from the chromosomal DNA and can replicate independently. In nature, they are used to carry variable genes to support the survival of the organism (e.g. resistance to antibiotics, virulence factors). The size of plasmids can vary from less than 1 kilobase pairs up to several megabase pairs whereas structure differ just slightly. Plasmids are composed of the gene for the plasmid-specific replication initiation protein (Rep), the iterons (repeating units), DnaA boxes (replication ignition factor) and an adjacent AT-rich region. For reproduction, smaller plasmids use replicative enzymes of the host whereas larger plasmids often carry their own genes for the replication.

1.1.2 Mode of action

In principle, there are at least two different possibilities in which mRNA can act as a tumour vaccination agent. In the first method, mRNA is either taken up by myocytes or immune cells like dendritic cells (DCs) after i.m. injection. In myocytes, mRNA is translated into the corresponding antigen. Then, the antigen is released by the cells and can be taken up by DCs, degraded into peptides and presented by major histocompatibility complex (MHC) class II molecules on the cell surface. This leads to an activation of $CD4^+$ T cells. The other possibility is the direct uptake of mRNA by DCs as illustrated roughly in Fig. 1. After translation and degradation, peptides are presented via MHC I molecules, which leads to an activation of $CD8^+$ T cells. Humoral and cellular immune reactions are possible. The humoral one takes place by

the presence of Interleukin (IL-) 4. $CD4^+$ T cells differentiate into Th_2 cells, which secrete IL-4/5/13. Consequently, B cells differentiate into plasma B cells, which produce antigen-specific antibodies to mark tumour cells for destruction, and memory B cells. For a cellular immune reaction, IL-12 is necessary. In this case, $CD4^+$ T cells differentiate into Th_1 cells, which secrete Interferon (IFN)-γ. First, $CD8^+$ T cells develop into cytotoxic T cells (Tc cells). Through the secretion of perforin and granzymes, apoptosis of tumour cells is induced. Moreover, the activation of macrophages leads to lysis of tumour cells due to nascent nitric oxide and reactive oxygen. T cells can also form memory cells. Just like the memory B cells, these cells can remain silent for a long time and get reactivated by another contact with the antigen. [14] Nevertheless, presentation of the applied antigen by MHC II receptors is not always guaranteed. By adding a secretion signal to the coding sequence of mRNA, which leads to secretion of the protein into the extracellular space and uptake as an exogenous protein, the MHC class II processing pathway can be achieved as well. [4]

1.1.3 Advantages of mRNA over proteins or DNA

Cancer therapy is one of the oldest approaches for the preclinical and clinical use of mRNA. In the beginning, it was used for an *ex vivo* transfection with DCs (*in vitro* pulsation of DCs). In contrast, the current research focus is more on direct *in vivo* transfection. [4] Besides the *in vitro* pulsation of DCs, mRNA can be administrated via several routes like intravenous, intradermal, subcutaneous, intranodal, intrasplenic or by a gene gun [15]. Vaccination with mRNA was more effective than with peptides because mRNA acts as a continuous source for generating new peptides. [6] There are several more reasons for the use of mRNA instead of the protein itself:

– mRNA can encode any peptide or protein.
– mRNA can encode not only one but several proteins.
– Only the sequences directly needed for the gene expression are necessary.
– Varying the protein just changes the sequence of mRNA, but not the physicochemical properties.

Consequently, the same delivery system and the preparation procedure can be used for different mRNA sequences. This is time- and cost-effective. On the contrary, changing a formulation with a protein, can lead to completely different properties, so that adjustments in the manufacturing process would be necessary. [16] In comparison with DNA, application of mRNA has led to equivalent transfection as shown by Wolff et al. [3] In addition, mRNA has several

advantages in the translation process. For example, mRNA does not have to enter the nucleus to be active since the mode of action takes place in the cytoplasm. Because of this, mRNA is not integrated into the genome so that mutagenesis cannot occur. Since it is degraded in the serum after several days, mRNA has just a transient effect. Hence, safety problems are reduced. [17] Furthermore, it is said, that mRNA has additional adjuvant effects on the innate immune system by costimulating pattern recognition receptors like Toll-like receptors on the surface of immune cells. [18] This so-called danger signal is needed for an effective adaptive immune response. [16] However, this multiple pattern recognition can entail severe immune reactions, particularly in susceptible individuals. Modifications of mRNA can counter these [19], but sometimes the co-dosing with an immunosuppressor is necessary. [7] In comparison to plasmids, synthetic mRNA is not categorised by the FDA as a genetically modified organism. [20]

Since single-stranded mRNA is not as stable as double-stranded DNA, modifications of the strand are necessary to increase the stability. mRNA is also active after lyophilisation [21] and can be stored in solution for two years at room temperature (RT) [22], but in contact with RNases, it degrades immediately. The median intracellularly half-life is said to be 7.1 h tested in mouse cell lines [23] and 10 h when using human hepatoma cells. [24] Values for the peak protein translation ranges from 6 [25,26] to 24 h [27], so that it is not clear whether the intracellular stability is high enough. A poly(A)tail at the 3' end and a cap at the 5' increase the stability, but also influence the translation. Both structures serve as frames for the coding sequences, so they have to be chosen carefully. [16,28] The open reading frame (ORF) is flagged by a start and stop codon with untranslated regions (UTRs) around it. The production of mRNA in comparison to DNA is quite simple, fast and cheap using *in vitro* transcription. DNA serves as a template for all structures except the 5'cap, which is done enzymatically. The DNA is digested by DNases afterwards. [4]

Until today, the problems of low stability and short half-life of mRNA have been solved by structural modifications, so that other hurdles are now in the focus. For an effective treatment with fewer side effects, it is necessary to target special organs and cells *in vivo*. Since mRNA is not the pharmacologically active agent, bioavailability is difficult to predict. The relationship between mRNA dose, the encoded protein and the corresponding effect has to be investigated carefully. [4]

Two types of mRNA can be used, non-amplifying mRNA (IVT-mRNA) and self-amplifying mRNA (replicon-mRNA). In comparison, the former one is smaller (2 to 3 compared to 9 to

10 kb) and does not contain further encoded proteins which lower the risk of unwanted immune responses. Due to its self-amplification, replicon-mRNA has a longer half-life and *in vivo*-expression can last almost 2 months. In contrast, replicon-mRNA is much more sensitive to structural modification. [29] For this work, only IVT-mRNA was used.

1.1.4 Necessity of delivery systems

For transport of mRNA, nanoparticulate formulations are often used. A suitable vehicle needs various functions, leading to heavy demands in development:

- Interactions with unwanted components in the serum, as well as aggregation, should be avoided.
- Drug delivery systems should enable transport over cell membranes, since large and highly charged molecules such as mRNA are normally not able to cross cellular membranes. [30,31] Furthermore, the anionic charge of mRNA hinders penetration into DCs. [11]
- Drug delivery systems should enable the uptake into cells as well as an endosomal release. [4] Those cells which take up naked mRNA spontaneously use endocytosis. Hence, mRNA is accumulated and degraded in the lysosomes and just a small amount is secreted into the cytoplasm.
- Although the stability of mRNA is increased by modification of the mRNA strand, it is still necessary to protect the mRNA from RNases which are ubiquitous in the human body.
- The drug delivery system should target e.g. dendritic cells (DCs), best located in the lymphatic organ because these cells are potent antigen-presenting cells (APCs).
- At the target site, the uptake of mRNA into cells as well as the translation of mRNA should be facilitated.
- The formulation of other factors needed for an effective transfection should be possible. As written before, several antigens are often needed. Although mRNA has self-adjuvating properties, the addition of adjuvants seems to be beneficial. [32] Encoding of immunomodulating molecules like CD40L or CD70 has led to a higher immune response to the antigen. [33] Factors which have an impact on the local microenvironment at the tumour site could also be essential.
- The possibility of a manufacturing under GMP-conditions is required for a successful application. [32]

1.1.5 Current challenges in clinical trials

Most of the clinical trials in the last 20 years were performed with the *ex vivo* administration of mRNA to DCs [34,35] which should not be part of this work. In the last years, focus was more on the direct administration of mRNA with targets like metastatic melanoma [36], renal cancer carcinoma [37] or prostate cancer. [38] In some of the earlier studies, the outcome was not as successful as expected [36,39–41] and also rare cases of severe side effects like a Bell palsy occurred [21,42], which raises questions concerning the safety. In general, application of mRNA-based vaccines was safe [40,43], well-tolerated and led to tumour antigen-specific immune responses [43]. Local side effects like pain, swelling or erythema and systemic adverse reactions like fever, fatigue or headache [21] can always occur for preventive vaccination procedures.

A weak immune response could not be the only explanation for the failure of such vaccines. Moreover, it seems to be due to a complex host-tumour relationship which comprises response, editing, escape, and adaption of the hosts immune system. [39,44] So far, the overall clinical benefit of cancer vaccination in comparison to general treatment is just about 20 %. [45] Therefore, modifications of the vaccinations are necessary. Independent on the active substance, targeted therapy bases on recognition of protein structures which are normally upregulated on tumour cells. Nevertheless, these structures can also be found on the surface of healthy cells which lowers the specificity. In addition, vaccination with just one antigen is not reasonable due to a possible resistance. Combinations of more than one antigen can increase the specificity, in case more receptors are upregulated on the tumour surface. The higher the difference between tumour and healthy cells, the higher the success of a therapy can be. Hence, mutated antigens seem to be beneficial over non-mutated antigens [43,46,47]. In addition, the delivery system has a huge influence on the immune response and needs to be optimised as well. [45]

Several clinical trials are performed to evaluate the therapeutic effect of mRNA, not only for treatment of cancer. In many of these studies, mRNA is applied nakedly without a delivery system (e.g. AGS-0003-LNG, AGS-003, IVAC mutanome/warehouse. In addition, lipid-based delivery systems are often used as well (e.g. Lipo-MERIT, TNBC-MERIT, mRNA-1325, mRNA-2416), which shows the suitability of these systems for the use as a delivery system for mRNA. [32,48]

1.2 Lipoplexes for nucleic acid delivery

1.2.1 Liposomes

Since liposomes were first mentioned in 1965 by Alec Bangham [49], they have been investigated intensively. In general, liposomes are spherical vehicles, consisting mainly of lipophilic phospholipids. In contrary to micelles, they have at least one lipid bilayer with an entrapped hydrophilic volume. Due to their similarity to cell membranes, liposomes are often used as model membranes whereas research focus is on their use as a drug delivery system. [50] Although liposomes are now investigated for more than five decades, only a few products are approved by the regulatory authorities and available on the market (DaunoXome®, AmBisome®, DOXIL®, Epaxal®, Lipodox®, Visudyne®, AMPHOTEC®, Marqibo®, ABELCELT®, Myocet®). [7,51] Reasons for the lack of market approvals are e.g. the missing long-term stability, a difficult scale-up of the production with high effort to fulfil all the regulatory norms and the recognition of liposomes by the mononuclear phagocytic system (MPS) followed by a fast clearance from the blood. [51] Despite these problems, liposomes were chosen as the delivery system for this work because they have many advantages:

– They are biocompatible and biodegradable along with a low toxicity and immunogenicity.
– The self-assembled structure of liposomes can be varied through the composition as well as the preparation method. For example, the size ranges from 20 nm up to a few micrometres while at the same time the number of bilayers can be tuned (Fig. 3).

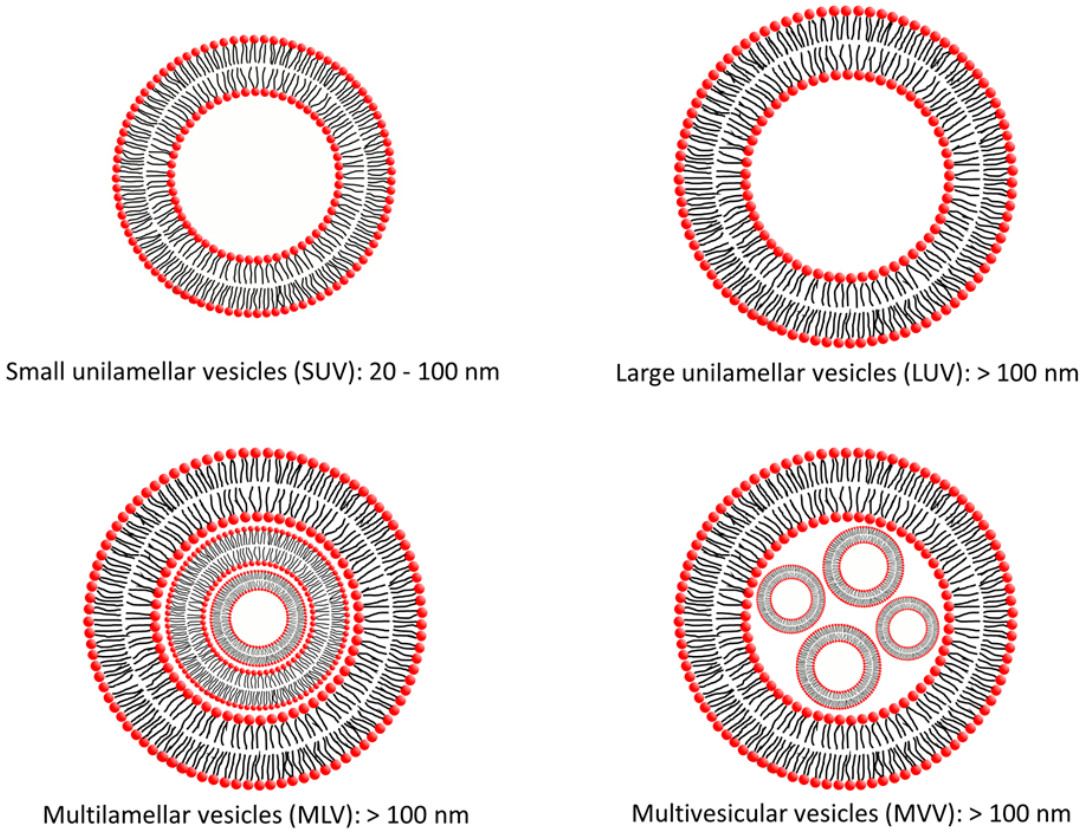

Figure 3: Classification of liposomes

– Due to the possibility of encapsulation of hydrophilic as well as lipophilic drugs, liposomes offer a wide range of formulation approaches. In general, by encapsulation, the toxicity and therefore the side effects of the therapeutic agent is reduced, which improves anticancer treatments. [51,52] It is possible to maintain a high drug concentration until the disintegration of the liposomes at the target region in the patient.
– Furthermore, active targeting by linkage of suitable structures like antibodies, proteins, Fab' fragments or carbohydrates on the surface, as well as passive targeting via the EPR-effect in tumour tissue, is feasible. [53]
– Due to the variability in properties, encapsulation and surface modifications, liposomes can be used for a wide range of therapies and also as a diagnostic agent as illustrated (Fig. 4). [54]

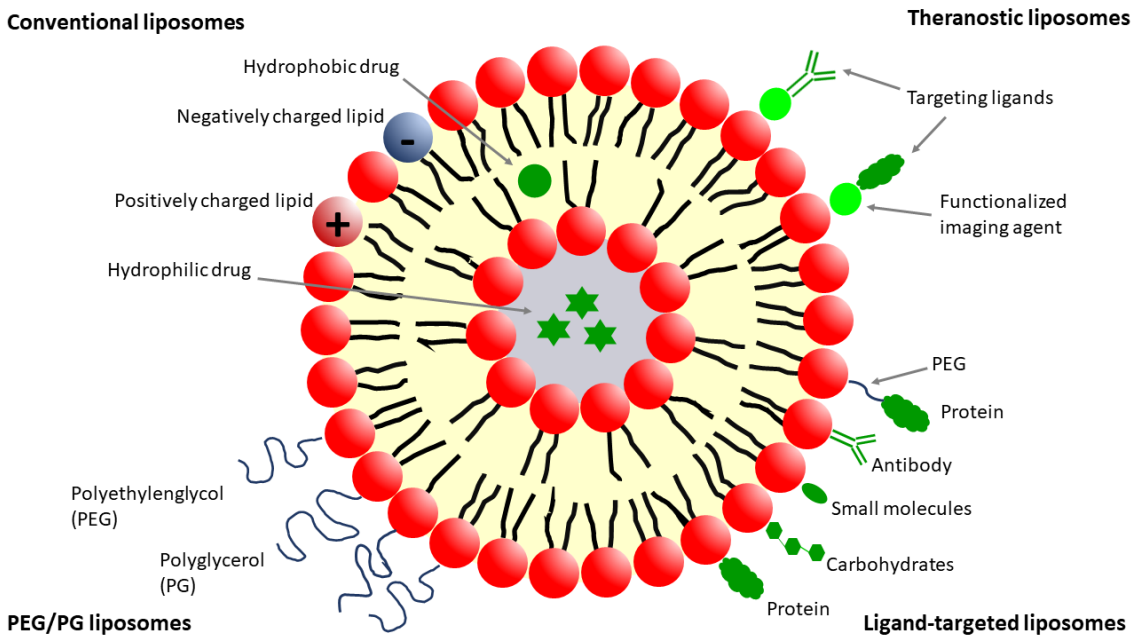

Figure 4: Different types of therapeutic liposomes (drawn after [54])

1.2.2 Mesomorphic phases

The formation of liposomes from lipids is an entropy-driven self-assembling process. Due to the molecular shape of the lipid [55], different mesomorphic phases exist (Fig. 5):

- **Lamellar phase (L_α):** The hydrocarbon chains are directed towards each other and the polar headgroups form the outer layer on both sides of the resulting bilayer. [56]
- **Cubic phase:** Different forms exist. The easiest one is an oil-in-water micelle assembly, where the hydrocarbon chains are all directed to one centre and the polar headgroups form the interface to the surrounding polar phase.
- **Reverse cubic phase:** Again, the easiest one is a water-in-oil micelle assembly, where the polar headgroups are all directed to one centre and the hydrocarbon chains form the interface to the surrounding lipid phase. [57]
- **Hexagonal phase (H_I):** Inwardly directed hydrocarbon chains form cylindrical aggregates with the polar headgroups as an interface to the surrounding polar phase.
- **Inverse hexagonal phase (H_{II}):** Cylindrical aggregates are formed by inwardly directed polar headgroups and hydrocarbon chains represent the interface to the surrounding lipid phase. [58]

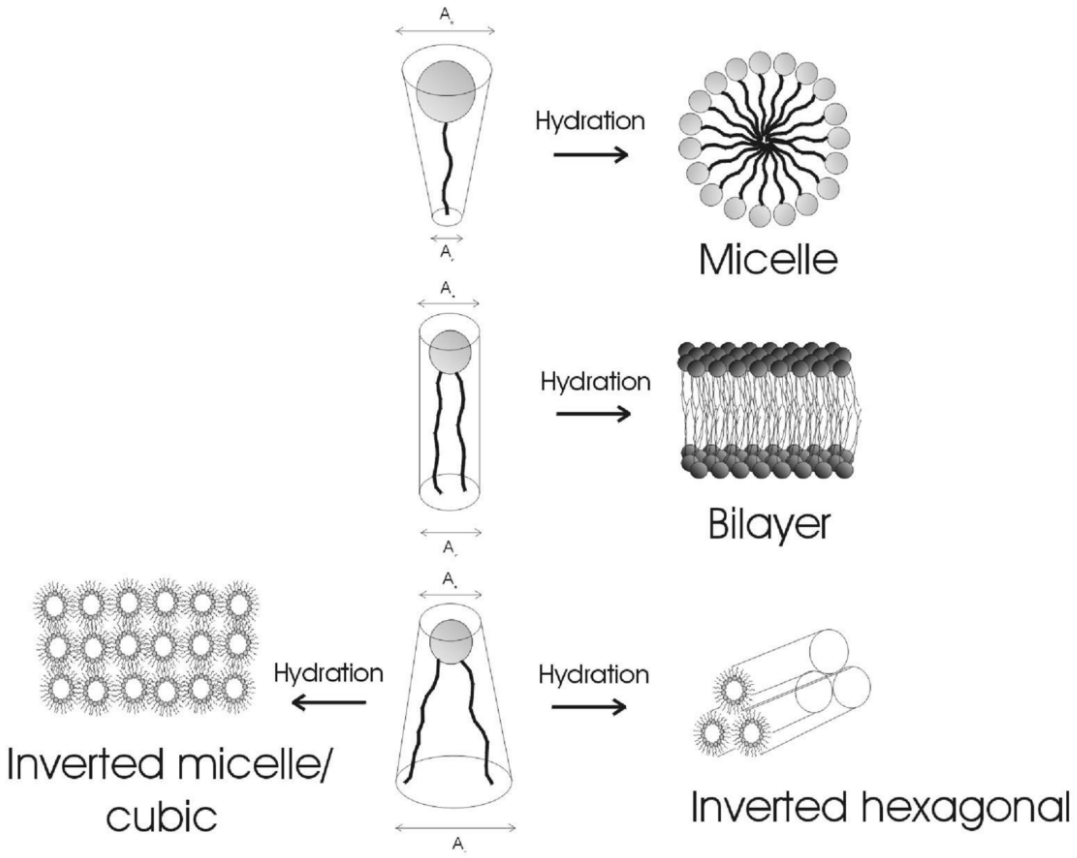

Figure 5: Exemplary illustration of lipid phases formed depending on the lipid shape (taken from [55])

For transport of nucleic acids and uptake of the liposomes into the cells by lipid membrane fusion [59], two phases and their transitions are most important. The lamellar structure represents stability since all cell membranes are associated in bilayers. Nevertheless, for transport of huge hydrophilic molecules, this structure is not beneficial. For uptake and release out of the endosome, the inverse hexagonal H_{II} phase is beneficial since it leads to a destabilisation. This mesomorphic phase is supposed to take place during the mitosis or invasion of viruses. [55] For evaluation of the ability of lipids to change from lamellar to hexagonal phase, the temperature of this transition can be measured. This transition depends on lipid shape, surrounding ionic conditions, hydration, temperature and pH. [60]

1.2.3 Lipoplexes for nucleic acid transport

Lipoplexes are the product of the formulation of nucleic acids with liposomes consisting of neutral, zwitterionic lipids like Egg-Phosphatidylcholine (EPC) or 1,2-Dioleoyl-sn-glycero-3-phosphocholine (DOPC) and a cationic lipid for complexation of the negative mRNA. Positively charged lipoplexes are associated with higher transfection efficiency in comparison to neutral or anionic lipoplexes. [61] Cationic lipids are associated with toxicity because they lead e.g. to cell shrinking, vacuolisation of cytoplasm or the disruption of the cell cycle. [62] Lipids generally consist of three parts – the hydrophobic chain, the hydrophilic headgroup and the linker between both. All three parts are considered to have an influence on the transfection and the toxicity. For example, cholesterol-based chains show higher transfection but have also a higher toxicity in comparison to aliphatic chains. [63] The cationic lipids normally have a carbon chain length from 8 to 18. One double bond in the chain is associated with the highest transfection efficiency, probably due to an increased fluidity of the membrane. [64] Single-tail chains are often more toxic than double-tail chains but can increase transfection as well. The linker bond between the hydrophobic chain and hydrophilic head can be either an ether, an ester or more recently also an amide or carbamate group. Ethers, like in 1,2-Di-O-octadecenyl-3-trimethylammonium propane (DOTMA), show good transfection but are too stable to be biodegradable. In contrast, esters like in 1,2-Dioleoyl-3-trimethylammonium-propane (DOTAP) result in lower toxicity because of a less stable bond, which can lead to degradation before reaching the target site. Carbamates or amides can circumvent these drawbacks. [65] The bonds are stable at neutral pH but are degradable in a more acidic area like the endosome. The headgroup bears the charge [63] which results in a higher impact on the transfection efficiency. [66] However, it also has a huge influence on the toxicity because the positive charge favors interactions with other components like proteins/enzymes. This leads to an increase in the particle size which can cause toxicity while circulating in the body. Furthermore, the charge is neutralised which normally decreases the transfection efficiency. In general, these effects are more pronounced for quaternary amines than tertiary amines. [63] Despite their toxic potential, cationic lipids are used to deliver mRNA because these lipids can serve as vaccine adjuvant as well. [67]

1.2.4 Selective targeting of lipoplexes

For tumour vaccination, activation of antigen-presenting cells (APCs) is prerequisite. Covalently bound mannose is one of the used ligands to target DCs as the most important antigen-presenting cells and can lead to higher transfection efficiency. [68,69]

Conversely, Kranz et al.[10] showed another approach to achieve a targeting. Instead of a molecular ligand, the composition of mRNA-lipoplexes was varied, which has resulted in a selective transfection after i.v. injection into mice. Naked mRNA, coding for luciferase, showed no measurable signal while mRNA in lipoplexes composed of DOTMA and 1,2-Dioleoyl-sn-glycero-3-phosphoethanolamine (DOPE), all with a size of 200 to 400 nm, showed a characteristic pattern. Cationic lipoplexes with a nitrogen to phosphate ratio (N/P = ratio of positive to negative charge in the complex) around 5/1 displayed expression of luciferase above all in the lungs and just rarely in the spleen. With the decrease of cationic lipid, the luciferase expression was shifted from the lungs to the spleen, so that neutral and negatively charged lipoplexes resulted in an expression exclusively in the spleen. The expression was reduced with an increase of negative charge. A higher amount of unbound mRNA is said to be responsible for that. Slightly positive lipoplexes (N/P from 2.5/1 to 1.8/1) were unstable by forming large aggregates after preparation so that these have been excluded from the experiments. This effect was also demonstrated with other cationic lipids like DOTAP. Although macrophages have the highest uptake of mRNA, the highest translation efficiency was shown in DCs. Furthermore it was shown, that lipoplexes are mainly taken up by macropinocytosis after binding to scavenger receptors. [10,70] Finally, these investigations have revealed that i.v. injection has advantages over local administration, tested with subcutaneous injection. [10] Nevertheless, local i.m. injection of lipid nanoparticles (LNPs) or cationic nanoemulsions (CNE) resulted in a strong stimulation of the immune system as well. [29,71]

1.3 Liposomal pathway after administrations to humans

The fate of the liposomal formulation depends on their way of administration. After intravenous injection, lipoplexes circulate in the blood stream depending on their properties. This circulation can be prolonged by stealth modification of the vesicular surface using polyethylenglycol (PEG) or polyglycerol (PG). [72] The distribution of the lipoplexes can be controlled via active targeting by addressing targets through binding of e.g. antibodies or proteins on the

liposomal surface or passive targeting by exploiting the physicochemical properties of the vesicles itself. Usually, differences in the properties of healthy and diseased tissue are required for the latter [73] as explained with the enhanced permeability and retention (EPR)-effect for tumours which is based on the leaky vasculature due to a rapid growth. [74,75] Finally, active and passive targeting cannot be separated completely since passive targeting enables accumulation of the particles in the target tissue. [76]

In this project, lipoplexes are supposed to be applied locally due to their high viscosity and missing size adjustment. Since skin is rich in DCs, an intracutaneous application is reasonable. The muscle as vaccination target is said to be favourable as well [77] since myocytes was shown to act as a depot for pDNA due to prolonged protein expression. [78] Casares et al.[79] revealed, that antigen presentation by DCs occurs after uptake of DNA into dermal or muscle cells. [79] Due to the local application, distribution issues are neglected and the focus is on the cell uptake of lipoplexes at the target site.

1.3.1 Cellular uptake

The uptake of naked mRNA was first investigated by Lorenz et al.[80], who found endocytosis as the main mechanism. This endocytosis is dependent on the binding to receptors of the scavenger family, which are expressed nearly everywhere in the body. Hence, the encoded antigen has been measured in almost all cell types. These receptors are concentrated in lipid rafts rich areas of the cells. Lipid rafts are liquid ordered phases in the cellular membrane which are surrounded by liquid disordered phases. Lipid rafts also contain proteins like receptors which can induce signal transduction. In addition, lipid rafts can form caveolae which are needed for endocytosis or transcytosis. Rafts are dynamic assemblies and have a high content of sphingolipids and cholesterol. [81]

Within the endocytic uptake, the pH of the emerging endosome is more acidic. The cytoplasm including the plasma membrane has the same physiological pH as the blood (7.4). After constriction of membrane lamellae, the formed early endosome has a pH of 6.2. Over time, the early endosome develops into the late endosome, which is more acidic with a pH around 5.0 to 5.5. After fusion with an early lysosome which contain hydrolytic enzymes and phosphatases for degradation of endogenous and exogenous components, late lysosomes are formed. The pH of these vesicles is around 4.6 to 5.0. [82,83] This pH decrease is necessary for maintenance of normal cell functions like processing of receptor-ligand complexes or the activity of the

degrading enzymes. [84] The mRNA accumulates in the lysosomes [80] which is quite typical for macromolecules taken up like this. [85] If they cannot escape before the formation of the late lysosome, the substances will be destroyed. Unfortunately, just small amounts of the mRNA can exit the endosome. In that case, the release happens spontaneously during vesicular rearrangements. [80] An endosomal escape is prerequisite for an assured and sufficient therapeutic effect. Until now, the actual uptake mechanism could not be identified explicitly. Endocytosis-independent uptake mechanisms are not excluded [80] and Diken et al.[86] described macropinocytosis as the mechanism for internalisation of mRNA into DCs. [86] However, the uptake of mRNA for all of the mechanisms is extremely low with less than 1 in 10 000. [4]

First attempts using cationic lipids to improve the transfection of DNA in cells have already been made during the late 1980s and the early 1990s [87–89], although the way of interaction was not clear at that time. A more detailed investigation to understand the interactions of liposomes with cells were done in 1995 by Wrobel and Collins [90] by using anionic liposomes. Cationic lipids like DOTAP and 3ß-[N-(N',N'-dimethylaminoethane)-carbamoyl]cholesterol (DC-Chol) mixed with DOPE are able to fuse with model membranes, while there is no fusion with DOPC. Furthermore, this fusion is independent on pH in a range from 4.5 to 7 as well as on the concentration of NaCl up to 150 mM. The same effect has been seen in mammalian cells. Furthermore, after blocking of the uptake route by depletion of adenosine-5'-triphosphate (ATP) or inhibition of clathrin-coated pits, also the lipid mixing has been inhibited. Hence, endocytosis is a prerequisite for lipid fusion although until now it is not completely clear why. [90] Until now, the endocytic pathway has been discussed for the uptake of liposomes [91] and has been proven for liposomes with different surface charge recently. Depending on the cell type as well as the surface charge, endocytosis was either caveolae- or clathrin-mediated and is a result of macropinocytosis. [92] In addition, endocytosis was also demonstrated for mRNA-based nanomedicines. [93,94]

1.3.2 Release of nucleic acids from lipoplexes

In 1996, Xu and Szoka [95] published their theory on the release kinetics of DNA from lipoplexes, which has not been refuted until today. [64,95] After the first contact with the cell surface, the lipoplex is internalised into the endosome. Subsequently, the endosomal membrane is destabilised by a flip-flop of anionic lipids, which can be found on the cytoplasmic side. This results in the formation of new complexes between these anionic lipids and the cationic ones from the lipoplexes. Hence, the DNA is released from the complex into the cytosol. In further

experiments, it has been proven that anionic lipids can displace DNA, thus leading to lipid mixing. This is also a reasonable explanation for the toxicity of some lipoplexes if this ion-pair formation takes place e.g. within the mitochondrial membrane. Furthermore, Xu and Szoka [95] have proven, that heparin and dextran sulfate as highly charged anionic polymers have the same property to form complexes with cationic lipid thus mimicking nucleic acid release *in vitro*. Similar to Wrobel and Collins [90], they have not been able to explain why lipoplexes first need to be taken up by endocytosis if lipid mixing and destabilisation occur anyway. [95]

In addition to the studies of Xu and Szoka [95], Hafez et al.[96] have investigated the detailed mechanism of the interaction between cationic lipid and the endosomal membrane. Due to electrostatic interactions, cationic lipid forms ion pairs with anionic lipids in an equimolar ratio. The cationic lipid normally tends to form bilayers due to a bigger ionised headgroup. While pairing with negatively charged lipids, neutralisation leads to the formation of an inverse hexagonal H_{II} phase. Consequently, the endosomal membrane is destabilised. Most anionic lipids are located on the cytoplasmic side of the endosome, but it seems like a small amount is enough to trigger this reaction. The mechanism is illustrated in Fig. 6 with siRNA as a model for all nucleic acids. [96]

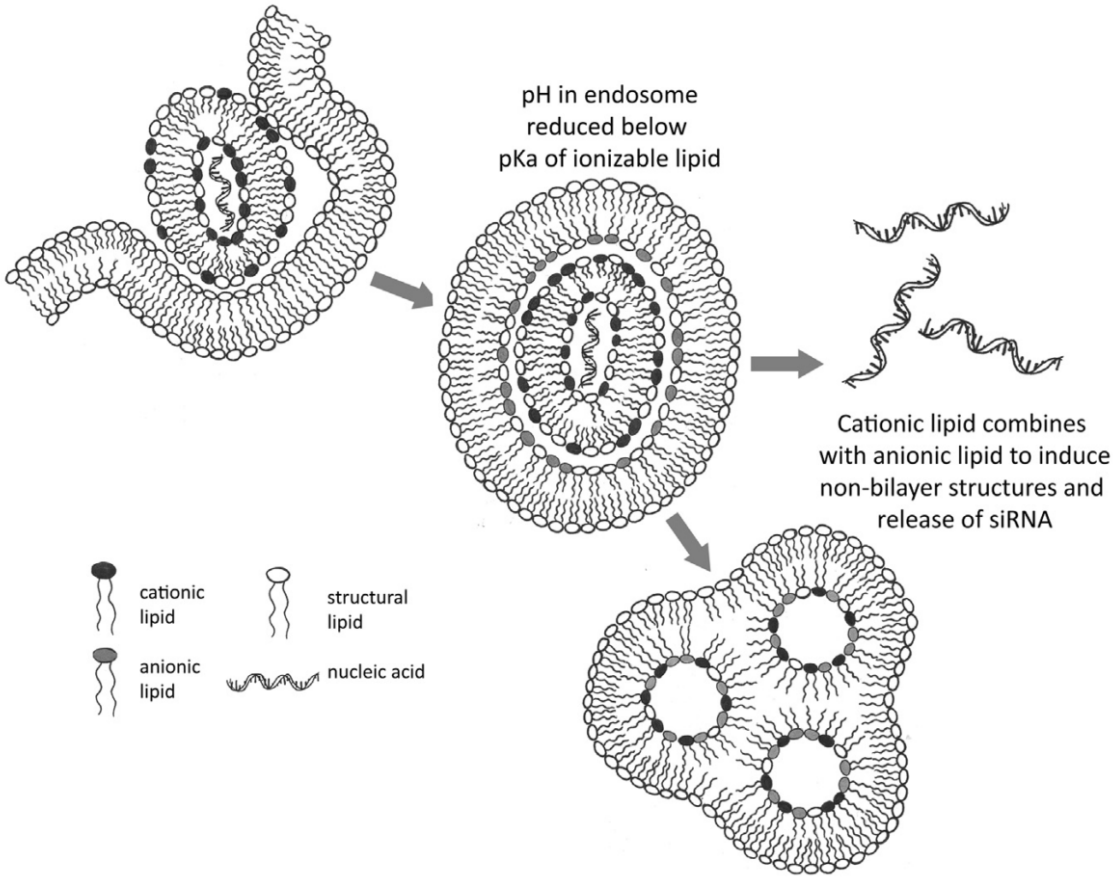

Figure 6: Presumed mechanism for endosomal release of lipoplexes (taken from [7])

According to these findings, a correlation between the lipid mixing and the release of DNA is obvious. However, four years later, Mui et al.[97] have shown that there this no correlation between the mixing and the transfection efficiency. [97] Already in 1997, it has been shown by Stegmann et al.[98], that lipid mixing is not always followed by DNA release and translation. They compared lipid mixing of either DOTAP or DOTMA alone and with DNA. The complex of both lipids and DNA has a lower tendency to fuse, probably due to a strong electrostatic interaction between the cationic lipid and the DNA as well as a likely different membrane structure of lipoplexes. Furthermore, they have determined the transfection of lipoplexes in Chinese hamster ovary (CHO-K1) cells while measuring the mixing of these lipoplexes with the cells. Experiments have exposed that there is no correlation between both events. The influence of DOPE has been investigated in addition. Lipoplexes (cationic lipid/DNA- ratio of 0.5) in combination with DOPE have had higher transfection than these lipoplexes alone (200-fold for DOTMA, 20-fold for DOTAP), which reveals the benefits of DOPE. Surprisingly, lipid mixing with DOPE has indeed increased transfection for DOTAP but has reduced

it for DOTMA. Obviously, the mechanism explained by Xu and Szoka [95] is taking place *in vitro*, but not exactly like this *in vivo*. [98]

1.3.3 Enhancement of endosomal release

One approach to enhance the endosomal release is the "proton sponge" effect by use of polymers, which is not part of this work and will not be discussed here. [99]

Another often-used possibility is the addition of the fusogenic lipid DOPE. Its quality to enhance transfection has already been mentioned above. Because of its ability to change between different liquid crystalline structures, it facilitates the destabilisation of the endosomal membrane. Normally in standard physiological conditions and neutral pH, pure DOPE forms the hexagonal H_{II} (non-bilayer) phase. In a mixture with a cationic lipid, DOPE is able to form bilayers. After contact with the anionic lipids in the endosome (described above), the cationic lipid is removed from the formulation by complexation. Consequently, DOPE forms again non-bilayer structures and supports the destabilisation of the membrane so that mRNA can be released. [64] The formation of the hexagonal phase is essential, which was also proven by Zuhorn et al.[100] in 2005. The cationic lipid SAINT-2 has been tested with DOPE and DPPE. Both facilitate the dissociation of DNA out of the complexes suggesting that the ethanolamine headgroup is responsible for this. The role of the PE head group is said to disturb the interaction between cationic lipid and DNA (by reaction of the PE phosphate group with the amine group of the cationic lipid and the amine group of PE with the phosphate group of the DNA). Transfection of DOPE has been higher compared to DOPC. DOPC forms lamellar structures where no dissociation of the lipoplexes is visible. After mixing with anionic liposomes, a mixed lamellar-hexagonal phase occurs which explains the low but nonetheless present transfection. [100]

As described earlier, cationic lipids alone have the property to destabilise the endosomal membrane, so that endosomal release can also occur without the addition of DOPE. Unfortunately, they are associated with toxicity. [63] Ionizable lipids like 1,2-dioleoyl-N,N-dimethyl-3-aminopropane (DODMA) offer a chance to overcome this problem. Jeffs et al.[101] investigated this pH-sensitive system for delivery of DNA. The apparent pK_a of DODMA in a lipid layer has been determined at 6.8. Therefore, the lipid is not completely charged at the physiological pH of 7.4, which avoids or at least reduces aggregation of proteins and facilitates a prolonged circulation in the extracellular fluids e.g. blood. While entering the acidic endosome, the headgroup gets ionised so that the ion pair formation with the anionic lipids is possible and the

DNA can be released. They discovered, that an optimal encapsulation of DNA into the lipids needs an acidic pH from 4 to 6 as well. [101] Although an overall neutrally charged vesicle seems to be optimal to avoid complete aggregation in the serum, it is necessary to have at least a small excess of positive charge. The charge is needed so that the vesicle can bind to the cell surface via electrostatic interaction and enhance cellular uptake via endocytosis. [102] Apart from that, it has to be considered that cell surfaces are coated with membrane proteins [103] and that the lipoplexes will be covered with a protein corona after administration into the human body. [104,105] Due to the complexity, this should not be considered within this thesis.

1.4 Structural analysis

As described above, detailed information on the structure is essential for a prediction of the *in vitro* and *in vivo* behaviour of mRNA formulations. Several techniques are available to gain insight into the molecular organisation, so for this work only some were accessible. As a primary method, small-angle scattering (SAS) techniques were used, whereas e.g. dynamic light scattering (DLS) and electrophoretic light scattering (ELS), differential scanning calorimetry (DSC) and the determination of free mRNA with RiboGreen® Assay, provided supporting information. Transfection experiments have been carried out to test the principal functionality and to correlate the findings with the biological behaviour.

Radiation describes the transport of energy through a medium or space and can be divided into particle radiation and electromagnetic radiation. The first describes the energy transport by the emission of particles such as neutrons or alpha- and beta radiation. In case of electromagnetic radiation, the energy is transported in the form of waves. Examples for this kind of radiation are X-rays, light and radio waves.

In the context of the SAS experiments, there are three relevant types of interaction between radiation and matter. Radiation can be absorbed entirely by matter (absorption). In the case of coherent scattering, scattered radiation is characterised by a fixed phase relation of the scattered waves. The phase relation is dependent on the structure of the scattering centre. Coherence can occur either temporally or spatially. The wavelength of the scattered light needs to be the same (coherent scattering). In case of incoherent scattering, there is no fixed phase relation between incident light and scattered light and the wavelengths of the scattered radiation differ. Due to the structure of the scattering centres, the waves are scattered into different directions

(incoherent scattering). For SAS measurements, the wanted information are transported by the coherent scattering, while the incoherent scattering generates the background noise. [106]

In addition, scattering is further characterised by the energy transfer from the incident radiation to the medium. In case of elastic scattering, the particle's kinetic energy before and after the scattering process is the same. No energy is transferred to the scattering centre. For inelastic scattering, the kinetic energy of the scattered particles or waves is lower since some of the energy is transferred to the scattering centre. The quantity of transferred energy provides information on the structure and properties of the tested material. [107]

Scattering patterns can either be static or dynamic. Static patterns grow out of intramolecular interference of the amplitudes generated by the atoms in a molecule. Due to that, the molecular structure can be analysed. Dynamic scattering patterns arise from the interference of various particles or molecules that move in a dispersed solution. Therefore, it can just be used to obtain information about the particle size but not about the molecular structure.

1.4.1 Small-angle scattering

Lots of studies show the feasibility of SAXS and SANS for investigation of lipoplexes, in a way that the mesomorphic structures can be determined. [108–114] In 1963, Kratky published first SAXS experiments with lamella-shaped particles. [115] In 1974, Atkinson et al.[108] carried out SAXS experiments with phosphatidylserine (PS) dispersions [108] and in 1987, Jousma et al.[116] characterised the multilamellar structure of liposomes composed of phosphatidylcholine (PC), PS and cholesterol after extrusion. [116] Nearly 20 years later, Lasic et al.[117] described a lamellar organisation for self-assembled DNA-lipoplexes composed of 1,2-Dioleoyloxy-3-dimethylamino-propane (DODAP) and cholesterol, where the DNA forms a lattice between the lipid layers. [117] Further experiments performed by Rädler et al.[113] and Salditt et al.[118] with a mixture of DOPC, DOTAP and DNA have proven the lamellar structure. [113,118] Shortly after, Koltover et al.[112] have been able to detect the inverse hexagonal phases alone and in coexistence with lamellar structures while using lipoplexes of DOPE and DOTAP [112]. Since then, several studies have been conducted to investigate lipoplexes of different compositions under various conditions. [119–122] Nevertheless, most studies have used lipoplexes with DNA or siRNA [123,124], but none were undertaken using mRNA. It has been shown that it is possible to detect mRNA alone or in combination using X-ray scattering as reviewed by Chen and Pollack. [125]

1.4.2 Differential scanning calorimetry

Another method for characterisation used in this thesis is the differential scanning calorimetry (DSC), which has been first mentioned in 1963. [126] The method can be used to determine the thermodynamical behaviour and complex formation of small molecules, polymers or lipid. A temperature program is applied to the sample as well as to a reference, while the amount of heat which is necessary to achieve this temperature is measured. Differences in the amount of heat can result from endothermic (e.g. melting) or exothermic (e.g. crystallisation) processes. For lipid formulations, the phase transition temperature (T_m) is a significant parameter since it represents the transition from the ordered gel-like state to the unordered liquid-like state of a lamellar order and is crucial for the stability of the system. Higher values for T_m mean more energy to destabilise the bilayers. The phase transition is dependent on the composition of the formulation and hydration of the lipids as well as the type and pH of the surrounding solvent. Depending on the geometry of the double bonds, unsaturated lipids can affect the packing of lipids. While the trans-position only has a slight influence on T_m, cis-double bonds can lead to a stronger decrease of T_m since the packing is no longer completely uniform. The packing of lipids can also be disturbed by impurities such as small molecules. [127] It has to be investigated if mRNA acts like an impurity. Furthermore, for storage liposomal formulations are often freeze-dried and result in an amorphous form. The glass transition temperature (T_g) is another parameter which can be determined to investigate the long-term stability. Summing up, DSC represents another important characterisation method for formulation development. [128]

1.4.3 Light scattering techniques

Two fundamental characteristics for lipoplexes are size and zeta potential. Lots of different factors have to be considered when adjusting the particle size. In addition, it is still not clear if size is a determining factor for transfection since there is inconsistent data concerning that. Some studies could not found a dependency [98,129,130] while others identified an influence of the size. [131,132] Some studies even described size as the major factor for transfection efficiency. [133,134] Nevertheless, some of the performed studies have shown, that large vesicles are not obstructive for transfection. For example, Turek et al.[135] showed, that DNA-lipoplexes with a size smaller than 250 nm have only transfected efficiently in the absence of serum, while the ones with sizes over 700 nm have shown good transfection with or without serum. Since large-size complexes showed higher transfection efficiency, it was assumed that the smaller particles show lower efficiency because the serum prevents an aggregation of these particles [135] as well

as inhibit the contact of the particles with the cell surface. [136] Studies indicate that large lipoplexes can induce the formation of large intracellular vesicles, which can be disrupted more easily and therefore deliver the DNA with higher efficacy. [137] For lipofection (transfection with liposomes or micelles), larger vesicles have maximum contact with the cells which increase the probability of endocytosis. [138] In contrast to that, by using colloidal gold nanoparticles Jiang et al.[139] showed that endocytosis was most efficient within the size range of 25 to 50 μm. [139] It is discussed that *in vitro* and *in vivo* application can require different particle sizes. [140]

In general, the size of nanoparticles cannot be increased too much to avoid e.g. pulmonary embolism, strokes or myocardial infarctions. The smallest capillaries have a diameter of 5 to 10 μm so that particles have to be much smaller than 5 μm and must not form aggregates. [141] The increase of the particle size after contact with serum due to formation of a protein corona has to be considered as well. [105,142] On the contrary, very small particles (< 100 nm) tend to form aggregates as well. [143] Local administration was in the focus of this thesis so that the size of the vesicles is not such an essential factor because distribution of the particles over the blood stream is not needed. Hence, the size of the lipoplexes was not adjusted throughout the preparation.

The zeta potential is defined as the potential difference between the stationary layer which is attached to a dispersed particle and the dispersion medium. It is measured as the overall charge of the lipoplexes and provides information on repulsive or attractive forces between particles. Aggregation, fusion or precipitation of particles is dependent on the charge so that zeta potential can predict the stability of the system. Furthermore, modifications of the surface can also be observed by a change in this potential. [144] Just like the size, the zeta potential can change after administration into the human body due to the formation of a protein corona. [142] The absorption of positively or negatively charged proteins on the particle surface can favour aggregation and increase the risk of an embolism or stroke.

1.4.4 Encapsulation efficiency

For the development of a structural model, it is necessary to know where the mRNA is located in the sample structure. Determination of free and bound mRNA gives information on the localisation of the mRNA molecules and can be done with the Quant-IT RiboGreen® Assay Kit provided by Thermo Fisher. The fluorescent dye only binds to free mRNA leading to a measurable fluorescence. By knowing the total concentration of mRNA in the sample, the complexed proportion can be calculated easily. [145]

1.4.5 Determination of ionizable properties

For the characterisation of formulations with an ionizable lipid, further characterisation is necessary to determine the pK_a. The 2-(p-toluidino)-6-naphthalenesulfonic acid (TNS) assay is a convenient method to perform an *in situ* measurement which was introduced by Eastman et al. in 1981. [146] The pK_a of the lipid incorporated into the lipid membrane is measured so that influences on the dissociation of the amine group by the neighboring lipids or the membrane itself are considered. [147–149]

The importance of the pK_a determination was emphasised by Jayaraman et al.[148] in 2012. In this study, novel amino lipids with pK_a values between 4.17 and 8.12 were synthesised by modification of the headgroup of the ionizable DLin-KC2-DMA. Importantly, there was no significant change in the molecular dimension of the hydrophilic region since a major change in the headgroup could lead to an alteration in the adoption of the inverted, non-bilayer structure. Lipids were formulated with siRNA in LNPs and tested for their *in vivo* hepatic gene silencing in mice. A pK_a range of 6.2 to 6.5 was found as an optimum for this effect. Nevertheless, lipids with the same pK_a showed differences in the potency, which indicated that the pK_a is just one parameter for an effective *in vivo* activity. In addition, mixing two lipids to achieve a special pK_a led to the same efficiency than one lipid with that pK_a. For similar structures, the *in vivo* hepatic gene silencing was driven by the pK_a rather than structural changes of the headgroup or the linker length. [148]

2 Aim of the thesis

mRNA nanomedicines have been gaining increasing interest for cancer therapy in the last years. They can be used for a wide range of therapeutic applications such as tumour therapy, vaccination or protein replacement therapy. Several products, most of them in for tumour therapy, have reached the level of clinical trials. Formulations are required for administration of the mRNA to achieve a protected and selective delivery as well as an efficient uptake and translation into the target cells. For a successful therapy, it is necessary to have detailed information of the molecular structure of the formulation for development of a structure-activity relationship and the selection of the suitable composition.

In this thesis, lipid-based carrier systems are used since barely any information about the structure of mRNA-lipoplexes is given. Most of the previous studies have dealt with DNA or siRNA. In the first part, cationic lipoplexes for local administration are used as a model system to characterise the structure when incorporating mRNA. DOPC acts as a matrix, into which the cationic lipid DOTAP is inserted in varying proportions. Several formulations with an excess of cationic lipid or negatively charged mRNA are prepared to investigated lipoplexes with different characteristic properties. The mRNA should be inserted into this highly concentrated DOPC matrix in a controlled way. It should be investigated if DOTAP acts as an anchor and is able to facilitate a controlled release of the mRNA.

Unfortunately, cationic lipids are related to toxicity. Hence, the second part of the thesis focuses on ionizable lipids, because these lipids propose to offer less toxicity with higher efficacy. The pK_a of the used formulation is evaluated to find the best composition to enhance endosomal release. In addition, the structural changes of the membranes are investigated as a function of the pH. Moreover, by addition of heparin and the concurrent reduction of the pH, cellular contact is mimicked and endosomal release is triggered. Again, the changes of the molecular structure and the release of mRNA can be determined to obtain information about the fate of the lipoplexes after administration into the human body as well as about their behaviour at the point of action.

3 Materials and methods

Partial results of the presented work have been published in: Ziller, A.; Nogueira, S. S.; Huehn, E.; Funari, S. S.; Brezesinski, G.; Hartmann, H.; Sahin, U.; Haas, H.; Langguth, P. Incorporation of mRNA in Lamellar Lipid Matrices for Parenteral Administration. Mol. Pharm. ***2017****, acs.molpharmaceut.7b01022.* [150]

3.1 Materials

3.1.1 Reagents and solvents

Ampuwa® (aqua ad iniectabilia)	Fresenius Kabi Deutschland GmbH, Bad Homburg vor der Höhe (Germany)
Adenosine 5'-Triphosphoric Acid Disodium Salt (ATP)	AppliChem GmbH, Darmstadt (Germany)
Boric acid	Sigma-Aldrich, St. Louis (USA)
Cell Proliferation Kit II (XTT)	Sigma-Aldrich, St. Louis (USA)
Chloroform anhydrous	Sigma-Aldrich, St. Louis (USA)
Citric acid	Sigma-Aldrich, St. Louis (USA)
Coenzyme A	P.J.K, Seoul (Korea)
D(+)-Glucose anhydrous	Merck Chemicals GmbH, Darmstadt (Germany)
Dithiothreitol (DTT)	AppliChem GmbH, Darmstadt (Germany)
D-Luciferin	Synchem UG & Co. KG, Felsberg (Germany)
Dulbecco's modified eagle medium (DMEM)	Sigma-Aldrich, St. Louis (USA)
D-(+)-Trehalosedihydrate from saccharomyces cerevisiae, BioReagent	Sigma-Aldrich, St. Louis (USA)

DPBS (Dulbecco's Phosphate Buffered Saline), no calcium, no magnesium	Gibco® - Life Technologies, Carlsbad (USA)
	Sigma-Aldrich, St. Louis (USA)
Eagle's minimal essential medium (EMEM)	Sigma-Aldrich, St. Louis (USA)
Ethylenediaminetetraacetic acid (EDTA)	Carl Roth GmbH, Karlsruhe (Germany)
	Sigma-Aldrich, St. Louis (USA)
Fetal bovine serum, 10 %	Sigma-Aldrich, St. Louis (USA)
Fetal calf serum (FCS)	Sigma-Aldrich, St. Louis (USA)
Formamide	Sigma-Aldrich, St. Louis (USA)
Glutamine	Sigma-Aldrich, St. Louis (USA)
Heparin sodium, BRP	Sigma-Aldrich, St. Louis (USA)
HEPES	Carl Roth GmbH, Karlsruhe (Germany)
Iscove's modified dulbecco's medium (IMDM)	Sigma-Aldrich, St. Louis (USA)
Isopropanol	Carl Roth GmbH, Karlsruhe (Germany)
jetPEI®	Polyplus-transfection,
	Illkirch-Graffenstaden (France)
Lipopolysaccharide (LPS)	InvivoGen, Toulouse (France)
Magnesiumsulfat * 7 H_2O	Carl Roth GmbH, Karlsruhe (Germany)
Mercaptoethanol	Carl Roth GmbH, Karlsruhe (Germany)
Messenger RNA	BioNTech AG, Mainz (Germany)
Opti-MEM™	Thermo Fisher Scientific GmbH, Dreieich (Germany)
Ovalbumin (OVA)	AppliChem GmbH, Darmstadt (Germany)

Passive lysis buffer	Promega Corporation, Madison (USA)
pCMV_GFP_2A_click_beatle luciferase (Plasmid DNA)	WG Prof. Grabbe/University hospital, Mainz (Germany)
Penicillin	Sigma-Aldrich, St. Louis (USA)
Pierce™ Firefly Luciferase Glow Assay Kit	Thermo Fisher Scientific GmbH, Dreieich (Germany)
Potassium phosphate monobasic	Sigma-Aldrich, St. Louis (USA)
Protamine sulfate salt from salmon, Grade X	Sigma-Aldrich, St. Louis (USA)
Puromycin	InvivoGen, Toulouse (France)
Quant-iT™ RiboGreen™ RNA Assay Kit	Thermo Fisher Scientific GmbH, Dreieich (Germany)
RNase Zap®	Ambion® - Life Technologies, Carlsbad (USA)
Roti®-Stock 100x TE-buffer	Carl Roth GmbH, Karlsruhe (Germany)
ROTIPUTAN® Ethanol	Carl Roth GmbH, Karlsruhe (Germany)
Sodium chloride	Carl Roth GmbH, Karlsruhe (Germany)
Sodium dodecyl sulfate (SDS)	AppliChem GmbH, Darmstadt (Germany)
Sodium hydroxide	Sigma-Aldrich, St. Louis (USA)
Sodium phosphate dibasic	Sigma-Aldrich, St. Louis (USA)
Sodium phosphate monobasic	Sigma-Aldrich, St. Louis (USA)
Streptomycin	Sigma-Aldrich, St. Louis (USA)
Thymidine (labelled with tritium)	PerkinElmer LAS GmbH, Rodgau (Germany)
2- (p-toluidino)-6-naphthalenesulfonic acid (TNS)	Sigma-Aldrich, St. Louis (USA)

Tricin PUFFERAN®	Carl Roth GmbH, Karlsruhe (Germany)
Trisodium citrate	Sigma-Aldrich, St. Louis (USA)
XTT Cell Proliferation Kit II	Sigma-Aldrich, St. Louis (USA)
Water RNase-free, Nuclease-free	Carl Roth GmbH, Karlsruhe (Germany)

3.1.2 Lipids

Cholesterol	Sigma Aldrich Co., St. Louis, Missouri (USA)
3ß-[N-(N',N'-Dimethylaminoethane)-carbamoyl]cholesterol (DC-Chol)	Avanti Polar Lipids, Inc., Alabaster (USA)
Didodecyldimethylammonium (DDAB)	Avanti Polar Lipids, Inc., Alabaster (USA)
1,2-Dioleoyl-N,N-dimethyl-3- aminopropane (DODMA)	Corden Pharma GmbH, Plankstadt (Germany)
1,2-Dioleoyl-sn-glycero-3-phosphocholine (DOPC)	Merck & Cie, Schaffhausen (Switzerland) Lipoid GmbH, Ludwigshafen (Germany)
1,2-Dioleoyl-sn-glycero-phosphoethanolamine (DOPE)	Lipoid GmbH, Ludwigshafen (Germany)
1,2-Dioleoyl-3-trimethylammonium-propane (DOTAP)	Merck & Cie, Schaffhausen (Switzerland) Lipoid GmbH, Ludwigshafen (Germany)
1,2-Di-O-octadecenyl-3-trimethylammonium propane (DOTMA)	Merck & Cie, Schaffhausen (Switzerland)
Egg-Phosphatidylcholine 80% (EPC 80, Lipoid E 80)	Lipoid GmbH, Ludwigshafen (Germany)
Egg-Phosphatidylcholine 100% (EPC 100, Lipoid E 100)	Lipoid GmbH, Ludwigshafen (Germany)

1,2-Dioleoyl-sn-glycero-3-phosphoethanolamine-N-(carboxyfluorescein) (PE-CF)	Avanti Polar Lipids, Inc., Alabaster (USA)

3.1.3 Laboratory disposables

Aluminium crucible with lid, 40 µl	Mettler-Toledo GmbH, Gießen (Germany)
Copper grids Quantifoil R1.2/1.3 200 mesh	Plano GmbH, Wetzlar (Germany)
DTS1060/DTS1070 folded capillary cell	Malvern Instruments GmbH, Herrenberg (Germany)
Nylon Wool Fibre, steril	Polyscience Europe GmbH, Hirschberg an der Bergstraße (Germany)
Omnifix®-F syringes, 1 ml	B. Braun Melsungen AG, Melsungen (Germany)
PARAFILM® M	Carl Roth GmbH, Karlsruhe (Germany)
Pierce™ Protein Concentrator PES, 100 K MWCO, 5 - 20 ml, 10 pk	Thermo Fisher Scientific GmbH, Dreieich (Germany)
Rotilabo® Disposable cuvette, PS, 1.6 ml	Carl Roth GmbH, Karlsruhe (Germany)
Safe-Lock Tubes, 0.5 ml/1.5 ml	Eppendorf AG, Hamburg (Germany)
SafeSeal SurPhob Filter Tip, 10 µl/200 µl/1000 µl	Biozym Scientific GmbH, Hessisch Oldenburg (Germany)
SiLibeads Typ ZY, 0.8 - 1.0 mm	Sigmund Lindner GmbH, Warmensteinach (Germany)
Sterican®, disposable cannulae, 0.6 x 60 mm, 23 G/0.8 x 40 mm, 21 G x 1 ½ , PP	Carl Roth GmbH, Karlsruhe (Germany)
Syringe filters, cellulose acetate, 0.2 µm, ø 25 mm	VWR International, Radnor (USA)

Tubes, Polypropylene, 15 ml/50 ml	Greiner Bio-One, Kremsmünster (Austria)
Twist top vials, 0.65 ml/2 ml	Sorenson™ BioScience, Salt Lake City (USA)
24-well plates CELLSTAR®, clear, steril	Greiner Bio-One, Kremsmünster (Austria)
96-well clear bottom well plates, black, steril, treated with TC	Biozym Scientific GmbH, Hessisch Oldenburg (Germany)
96-well plate LUMITRAC 200 immunology plate	Greiner Bio-One, Kremsmünster (Austria)

3.1.4 General equipment

ABIMED Pipettes, 10 µl/200 µl/1000 µl	Kinesis GmbH, Langenfeld (Germany)
Centrifuge 5804 R	Eppendorf AG, Hamburg (Germany)
Centrifuge Heraeus® Multifuge® 1 L-R	Thermo Fisher Scientific GmbH, Dreieich (Germany)
Cryoplunge 3 System	Gatan, Inc., München (Germany)
Drying cabinet	Fa. BINDER GmbH, Tuttlingen (Germany)
DSC 1 STAR^e System	Mettler-Toledo GmbH, Gießen (Germany)
Glass flat-head stopper, NS 14/23	DURAN Group GmbH, Mainz (Germany)
Harvester 96	Tomtec, Inc., Hamden (USA)
Incubator CB 210	Fa. BINDER GmbH, Tuttlingen (Germany)
Laminar Flow Cabinet SKANAIR VFC 120	SKAN AG, Allschwil (Switzerland)
LIEBHERR Comfort Freezer	Liebherr-International Deutschland GmbH, Biberach an der Riß (Germany)

Nanodrop™ 2000 Spectrophotometer	Thermo Fisher Scientific GmbH, Dreieich (Germany)
Nylon wool column	Do-it-yourself construction, WG Prof. Grabbe/University hospital, Mainz (Germany)
pH meter pH 538	LaboTec GmbH & Co. KG, Dillenburg-Manderbach (Germany)
Refrigerated Condensation Trap RT 400	Thermo Fisher Scientific GmbH, Dreieich (Germany)
Rotavapor R-3 with Vacuum Pump V-700 and Vacuum Controller V-850	BÜCHI Labortechnik GmbH, Essen (Germany)
SAVANT Speed Vac SVC 200	Thermo Fisher Scientific GmbH, Dreieich (Germany)
Semi-Micro-Balance LE225D-OCE	Sartorius AG, Göttingen (Germany)
SpeedMixer™ DAC 150.1 CM	Hauschild & Co KG, Hamm (Germany)
Storage vial kit, 12 ml - 19 x 65/4 ml - 15 x 45, amber	Agilent Technologies, Santa Clara (USA)
TECAN infinite F200	Tecan Group Ltd., Männedorf (Switzerland)
Test tubes 16 x 100 mm, NSH 14/23	DURAN Group GmbH, Mainz (Germany)
Transmission electron microscope FEI TECNAI T12	Thermo Fisher Scientific GmbH, Dreieich (Germany)
Ultrasound bath RK 510	Brandelin, Berlin (Germany)
Vortexer RS-VF 10	Phoenix Instrument GmbH, Garbsen (Germany)
Zetasizer Nano ZS	Malvern Instruments GmbH, Herrenberg (Germany)

3.1.5 Data progression

Excel 2013/2016	Microsoft Corporation, Redmond (USA)
Fit2D	ESRF, Grenoble (France)
Origin 7.5	Additive GmbH, Friedrichsdorf (Germany)
Zetasizer Software 7.11	Malvern Instruments GmbH, Herrenberg (Germany)

3.2 Methods

3.2.1 Nucleic acids

mRNA

The mRNA used in this work had a modified structure for an increased stability and was synthesised and provided by BioNTech AG (Mainz, Germany) [151]. For cell experiments, the encoding proteins were either luciferase or green fluorescent protein (GFP). For structural analysis, noncoding out of specification- (OOS) mRNA was used instead. The total length of the mRNA strand was about 2000 bases including the poly-A tail. The stretched length of the mRNA strand is approximately 560 nm while the coiled length is around 30 to 70 nm. [152–154]

OOS-mRNA needed to be highly concentrated. Pierce™ Protein Concentrators with a molecular weight cutoff of 100 K were filled with the mRNA and centrifuged with Centrifuge 5804 R at 3000 RMP maximum until the needed concentration was achieved. The final concentration was determined with the Nanodrop™ 2000 Spectrophotometer.

Plasmid DNA

Plasmid DNA in water was provided by the working group of Prof. Dr. Grabbe from the University hospital (Mainz, Germany). Two plasmids (pGL3 and 1699), differing in their molecular weights, were tested at the beginning (data not shown) and 1699 was used for further experiments due to its higher efficiency.

3.2.2 RNase-free working

RNases, which is the abbreviation for ribonucleases, are enzymes which degrade RNA by cleaving the phosphodiester bonds between the nucleotides. These enzymes can be found ubiquitously in and on the human body and serve as a protective barrier against foreign RNA like from bacteria. Therefore, they are considered stable and just small amounts are sufficient to destroy mRNA. Although RNases are essential for the human body, they have to be eliminated for development and manufacturing of RNA-lipoplexes. Therefore, some arrangements have to be taken. It is always necessary to wear gloves and change them after contact with skin or unclean surfaces. As necessary for all parenteral administrations, a bench with laminar air flow and aseptic techniques is needed to avoid contamination of samples. In addition, contact with RNases can be prevented. Chemicals, water and laboratory disposables like tips are available in an RNase-free condition. Glassware needs to be heated up to 300 °C for at least three hours. At least, all surfaces and plastic items which are not available RNase-free can be treated with RNaseZAP (Ambion®, Thermo Scientific™, Darmstadt, Germany) to be decontaminated.

Same procedures have to be done while working with DNA. Although DNA is more stable, degradation via DNases can occur as well.

3.2.3 mRNA integrity

The integrity of mRNA in the formulations after preparation was tested with the commercially available RNA 6000 Nano Kit using the Agilent 2100 Bioanalyzer (Agilent, Santa Clara, USA) lab-on-chip system that is based on a capillary electrophoresis. This system is similar to gel electrophoresis but is more comfortable and less amount of sample is required.

Samples were mixed with an equal amount of formamide buffer (23.8 M formamide, 8.7 mM SDS, 18.0 mM EDTA) before testing. A 1 µl sample corresponding to a mRNA-concentration of 25 to 250 ng/µl was filled into the wells in an appropriate chip. An electrical field is applied and hence, the mRNA moves through the microchannels which are filled with a sieving polymer and a fluorescent dye. Electropherograms were obtained by reaction with a fluorescent dye and translated into gel-like images (bands).

3.2.4 Lipoplex preparation

Lipids were dissolved in chloroform (or ethanol) and the stock solutions were stored in the freezer at - 25 °C. Lipoplexes were produced by two different methods, the lipid film method and the dual asymmetric centrifuge (DAC).

Lipid film method

For the preparation of the lipoplexes, the appropriate amount of lipids were pipettes into a glass tube to obtain a homogenous mixture of lipid. The organic solvent was removed via rotary evaporation with a Büchi® Rotavapor R-3 or via centrifugal evaporation with a Savant® Speed Vac SVC 200. Dried lipid films were stored in the freezer at - 25°C and were thawed before further usage.

Lipid amounts for samples containing DOPC and DOTAP are calculated in mol% (Table 1) while lipid amounts for samples with EPC 80 % and DOTMA or DODMA are stated in mg/ml.

Table 1: Exemplary calculation for liposomes containing 90 mol% DOPC with 10 mol% DOTAP with a total lipid concentration of 100 mg/ml

- $\boldsymbol{DOPC}: \mathbf{0.9\ mol} * \mathbf{786.113}\,\frac{\boldsymbol{g}}{\boldsymbol{mol}} = \mathbf{707.502\ g}$

- $\boldsymbol{DOTAP}: \mathbf{0.1\ mol} * \mathbf{698.542}\,\frac{\boldsymbol{g}}{\boldsymbol{mol}} = \mathbf{69.854\ g}$

- $\mathbf{707.504\ g + 69.854\ g = 777.358\ g}$

- $\boldsymbol{DOPC}: \frac{\mathbf{777.358 g}}{\mathbf{100 mg}} = \frac{\mathbf{707.502 g}}{\boldsymbol{x}} \rightarrow\ \boldsymbol{x} = \mathbf{91.01\ mg}$

- $\boldsymbol{DOTAP}: \frac{\mathbf{777.358 g}}{\mathbf{100 mg}} = \frac{\mathbf{69.854 g}}{\boldsymbol{x}} \rightarrow - \boldsymbol{x} = \mathbf{8.99\ mg}$

For the DOPC/DOTAP-lipoplexes, a 0.27 M trehalose [155] solution containing the mRNA was added to obtain a lipid concentration of 100 mg/ml. For the EPC/DOTMA or EPC/DODMA-lipoplexes, a buffer solution with 10 mM HEPES and 0.1 mM EDTA containing the mRNA was added to obtain a lipid concentration of 100 mg/ml. The suspensions

were vortexed at RT for 10 sec and allowed to stand overnight or at least for 8 h also at RT for full hydration. If the lipid film was not completed hydrated afterwards, further vortexing was applied until the dispersion was homogenous.

Dual Asymmetric Centrifuge

For the preparation of the lipoplexes, the appropriate amount of lipids (calculated in mol%) was pipetted into a sterile Twist top vial. The organic solvent was removed via centrifugal evaporation with a Savant® Speed Vac SVC 200. A small amount of the buffer containing the mRNA or plasmid DNA was added together with an appropriate amount of SiLibeads Type ZY 0.8–1.0 mm for a better mixing. In a Dual Asymmetric Centrifuge SpeedMixer™ DAC 150.1 CM, vials were mixed for 10 min at 3000 RPM. The rest of the buffer was added and the content was mixed again at 3000 RPM for 10 min. If dilution of the sample was necessary, the appropriate amount of buffer was added and the sample was mixed again at 3000 RPM for 30 sec.

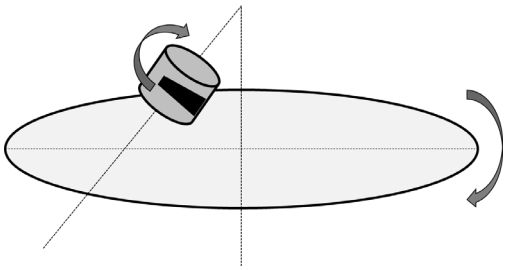

Figure 7: Schematic illustration of a dual asymmetric centrifuge

For calculation of the N/P ratio, the molar mass of the cationic lipid (e.g. DOTAP: 670 g/mol) was used for one cationic charge while the molar mass of one nucleotide (330 g/mol) was assumed for one negative charge. Consequently, the same amount (in mg) of DOTAP and mRNA lead to a N/P ratio of 2/1.

The principle of the DAC is displayed in Fig. 7. The adapter with the vial containing the mixture moves in two different directions. This movement lead to special forces which are responsible for the liposomal formation.

3.2.5 Dynamic light scattering

Dynamic light scattering (DLS), also known as photon correlation spectroscopy (PCS), was used for determination of the size distribution profile of the lipoplexes. For measurement, the particles are dispersed in a fluid, so that the hydrodynamic diameter is determined with this method. The dispersed particles show the Brownian motion. Larger particles move more slowly, while smaller particles move faster (because they are pushed more easily by the water molecules). DLS measures the speed of this motion. When light hits a particle, it gets scattered in all directions. The scattered light of different particles interferes. Due to the Brownian motion, the distance between the particles always changes which lead to fluctuations in the scattering intensity. If this change in fluctuation is observed over a time period, it can give information over the velocity and therefore over the size of the particles. For calculation of the diameter, the Stokes-Einstein equation is used:

$$d_H = \frac{kT}{3\pi\eta D}$$

Equation 1: Stokes-Einstein equation from the diffusion coefficient D used for the size calculation

where d_H is the hydrodynamic diameter, k is the Boltzmann constant, T is the absolute temperature of the system, η is the viscosity of the solution and D is the translational diffusion coefficient. D defines the velocity of the Brownian motion and contains e.g. the temperature. In addition, the speed of the Brownian motion is dependent on the particle size, the viscosity and the temperature. For determination of the particle size, the viscosity and temperature have to be constant.

With the Zetasizer Nano ZS®, the so-called non-invasive backscatter (NIBS) detection can be used. [156] The angle of detection is 173° instead of 90° which avoids multiple scattering and minimises the detection of scattering caused by bigger particles like dust. Furthermore, artefacts due to multiple scattering are prevented.

For measurement of DOPC/DOTAP-lipoplexes, samples were diluted with a 0.27 M trehalose solution to a final lipid concentration of 0.1 mg/ml and measured at 25 °C with a Malvern Zetasizer Nano ZS®.

For measurement of EPC/DOTMA or EPC/DODMA-lipoplexes, samples were diluted with a 5 mM solution of NaCl to a final lipid concentration of 0.1 mg/ml and measured at 25 °C with a Malvern Zetasizer Nano ZS®.

3.2.6 Zeta potential

The electrostatic interactions of particles dispersed in a fluid and ions can be described by the zeta potential, which is illustrated in Fig. 8. A liquid layer around a charged particle occurs and can be divided into two parts. The inner layer is called the Stern layer and includes ions which are strongly bound to the surface of the particle. The outer diffuse layer includes ions which are just associated loosely. The particle appears to be neutral. While moving in the fluid, the Stern layer is moving together with the particle which results in the hydrodynamic diameter. Some ions from the diffuse layer are removed by friction which leads to a potential of the particle. This is named the zeta potential and means the potential on the surface of the hydrated particle, also called the slipping plane.

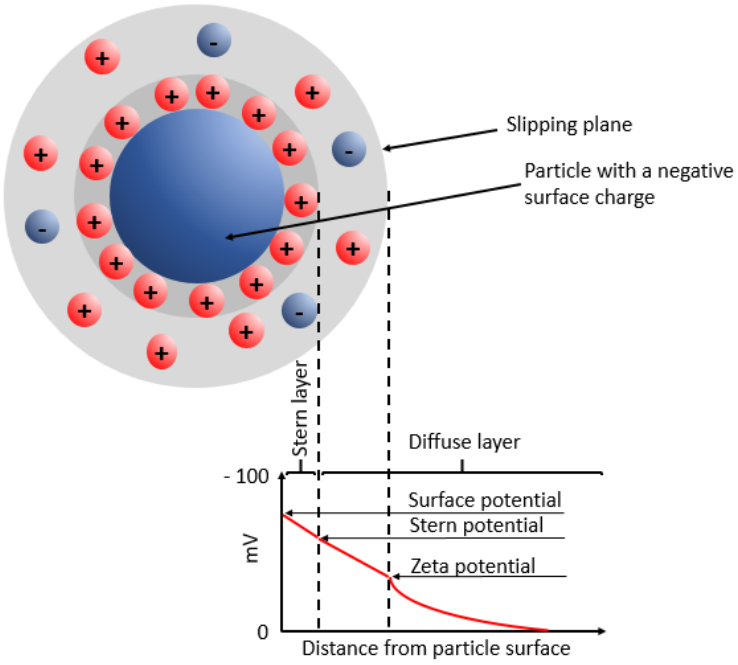

Figure 8: Principle of zeta potential and surface layers

Charged particles have the tendency to move in an electric field, which is called electrophoresis. This phenomenon is used to measure the zeta potential. An electric field is applied and the particles migrate to the oppositely charged electrode. The velocity increases with a higher charge. The electrophoretic mobility can be evaluated by using the Henry equation:

$$U_E = \frac{2\,\varepsilon\,\zeta\,f(k_a)}{3\,\eta}$$

Equation 2: Henry equation for calculation of electrophoretic mobility

where U_E is the electrophoretic mobility, ε the dielectric constant, η the viscosity of the solvent, ζ is the measured zeta potential and f(k_a) the Henry's function, which means the ratio of the radius of the particle to the thickness of the electrical double layer. F(k_a) can be either 1.5 or 1.0. For measuring in polar solutions with moderate electrolyte concentrations, where particles are much larger than the double layer thickness, f(k_a) is set to 1.5. This is called the Smoluchowski approximation. 1.0 is used in non-polar solutions, where particles are smaller than the double layer thickness. This is called the Hückel approximation.

The zeta potential is a good indicator of the stability of a system in a biological environment. Particles may tend to aggregation. If the repulsive forces are stronger than the attractive forces, aggregation is prevented. Repulsive forces can be induced by increasing electrostatic repulsion between the particles. Stable dispersions typically have a zeta potential higher than + 30 mV or lower than - 30 mV. Nevertheless, other factors like the nature of the counter ions or the pH can also have an influence on the interactions between the particles.

For measurement of DOPC/DOTAP-lipoplexes, samples were diluted with a 0.27 M trehalose solution to a final lipid concentration of 0.08 mg/ml and measured at 25 °C with a Malvern Zetasizer Nano ZS® using the Smoluchowski approximation.

For measurement of EPC/DOTMA or EPC/DODMA-lipoplexes, samples were diluted with a 5 mM NaCl solution to a final lipid concentration of 0.125 mg/ml and measured at 25 °C with a Malvern Zetasizer Nano ZS® using the Smoluchowski approximation.

3.2.7 Differential scanning calorimetry

DSC is a thermal analysis technique to determine the heat capacity of a material (Fig. 9). As a function of time, the differences in the amount of heat to increase the temperature of a sample in comparison to a reference of equal mass is measured. Differences in the amount of heat result from either endothermic or exothermic processes such as melting, curing, glass transition or phase changes. Changes in the heat flow relate to changes in the heat capacity of a sample.

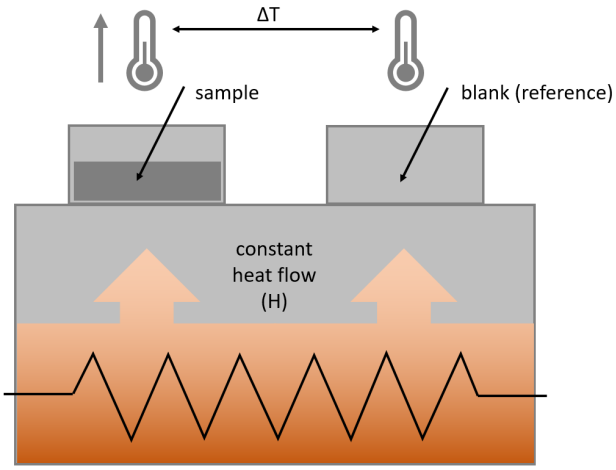

Figure 9: Active principle of differential scanning calorimetry

A characteristic parameter for lipids is the phase transition temperature (T_m). At this point, lipids change from an ordered gel state, with fully extended and closely packed hydrocarbon chains, to the disordered liquid crystalline phase, where the hydrocarbon chains are fluid and orientated in a random manner (Fig. 10). For example, DOPC has a T_m around - 20 °C so that liposomal membranes which are mainly composed of DOPC are always in the liquid crystalline phase when handling at RT. Despite, the determination of the phase transition with DSC can be used for evaluation of the stability of model membranes like liposomes. The higher the T_m of a liposomal membrane is, the more energy is necessary to destabilise the system. The input of higher energy level characterises a more stable membrane system. DSC can also be used easily for comparison of various lipid compositions. Furthermore, the influence of added mRNA can be investigated. Due to changes in the structural arrangement of the lipid membrane, an altered T_m is plausible. [157]

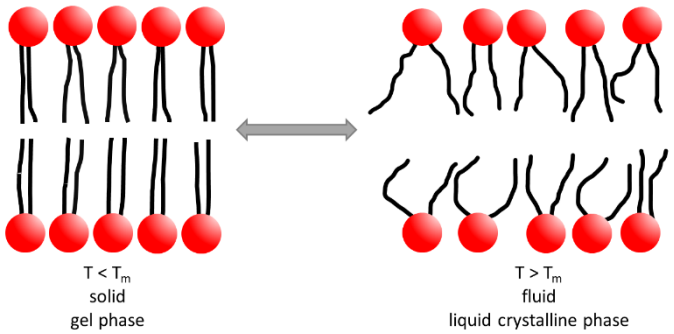

Figure 10: Lipid transition between solid and fluid phase at the phase transition temperature T_m

For determination of the phase transition temperature, 20 µl of each formulation was filled into an aluminium crucible (Mettler-Toledo, aluminium crucible standard, 40 µl, with pin and lid), hermetically sealed and measured together with a trehalose sample as a reference since all samples were measured in presence of trehalose. The samples were cooled to - 40 °C with liquid nitrogen and subsequently heated up to 20 °C. The cooling rate was 2 °C/min while the heating rate was set to 1 °C/min. Reaching - 40 °C the temperature was held constant for 5 min. The temperature program was repeated once.

3.2.8 RiboGreen Assay

Determination of free mRNA

The amount of mRNA which is encapsulated in the lipoplexes was determined by measurement of the amount of mRNA which is not bound to the lipoplexes. This was carried out with the commercially available Quant-iT™ RiboGreen® RNA Assay. [145]After dilution of the samples, fluorescent dye was added and fluorescence intensity was detected with TECAN infinite F200. In total, samples were diluted 1:16000 with TE-buffer for measurement (1:8 before the RiboGreen® RNA Assay, 1:2000 while performing the assay) to a final mRNA concentration between 20 ng/µl and 1 µg/ml. The used wavelengths were 465 nm for excitation and 535 nm for emission. Samples were measured in 96-well clear bottom plates from below and the gain was adjusted to 130 for comparison of different measurements. The amount of free mRNA was subtracted from the total amount of mRNA to obtain the encapsulated or bound amount of mRNA.

Release of mRNA from lipoplexes

For measuring the release of mRNA after mimicking cellular contact, Quant-iT™ RiboGreen® RNA Assay was used again. To mimic the cellular contact, samples were mixed 1:4 with a buffer of pH 7.5 or 5 and an appropriate amount of heparin or liposomes composed of DOPG (5-fold excess of negative to positive charge). Samples were treated as described above and the amount of free mRNA was determined at several time points (5, 10, 20, 40, 60 min) after mixing. For each time point, a fresh aliquot was used.

3.2.9 Cryo-Transmission electron microscopy

The tested lipoplex was composed of 95 mol% DOPC, 5 mol% DOTAP and 10 mol% mRNA (with regard to the total lipid concentration) in 0.27 M trehalose and prepared with the lipid film method as described above with a lipid concentration of 10 mg/ml.

First, the carbon coatings of the copper grid Quantifoil R1.2/R1.3 were treated with a plasma cleaner to become hydrophilic. Under controlled humidity, 50 µl of the diluted sample with a 0.5 mg/ml lipid concentration were transferred to the copper grids. For sample preparation, a modified version of the Cryoplunge Gatan CP3 was used. Excess sample were blotted by a filter paper for 1 sec. The copper grid with the sample dropped into liquid ethane for rapid cooling and was then transferred into liquid nitrogen. By constant cooling, the sample was transferred and measured in the transmission electron microscope TECNAI 12 in the Institute of Zoology at the Johannes Gutenberg-University Mainz.

3.2.10 Transfection efficiency

Transfection efficiency of mRNA lipoplexes

C2C12 myoblast cells were cultured in Dulbecco's modified Eagle's medium (DMEM) supplemented with 10 % fetal bovine serum (not inactivated) at 37 °C in an atmosphere with 5 % CO_2. Cells were seeded in 96-well plates with a density of 5×10^3 cells per well for both luciferase and XTT assay. After 24 h, the cells were washed with phosphate-buffered saline (PBS) and the appropriate amount of diluted lipoplexes containing 1 µg of luciferase-encoded mRNA in Opti-Mem™ medium was added to each well. Cells were incubated for 6 h and the culture media was replaced with fresh culture medium afterwards. The culture media were removed after 24 h and cells were washed with 0.5 ml of PBS. 0.05 ml of PBS and reporter lysis buffer were then added to each well to lyse the cells. Additionally, the viability (which means the 24 h survival of the cells) was tested with XTT Cell Proliferation Kit II. Readout was done after 2 h. All measurements were performed with a TECAN infinite P200 PRO. The wavelengths for measurement were set to 450 and 630 nm. Untreated cells were used as positive control, so that viability was calculated using the following equation:

$$Cell\ viability = \frac{(treated\ cells - blank)}{(untreated\ cells - blank)} * 100\%$$

Equation 3: Calculation of cell viability

Transfection efficiency of DNA-lipoplexes

HEKs or DC2.4 were harvested with PBS supplemented with 2 mM EDTA when they have been 80 % confluent. Cells were washed with medium, centrifuged (8 min at RT with 300 g) and resuspended in 5 ml culture medium. Cells were counted and seeded at a density of $2x10^5$ cells/ml 24 h before the transfection (500 µl in 24-well plates correspond to 10^5). The following day, the serum-containing medium was removed, cells were washed twice with 200 µl PBS and transferred to 500 µl serum-free transfection medium (EMEM). The liposomes/lipoplexes were diluted 1:20 with serum-free transfection medium and the appropriate amount of lipoplex containing 1 µg DNA was added to each well. All samples were done in triplicates. Same DNA transfected with jetPEI® (commercially available transfection reagent composed of a linear polyethylenimine derivate) was used as positive control. The cells and cells transfected with DNA without transfection reagent were used as negative control. The serum-free medium was removed after 6 h of transfection and replaced with 1 ml of culture medium. Incubation was done for 48 h at 37 °C (under 5 % CO_2 for HEK cells, under 10 % CO_2 for DC2.4). After incubation, the medium was removed completely, and the cells were lysed with 100 µl of passive lysis buffer (Promega, Mannheim) for 10 to 15 min at RT. Lysates were stored at - 20 °C until measurement. For measurement, 20 µl of the lysate were transferred to a 96-well LUMITRAC plate and measured at the microtiter plate luminometer. The advice ads 100 µl of Firefly substrate to each sample and measures the luminescence for 10 sec after a delay of 3 sec. The Firefly substrate contains the protein luciferin, ATP and magnesium and can produce a greenish yellow light (550 to 570 nm) in the presence of oxygen.

The medium for DC2.4 cells is composed of Iscove's Modified Dulbecco's Medium (IMDM) with 5 % of fetal calf serum (FCS), 2 mM of glutamine, 100 U/ml Penicillin, 100 µg/ml Streptomycin and 50 µM ß-Mercaptoethanol.

The medium for HEK cells is composed of Dulbecco's Modified Eagle Medium (DMEM) with 10 % of FCS, 100 U/ml Penicillin and 100 µg/ml Streptomycin.

DC-TC-Coculture with transfected DC2.4 with DNA-lipoplexes

DC2.4 cells were harvested, washed and counted. 24 h before the transfection, cells were seeded in a 96-well flat bottom plate at a cell density of $5x10^5$ cells/ml (100 µl/well). At the transfection day, the serum-containing medium was removed, cells were washed with PBS twice and 100 µl of serum-free transfection medium was added. Autoproliferation of DC2.4

was inhibited by addition of 0.5 mg/ml puromycine 45 min prior to transfection. After excessive washing of the cells, liposomes/lipoplexes were diluted 1 to 10 with serum-free medium. Triplicates were done for 100 ng, 200 ng, 300 ng and 400 ng DNA/well and transfected for 48 h.

Following samples were transfected:

1. Liposome/Lipoplex (pCMV_sOVA)
2. Liposome/Lipoplex (pEF_IKK2_wt)
3. Liposome/Lipoplex (pCMV_sOVA + pEF_IKK2_wt)
4. Liposome/Lipoplex (pCMV_sOVA) + LPS
5. OVA-Protein + Liposome/Lipoplex (pEF_IKK2_wt)
6. Liposome/Lipoplex (Control plasmid)
7. Liposome/Lipoplex (Control plasmid) + LPS

For sample 5, DC2.4 cells were first loaded with soluble ovalbumin (OVA)-protein and transfected the following day. Lipopolysaccharide (LPS) was added after 48 h of incubation and was left there for 16 h. Cells, cells with LPS, cells with OVA, cells with OVA and LPS and T-cells were used as controls. 6 h after transfection, the transfection medium was replaced by culture medium.

T-cells were isolated out of spleens of OT-I and OT-II mice by using a nylon wool column. Spleens were taken out, ground, the erythrocytes were lysed, and the cells were given on to an equilibrated nylon wool column. After incubation at 37 °C for 45 min, the bigger spleen cells adhered while the smaller T-cells could be eluted (drop speed: 1 drop/sec). T-cells were collected, washed, counted and adjusted to $5x10^5$ cells/ml. 100 µl of OT-I or OT-II T-cells were added to each well of DC2.4. After incubation or 72 h, the plates were pulsed radioactively to relate to the proliferation of the T-cells. 0.75 µCi ^{3}H-marked thymidine (corresponds to 27750 Bq) was added to each well and the plates were incubated for 18 h. Afterwards, the plates were harvested and measured in the ß-counter.

3.2.11 Small-angle scattering

Small-angle scattering is a scattering technique where the coherent and elastic scattering of collimated radiation after interaction with sample structures is detected at very low angles (0.01 to 30 Å). The applied wavelengths are much smaller than the detectable structures. With these techniques, information on size, shape and orientation of particles and even their inner structures can be obtained.

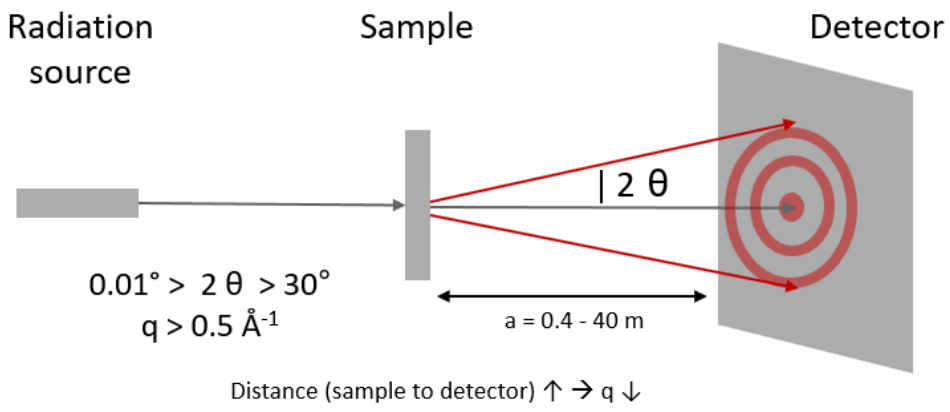

Figure 11: Principal experiment setup of SAS

SAS can be divided into SAXS using X-ray and SANS using neutrons. For both, radiation needs to be parallel (collimated) and the used slit defines the shape of the beam (e.g. square or circle). Furthermore, the measured size range can be adjusted by wavelength and distance (a) between the sample and the detector. The principle setup for both methods is comparable as shown in Fig. 11. The difference in the scattering of a macromolecular specimen to a solvent of low molecular mass is estimated. As a result, the particle scattering (SLD) correspond to the excess scattering length density with respect to the solvent. With SAXS, an equivalent technique exists in the anomalous scattering (ASXAS), but it depends on heavy elements so that it is not applicable for the mRNA-lipoplexes in this thesis. [158]

The SLD is an often-used parameter to describe the strength of the interaction between the neutron and the nucleus (SANS) or the X-ray and the atomic shell (SAXS). SAXS interacts with electrons in the atomic shells, thus the scattering power (cross section) of atoms for X-ray photons increase with the atom number z. For neutrons (SANS), the cross section is different for each isotope. In contrast to X-ray photons, neutrons of SANS interact with the atomic nucleus in an isotope dependent way. Thus, scattering depends on the isotope and

magnetic fields as well. For SAXS experiments, the SLD consequently correlates with the number of electrons and thereby also with the atomic number z. In case of SANS, the SLD correlates with the proton concentration. Comparing the intensity of both SAS methods, the probability for scattering is around 1000 times higher for neutrons by contrast with X-rays. However, the intensity for SANS measurements is lower because high flux reactor as a radiation source are much weaker compared to synchrotrons.

By nuclear interaction phase, hydrogen has a negative SLD, while deuterium (a hydrogen isotope with one neutron more in the core) has a strongly positive one. Consequently, the neutron scattering of one system can be varied by hydrogen-deuterium contrast variation, so that different structural parts can be investigated. Each material has a characteristic neutron SLD and since H_2O and D_2O represent the outer limits of the range of SLDs, every possible SLD of a bio-system can be mimicked by a mixture of H_2O/D_2O. As illustrated further down (Fig. 13), the point of mimicking a systems SLD so that it gets invisible for detection is called the contrast matching point. [159]

Lipoplexes are considered to be (partially) ordered and centre-symmetric. Such systems show characteristic Bragg peaks caused by Bragg diffraction. [160] Two beams with identical wavelength and phase are scattered off two different atoms with distance d. This so-called constructive interference occurs when the path difference is equal to an integer multiple of the radiation wavelength.

Using the Bragg peaks, d-spacing can be calculated as another indicative parameter with the following equations:

$$d = \frac{n\,2\,\pi}{q_{\max(n)}}$$

Equation 4: Calculation of d-spacing

$$q = \frac{4\,\pi}{\lambda} * \sin\theta$$

Equation 5: Calculation of the scattering vector (momentum transfer)

with q as the momentum transfer, the reflex order n and the peak position q_{max} of the Bragg peak, the wavelength λ and the angle θ.

The scattering vector describes the difference in the incident wave k_0 and the expiring wave k_S and characterise the momentum transfer from the particle to the wave (Fig. 12).

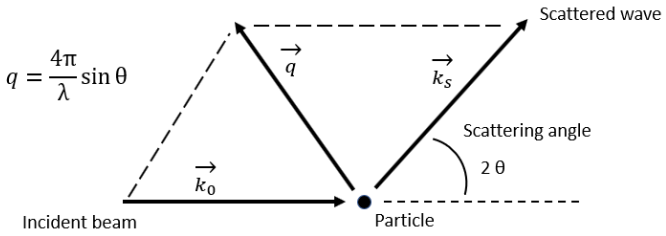

Figure 12: Scattering vector q

For evaluation of the exact peak position and for further analysis of the scattering curves, the Lorentz function can be applied and gives information about peak area and the peak width at half-height (FWHM):

$$y = y_0 + \frac{2\,A}{\pi} \frac{\omega}{4\,(x - x_c)^2 + \omega^2}$$

Equation 6: Lorentz function for peak analysis

with y_0 as the offset, x_c as the peak centre, ω as the FWHM and A as the peak area.

Small-angle X-ray scattering

The SAXS experiments were carried out at different facilities (Table 2).

Table 2: Overview of the performed SAXS experiments

Facility [Beamline]	**ESRF Grenoble [ID02], France / Synchrotron**
Set up	**Source:** U21.4 and U35 undulator **Monochromator:** cryogenic (liquid nitrogen) cooled Si-111 channel-cut, focusing toroidal mirror **Detector:** Rayonix MX-170HS **Beam size (vert. x hor.):** 200 μm x 400 μm **Divergence (vert. x hor.):** 20 μrad x 40 μrad **Wavelength range:** 0.1 nm (0.073 nm – 0.16 nm) **Energy range:** 12.4 keV **Energy resolution:** 1/100 $\Delta\lambda/\lambda$ **Flux at sample position:** $10^{14\ \text{photons/sec}}/_{100\ \text{mA}}$
Conditions	**Samples:** EPC 80 % with DOTMA or DODMA and mRNA **Buffers:** phosphate buffer with two different pH values (7.5/5) and hepes **Concentration for measurement (lipid):** 25 mg/ml **q-range:** 0.005916 – 0.645377 $Å^{-1}$ **Temperature:** RT
Performed experiments	Structural investigation of mRNA-lipoplexes in dependence of the pH
Data analysis	1. Raw data conversion with the instrument software 2. Data analysis with Origin 7.5 (Plotting of pure scattering curve + Lorentz fit for peak properties)
Facility [Beamline]	**BESSY II (HZB) Berlin [mySpot], Germany / Synchrotron** [161]
Set up	**Source:** 7T-WLS-1 (Wavelength Shifter) **Monochromator:** Multiple Crystal (Si 111, Si 311) and Multilayer mirror (B4C/Mo, 2nm period) **Flux:** $1e^{12}$-$1e^{13}$ **Detector:** Mar X-ray CCD **Energy range:** 4 – 30 keV **Energy resolution:** 1/8000 – 1/500 $\Delta\lambda/\lambda$ **Polarisation:** horizontal **Divergence horizontal/vertical:** 1 mrad

	Focus size (hor. x vert.): 400 x 400, 400 x 50 µm
Conditions	**Samples:** EPC 80 % with DOTMA or DODMA and mRNA **Buffer:** phosphate buffer with eight different pH values (8.0/7.5/7.0/6.5/6.0/5.5/5.0/4.5) **Concentration for measurement (lipid):** 25 mg/ml **q-range:** 0.000185 – 1.136304 $Å^{-1}$ **Temperature**: RT
Performed experiments	Structural investigation of mRNA-lipoplexes in dependency of the pH
Data analysis	1. Raw data conversion with Fit 2 D 2. Data analysis with Origin 7.5 (Plotting of pure scattering curve + Lorentz fit for peak properties)
Facility [Beamline]	**EMBL (DESY) Hamburg [P12], German / Synchrotron** [162]
Set up	**Source:** Petra U29 undulator **Monochromator:** Double crystal Si (111) **Energy range:** 10 keV (4 – 20 keV) **Wavelength range:** 0.6 – 3 Å **Flux:** 5 x 10^{12} ph/s **Beam size at sample:** 0.2 x 0.3 mm^2 (FWHM) **Slits:** Individually motorised blades of Hybrid Scatterless in a module from Xenocs **Focal spot:** 0.2 x 1.2 mm **Detector:** Pilatus 2M pixel detector (253 x 288 mm^2) **Sample - detector distance:** 1.6 – 6.1 m **Particle size range:** 1000 Å – 8 Å **Energy resolution:** 1/1000 $\Delta\lambda/\lambda$ **Sample changer:** EMBL/ESRF new generation
Conditions	**Samples:** DOPC with DOTMA or DODMA and mRNA / DOPC with DOTAP and mRNA **Buffer:** phosphate buffer with eight different pH values (8.0/7.5/7.0/6.5/6.0/5.5/5.0/4.5) / trehalose solution **Concentration for measurement (lipid):** 12.5 or 25 mg/ml **q-range:** 0.002732 – 0.507534 $Å^{-1}$ **Temperature:** RT **Sample - detector distance:** 3.0 m
Performed experiments	Structural investigation of mRNA-lipoplexes in dependency of the pH Preliminary experiments for LNLS (data not shown)
Data analysis	1. Raw data conversion with the instrument software

	2. Data analysis with Origin 7.5 (Plotting of pure scattering curve + Lorentz fit for peak properties)
Facility [Beamline]	**LNLS (CNPEM) Campinas [SAXS1], Brazil / Synchrotron**
Set up	**Source:** Bending Magnet D01 exit B (15°) **Monochromator:** W/B4C Multilayer (500 double layers) on Si substrate **Detector:** Pilatus 300K **Energy range:** 8 keV **Energy resolution:** 1/10 $\Delta\lambda/\lambda$ **Beam size at sample:** 1.5 mm^2 x 1 FWHM **Flux density at sample:** 10^{10} – 10^{12} (ph/s)/mm^2 **Particle size range:** 1 – 100 nm
Conditions	**Samples:** EPC 80 % with DOTMA or DODMA and mRNA / DOPC with DOTAP and mRNA **Buffer:** phosphate buffer with two different pH values (7.5/5) with heparin/ D_2O and H_2O with trehalose **Concentration for measurement (lipid):** 12.5 mg/ml **q-range:** 0.012978 – 0.470028 $Å^{-1}$ **Temperature:** RT
Performed experiments	Time-dependent structural changes of lipoplexes by mimicking cell contact Comparison of structure after mixing with D_2O and H_2O and different trehalose concentration
Data analysis	1. Raw data conversion with the instrument software 2. Data analysis with Origin 7.5 (Plotting of pure scattering curve + Lorentz fit for peak properties)

A wide range of pH was measured within these experiments. To ensure that the salt composition was always nearly the same, Sörensen phosphate buffer was used. With different ratios between two salts, buffers with a pH range of 4.9 to 8.0 can be prepared.

First, solution A was prepared with potassium dihydrogen phosphate (9.078 g/1000 ml) and solution B with disodium hydrogen phosphate-dihydrate (11.876 g/1000 ml) in RNase-free water. To achieve the appropriate pH, the number of ml in Table 3 is taken from solution B and filled up to 100 ml with solution A.

Table 3: Preparation of Sörenson phosphate buffer (required amounts of solution B for 100 ml)

pH	.0	.1	.2	.3	.4	.5	.6	.7	.8	.9
4										0.60
5	0.95	1.35	1.80	2.30	3.00	3.90	4.90	6.20	7.90	9.80
6	12.1	15.0	18.4	22.1	26.4	31.3	37.2	43.0	49.2	55.2
7	61.2	67.0	72.6	77.7	81.8	85.2	88.5	91.2	93.6	95.3
8	96.9									

For pH 4.5, a buffer with just potassium dihydrogen phosphate (6.8 g/1000 ml) was utilised.

The experiments at the **ESRF** and **BESSY** synchrotron sources were performed to investigate the structural differences between lipoplexes with a cationic (DOTMA) and ionizable (DODMA) lipid at different pH. Lipoplexes composed of EPC 80 % and different proportions of DOTMA or DODMA and mRNA were prepared with the lipid film method as described above. For these measurements, lipoplexes were diluted 1 to 4 with buffer to a final lipid concentration of 25 mg/ml and measured afterwards (no accurate time). One of the buffers was used to subtract the background although in some cases, background was not subtracted with 100 %.

The experiments at the **EMBL** synchrotron source were carried out to repeat the experiments performed at BESSY with DOPC instead of EPC 80 %. Lipoplexes composed of DOPC and different proportions of DODMA with and without mRNA were prepared with the lipid film method as described above. As reference, one formulation with DOTMA was used. For these measurements, lipoplexes were diluted 1 to 8 with buffer to a final lipid concentration of 12.5 mg/ml and measured afterwards (no accurate time). For all samples, the appropriate buffers were measured to subtract the background although in some cases, background was not subtracted with 100 %.

The experiments at the **LNLS** synchrotron source were performed to investigate time dependence of the structural changes between lipoplexes with a cationic (DOTMA) or ionizable (DODMA) lipid at different pH after mimicking cell contact. Lipoplexes composed of EPC 80 % and different proportions of DOTMA or DODMA and mRNA were prepared with the lipid film method as described above. Samples were diluted with a mixture of buffer

and an appropriate amount of heparin to a final lipid concentration of 12.67 mg/ml and measured immediately after mixing and 2.5, 5, 10, 20 min and for some samples also at 40 min. For each sample and time point, a separate solution was prepared. (Preliminary experiments with the same lipoplexes were performed at the **EMBL** synchrotron source. Due to a sample holder instead of a flow-through cell as used for all other measurements, each sample was measured at different time points after mixing. Data is not evaluable and hence, not shown here.) In addition to SANS experiments at **FRM II** facility, two DOPC/DOTAP-lipoplexes with low and high amount of mRNA were measured to investigate the effect of dilution with high concentrated trehalose solutions on the membrane spacing. Lipoplexes were prepared with lipid film method as described above. Both samples were diluted with H_2O and D_2O containing a low and a high concentration of trehalose. For all samples, the appropriate buffers were measured to subtract the background although in some cases, background was not subtracted with 100 %.

Small-angle neutron scattering

As named above, the scattering effect which is dependent on the isotope is used for this measurement technique. Hydrogen has a negative SLD, while deuterium has a strongly positive one. The scattering of one system can be varied by contrast variation, so that different structural parts can be investigated. [163] Each material has a characteristic neutron SLD and since H_2O and D_2O represent both outer limits of the range of SLDs. Every possible SLD can be mimicked by a mixture of H_2O/D_2O as solvent. The point of mimicking a systems SLD so that it gets invisible for detection is called the matching point. The principle of contrast variation is illustrated in Fig. 13, together with neutron SLDs for typical macromolecules. The SLD for RNA, proteins and water changes due to exchangeable protons of the molecules [159]. Another way of varying the SLD is the deuteration of the sample e.g. by using deuterated lipids. This method was not used within this thesis. Since the lipoplexes were prepared with a very high concentration, the required amount of lipid would be very high.

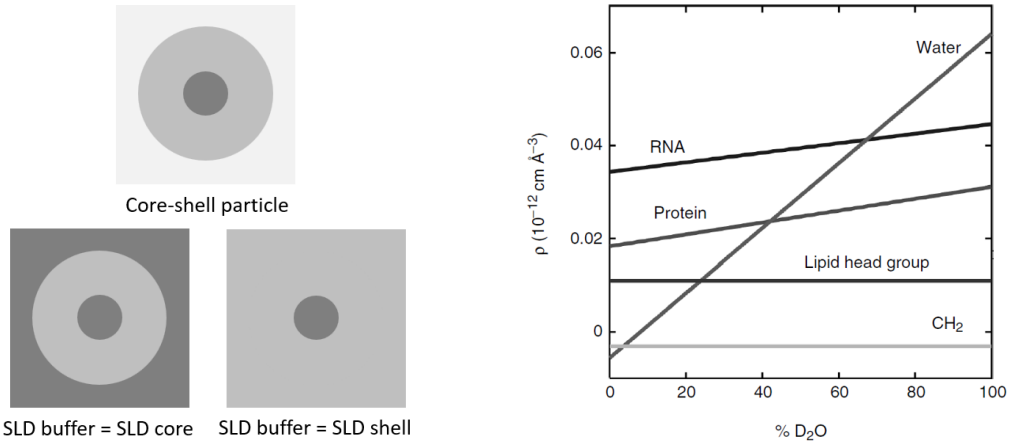

Figure 13: Principle of contrast variation [left] and average SLD for typical macromolecules (taken from [159]) [right]

The Guinier plot gives information on the gyration radius and is suitable for analysis of SAXS and SANS data. When evaluating SANS data, the Kratky-Porod plot can be used to determine the membrane span. This plot is not commonly used for SAXS since the contrast of liposomes in H_2O is really low for X-rays.

$$\ln(I(g) = \ln(I_0) - \frac{R\,g^2}{3} * q^2 \qquad \ln\left(I_d(q)\right) = \ln(I_{d0}) - {R_d}^2 * q^2$$

Equation 7: Logarithmic plot for Guinier [left] and Kratky-Porod [right] function

$$d = R_d * \sqrt{12}$$

Equation 8: Membrane thickness

with R_d as the thickness radius obtained from the logarithmic evaluation of the thickness profile $I_d(q)$ which is determined from the middle part of the scattering profile I(q) which is multiplicated by the thickness factor q^2. [164]

The SANS experiments were carried out at two different facilities (Table 4).

Table 4: Overview of the performed SANS experiments

Facility [Beamline]	**FRM II (JCNS) Garching [KWS-2], Germany / High flux reactor**
Set up	**Neutron flux:** 2.5 x 10^7 N/(cm^2 sec) **Beam cross section:** 8 x 10 mm **Wavelength range:** 0.4533 nm (0.4 – 1.5 nm) **Detector:** ^{6}Li (60 x 60 cm^2) **Detector distance:** 2, 4, 8, 14 and 20 m **Energy range:** 10 or 20 % ($\Delta\lambda/\lambda$)
Conditions	**Samples:** DOPC with DOTAP and mRNA **Buffer:** mixture of H_2O- and D_2O-buffers for eight different D_2O contents (0, 11.11, 16.16, 22.22, 33.33, 44.44, 55.56, 66.67, 77.78 %) containing 1.31 M trehalose **Concentration for measurement (lipid):** 10 mg/ml **q-range:** 0.00309 – 0.47395 $Å^{-1}$ **Temperature:** RT **Detector distance:** 2, 8 and 20 m
Performed experiments	Detailed structural investigation of mRNA-lipoplexes for proof of structural model
Data analysis	1. Raw data conversion with the instrument software 2. Data analysis with Origin 7.5 (e.g. Guinier plot)
Facility [Beamline]	**NIST Delaware [nSoft], USA / Medium flux reactor**
Set up	**Source:** Neutron Guide (NG-B) **Beam cross section:** 60 x 60 mm **Monochromator:** Mechanical velocity selector with variable speed and pitch **Particle size range:** 1 – 200 nm **Wavelength range:** 4 – 20 Å **Detector:** ^{3}He position-sensitive proportional counter (640 x 640 mm) with a 5.08 x 5.08 mm resolution **Source – sample distance:** 1 – 3 m **Sample – detector distance:** 1.3 – 5.2 m **Energy resolution:** 9 – 30 % ($\Delta\lambda/\lambda$) (FWHM)
Conditions	**Samples:** DOPC with DOTAP and mRNA, pure DOPC **Buffer:** mixture of H_2O- and D_2O-buffers for three different D_2O contents (77.78, 85, 90 %) containing 0.27 or 1.31 M trehalose **Concentration for measurement (lipid):** 10 mg/ml or 100 mg/ml

	q-range: 0.006 – 0.5 $Å^{-1}$ **Temperature:** RT **Detector distance:** 10 m
Performed experiments	Detailed structural investigation of mRNA-lipoplexes and the osmotic effect of Trehalose
Data analysis	1. Raw data conversion with the instrument software 2. Data analysis performed by the instrument's scientists

SANS experiments at the **FRM II** facility were carried out to get a further insight into the molecular structure of the DOPC/DOTAP-lipoplexes. The KWS-2 instrument of the Jülich centre of neutron scattering (JCNS) at the FRM II high flux reactor of the Maier-Leibnitz research centre (MLZ) at Garching was used. Lipoplexes were prepared with lipid film method as described above and were composed of DOPC and DOTAP and two different proportions of mRNA. Previous experiments (data not shown) pointed out, that dilution in the cuvettes with 0.27 M trehalose solution led to strong aggregation and sedimentation so that measurements could not be performed. Therefore, samples were diluted with 1.31 M trehalose solution to a final lipid concentration of 10 mg/ml. Buffers for contrast variation were composed of either H_2O or D_2O containing 20 m/g glucose, 2.38 mg/g HEPES and 9 mg/g NaCl and different proportions of D_2O (0, 11.11, 16.16, 22.22, 33.33, 44.44, 55.56, 66.67 and 77.78 %). For 0 to 22.22 % of D_2O, cuvettes with a thickness of 1 mm and a sample volume of 200 µl and for all others 2 mm cuvettes with a volume of 400 µl were used. Measurements were carried out at three different sample-detector distances, whereas measurement time needed to be adjusted to the distance (Table 5). For each sample, the appropriate buffers were measured under similar conditions to subtract the background. Transmission of samples was measured in addition and used to calculate the real D_2O content. The content of D_2O (%) differed from the calculated content because of the high proportion of trehalose which changed the number of hydrogen atoms as well as the density of the buffer.

Table 5: Measurement schedule of experiments performed at FRM II – KWS-2 (in min/sample) showing the measured time in min

Sample / D_2O [%]	20 m Sample	20 m Buffer	8 m Sample	8 m Buffer	2 m Sample	2 m Buffer	Transmission
0	30	50	20	30	10	10	1
11.11	50	50	20	30	10	10	1
16.16	50	50	20	30	10	10	1
22.22	50	50	20	20	10	10	1
33.33	-	-	20	30	10	10	1
44.44	-	-	10	15	5	5	1
55.56	30	30	10	15	5	5	1
66.67	20	20	10	15	5	5	1
77.78	20	20	10	15	5	5	1

Experiments at the **NIST** facility were carried out to extend the data from the experiments at FRM II and to investigate the osmotic effect of high concentrations of trehalose on the lipid membrane. Samples were shipped to Delaware by flight. Lipoplexes were prepared with lipid film method as described earlier and composed of DOPC with two different amounts of DOTAP and the same amount of mRNA. Further on, pure DOPC was used as a reference system. All three samples were measured pure with the final concentration of 100 mg/ml and diluted to 10 mg/ml with different buffers. Buffers were composed as buffers used at FRM II, but with higher proportions of D_2O (77.77 %, 85 %, 90 %) and either 0.27 M or 1.31 M trehalose. All buffers were measured to subtract the background.

3.2.12 Determination of pK_a

For further characterisation of ionizable lipids, TNS assay is applied to determine the apparent pK_a of each formulation. With this assay, the pK_a can be measured *in situ* while the lipid is incorporated into the lipid membrane of the formulation. Therefore, influences on the amine group by neighbouring lipids or the membrane itself are considered. The negatively charged fluorescent dye is only attracted to the ionizable lipid when the ionizable lipid is charged. With a subsequent adsorption to the membrane, the TNS gets more lipophilic which leads to a removal of the water molecules that otherwise quench the fluorescence [147]. By lowering the

pH, the positive charge increases and so does the fluorescence. A 100 % fluorescence is assumed when the ionizable lipids are completely ionised. Nevertheless, the TNS concentration used in the assay is much lower in comparison with the amount of the ionizable lipid. Hence, it is assumed that a small fraction of ionised lipid is enough for the determination [149]. By using curve-fit analysis (Boltzmann equation), the apparent pk_a can be determined at the point, where 50 % of the lipid is charged.

Lipoplexes composed of EPC 80 % or DOPC and DOTMA or DODMA were prepared with the lipid film method as described earlier. Same compositions were tested with or without mRNA. Pure lipids were measured as a reference. Different buffers were used to obtain a pH range from 3 to 10 (10 mM citrate: 3, 4, 5, 6; 10 mM phosphate: 6, 7, 8; 10 mM borate: 9, 10). For some of the experiments, buffers contained 150 mM NaCl. 90 µl of each buffer and 2 µl of a 300 µM stock solution of TNS in DMSO were added to a 96-well plate. Lipoplexes were diluted with water to a final concentration of 22 µM (either total lipid or cationic lipid concentration) and 10 µl of this dilution was added as well. The fluorescence was measured using the TECAN infinite F200 with 360 nm as excitation wavelength and 430 nm as wavelength for emission. The signal was normalised to either pH 3 or 4 and plotted against the pH.

The experiments were carried out under different conditions as explained in chapter 4.2.2.

3.2.13 Overview of tested formulations

In Tables 6 to 13, all tested samples with the implemented experiments are listed.

Table 6: Tested systems with EPC 80 % as matrix lipid and different proportions (mol%) of DOTAP and mRNA with the resulting N/P ratios (+/-) (taken from [150])

mRNA	**0**		**5**		**10**	
DOTAP						
0	0	*	0	*	0	*
5	0	*	1/1	*	1/2	*
10	0	*	2/1	*	1/1	*

Table 7: Tested systems with DOPC as matrix lipid and different proportions (mol%) of DOTAP and mRNA with the resulting N/P ratios (+/-) (taken from [150])

mRNA	0		2.5		5		10		20	
DOTAP										
0	0	* # $	0	*	0	* #	0	*	0	* °
1	0	#			1/5	#				
2	0	#			1/2.5	#				
2.5	0	*	1/1	*	1/2	* #	1/4	*	1/8	* + x
3	0	#			1/1.67	#				
4	0	#			1/1.25	#				
5	0	* #	2/1	* § /	1/1	* # $	1/2	* § &/	1/4	* + x
7.5									1/3	+ x
10	0	* #	4/1	*	2/1	* # $	1/1	*	1/2	* + x °
11.4									1/1.75	+ x
13									1/1.5	+ x
15									1/1.33	+ x
16									1/1.25	+ x
17.4									1/1.12	+ x
20									1/1	+ x °
25									1.25/1	+ x
30									1.5/1	+ x °
35									1.75/1	+ x
40									2/1	+ x °
45									2.25/1	+ x
50									2.5/1	+ x °

Table 8: Implemented measurements for samples listed in Tables 5 and 6

+	Zeta potential
x	Free mRNA
#	DSC
°	Transfection efficiency
*	SAXS – Mainz University
/	SAXS – EMBL (Hamburg)
&	SAXS – LNLS (Campinas)
§	SANS – FRM II (Garching)
$	SANS – NIST (Delaware)

Table 9: Tested systems with EPC 80 % as matrix lipid and different proportions (mg/ml) of DOTMA or DODMA and mRNA with the resulting N/P ratios (+/-)

mRNA	**0**		**2.5**		**5**		**10**	
cat. lipid								
DOTMA								
0	0	*			0	*	0	*
2.5	0	°			1/4	& °		
5	0	* °			1/2	* & °	1/4	*
10	0	*	2/1	& x	1/1	* +&°	1/2	*
20	0	°			2/1	°		
50	0	°						
DODMA								
0	0	* °			0	*	0	*
2.5	0	°			1/4	& °		
5	0	* °			1/2	* & °	1/4	* +
10	0	* °	2/1	& x	1/1	* +&°	1/2	* +
20	0	°			2/1	°		
50	0	°			5/1	°		

Table 10: Tested systems with DOPC as matrix lipid and different proportions (mg/ml) of DOTMA or DODMA and mRNA with the resulting N/P ratios (+/-)

mRNA	0	2.5	5	10
cat. lipid				
DOTMA				
10			1/1 / °	
DODMA				
10			1/1 / °	
20			2/1 / °	

Table 11: Implemented measurements for samples listed in Tables 8 and 9

*	SAXS – ESRF (Grenoble)
+	SAXS – BESSY (Berlin)
&	SAXS – LNLS (Campinas)
/	SAXS – EMBL (Hamburg)
°	TNS Assay
x	Free mRNA

Table 12: Tested systems with EPC 100 % as matrix lipid, different cationic or ionizable lipids (20 mol%) and plasmid DNA (1 mg/ml)

DOPE	0	20
cat. lipid		
DOTAP	* + x	* + x
DDAB	* + x	* + x
DC-Chol	* + x	* + x
DOTMA	* + x	* + x
DODMA	* + x	* + x #

Table 13: Implemented measurements for samples listed in Table 12

*	Size
+	Zeta potential
x	Transfection efficiency
#	T-cell proliferation

4 Results

4.1 mRNA-lipoplexes of DOPC and DOTAP

Partial results of the presented work have been published in: Ziller, A.; Nogueira, S. S.; Huehn, E.; Funari, S. S.; Brezesinski, G.; Hartmann, H.; Sahin, U.; Haas, H.; Langguth, P. Incorporation of mRNA in Lamellar Lipid Matrices for Parenteral Administration. Mol. Pharm. 2017, acs.molpharmaceut.7b01022. [150]

Partial results of the presented work have been taken from the unpublished thesis of Dr. Eva Hühn ("Rational Design of Sustained Release Liposomal mRNA Formulations for Parenteral Administration and Image-Guided Assessment of in Vivo Performance, 2013"). [165]

4.1.1 SAXS experiments

First experiments were performed with lipoplexes composed of EPC 80 % and DOTAP with different amounts of mRNA using small-angle X-ray scattering (SAXS). Scattering of such samples shows typical features of lipid systems. First, Bragg peaks indicated the molecular structure, which can be derived from the ratio of the reoccurring peak positions on the q-scale as listed in Table 14.

Table 14: Determination of the molecular structure with the help of the peak position

Molecular structure	**Peak position at q-scale**
Lamellar	1, 2, 3, 4, 5, …
Cubic	1, √2, √3, 2, √5, …
Hexagonal	1, √3, 2, √7, 3, …

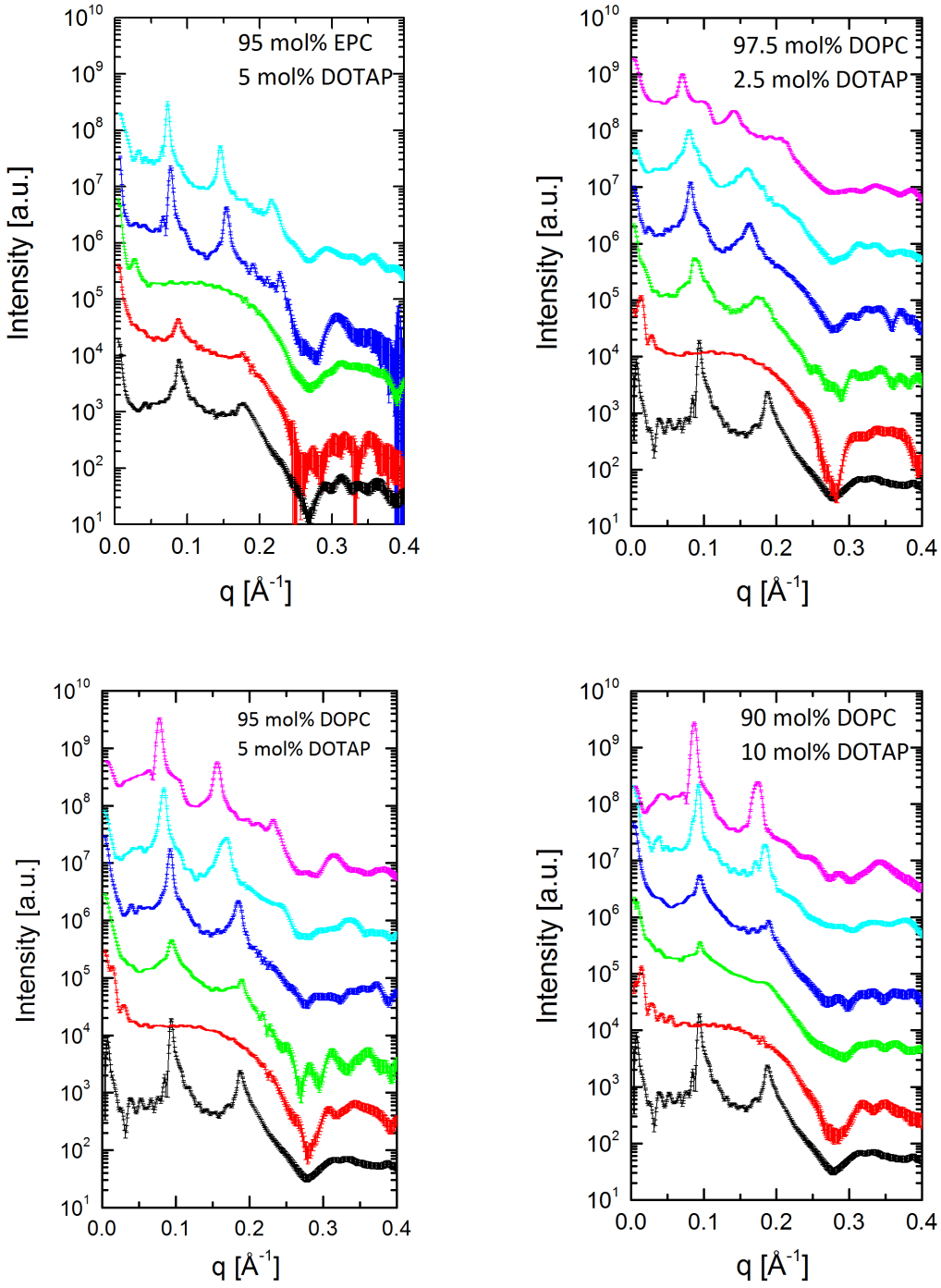

Figure 14: X-ray scattering data of lipoplexes composed of either EPC 80 % [top left] *(with pure EPC 80 % [black], EPC 80 % in presence of 5 mol% mRNA [red], EPC with 5 mol% DOTAP [green], EPC 80 % with 5 mol% DOTAP and 5 mol% mRNA [blue], and EPC 80 % with 5 mol% DOTAP and 10 mol% mRNA [cyan])* or DOPC [top right and bottom] *(with pure DOPC [black], DOPC with 2.5, 5 or 10 mol% DOTAP [red], DOPC with 2.5, 5 or 10 mol% of DOTAP and 2.5 mol% mRNA [green], DOPC with 2.5, 5 or 10 mol% of DOTAP and 5 mol% mRNA [blue], DOPC with 2.5, 5 or 10 mol% of DOTAP and 10 mol% mRNA [cyan], and DOPC with 2.5, 5 or 10 mol% of DOTAP and 20 mol% mRNA [purple])* with different amounts of DOTAP and mRNA (taken from [150])

Scattering data can be seen in Fig. 14 [top left]. Lipoplexes with pure EPC 80 % showed typical Bragg peaks. The positions indicated a lamellar lipid structure. As soon as EPC 80 % was mixed with DOTAP, the Bragg peaks disappeared, and the signal was dominated by the unstructured signal resulting from the individual bilayer scattering (form factor) between 0.05 and 0.25 Å. Just a small peak at 0.0027 $Å^{-1}$ indicates a large distance of about 230 Å between the lipid bilayers due to electrostatic interaction because of the introduced positive charge of DOTAP. After incorporation of mRNA into the lipoplexes, Bragg peaks were recovered, and positions referred to a lamellar structure again, which can be seen as integer multiples of the first q-value. For 5 mol% of mRNA, two clear Bragg peaks could be seen while for 10 mol% of mRNA, three clear Bragg peaks appeared. Furthermore, the peaks shifted to smaller q values with higher amounts of mRNA.

Since EPC 80 % is a natural lipid mixture composed of 80 % egg-PC (mainly POPC), lipid composition varies slightly. To ensure consistent quality for pharmaceutical development and production, DOPC as a pure and synthetic lipid was chosen for further experiments. SAXS experiments were repeated with a wider range of compositions including three different amounts of DOPC and increasing proportions of mRNA. Results from DOPC-lipoplexes (Fig. 14) illustrated similar behaviour as lipoplexes with EPC 80 %. Briefly, pure DOPC showed a lamellar order indicated by two Bragg peaks. After incorporation of DOTAP, the resulting form factor between 0.05 and 0.25 Å and a small peak at around 0.027 Å referred to a loss of structure. Comparable to EPC 80 %, the small peak resulted from an extended d-spacing at 230 Å. Again, with the incorporation of mRNA in the DOPC/DOTAP-lipoplexes, Bragg peaks recovered while peak positions were shifted to smaller q-values in comparison to pure DOPC. With increase amounts of mRNA, this shift became greater.

D-spacing of all samples were analysed carefully and showed a typical behaviour of insertion. All results were plotted against the DOTAP/mRNA (N/P) ratio, irrespective of the DOPC/DOTAP ratio. For example, lipoplex with 2.5 mol% DOTAP and 5 mol% mRNA and lipoplex with 5 mol% DOTAP and 10 mol% mRNA have the same N/P ratio (1/2), thus they were plotted at the same position.

With an excess of DOTAP (N/P ratio > 1), d-spacing as a function of N/P ratio changed only marginally. Close to the equilibrium and for samples with an excess of mRNA (N/P ratio < 1), d-spacing increased monotonously. For similar N/P ratios, similar d-spacings could be found. In conclusion, d-spacing was not dependent on the molar fraction of DOTAP but on the ratio of the amount of DOTAP and mRNA as it is illustrated in Fig. 15 [top].

4.1.2 Further characterisation

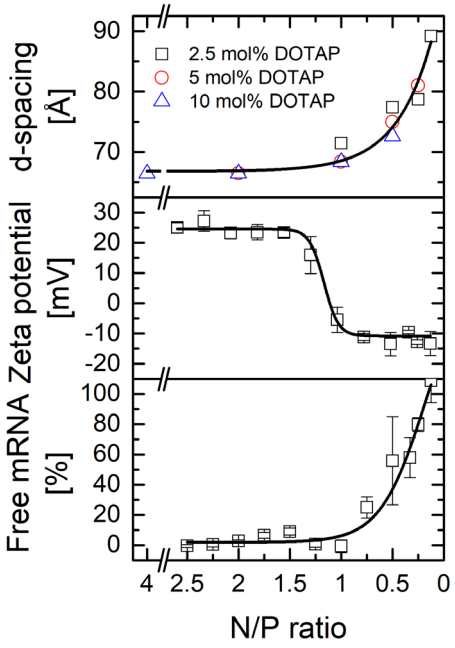

Figure 15: Characterisation of lipoplexes showing the d-spacing of lipoplexes with different proportions of DOPC, DOTAP and mRNA [top], zeta potential of lipoplexes with different amounts of DOPC, DOTAP and 20 mol% mRNA [middle] and amount of free mRNA from DOPC with different amounts of DOTAP and 20 mol% mRNA [bottom]; plotted as a function of the N/P ratio (taken from [150])

The amount of free mRNA was quantified with the commercially available Quant-iT™ RiboGreen™ RNA Assay Kit (Fig. 15 [bottom]). The dye shows fluorescent only when it binds to mRNA which is not bound to lipid membranes and therefore accessible. With an excess of DOTAP (N/P ratio > 1), there was no free mRNA since no fluorescence is detectable. With an excess of mRNA (N/P ratio < 1), the fluorescence and thus the amount of free mRNA increased. In addition, zeta potential measurements were performed (Fig. 15 [middle]). Pure DOPC showed negative values, while there was a positive potential after incorporation. By incorporating both DOTAP and mRNA, the measured potential reflected the N/P ratio of the lipoplexes. Samples with a N/P ratio higher than 1 showed a positive zeta potential. This was not unexpected since there was an excess of DOTAP. With an excess of mRNA and therefore a N/P ratio lower than 1, the zeta potential switched to negative values. For better comparison, the fraction of free mRNA and the zeta potential were plotted over the same axis as for d-spacing. There seems to be a characteristic change at the N/P ratio of 1/1. First, d-

spacing as well as the amount of free mRNA started to increase at this ratio. Furthermore, a change in the slope of the zeta potential occurred at this N/P ratio. Measured potentials above this ratio were positive, the ones below negative. Consequently, binding of mRNA to DOTAP seemed to occur in a manner of 1 to 1 (mol% to mol%). One molecule of DOTAP with one positive charge could bind one nucleotide of the mRNA strand with one negative charge.

4.1.3 Determination of phase transition temperature

For further analysis and proof of a homogenous insertion of DOTAP into the DOPC membrane, phase transition temperature (T_m) was measured by the use of differential scanning calorimetry (Fig. 16). At this point, transition from gel to liquid-crystalline phase can be observed and hence, it represents an indicator for the stability of a system. The higher this temperature is, the more energy is necessary to unstable it. Both samples with and without mRNA were tested.

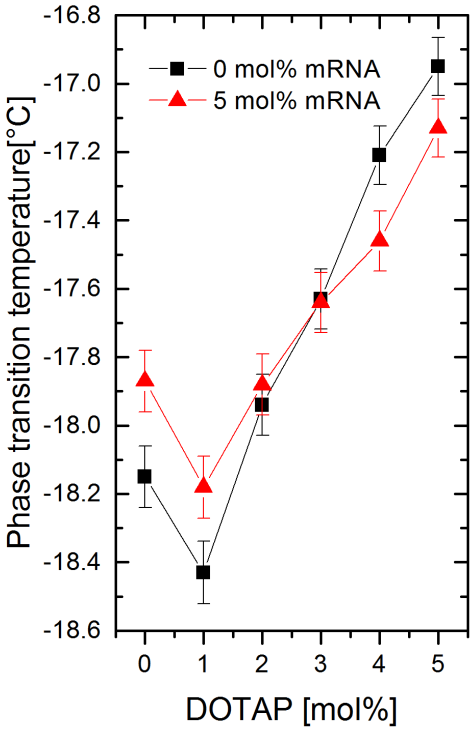

Figure 16: Phase transition temperature of lipoplexes with different proportions of DOPC, DOTAP and mRNA; plotted as a function of the amount of DOTAP (taken from [150])

For all the lipoplexes, T_m was in the sub-zero temperature range. Pure DOPC had a transition temperature at around - 18°C, while with mRNA it was slightly higher. Increasing DOTAP

concentration in the samples, T_m of the samples first decreased, but then increased constantly as a function of the DOTAP content. The insertion into the gel and the liquid crystalline phase and also the molecular interactions in both phases have to be taken into account when investigating the influence of DOTAP on the phase transition of DOPC. [166,167]

In general, insertion of a non-interacting solute into the liquid-crystalline (fluid like) phase is expected to lead to a decrease of T_m as a function of the solute concentration as is stated in:

$$\Delta T_m = -\left(\frac{RT_m^2}{\Delta H}\right) \cdot x_a$$

Equation 9: Calculation of the shift of the phase transition temperature

with ΔT_m as the shift of the phase transition temperature, R as the gas constant, ΔH as the melting enthalpy and x_a as the molar fraction of the solute in the solvent.

In contrast, insertion of DOTAP into the DOPC matrix just led to a first decrease for the lowest fraction, followed by an increase of the transition temperature for higher fractions. This increase in stability could be explained by interactions between both lipids. There is a strong attraction between the positively charged trimethylammonium headgroup of DOTAP and the negatively charged phosphate group of the zwitterionic DOPC. The more DOTAP was incorporated, the stronger these attractions were which then led to an increased stability. For lipoplexes with mRNA, the same temperature course with only minor shifts in comparison to the mRNA-free lipoplexes could be seen. This indicate, that mRNA did not act like a disruptive factor, but the lipid system remained also on the binding of mRNA. Hence, in presence of mRNA, DOTAP could be inserted homogenously into the DOPC matrix without phase separation since this would have led to a reversion back to the phase transition temperature of pure DOPC. In addition, results of zeta potential measurements supported these findings. The effects on the zeta potential indicated that both mRNA and DOTAP could be inserted into the membranes.

4.1.4 Cryo-TEM pictures

CryoTEM pictures indicated lipoplexes with different appearance (Fig. 17).

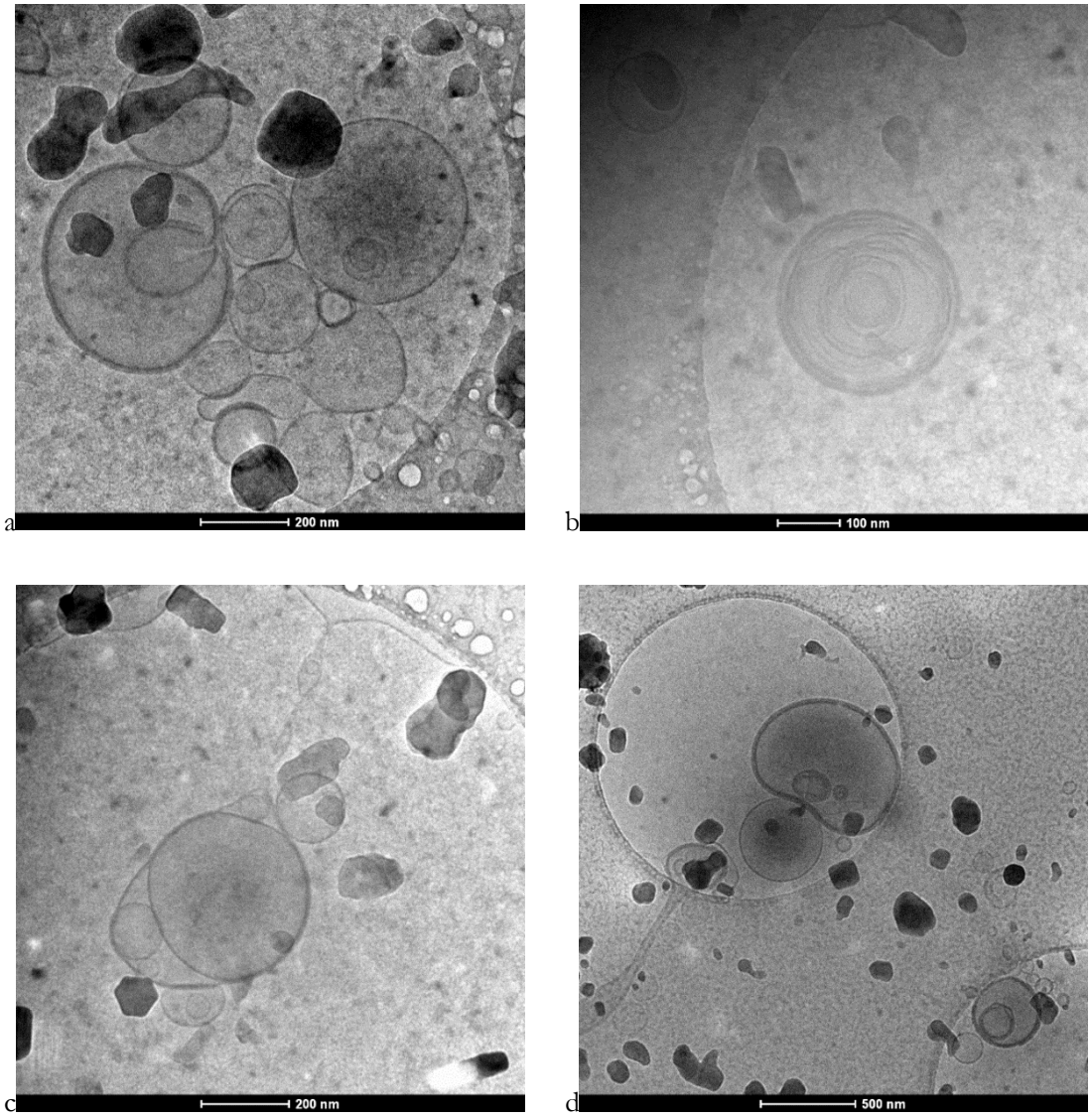

Figure 17: CryoTEM pictures of lipoplexes with 95 mol% DOPC, 5 mol% DOTAP and 10 mol% mRNA

Most of the vesicles had one or two lamellae. The membrane thickness differed slightly as is can be seen in Fig. 17 [d]. A thicker membrane can result from the accumulation of mRNA on the surface. The size ranged from 50 nm to about 500 nm. Most of the vesicles had a round shape while some of the lipoplexes appeared to be oval as well. Pictures revealed that some smaller vesicles were enclosed by larger vesicles forming multivesicular vesicles (MVV). In Fig. 17 [b], a typical multilamellar vesicle (MLV) with several membranes is depicted. With

regard to the lipid film method as the preparation method, it would have been expected that more of the vesicles form MLV. Further on, the addition of negatively charged mRNA would favour the arrangement in lipid layers because it reduces the repulsion force between the negatively charged lipid membranes. Possibly, the higher dilution of the liposomal suspension which was needed for this technique favours the formation of more unilamellar vesicles instead of MLV. Fig. 17 [a] showed some tendency of aggregation which was not that obvious in the other pictures. This aggregation is likely to be caused by the electrostatic interaction between the positively charged liposomal surface and the negatively charged mRNA which then impedes an electrostatic repulsion between the cationic liposomes. This indicates that the mRNA is not only encapsulated into the vesicles but is also bound on the surface of the liposomes. Nevertheless, this phenomenon must be investigated more deeply since the pictures just show a small part of the whole sample and it could be due to the special preparation for CryoTEM.

Contamination of ice crystals due to a high content of evaporated water appeared but did not impede a qualitative analysis.

4.1.5 Transfection efficiency

For evaluation of principal functionality, cell culture experiments were performed. Before application to the cells, lipoplexes needed to be diluted. Therefore, it was tested if the structure of the lipoplexes remain the same while dilution. As an example, three different compositions with 90 mol% DOPC, 10 mol% DOTAP and 5, 10 and 20 mol% mRNA were measured with SAXS. The molecular structure was determined for four concentrations (100, 10, 2 and 0.5 mg/ml.) as it can be seen in Fig. 18. As expected, the intensity decreased with lower lipoplex concentrations but, nevertheless, peak positions remained the same which indicate a preservation of the molecular organisation of the lipoplexes. Hence, the characterisation of the structure for the concentrated lipoplexes can be directly correlated with the results from the biological investigation.

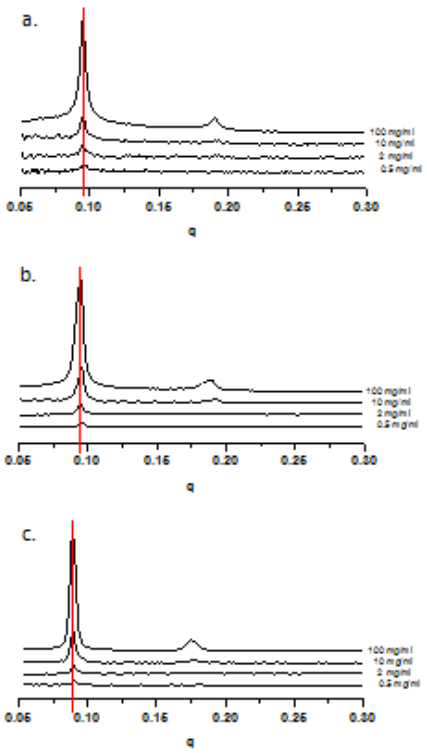

Figure 18: Scattering curves (SAXS) from DOPC with 10 mol% DOTAP and 5 mol% mRNA [top], 10 mol% mRNA [middle] and 20 mol% mRNA [bottom], diluted up to a lipid concentration of 0.5 mg/ml (taken from [150])

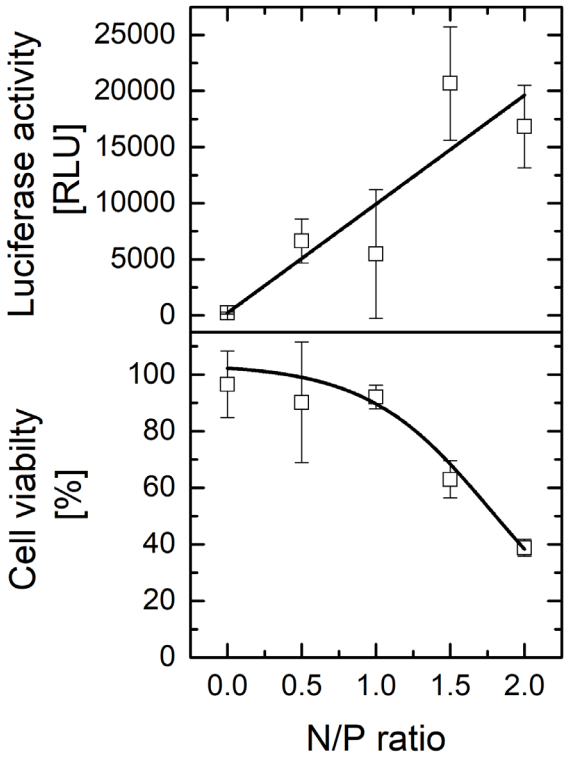

Figure 19: Transfection in C2C12 cells [top] and cell viability [bottom] of lipoplexes with DOPC, different amounts of DOTAP and 20 mol% mRNA (taken from [150])

In Fig. 19, results from the cell culture experiments using C2C12 murine myoblasts show that the mRNA inserted into the lipid membranes was functional. The luciferase activity was dependent on compositions and hence on the characteristic of the respective formulation. An excess of DOTAP was associated with higher signals. Nevertheless, systems with an excess of mRNA showed activity as well. In addition, cell viability test led to contrary results. With higher amount of DOTAP, cell viability decreased because of the toxicity of cationic lipids in general.

To ensure the applicability in different systems, the lipoplexes needs to be investigated in further *in vitro* and *in vivo* studies. The systems are supposed to work as a depot for local administration so that the release of mRNA should be investigated as well. For each route of application (e.g. intradermal, intramuscular or intratumoural), the most suitable formulation needs to be identified.

4.1.6 SANS experiments

The information gained from the previous described methods was used to characterise the lipoplexes composed of DOPC and DOTAP and for the development of a structural model. Nevertheless, it was not possible to proof the exact position of the mRNA. It could just be assumed that the mRNA appears to be a layer on the top of each lipid bilayer and forms clusters by interacting with the cationic headgroup of DOTAP. Therefore, SANS measurements were performed to proof the developed structural model. Using contrast variation, it should be possible to mimic the lipid bilayer and figure out the exact location of the mRNA.

Two characteristic samples with 5 mol% DOTAP and either 2.5 or 10 mol% mRNA were used to investigate both an excess of DOTAP and mRNA. Unfortunately, first measurements carried out at the KWS-2 instrument at FRM II in Garching failed by sample preparation. Samples needed to be diluted to a lipid concentration of 10 mg/ml. Stabilisation of samples was necessary due to a long measurement time. Consequently, a higher content of trehalose (1.31 M instead of 0.27 M) was chosen for dilution of the samples and experiments at the instrument in Garching were repeated. Aggregation could be prevented. Both samples were adjusted to a lipid concentration of 10 mg/ml and nine different contents of D_2O. Measurement were performed at three different detector distances to achieve a broader q-range (2, 8 and 20 m).

With the higher content of trehalose, another problem appeared. Trehalose has a lot of hydrogen atoms. By addition of a higher proportion, the initial ratio of deuterium to hydrogen is shifted in favour of hydrogen, additionally the density is modified. Consequently, the real content of D_2O differed from the initially calculated one. This phenomenon was not considered before the experiments. Therefore, the real contents of D_2O needed to be calculated afterwards from the neutron transmission values and are listed in Table 15. The transmission of each buffer was measured and compared to the transmission of buffers with a known D_2O content. As expected, D_2O contents were lower as initially calculated. Just for 0 and 11.11 %, the measured D_2O content was higher which is due to changes in the density caused by the high content of trehalose (1.31 M).

Table 15: Comparison of calculated and real amount of D_2O due to high content of trehalose (1.31 M)

D_2O calculated [%]	D_2O real [%]
0	4.64
11.11	12.7
16.16	15.63
22.22	20.39
33.33	28.55
44.44	34.09
55.56	39.82
66.67	46.29
77.78	54.05

Each contrast has to be analysed separately and different information can be gained by evaluation of 2, 8 and 20 m. Background subtraction was corrected with the Porod plot. Data of all distances was merged. The linear part of the 20 m data at very low q-values was treated with the Guinier plot to gain forward intensity and radius of gyration of the particle, which describes the radius measured from the centre of mass. The Kratky-Porod plot was used for the linear part of the 8 m data at q values between 0.0004 to 0.001 Å to observe the thickness of possible flat areas (layer span thickness) within the system, which can occur due to bilayer membranes of the lipids. Exemplary, data treatment is shown for one sample with one D_2O contrast in Fig. 20. Procedure was done for all contrasts and results are listed in Table 16.

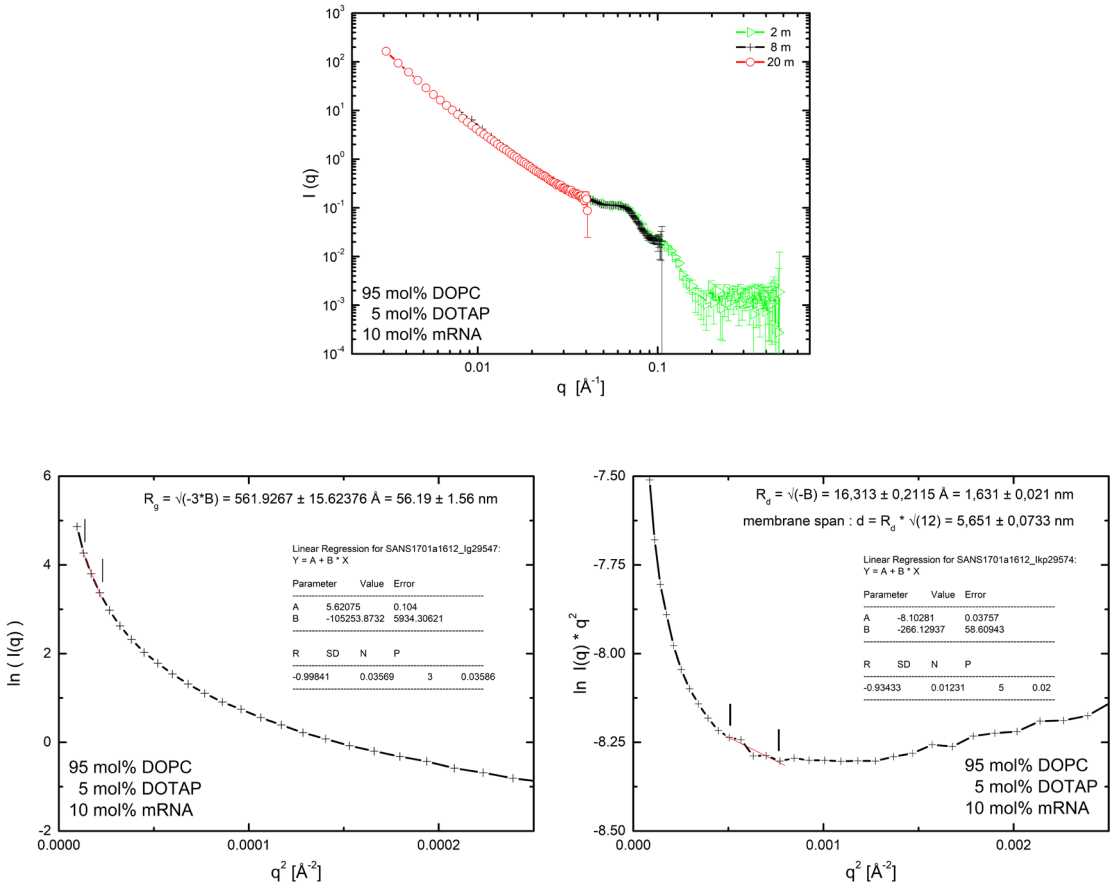

Figure 20: Scattering profile [top], Guinier plot [bottom left] and Kratky-Porod [bottom right] of lipoplexes with 95 mol% DOPC, 5 mol% DOTAP and 10 mol% mRNA in 54 % D_2O

Table 16: Results for radius of gyration as obtained from the Guinier plot and layer span thickness resulting from the Kratky-Porod plot

Sample [% D_2O real]	Radius of gyration [nm]	Layer span thickness [nm]
95 mol% DOPC / 5 mol% DOTAP / 2.5 mol% mRNA		
4.64	54.77	3.87
12.7	52.36	20.1
15.63	57.03	19.39
20.39	55.88	19.74
28.55	-	8.78
34.09	-	9.3
39.82	56.19	10.0
46.29	56.12	4.51
54.05	53.2	5.64
95 mol% DOPC / 5 mol% DOTAP / 10 mol% mRNA		
4.64	42.9	3.87
12.7	49.16	5.17
15.63	54.32	7.68
20.39	53.20	4.47
28.55	-	7.37
34.09	-	6.73
39.82	48.28	5.7
46.29	48.36	4.83
54.05	48.26	5.65

Depending on the D_2O content, certain structures within the lipoplex are matched and the not matched parts can be observed. A DOPC/DOTAP bilayer has a thickness between 33 and 44 Å (3.3 to 4.4 nm) depending on the composition [168]. Close to the matching point of the mRNA around 67 %, membrane thickness has to correspond to the thickness of pure DOPC/DOTAP. Unfortunately, this D_2O content could not have been measured due to the high content of trehalose. Despite, these values could be proven for both samples since the D_2O content of 46.29 % is quite close to the matching point of the mRNA and resulted in a

layer span thickness of 4.51 or 4.83 nm. The lowest content (4.64 %) shows the pure mRNA. The values show that the mRNA forms a thinner layer in comparison to the lipid membrane which is in line with the developed structural model.

The mRNA is expected to form another layer on top of each side of the lipid bilayer. Hence, membrane thickness has to be higher than for pure DOPC/DOTAP membrane. Increasing the D_2O content (12.7, 15.63 and 20.39 %), the layer span thickness is supposed to reflect the mRNA accumulated on the lipid membrane, so the values have to be higher. The sample with 10 mol% shows a layer span thickness which indicate that one mRNA layer is on top of one lipid bilayer (7.58 nm for 15.63 %) which is in accordance to the developed model. In case just one side of the lipid bilayer is covered with mRNA. It has to be evaluated if a lipid bilayer can also be covered with mRNA from both sides. For the sample with 2.5 % mRNA, the values are much higher (19.39 to 20.1 nm). In the earlier performed SAXS experiments, this low content of mRNA led to a strong decrease of the d-spacing of the lipid bilayers in comparison to the same lipid sample without mRNA since the mRNA compensates the electrostatic repulsion of the cationic membrane surface. Possibly, more layers of mRNA and lipid bilayers stick together and cannot be measured separately which led to such high values. In the same experiment, 10 mol% of mRNA increased the d-spacing in comparison to 2.5 mol% mRNA which was caused by a higher anionic charge and an increased requirement of space. Hence, lipid bilayers do not stick together which is accordance with the above-mentioned layer span thickness.

The values for the gyration radius are all around 50 nm. This seems to be quite small. The CryoTEM-pictures (see Ch. 3.1.4) revealed vesicles with sizes ranging from 50 to a few hundred nm. In addition, DLS experiments (data not shown) from the SANS experiments showed larger particles as well. These results can be caused by the curved instead of a linear Guinier plot at small q-values which can happen in samples that tend to aggregation. Due to that, the Guinier plot could just be performed with the minimum amount of data points.

A crucial tool is the determination of the matching point. The matching point constitutes the D_2O content, where the according substance has the same scattering length as the buffer. With the help of values based on literature (e.g. matching point of lipids: 11 %), it should be simple to determine the single components of the according structure. The matching point can be determined for the whole sample as well as for a single appearing peak to investigate the composition of the causing structure. It is also important to analyse the side peaks because they can give information on structural details.

For the matching point of the whole sample, Guinier plot is applied to calculate the matching point of the whole particle. Therefore, a linear area in the 20 m data is used to determine I_0 and its root is plotted over the corresponding D_2O content. At y=0, the matching point of the whole particle can be determined. Both can be seen in Fig. 21. The graph is based on the real D_2O values as listed in Table 15. In case of the sample with 5 mol% DOTAP and 2.5 mol% mRNA, the matching point occurred to be at a D_2O content of 6.6 %. For the formulation with 10 mol% mRNA, it appeared to be 6.7 %.

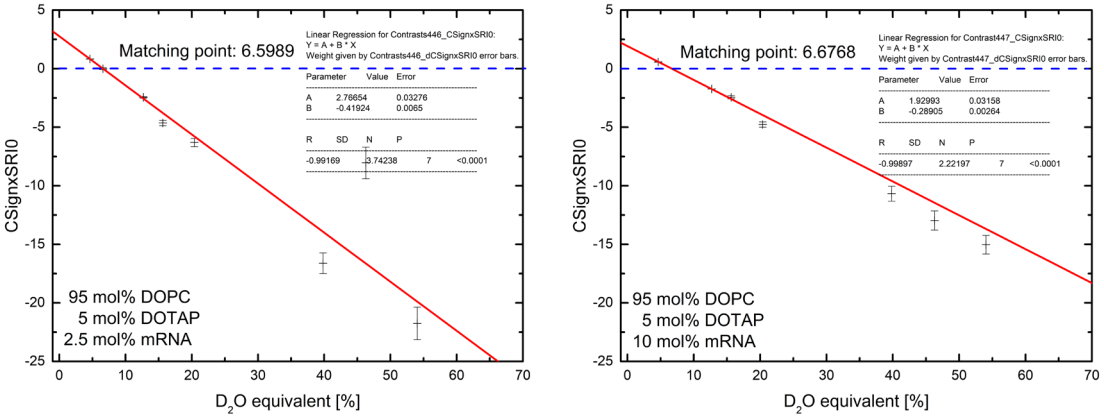

Figure 21: Matching point of lipoplexes with 95 mol% DOPC, 5 mol% DOTAP and a low [left] and a high [right] content of mRNA

Lipids constitute the largest proportion in the formulation, so the matching point could be expected around 11 %. If the mRNA (matching point: 67 %) had a strong impact on the formulation structure, the matching point would be shifted to higher D_2O contents. The matching point was shifted to lower contents, so that another ingredient seemed to have an impact in both samples. Since there was a large amount of trehalose in the samples (1.31 M), an influence of trehalose is expected. Normally, the errors are larger with lower contents. As it is obvious in Fig. 21, the error got larger with a higher content of D_2O. This can be explained with the help of the Guinier plots. Instead of a linear course, the plot is curved at the smallest q-values which indicates aggregation of particles. With higher amounts of D_2O, the aggregates got more visible. However, since the data points are nearly on one line, separation could not have been observed.

Next step in evaluation would be the determination of the matching points of each peak to receive information on the structure which caused the respective peaks. Hence, exact structural characterisation would be possible. Nevertheless, with the currently available data, this analysis

is not possible. Reference measurement with empty liposomes containing DOPC alone and DOPC with different contents of DOTAP are needed. Although such data can be found in the literature, it cannot be used for these experiments. Since the high content of trehalose influences the scattering profile, the references measurements have to be performed in the same buffer. Further experiments are planned to complete the data set. Therefore, analysis of the single peaks is not part of this work. With these reference measurements, it will also be easier to evaluate the data. Until now, the influence of the trehalose on the results cannot be clarified completely.

Comparison between SAXS and SANS

For comparison, samples with the same composition were also tested at the BioSAXS beamline at EMBL in Hamburg. Scattering curves from SAXS and SANS were plotted together in Fig. 22. For better comparison, just the data from 2 and 8 m are shown since most of the information is in this q-range.

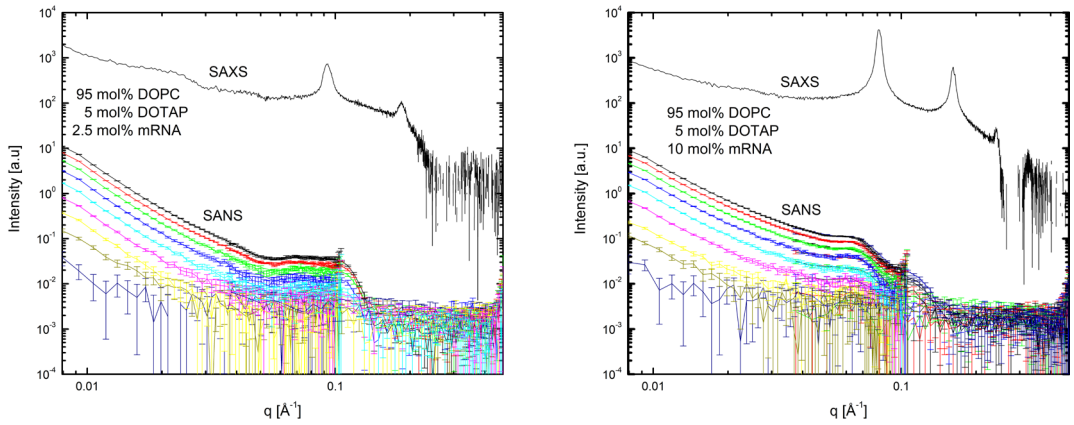

Figure 22: Comparison of SAXS [highest one] and SANS [lower ones, 77.77 % to 0 % D_2O from top to bottom] curves from lipoplexes with 95 mol% DOPC, 5 mol% DOTAP and a low [left] and a high [right] content of mRNA

The highest curves, which has a different appearance, is the SAXS curves while the curves beyond show the different D_2O contents from 77.77 % at the top going down, in linear steps of 11.11 %, to 0 % at the bottom; with 16.16 % as an additional measuring point. As expected, the plot revealed varied intensities of the scattering curves generated by SAXS and SANS. This is due to higher concentration for SAXS but also stronger scattering effects for electrons. Moreover, peaks generated by SAXS were much clearer while the peaks for SANS formed just

shoulders instead of peaks. These narrow peaks are caused by the strictly monochromatic radiation used at a SAXS beamline which results in very small energy resolutions (e.g. 10^{-3} $\Delta\lambda/\lambda$ for the ID02 beamline at ESRF facility). In contrast, the energy resolution of the radiation used in SANS experiments is higher (e.g. 20 % ($\Delta\lambda/\lambda$) for the KWS-2 instrument at the FRM II facility) which lead to strong smearing of the peaks. The scattering intensity of the SANS curves increased with higher D_2O contents due to stronger coherent scattering of deuterium compared to hydrogen. SAXS data confirmed the results illustrated earlier in Ch. 4.1.2. The peak positions revealed a lamellar structure with two orders which is dependent on the composition. With an excess of DOTAP, peaks positioned at 0.093 $Å^{-1}$ and 0.186 $Å^{-1}$ while the excess of mRNA resulted in peaks at 0.081 $Å^{-1}$ and 0.162 $Å^{-1}$ which meant a bigger d-spacing for the latter sample.

Analysis of the peaks generated by SANS was more difficult. The sample with an excess of mRNA pictured two peaks which were shifted to smaller q-values in comparison to the SAXS curve. The excess of DOTAP led to one broad peak which was assembled by several peaks. Possible 2nd order peaks were difficult to determine because of the strong background noise at larger q-values. Although samples had the same composition, peak pattern appeared differently. Both samples were prepared in 0.27 M trehalose. For SAXS, samples were diluted with the same concentration while a solution with 1.31 M trehalose was utilised for SANS. This was the only difference in the measured sample so that further analysis of this phenomenon was necessary.

Therefore, the sample with 5 mol% DOTAP and 10 mol% mRNA was measured with either 0.27 M or 1.31 M trehalose at the SAXS1 beamline at LNLS in Campinas. Furthermore, H_2O and D_2O was used as base for dilution medium to exclude a possible influence. Scattering curves of all four conditions are illustrated in Fig. 23. Samples with D_2O were shifted along the y-axis, just for a better display. Further analysis of the peak pattern can be seen in Fig. 23 as well. Variations between H_2O and D_2O appeared just for the peak areas but not for the d-spacing. Unfortunately, the scattering curves showed two lamellar systems although this sample normally just caused one lamellar system as it can be seen in other experiments. The main system appeared around 85 Å and the second one at 68 Å. Dilutions with the lower amount of trehalose showed four peaks whereas the higher amount led to just three peaks. While the peaks at a spacing of 85 Å just shifted slightly by increase of the trehalose content, there was a clear shift for the peaks from 68 Å to 60 Å.

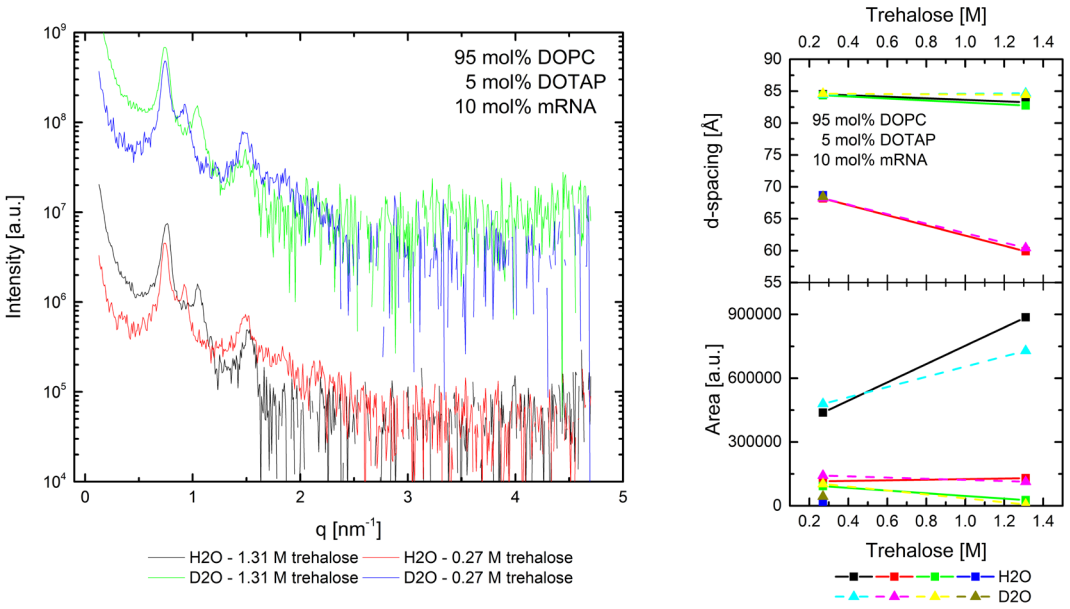

Figure 23: SAXS curves [left] and peak analysis [right] of lipoplexes with 95 mol% DOPC, 5 mol% DOTAP and 10 mol% mRNA mixed with 0.27 and 1.31 M trehalose in either H_2O or D_2O

SANS measurement in cooperation with NIST (Delaware)

Further investigation on the effect of the high trehalose content was done at the *n*Soft instrument at NIST in Delaware. Two samples with 10 mol% mRNA and either 5 or 10 mol% DOTAP as well as pure DOPC with 100 mg/ml as reference were prepared. Samples were measured pure and diluted with 0.27 M or 1.31 M trehalose solution. Since equivalent D_2O contents were always lower because of the high trehalose amount, 77.78, 85 or 90 % were adjusted to achieve a preferably high D_2O content. Nevertheless, the equivalent content of D_2O was not determined within this experiment.

Fig. 24 displays results for pure DOPC and mixed with two different D_2O contents as well as the two trehalose amounts. Intensity of pure DOPC was higher because samples was measured without dilution. A shift to larger q-values was observed and d-spacing was calculated by the help of the peak position. More trehalose correlated with a stronger shift since the shift for 0.27 M was 7 Å and for 1.31 M trehalose about 10 Å. In contrast, D_2O concentration had no influence.

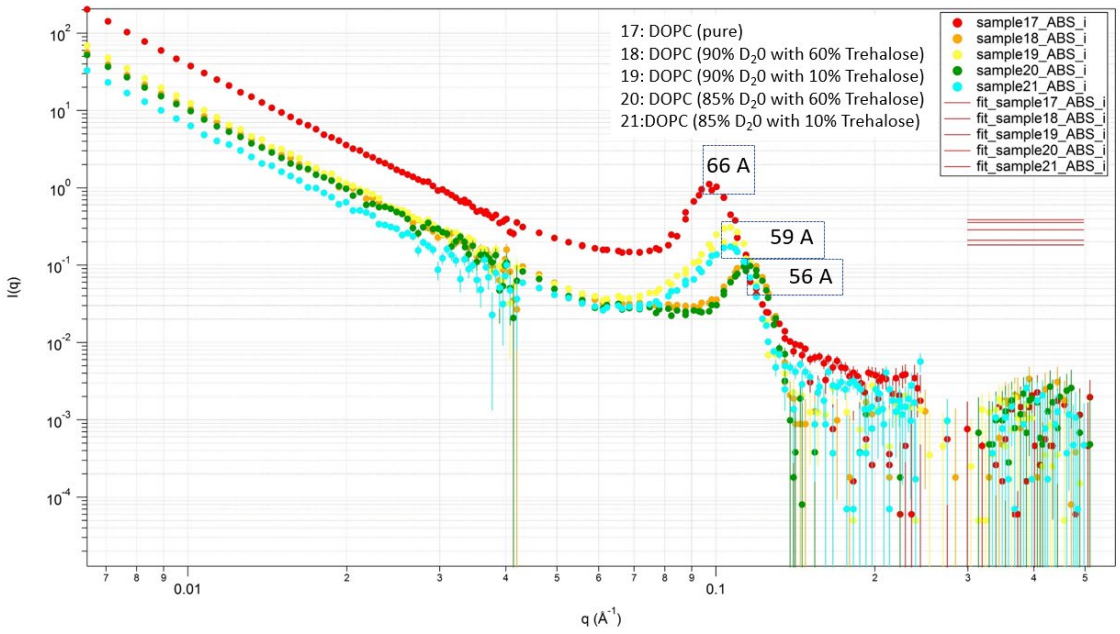

Figure 24: Scattering curves of pure DOPC and mixed different amounts of D_2O and trehalose

This comparison was done similar for both samples as illustrated in Fig. 25. D-spacing differed for the pure samples with a larger spacing for the sample with less DOTAP (5 mol%: 73 Å and 10 mol%: 69 Å). All measured conditions (90 and 85 % D_2O for 0.27 and 1.31 M trehalose and 77.78 % D_2O for 0.27 M trehalose) resulted in a comparable shift. Peaks for the sample with 5 mol% DOTAP were shifted 16 Å while the shift for 10 mol% DOTAP was just 9 Å. For the latter, peaks of the generated scattering curve just differed in intensity but not in shape. Scattering curve of the formulation with 5 mol% DOTAP showed various appearance. Peaks generated by 0.27 M trehalose were more defined than the peaks for the high concentration.

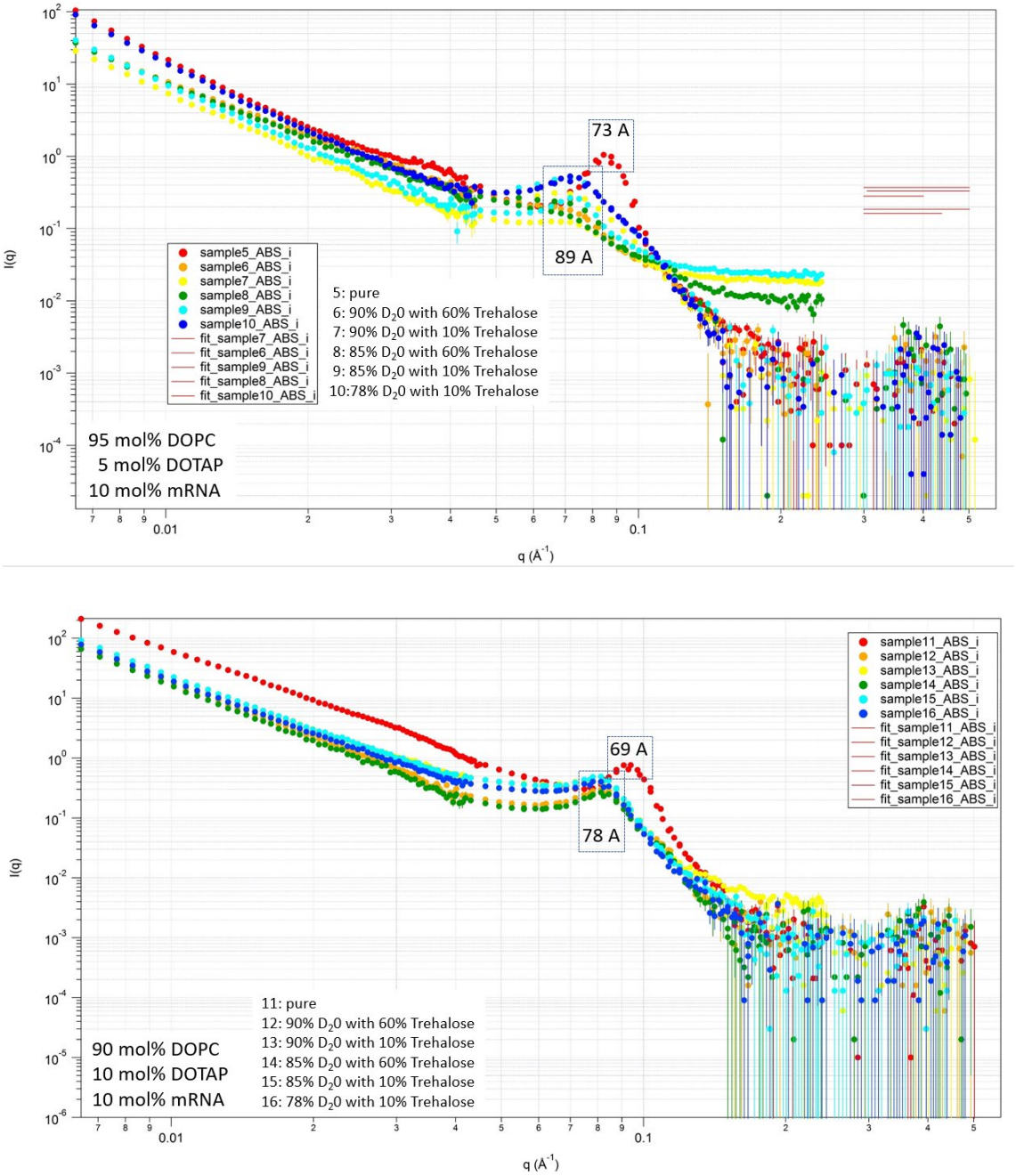

Figure 25: Scattering curves of lipoplexes with 5 mol% [top] and 10 mol% DOTAP [bottom] with different amounts of D_2O and trehalose

Comparison of the pure samples are presented in Fig. 26. Pure DOPC showed a peak at the highest q-value. With the addition of DOTAP and mRNA, peaks shifted to smaller q-values whereas lower amount of DOTAP related to a stronger shift. This is in line with earlier results.

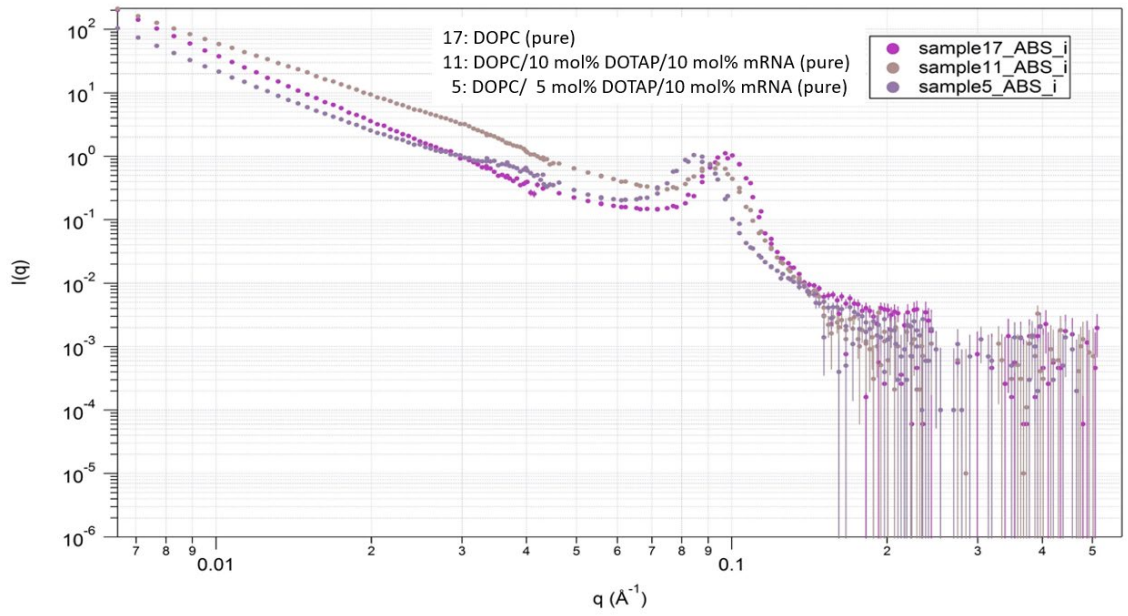

Figure 26: Comparison of pure DOPC and two lipoplexes with 5 and 10 mol% DOTAP and 10 mol% mRNA

4.1.7 Reproducibility of preparations

Beamtime at a synchrotron is rare so that samples can often just be measured once. Despite, reproducibility is an important criterion for the preparation of pharmaceutical formulations. Preparation of the same sample by different persons as well as repeated measurements and measurements at different facilities should lead to the same results. For this work, samples could be prepared by different persons and could also be measured at different beamlines. [165] A comparison of these samples is shown in Table 17.

Concentration for measurement varied between the different experiments, but this has no influence on the d-spacing as shown earlier in Ch. 4.1.5. Samples were prepared and diluted with a 0.27 M trehalose solution. The d-spacing for the samples prepared by Eva Hühn represented both peaks of the lamellar system. It is evident, that results from earlier measurements by Eva Hühn could be replicated successfully. [165] Lamellar orders were identical and d-spacing varied in an acceptable range.

Just for the sample with 5 mol% DOTAP and 10 mol% mRNA one repetition led to a different result. Since this is one out of four experiments, it could be an artefact or due to insufficient transportation to the facility. The sample had to be carried to Brazil and sufficient and continuous refrigeration during the trip could not be guaranteed.

Table 17: Properties of same MLV sample prepared for different beamtimes

100 mol% DOPC				
Producer	Eva Hühn	Antje Ziller		
Facility	Mainz University	NIST		
Lamellar systems	1 (2 orders)	1 (2 orders potentially)		
Experiment	SAXS	SANS		
D-spacing	66.5 Å	66 Å		
95 mol% DOPC / 5 mol% DOTAP / 2.5 mol% mRNA				
Producer	Eva Hühn	Antje Ziller		
Facility	Mainz University	EMBL (DESY)		
Experiment	SAXS	SAXS		
Lamellar systems	1 (2 orders)	1 (2 orders)		
D-spacing	66.5 Å	67.9 / 68.5 Å		
95 mol% DOPC / 5 mol% DOTAP / 10 mol% mRNA				
Producer	Eva Hühn	Antje Ziller	Antje Ziller	Antje Ziller
Facility	Mainz University	EMBL (DESY)	NIST	LNLS
Experiment	SAXS	SAXS	SANS	SAXS
Lamellar systems	1 (2 orders)	1 (2 orders)	1 (2 orders potentially)	2 (2 orders)
D-spacing	75.0 Å	75.6 / 75.9 Å	73 Å	84.5 / 84.4 Å 68.2/ 68.7 Å
90 mol% DOPC / 10 mol% DOTAP / 10 mol% mRNA				
Producer	Eva Hühn	Antje Ziller		
Facility	Mainz University	NIST		
Experiment	SAXS	SANS		
Lamellar systems	1 (2 orders)	1 (2 orders potentially)		
D-spacing	68.4 Å	69 Å		

4.2 mRNA-lipoplexes with ionizable lipoplexes

The evaluation of lipoplexes with ionizable lipids was the overall aim of the following work. By using the homologous lipids DOTMA and DODMA, the structural behaviour of formulations with ionizable lipids in comparison with permanently cationic lipids could be investigated. Both are nearly the same lipids but differ slightly in their headgroup. DOTMA has a quaternary amine which lead to a constantly charged headgroup. In contrast, DODMA has a tertiary amine resulting in a pH-dependent protonation so that the positive charge is affected by the actual environment. Both lipids were embedded in a zwitterionic base lipid, which was either EPC 80 % or DOPC.

After subtraction of the buffer scattering, the Lorentz fit was applied to determine the exact peak position and area. The absolute values of the areas can just be compared while measuring at the same beamline since the intensity between different beamlines differs. D-spacing was calculated from the peak position according to Eq. 5. Both the scattering curve prior to fitting and the data obtained by fitting are used for evaluation and will be discussed. Peak analysis is shown in the results part while the corresponding scattering curves can be found in the appendix. For better comparison, scattering curves are plotted semi-logarithmic while a linear plot was used for fitting.

4.2.1 pH dependent structural changes

I. Comparison of structures at pH 7.5 and 5 with EPC 80 %-lipoplexes using SAXS

Figs. 27 to 29 show the results of the different formulations plotted over the amount of added mRNA. For better comparison, both pH values are placed in the same graph. Data of pH 5 is marked with solid line and squares while dashed lines and triangles are used for pH 7.5. In addition, each occurring peak is marked with another colour.

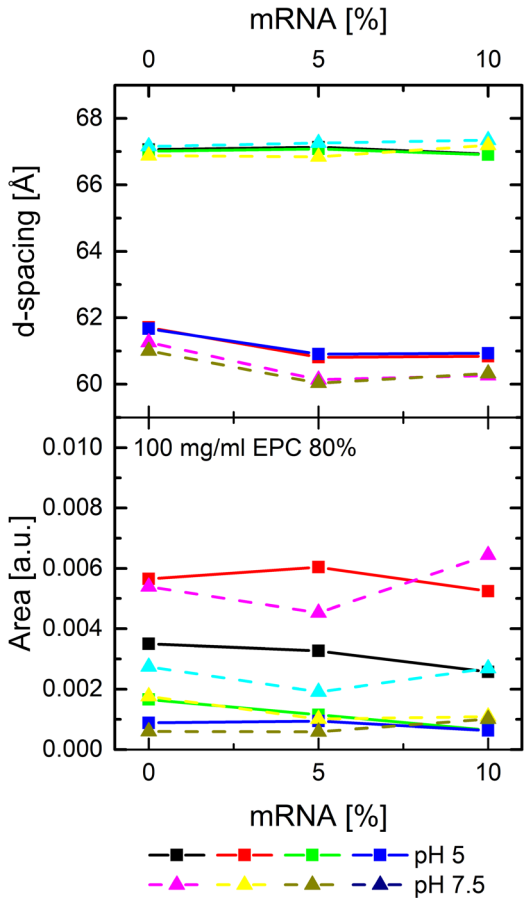

Figure 27: Peak analysis of lipoplexes with EPC 80 % and different amounts of mRNA, measured in pH 7.5 and 5

Exemplary for Fig. 27, four different peaks appeared at pH 5 as well as four peaks at pH 7.5. According to the peak positions (Table 14), a lamellar structure of all lipoplexes can be assumed. In comparison, more peaks (especially $q > 2$) are visible with the semi-logarithmic plot (Appendix I). Therefore, some of the peaks at q-values higher than 2 were not available for fitting since the linear plot was used for the Lorentz fit. Considering the position, these peaks always belonged to one of the present lamellar orders and therefore, indicate only a higher level of order/structure.

Pure EPC 80 %-lipoplexes, as it can be seen in Fig. 27, formed two orders of lipid lamellae around 61 and 67 Å, which also existed after addition of 5 and 10 % of mRNA. The constant area of each peak indicated a continuance of the orders. Just slight differences between both pH values appeared. Both lamellar orders formed a double peak, which indicated two in parallel existing lamellar systems.

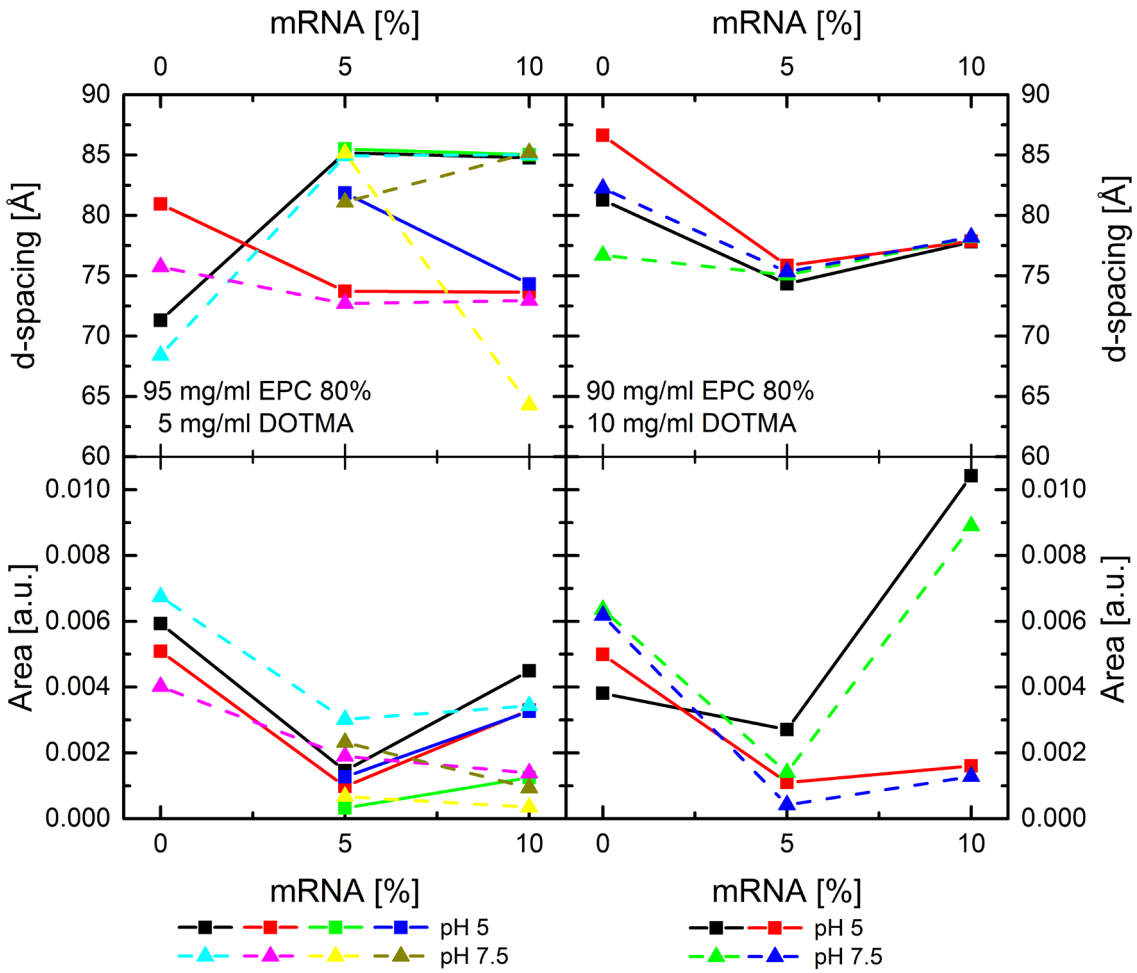

Figure 28: Peak analysis of lipoplexes with EPC 80 % and different amounts of DOTMA and mRNA, measured in pH 7.5 and 5

Afterwards, lipoplexes with 5 and 10 % of DOTMA were measured to investigate structure with a permanently charged lipid. Formulations without mRNA showed rather broad peaks, while the peaks got sharper after addition of mRNA (Fig. 28). Due to these broad peaks, a direct comparison between the formulations without and with mRNA is difficult. Fitting of these broader peaks is sometimes not explicit and can lead to varying peak positions and larger peak areas than actually present. In comparison to pure EPC 80 %, lipoplexes with DOTMA but without mRNA had a larger range of d-spacing while the intensity was similar. In the presence of mRNA, lipoplexes with a higher amount of DOTMA showed also a higher degree of structure. With 5 % DOTMA, two lamellar system with up to three successive peaks were detected. Furthermore, peaks were not separated completely. The area of the peaks changed just slightly while increasing the amount of mRNA. In contrast, lipoplexes with 10 % of

DOTMA showed just one lamellar order with up to four successive peaks. There was also a strong increase of the peak area of the main peak with an increase of mRNA from 5 to 10 %, which could be observed for both pH values.

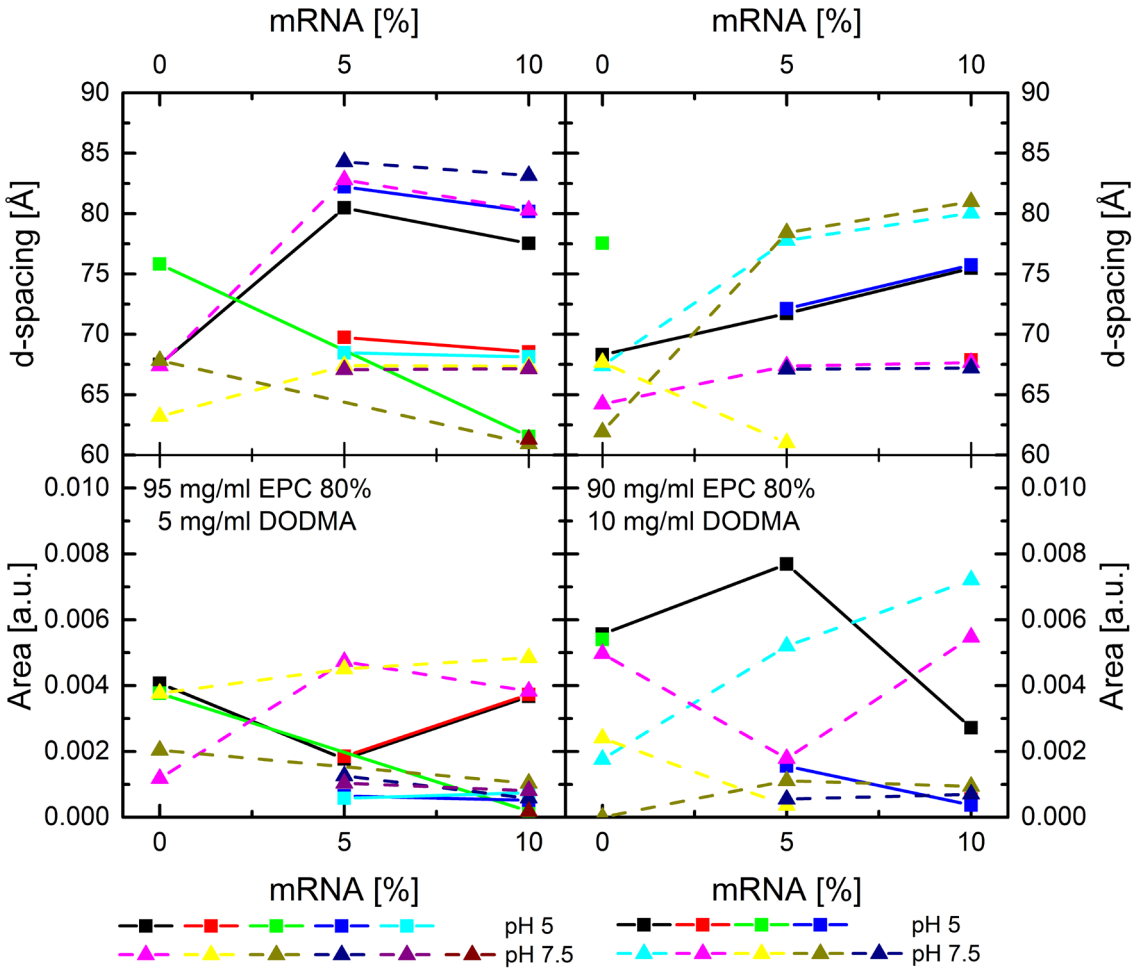

Figure 29: Peak analysis of lipoplexes with EPC 80 % and different amounts of DODMA and mRNA, measured in pH 7.5 and 5

Same experiments were carried out with 5 and 10 % of DODMA (Fig. 29). Results for d-spacing and peak area were in the same magnitude as for DOTMA. Although more peaks were visible for lipoplexes with DODMA, samples had a lower degree of structure. For 5 % of DODMA, not all peaks could be assigned to a lamellar order which was the same for both pH values. Lipoplexes with 10 % of DODMA behaved differently. For pH 7.5, two lamellar orders could be detected while still double peaks appeared. By lowering the pH to 5, only one lamellar

system was measured. For both 5 and 10 % DODMA, a slight increase of the d-spacing could be observed with the increase of mRNA while there was no clear change in the peak areas.

II. Investigation of pH dependent structural transition with EPC 80 %-lipoplexes

The experiments performed at the ESRF showed differences in the structure of lipoplexes with DOTMA and DODMA when mixed with a buffer of neutral or acidic pH. Further measurements on this behaviour were necessary to investigate a wider range of pH values and find the pH at which the transition of structure takes place. These experiments were performed at the mySpot beamline at BESSY in Berlin. Due to a time limitation, only characteristic samples of the ones measured at ESRF were chosen. Three lipoplexes with DODMA varying in the N/P ratio and one lipoplex with DOTMA as a reference were used. Again, the scattering curves prior to fitting and the results from Lorentz fit were included into the evaluation. d-spacing was calculated and plotted over the tested pH values, same was done for the peak area. Square data points and solid lines were used to illustrate the 1st order peaks while triangle data points and dashed lines were used for 2nd order peaks. Peaks are numbered consecutively. Compared to the scattering curves of ESRF data, the 3rd peaks did not occur, also not in the semi-logarithmic graphs. Due to the higher intensity of ESRF beamline, this was not unexpected.

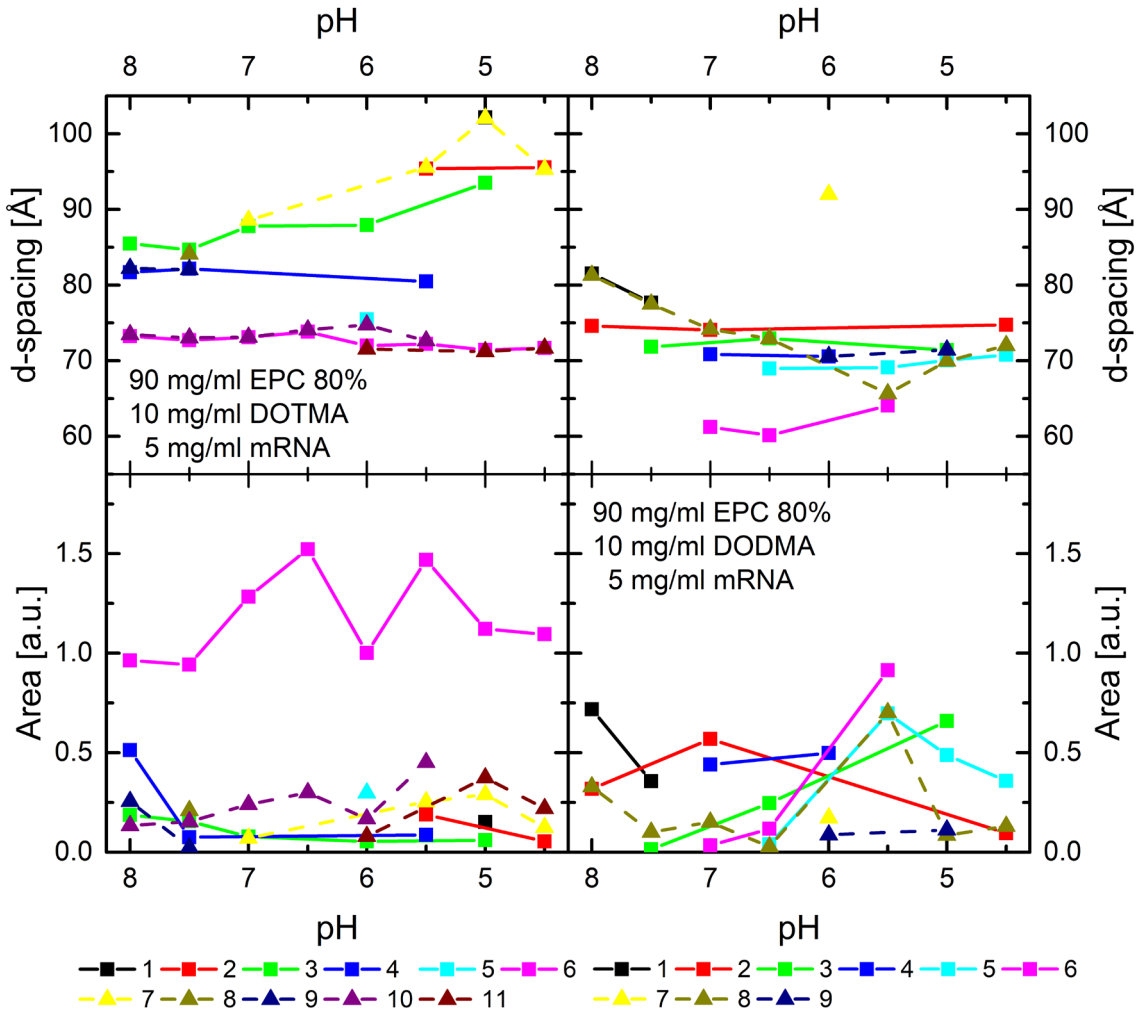

Figure 30: Peak analysis of lipoplexes with EPC 80 %, 10 mg/ml DOTMA or DODMA and 5 mg/ml mRNA, measured from pH 8 to 4.5

In Fig. 30, results from two formulations with the same composition (90 mg/ml EPC 80 % and 5 mg/ml mRNA) but with either 10 mg/ml DOTMA (left) or DODMA (right) are illustrated. Both samples showed different behaviour after mixing with various pH buffers between 8 and 4.5. At neutral pH, values for d-spacing (70 to 85 Å) were comparable while the range of d-spacing at acidic pH developed differently. For both lipoplexes, some peaks remained at the same d-spacing (peak 4, 5, 6, 10, 11 for DOTMA and peak 2, 3, 4, 5 for DODMA). Development of the remaining peaks showed differences. Peaks for the DOTMA sample increased in d-spacing (peak 2, 3, 7). Peaks for the DODMA samples either increased (peak 6, 8) or decreased in d-spacing (peak 1, 8). Peaks appearing for the DOTMA sample drifted apart from each other (peak 3, 4) whereas peaks for the formulation with DODMA seemed to fuse together (peak 5, 6). This led to smaller values and a tighter range of d-spacing compared to DOTMA (DODMA: 70 to 75 Å, DOTMA: 70 to 105 Å). This means, DODMA had just one

lamellar system while DODMA showed two systems with different spacing. Comparing the area as a proportion of the total amount of structural elements, differences can be seen as well. The lipoplexes with DOTMA had one dominating peak which did not change over the pH range. All the other peaks were less than half of this area and just varied slightly. The formulation with DODMA did not show one dominant peak. Nevertheless, it can be seen that the area of some peaks increases with lowering the pH (peak 5, 6, 8) which underlines the phenomenon of the peak fusion. This can also be seen in the scattering curve of this sample, that shows less but larger peaks at acidic pH.

In Fig. 31, data of the other tested samples is illustrated. One sample contains 5 mg/ml DODMA and 10 mg/ml mRNA (left) and one sample is composed of 10 mg/ml DODMA and also 10 mg/ml mRNA (right). In comparison to the DODMA samples discussed above, both similarities and differences are visible. First, the tendency of peak fusion with a reduction in the number of peaks was apparent.

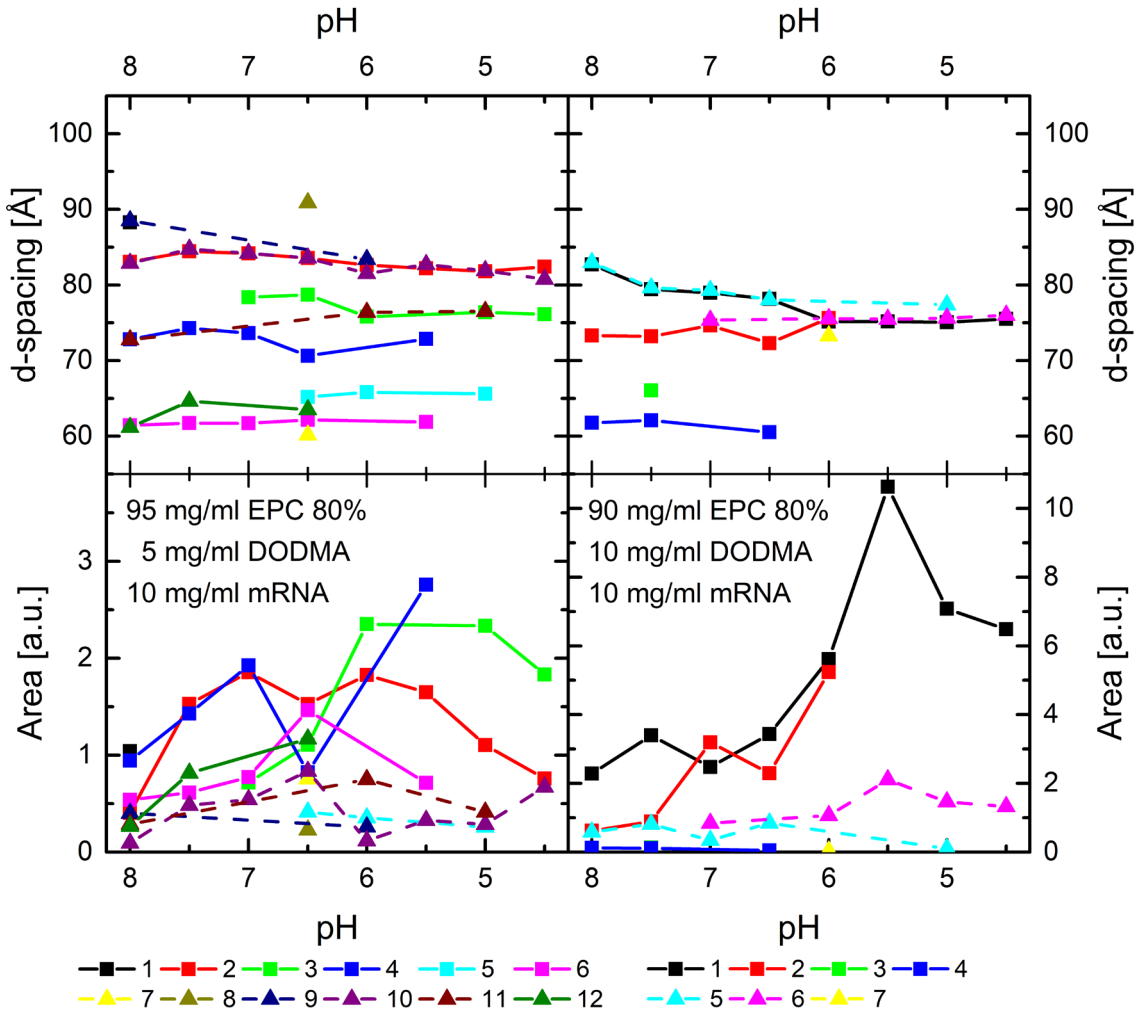

Figure 31: Peak analysis of lipoplexes with EPC 80 %, different amounts of DODMA and 10 mg/ml mRNA, measured from pH 8 to 4.5

For lipoplexes with 5 mg/ml of DODMA, more peaks occurred in comparison with the others which was visible above all for neutral and slightly acidic pH values. The scattering curve revealed that most of the peaks were not completely separated. Moreover, the range of d-spacing was quite large with varying between 60 and 90 Å. Three different lamellar systems were clearly visible. Lowering the pH to 5 and 4.5, most of the peaks disappeared finally. Due to the shift of certain peaks, d-spacing of the lamellar systems approached a range between 75 and 85 Å at a pH of 4.5, which is slightly higher than the range of the first DODMA sample. Nevertheless, the final peaks at pH 4.5 were also no clear single peaks but double peaks as it can be seen in the scattering curve. Again, the illustrated peak area emphasised the peak fusion since the area of the 1st order peaks increased through fusion.

The formulation with 10 mg/ml of DODMA and mRNA showed the observed phenomenon in the strongest manner. This composition led to less peaks compared to all the others while the range of d-spacing (60 to 85 Å) at neutral pH was comparable. Despite, three different lamellar systems were visible. The one system around 60 Å showed just one order and disappeared at pH 6. At the same pH, the two main lamellar systems below and above 75 Å fused to one lamellar system. This effect is supported by the illustrated peak area below. Peak 1 and 2 fused together followed by a strong increase of the resulting peak area. The same event happened with the 2nd order peaks 5 and 6. Surprisingly, the peak area of this sample was much higher than the others (see different scale). 1st order peaks showed larger areas than 2nd order peaks. In general, this effect is expected and was also observed for all samples but to a different degree.

III. Investigation of pH dependent structural transition with DOPC-lipoplexes

EPC 80 % is a natural lipid mixture which contains around 20 % of other lipid components like PC, which is mostly POPC. For pharmaceutical products, a consistent composition and quality is necessary. Therefore, the synthetically produced DOPC was used instead of EPC 80 %. The further experiments to analyse the pH transition of these samples were carried out at the BioSAXS beamline of EMBL at DESY in Hamburg. For better comparison with earlier measurements, a formulation with 10 mg/ml DODMA was prepared. Since higher amounts of ionizable lipids seem to have a higher influence on the structure, one formulation with 20 mg/ml of DODMA was tested. As a reference, 10 mg/ml DOTMA was used again. All samples contained 5 mg/ml mRNA. For a better outcome, 10 mg/ml DODMA were also tested without the addition of mRNA. Data was analysed as before and d-spacing and area of each sample was plotted about each other.

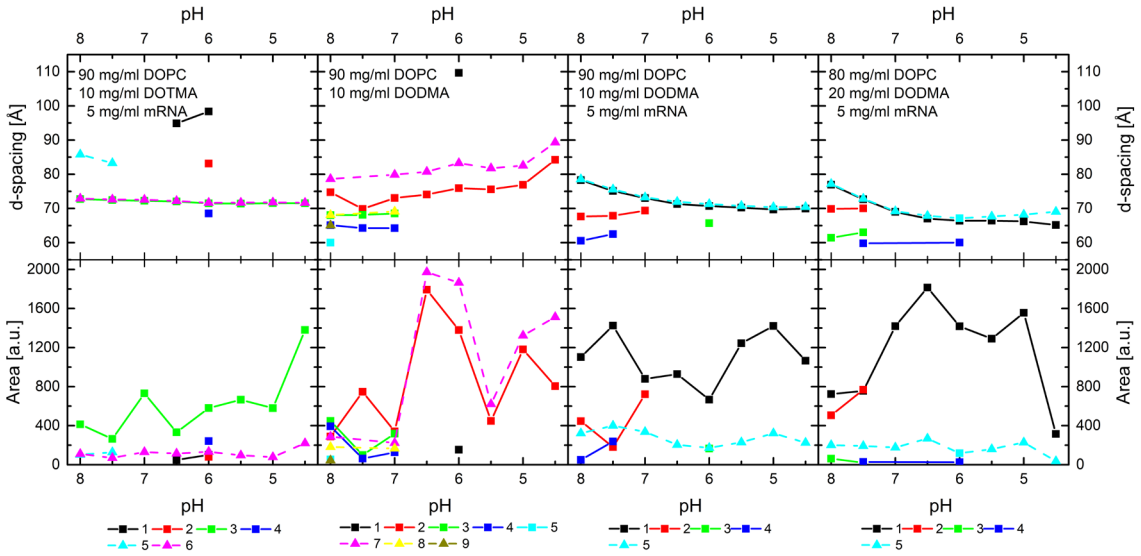

Figure 32: Peak analysis of lipoplexes with DOPC, different amounts of DOTMA or DODMA with or without 5 mg/ml mRNA, measured from pH 8 to 4.5

In Fig. 32, peaks of all measured samples are illustrated comparative. Square data points and solid lines are used for the 1st order peaks and triangle data points and dashed lines for 2nd order peaks. At first glance, there were less peaks for all samples with DOPC, but the general course over the pH range resembled the formulations with EPC 80 %.

The reference sample with DOTMA can be seen on the left side. Next to some single peaks (peak 1, 2, 4, 5), just one main lamellar system with a first and second order (peak 3, 6) can be observed around 72 Å. Both orders behave identically. D-spacing decreased marginally from 72.7 and 72.9 Å to 71.5 and 71.6 Å. Furthermore, the peak areas also just increased slightly while the 1st order peak was the dominating structure. At pH 8 and 7.5, there was another lamellar system at around 85 Å. In contrast to the diagram, two orders were observable in the scattering curve (Appendix II). Due to the position and size, the 1st order peak could not be fitted.

Second column in the diagram represents the reference sample without mRNA. At pH 8 to 7, d-spacings ranged from 60 to 75 Å with two lamellar systems with each 1st and 2nd order peaks. With lowering the pH, most of the peaks disappeared. One lamellar system remained until pH 4.5 whereas the d-spacing of both peaks increased to a range of 85 to 90 Å. The course of d-spacing of 1st and 2nd order peaks over the pH range was not on the top of each other as it would have been expected. Furthermore, peak area of the 2nd order peak seemed to be larger than the area of the 1st order peak. As visible in the scattering curve of this formulation, peaks got quite broad by decreasing the pH. At neutral pH, DODMA was nearly uncharged and

behaved more like pure DOPC. With a more acidic pH, headgroups got protonated and led to electrostatic interaction between the bilayers. Due to the broad peaks, fitting is not always exact so that peak position and area can differ which is a possible explanation for this phenomenon. Furthermore, the scattering curves revealed that all the peaks from one order fused together.

The lipoplexes with 10 and 20 mg/ml DODMA showed similar peak distributions. The range of d-spacing at pH 8 was between 60 and 80 Å for both. Furthermore, one lamellar system with 1st and 2nd order appeared over the whole pH range. As for the samples with EPC 80 %, peaks were drifting together so that the range of d-spacing become narrower with lower pH values (see peak 1, 2 for sample with 10 mg/ml and peak 1, 3 for sample with 20 mg/ml DODMA). The scattering curves of both samples pointed out, that the peaks were not completely separated even before the fusion around pH 7. The course of the peak area underlined this behaviour although it was more pronounced with 20 mg/ml of DODMA. After the fusion of peak 1 and 2, the area of this peak proliferated. For both samples, 1st order was in greater proportion as it was also indicated by a much larger peak area of the 1st order compared to the 2nd order peak. Compared to the formulation without mRNA, clear and narrow peaks developed by lowering the pH.

IV. Determination of pK_a out of the scattering data

The pK_a is the pH at which 50 % of the headgroups are said to be ionised. This ionisation is associated with structural changes due to electrostatic interactions which are supposed to be visible in the scattering experiment. Hence, the scattering profiles are supposed to give information concerning the pK_a. The data was analysed with regard to structural changes at specific pH values. The observations for both samples with DODMA and DOTMA are listed in the Tables 18 and 19.

Table 18: Structural behaviour of lipoplexes with EPC 80 % and DOPC as matrix lipid and different proportions of DODMA and mRNA

Basis	DODMA [mg/ml]	mRNA [mg/ml]	Behaviour
BESSY 02/2015			
EPC 80 %	10	10	Distinct transition at pH 6 with a loss of peaks and an occurrence of one new structure due to peak fusion
EPC 80 %	10	5	Gradual transition with a change in structure around pH 5.5 to 5
EPC 80 %	5	10	Gradual transition with a loss of some structures at pH 5 and 4.5
EMBL 12/2017			
DOPC	20	5	Gradual transition with a peak fusion at pH 7.5
DOPC	10	5	Gradual transition with a peak fusion at pH 7
DOPC	10	0	Gradual transition with a loss of peaks at pH 6.5

Table 19: Structural behaviour of lipoplexes with EPC 80 % and DOPC as matrix lipid and different proportions of DOTMA and mRNA

Basis	DOTMA [mg/ml]	mRNA [mg/ml]	Behaviour
BESSY 02/2015			
EPC 80 %	10	10	Gradual transition over the whole pH range, but no loss of peaks
EMBL 12/2017			
DOPC	10	5	No transition over the whole pH range

4.2.2 Determination of pK_a without SAXS

The TNS assay was performed in different ways. As a first test, pure EPC 80 % and samples with half of EPC 80 % and DOTMA or DODMA were used to test the suitability of the TNS assay for this kind of samples. The number of added samples was adjusted to 22 µM in 102 µl per well.

The total volume of sample per well was doubled to 204 µl due to the responsiveness of the fluorimeter. However, fluorescence of EPC 80 % was too low, so the lipid concentration of stock solution was increased tenfold (to 220 µM). Despite this increase, the fluorescence intensity of pure EPC 80 % was still lower. Since the fluorescence intensity was always normalised to pH 3, comparison with the other samples was not impeded. Fig. 33 [left] illustrates the expected behaviour of all three samples. Higher fluorescence intensity is correlated with a stronger binding of TNS to the cationic charged lipid headgroup. With the shift to neutral pH values, charge of ionizable lipids is reduced what led to less binding of TNS. This effect can be seen for the sample with DODMA whereas the intensity of the sample with DOTMA remained constant. Furthermore, intensity for EPC 80 % remained constant as well but with a much lower absolute intensity as explained earlier.

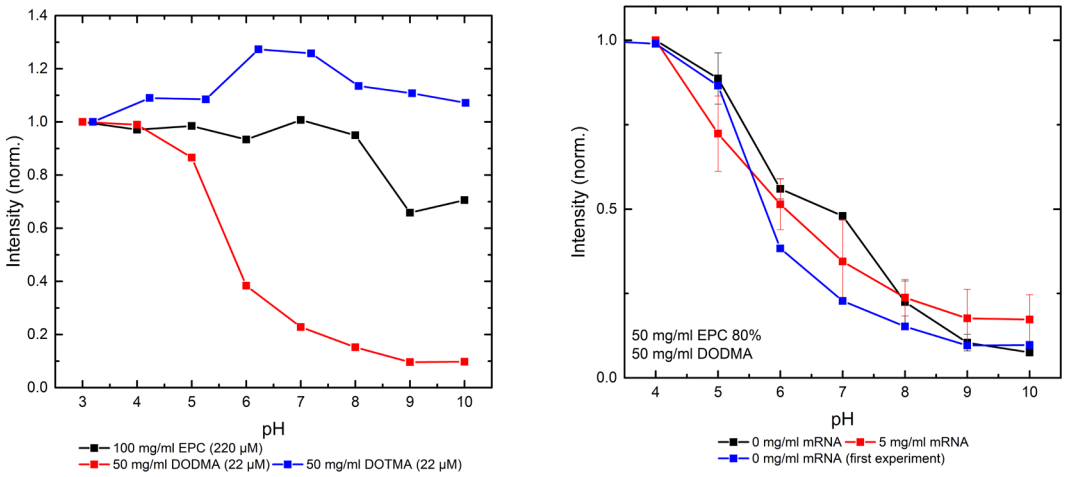

Figure 33: Reference measurements for TNS assay at different pH values [left] and comparison of intensity of lipoplexes with 50 mg/ml DODMA with and without mRNA at different pH values [right] (test conditions 1 and 2)

Further experiments were carried out to investigate whether the amount of ionizable lipid in the formulation influences the apparent pK_a. Therefore, 2.5, 5, 10 and 20 mg/ml DODMA was tested in comparison to the same amounts of DOTMA as reference. In addition, all of them were also prepared with 5 mg/ml mRNA to see a possible impact of that as well. Proofing reproducibility, two individual samples for 20 mg/ml were used. Due to better responsiveness, fluorescence was now measured with a TECAN infinite F200. Furthermore, measured lipid amount per well was 100-fold higher than in the first experiments while the total volume per well was 102 µl.

Samples were measured in duplicates to grasp an idea of the standard deviation. For comparison with the first experiments, lipoplexes with 50 mg/ml of DODMA were tested again and results are illustrated in Fig. 33 [right] after normalisation of intensity. It is obvious, that the tested concentration did not have an influence on the measurement since the course of the graphs is similar within the standard deviation. The addition of mRNA did not have an influence as well. Nevertheless, standard deviation was higher compared to the formulation without mRNA. This could be due to some aggregation of sample which favours inaccuracies in pipetting. Fig. 34 shows the overview of all the other tested samples. Again, most of the samples with mRNA had higher standard deviations than the formulations without mRNA while the standard deviation differed quite a lot between the different compositions. Nevertheless, the expected course was visible since a decrease in the intensity was provable for all DODMA samples. In comparison, samples with DOTMA led to less decrease in fluorescence intensity

while higher amounts of DOTMA showed more pronounced results. Findings were reproducible since all samples with 20 mg/ml DODMA and DOTMA with and without mRNA led to comparable results.

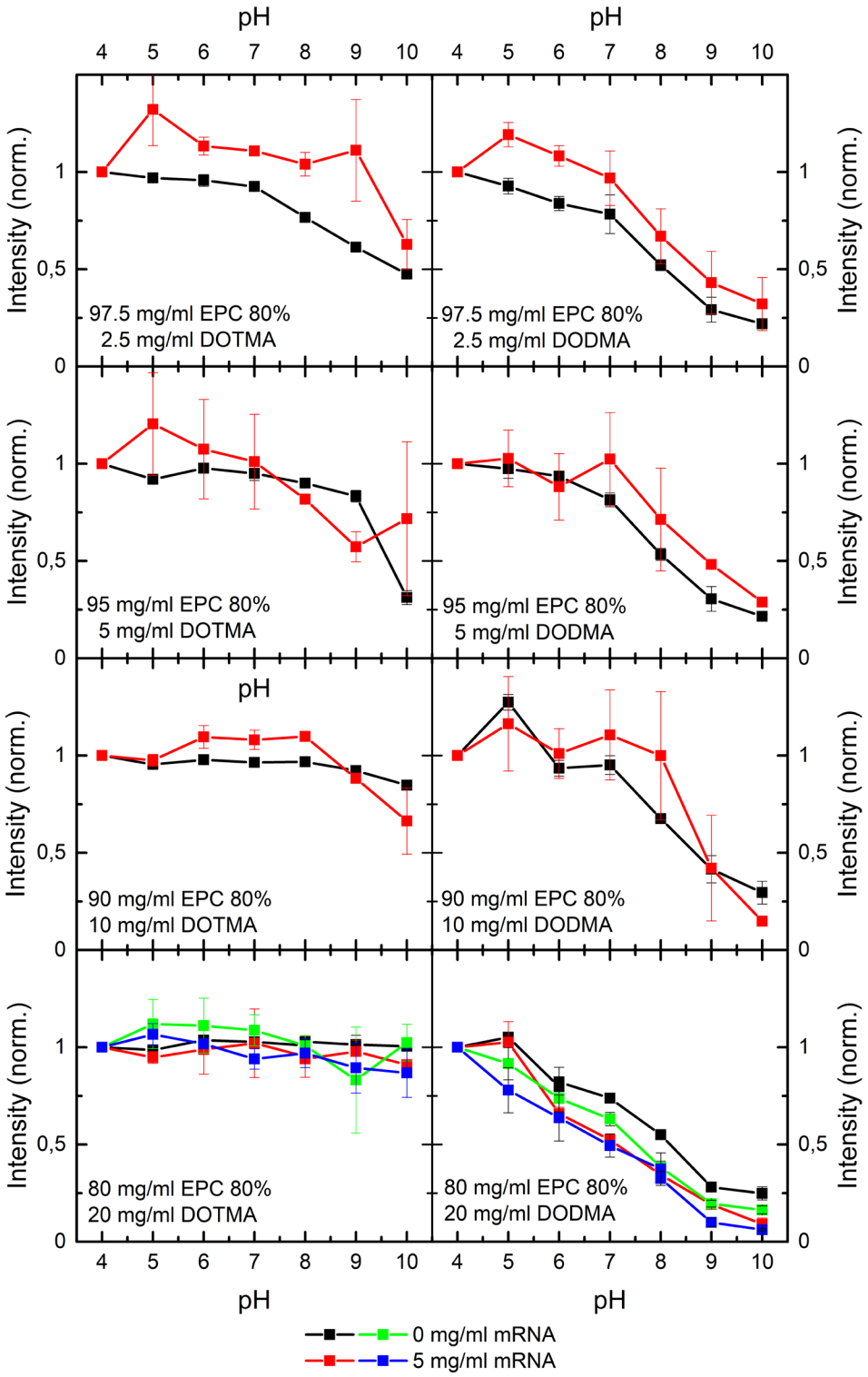

Figure 34: TNS assay of lipoplexes with EPC 80 %, different amounts of DOTMA or DODMA with or without mRNA (test conditions 2)

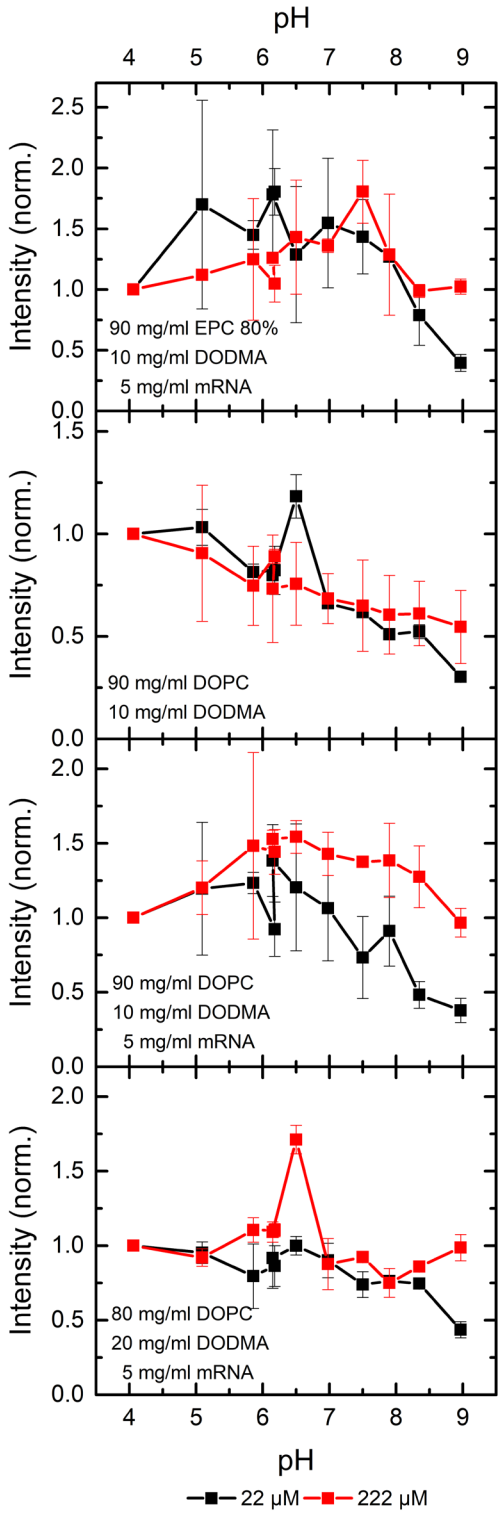

Figure 35: TNS assay of lipoplexes with DOPC, different amounts of DODMA with or without mRNA (test conditions 3)

The previous experiments focused on the total lipid concentration as basis for the calculation of added sample. Depending on the composition, this led to different amounts of ionizable or cationic lipid per well. The fluorescence is related to the amount of bound TNS which of course will be higher for more ionizable lipid. Then again, the fluorescence intensity is normalised. Hence, influence of the absolute amount of ionizable lipid was not clear. Therefore, next experiments were carried out with focus on the amount of ionizable lipid. Furthermore, EPC 80 % as base lipid was exchanged with DOPC. For comparison, one formulation still contained EPC 80 %. Influence of lipid concentration should be investigated as well. In addition to 22 µM, 222 µM as cationic lipid concentration was tested as well. Furthermore, buffers contained 150 mM of NaCl to mimic physiologic conditions. All samples were measured in duplicates. Results are presented in Fig. 35. The expected decrease of intensity with higher pH values was not as obvious as with the previous experiments. While formulation with EPC 80 % showed good results in previous experiments, a tendency of decrease was just slightly visible for 22 µM. A test with 222 µM led to no response. This phenomenon was also pronounced for all samples. In addition, high standard deviations impeded the evaluation.

Table 20 shows a summary of the conditions used in the experiments with the help of two different compositions. The calculation can be seen underneath with the composition of 50 mg/ml EPC 80 % and 50 mg/ml DODMA as an example (Table 21). All samples were calculated in the same way.

Table 20: Different test condition for TNS assay

#	Composition	Amount of formulation per 102 µl	Conc. of cationic lipid	Conc. of total lipid	Buffers
1	50 mg/ml EPC 80 %, 50 mg/ml DODMA	0.01616 µl	11.8 µM	22 µM	3 – 10, no NaCl
2	50 mg/ml EPC 80 %, 50 mg/ml DODMA	1.614 µl	1.18 mM	2.2 mM	4 – 10, no NaCl
	90 mg/ml EPC 80 %, 10 mg/ml DODMA	1.702 µl	250 µM	2.2 mM	4 – 10, no NaCl
3	90 mg/ml EPC 80 %, 10 mg/ml DODMA	0.1505 µl	22 µM	0.19 mM	4 – 9, 150 mM NaCl
	90 mg/ml EPC 80 %, 10 mg/ml DODMA	1.5 µl	220 µM	1.9 mM	4 – 9, 150 mM NaCl

Table 21: Calculation of formulation amounts needed for TNS assay

- 22 µM of lipid in 102 µl solution in 96-well plate correspond to 0.000022 mol/l
- 50 % EPC 80 % (MW = 768 g/mol) + 50 % DODMA (MW = 670.575 g/mol) result in an average MW of 719.288 g/mol
- 719.288 g/mol * 0.000022 mol/l = 0.0158 mg/ml lipid concentration
- 0.0158 mg = 1000 µl → 0.001616 mg of lipid in a well with 102 µl
- concentration of samples is 100 mg/ml → 0.01616 µl of formulation for one well (Stock solution: 1.616 µl of sample in 1000 µl of water = 0.1616 mg/ml)
- 0.01616 µl formulation correspond to 0.000808 mg DODMA (50 mg/ml per well
- 0.000808 mg in 102 µl → 0.00792 mg/ml
- 0.00792 mg/ml correspond to 0.0118 mmol/l (MW of DODMA: 670.575 g/mol)

Determination of pK_a

The pK_a represents the point with half of the maximum fluorescence and can be determined with the help of a sigmoidal fit (Boltzmann). Unfortunately, this fit converged just for the sample with 50 mg/ml DODMA. For the remaining formulations, the pK_a could only be determined manually at the normalised intensity of 50 %. In order to ensure comparability, all samples were evaluated in the same way.

The listed values in Table 22 highlight several dependencies. The pK_a was dependent on the amount of DODMA as higher properties shifted the pK_a to smaller values. Furthermore, the complexation of mRNA had an influence. As long as there was an excess of ionizable lipid over mRNA, there was a left shift of the pK_a. With equal amounts or excess of anionic charge, the pK_a values were shifted to higher values. The exchange of EPC 80 % with DOPC as base lipid led to different values. Finally, the influence of the test conditions has to be evaluated in detail. The pK_a of the formulation with 50 mg/ml DODMA fluctuated within one unit with different conditions. In contrast, the formulation with 10 mg/ml DODMA and 5 mg/ml mRNA were in the same range of pK_a although measurements were performed with and without addition of NaCl.

The determination of the pK_a for the formulations containing DOTMA was just possible for very few samples, as listed in Table 23. This was not surprising. Since DOTMA has a permanently charged headgroup, a variation in the pH must not change the lipid status.

The evaluated data showed quite high standard deviations. Hence, experiments need to be repeated under ideal conditions to proof the present results.

Table 22: pK_a values for lipoplexes with EPC 80 % or DOPC, different amounts of DODMA with or without mRNA (measured with the test conditions listed in Table 20)

Basis	DODMA [mg/ml]	mRNA [mg/ml]	pK_a
Test condition # 1			
EPC 80 %	0	0	- *
EPC 80 %	50	0	5.754
Test condition # 2			
EPC 80 %	50	0	6.729
EPC 80 %	50	5	6.065
EPC 80 %	20	0	8.179 / 7.544
EPC 80 %	20	5	7.142 / 6.997
EPC 80 %	10	0	7.9
EPC 80 %	10	5	8.502
EPC 80 %	5	0	8.136
EPC 80 %	5	5	8.904
EPC 80 %	2.5	0	8.085
EPC 80 %	2.5	5	8.687
Test condition # 3 (22 µM)			
DOPC	20	5	8.839
DOPC	10	0	8.396
DOPC	10	5	8.336
EPC 80 %	10	5	8.791

Table 23: pK_a values for lipoplexes with EPC 80 %, different amounts of DOTMA without mRNA (measured with the test conditions listed in Table 20)

Basis	DOTMA [mg/ml]	mRNA [mg/ml]	pK_a
Test condition # 2			
EPC 80 %	5	0	9.621
EPC 80 %	2.5	0	9.783

4.2.3 mRNA-release dependent structural changes

I. Investigation on structural changes with SAXS

After uptake into a cell, lipoplexes needs to be released out of the endosomes to have an effect. Since this release is crucial and formulations often end up being digested in the late endosome/lysosome, it has to be investigated more in detail. Furthermore, a change in the molecular structure of liposomal systems is necessary to facilitate this release. Therefore, measurements were done to investigate the structural changes after addition of heparin which mimic a cellular contact. Moreover, experiments were carried out at two different pH. pH 7.5 represented the condition around and inside the cell while pH 5 should mimic the acidic condition in the endosome. The experiments were carried out at the SAXS1 beamline at the LNLS in Campinas. Four different compositions were tested with either DOTMA or DODMA. Samples were mixed with the buffer and the adequate amount of heparin (fourfold excess of positive charge over the negative charge of the mRNA, neglecting the positive charge of the lipid). After mixing, samples were measured immediately which was around 60 to 90 sec and after 2.5, 5, 10 and 20 min. Some samples were also measured after 40 min. Due to time and sample limitations; this was not possible for all samples. Data was treated in the same ways as before.

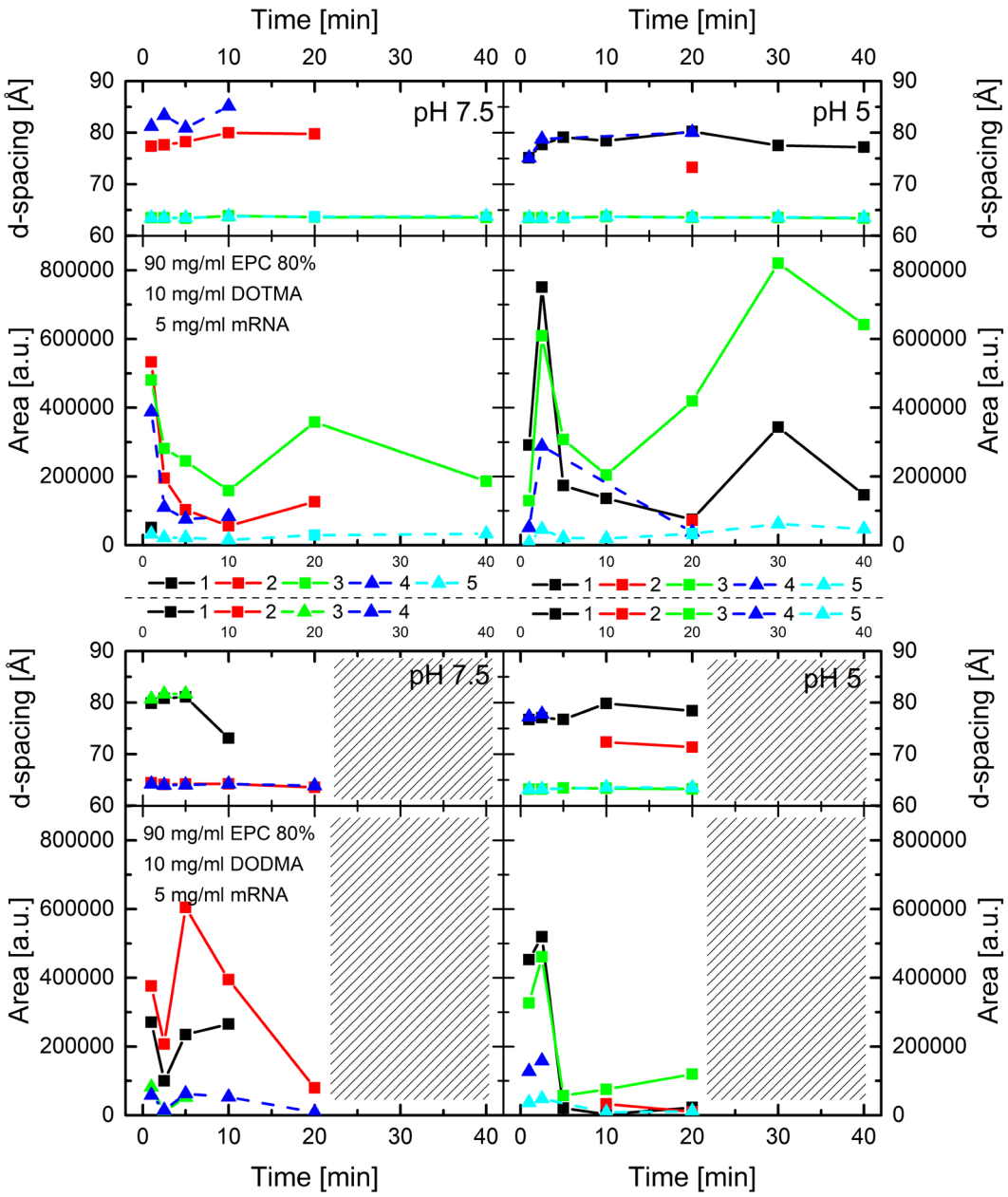

Figure 36: Peak analysis of lipoplexes with EPC 80 %, 10 mg/ml DOTMA or DODMA and 5 mg/ml mRNA after addition of heparin in pH 7.5 and 5

In Fig. 36, results of the first two samples with 10 mg/ml DOTMA [top] or DODMA [bottom] and 5 mg/ml mRNA are shown. Data of pH 7.5 is on the left, data of pH 5 on the right side. The formulation with DOTMA can be seen on the top. For both pH, there were two lamellar systems with two orders around 60 to 80 Å. Peak areas for the 1st order had comparable values at the beginning. During time, the proportion of the lamellar systems shifted which led to one dominating lamellar system while the other one disappeared. For pH 7.5, this shift happened faster since the 2nd order peak 4 disappeared after 10 and 1st order peak 2 after 20 min. In

addition, peak area of peak 2 decrease continuously. At the scattering curve, this peak was still visible, but it was too small to be fitted. In general, the decrease of the peak areas indicated a disintegration of the system. For pH 5, both lamellar systems existed until 40 min. Just one 2nd order peak disappeared after 20 min. The development of the peak areas underlined the shift since peak 3 increased while peak 1 decreased. Larger peak areas in comparison to pH 7.5 indicated stronger structures for this pH.

The sample with DODMA was just measured until 20 min which impeded a complete comparison. Two lamellar systems at the same range of d-spacing occurred. At pH 7.5, one lamellar order remained while peak 1 and 3 disappeared. Peak area of the dominating peak 2 got smaller as well which entailed a disintegration. Same happened for pH 5, but there were still two peaks at 70 and 80 Å. By a look at the scattering curve, these were no real peaks but part of a shoulder at the left side of the main peak. With the available data set, it is not possible to predict of the areas would increase after 20 min as it happened with the DOTMA sample at pH 5.

More samples with 10 mg/ml of DOTMA or DODMA but just 2.5 mg/ml of mRNA were measured and illustrated in Fig. 37. First, it is obvious that the peak distribution changed for the formulation with DOTMA. Above all, smaller peaks could not always be fitted that accurate as for the samples with higher amount of mRNA. The range of d-spacing enlarged from 60 to 130 Å with four lamellar systems at pH 5 and three at pH 7.5. At acidic pH, two systems dominated at the beginning whereas one increased and one decreased during time, observable also by the change of the areas of peak 3 and 4. Moreover, some of the structures disappeared completely (peak 1, 5, 6). Scattering curve at pH 5 showed, that the shift of the two main peaks happened in the same way. By a look at the peak area, it is not so obvious since areas change similar. This can be due to the broadness of peak 2.

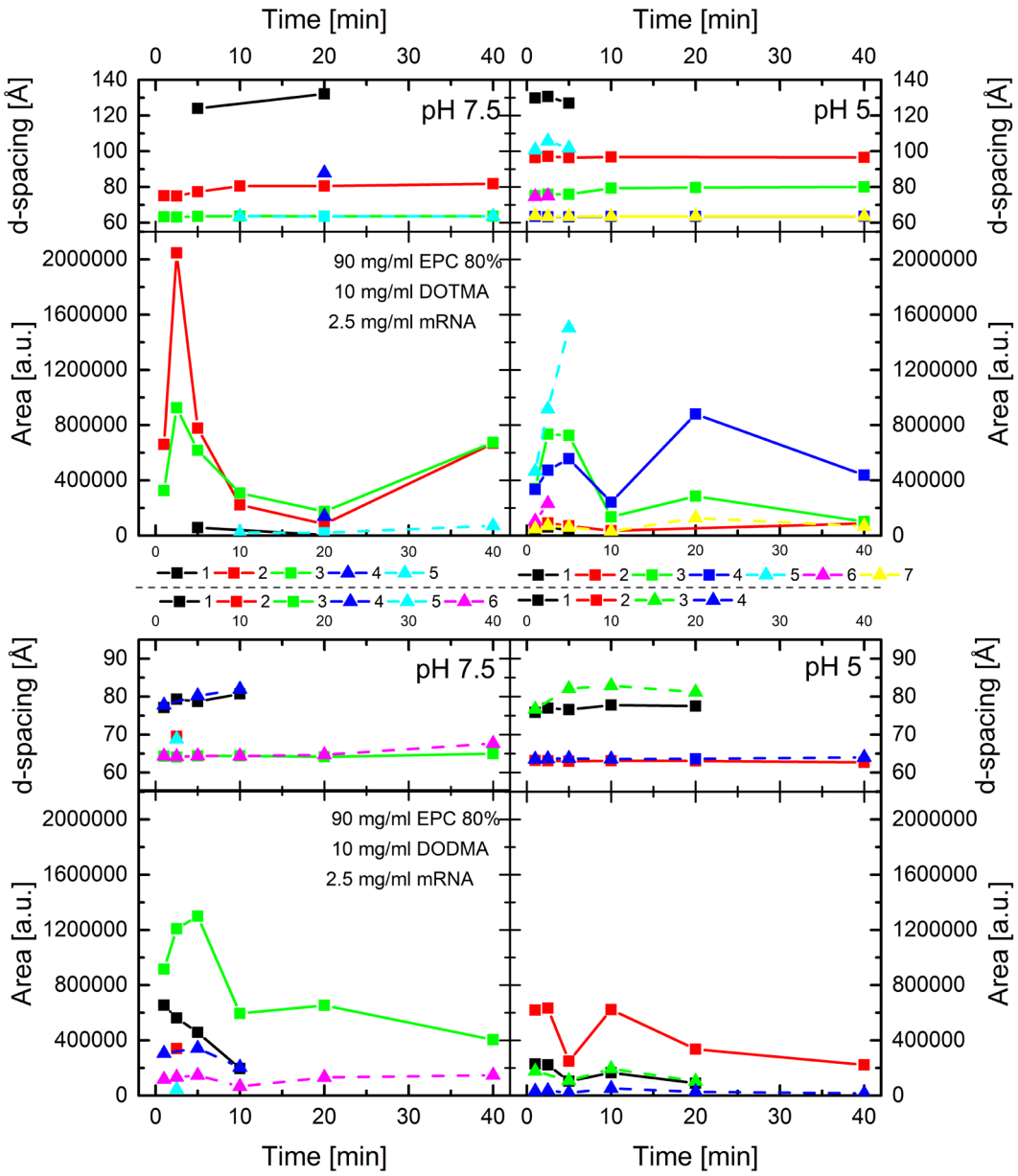

Figure 37: Peak analysis of lipoplexes with EPC 80 %, 10 mg/ml DOTMA or DODMA and 2.5 mg/ml mRNA after addition of heparin in pH 7.5 and 5

Same sample with DODMA showed a peak pattern which is more comparable to the samples with 5 mg/ml mRNA. Two lamellar systems around 60 to 80 Å occurred while one of them disappear after 20 min for both pH 5 and 7.5. Peak areas at pH 5 were slightly smaller than pH 7.5 and both indicated the disintegration of the lamellar structures.

With the next samples, illustrated in Fig. 38, the amount of DOTMA and DODMA was lowered to 5 mg/ml with 5 mg/ml mRNA. In general, scattering curves indicated, that the peaks of the 1st order were not separated. The range of d-spacing was slightly higher and ranged from 60 to 90 Å, whereas there was also one peak at 120 Å for the DOTMA formulation at pH 5.

For the lipoplexes with DOTMA, three lamellar systems occurred over the whole time while the peak around 75 Å had no 2nd order. This peak was much lower than the two surrounding ones but had a much larger area after 20 min. One dominating systems at the beginning, resulted in three quite consistent peaks which was underlined by the peak area (see peak 2, 3, 5). The peak pattern for pH 7.5 did not differ from the acidic pH. The scattering curve demonstrated again a shift in the dominating lamellar system, which could be seen for both 1st and 2nd order. Area of peak 1 and 3 were similar but drifted apart during time.

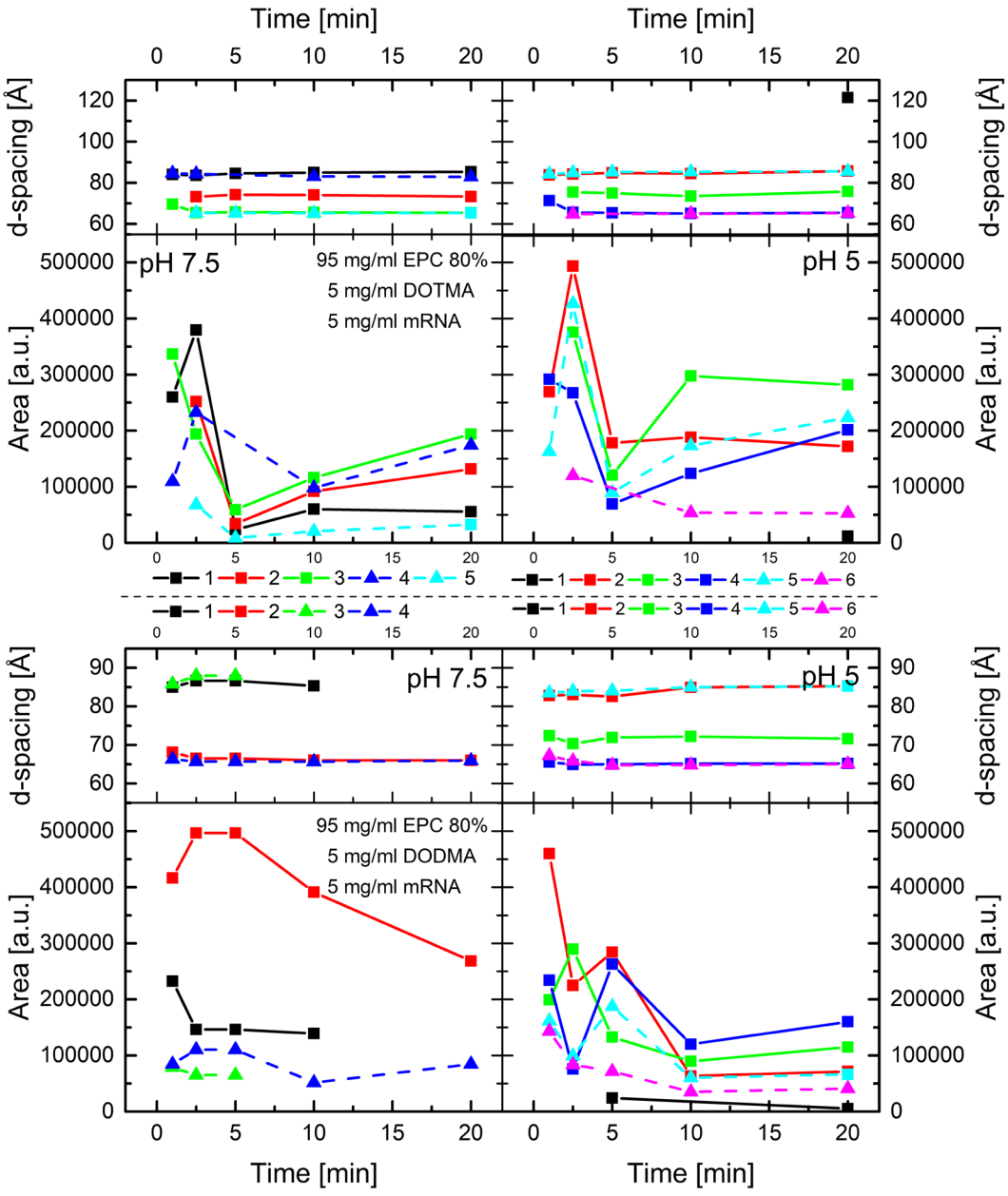

Figure 38: Peak analysis of lipoplexes with EPC 80 %, 5 mg/ml DOTMA or DODMA and 5 mg/ml mRNA after addition of heparin in pH 7.5 and 5

The same composition but with DODMA showed clear differences between pH 7.5 and 5. For pH 5, two lamellar systems with 1st and 2nd order (around 65 and 82 Å) and one lamellar system in between at around 72 Å remained over the whole 20 min. One dominating system at the beginning, changed to three consistent systems after 20 min. The course of peak areas stressed this as well. By mixing this sample with pH 7.5, just two lamellar systems occurred where just one remained. Furthermore, peak area indicated a much larger 1st order peak in comparison to the other three peaks. Summing up, the diagram of the DODMA sample at pH 5 is comparable to the DOTMA sample both at pH 7.5 and 5.

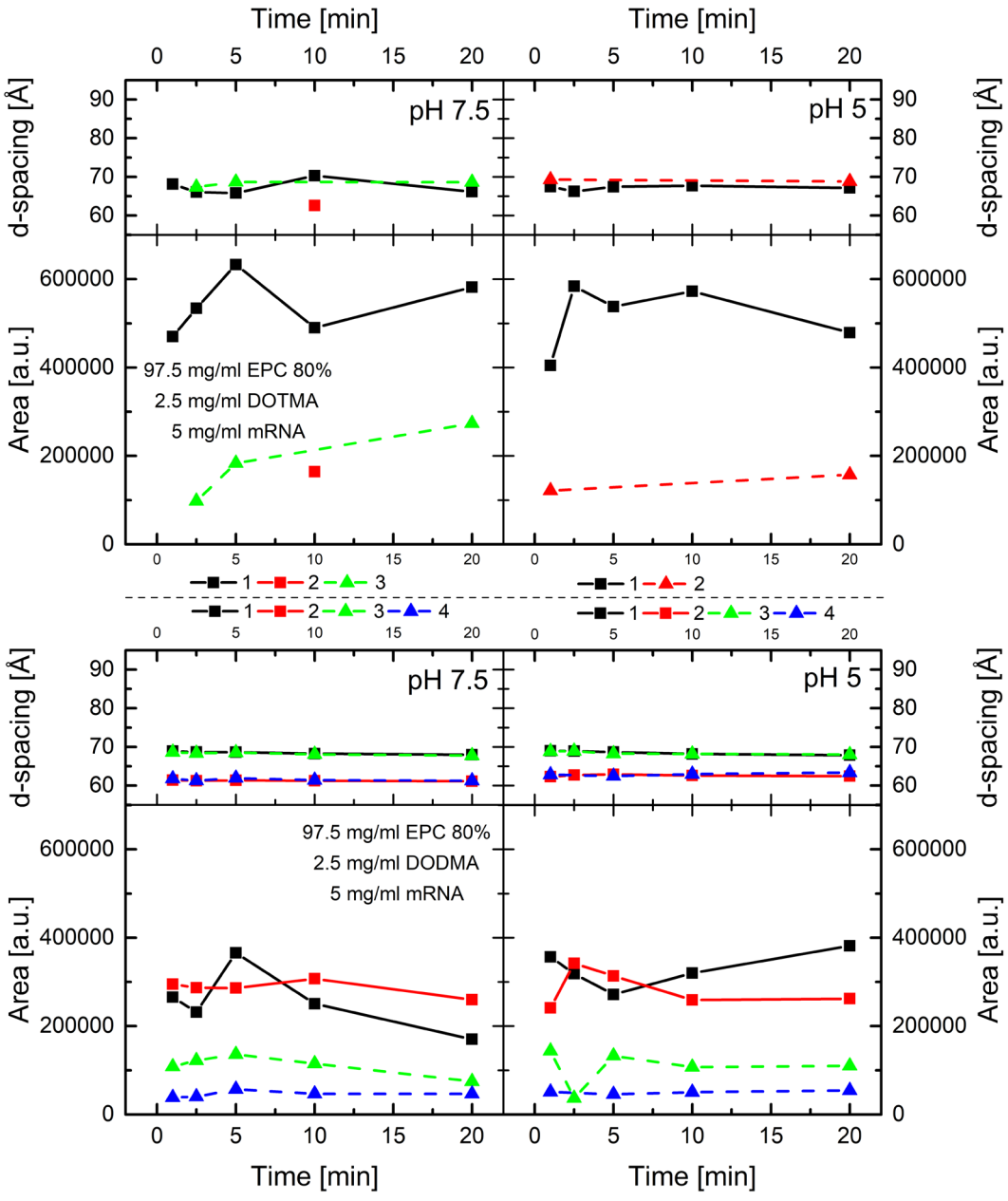

Figure 39: Peak analysis of lipoplexes with EPC 80 %, 2.5 mg/ml DOTMA or DODMA and 5 mg/ml mRNA after addition of heparin in pH 7.5 and 5

The amount of DOTMA or DODMA was again reduced to 2.5 mg/ml with a mRNA concentration of 5 mg/ml. Data are shown in Fig. 39. The lipid structures were really reduced within these samples. For both pH values, the formulation with DOTMA had just one lamellar system which remained constant during the time. The 2nd order always remained but could not be fitted for all data points. As expected, 1st order peak had a much larger area. The peaks were even broader at pH 7.5 with a slight tendency for peak splitting after 10 min.

The sample with DODMA showed two lamellar systems in a smaller range of d-spacing (60 to 70 Å), which did not change in position or area during the time. The scattering curves revealed a huge peak splitting into two peaks at the top. This splitting was more pronounced at pH 7.5. In general, DODMA samples formed more accurate peaks than the DOTMA samples.

II. Investigation of mRNA release

In parallel to the SAXS studies concerning the structural changes, the RiboGreen® Assay was used to investigate the release of mRNA after a cellular trigger. Two formulations with 90 mg/ml EPC 80 %, 2.5 mg/ml mRNA and 10 mg/ml of either DOTMA or DODMA were prepared as explained earlier. Samples were mixed with a buffer of pH 5 and an appropriate amount of heparin or DOPG (fivefold excess of positive charge over the negative charge of the mRNA, neglecting the positive charge of the lipid) and the resulting amount of free mRNA was detected at several time points after mixing. The formulation containing DODMA was tested over 120 min, while the lipoplex with DOTMA was tested twice over shorter intervals. Results are shown in Fig. 40. The amount of free mRNA at neutral pH and without the addition of heparin was set as starting point. Around 5 % of the added amount was determined as free which is quite low and in line with similar experiments performed with lipoplexes composed of DOPC and DOTAP. After imitation of cellular contact by adding heparin or DOPG, an increase of free mRNA was observed. Heparin led to a higher release up to 18 % of the added amount of mRNA for both samples while the addition of DOPG just led to a doubling of the free mRNA.

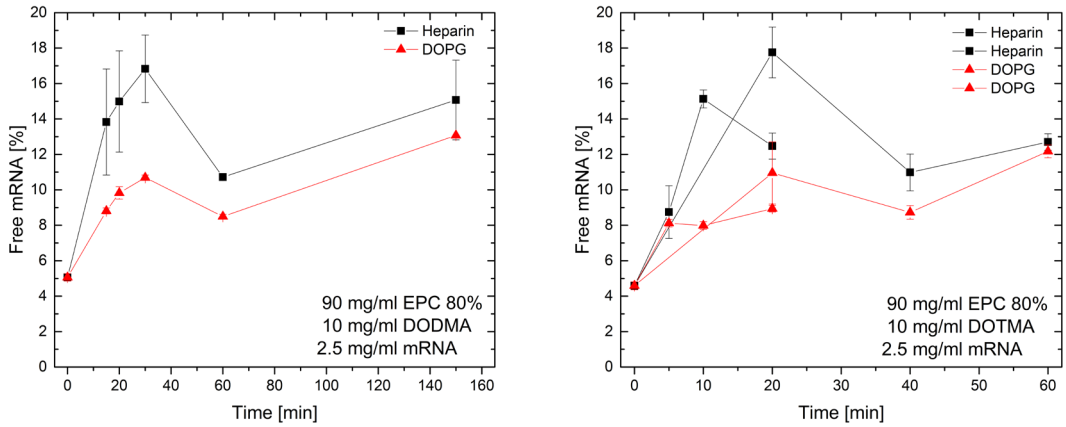

Figure 40: mRNA release out of lipoplexes with EPC 80 %, 10 mg/ml DOTMA or DODMA and 2.5 mg/ml mRNA after addition of heparin or DOPG

4.3 DNA-lipoplexes

As explained earlier, mRNA has several advantages over DNA. Despite, the usage of DNA for vaccination or related strategies is still common. Therefore, lipid systems were also utilised for the encapsulation of plasmid DNA (pDNA). The influence of several cationic or ionizable lipids, also in presence of DOPE, was investigated: DOTAP, DC-Chol, Didodecyl dimethylammonium bromide (DDAB), DOTMA and DODMA. Lipoplexes were composed of either 80 mol% EPC 100 % and 20 mol% of cationic or ionizable lipid or 60 mol% EPC 100 %, 20 mol% cationic or ionizable lipids and 20 mol% DOPE with 1 mg/ml of pDNA. For preparation, DAC was applied as described earlier.

4.3.1 Characterisation of lipoplexes with different cationic lipids

Determination of size and zeta potential was used for characterisation. Results are shown in Figs. 41 and 42. Except for DODMA, size was nearly 200 nm with a PDI ranging from 0.2 to 0.3. Slight changes occurred with the addition of DOPE. Lipoplexes composed of EPC 100 % and DODMA had a size of 600 nm which decreased to 400 nm with the addition of DOPE. PDI changed from 1 to 0.6 through the presence of DOPE. Zeta potential was positive for all formulations. The combination of EPC 100 % and DOTAP showed the highest value around 50 mV while EPC 100 %, DC-Chol and DOPE achieved the smallest potential with nearly 25 mV. In general, zeta potential was lower for the formulations with DOPE. Just in the case of DODMA, it was the opposite.

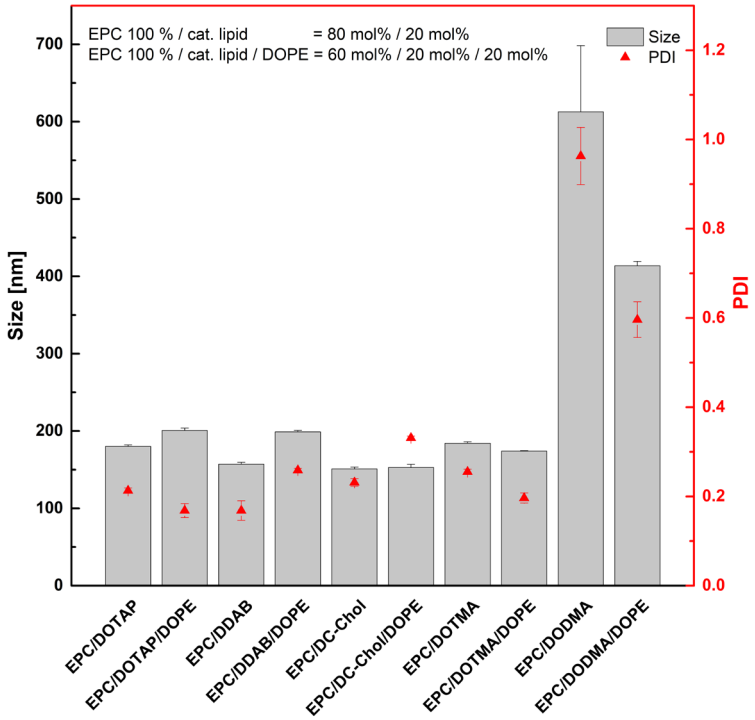

Figure 41: Size distribution of lipoplexes with EPC 100 %, different cationic or ionizable lipids with or without DOPE

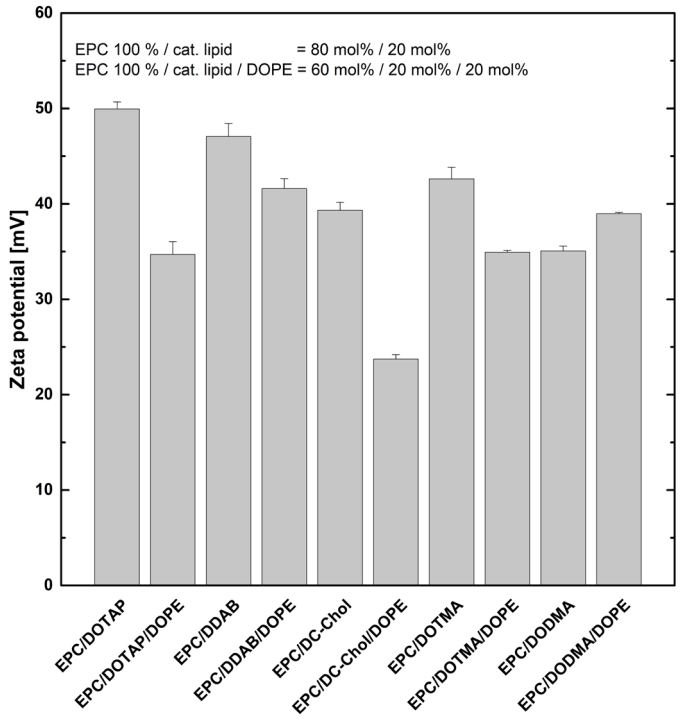

Figure 42: Zeta potential of lipoplexes with EPC 100 %, different cationic or ionizable lipids with or without DOPE

4.3.2 Transfection efficiency in DC2.4

The result of the transfection experiments with DC2.4 is depicted in Fig. 43. Transfection efficiency differed depending on the composition. Best transfection was caused by the positive control jetPEI® as none of the samples reach 100 % of transfection. Formulations with DOTAP, DC-Cholesterol and DDAB showed no significant effects. The formulations with DOTMA and DODMA caused a significant increase in the uptake in comparison to free DNA. The formulation with DOTMA and DOPE did not reach a significantly higher uptake than DOTMA without DOPE, while the formulation with DODMA and DOPE showed even higher uptake rates. Consequently, formulation with DODMA and DOPE was selected for further experiments.

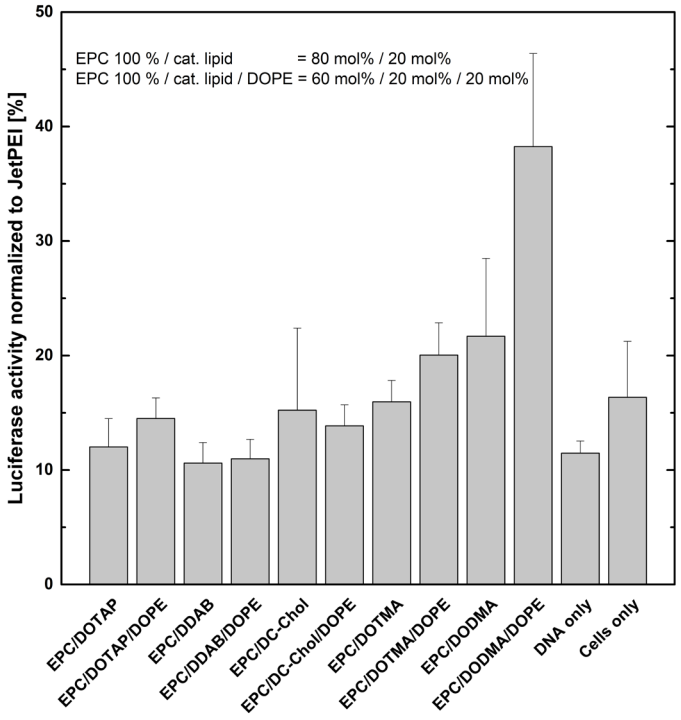

Figure 43: Transfection efficiency of lipoplexes with EPC 100 %, different cationic or ionizable lipids with or without DOPE

4.3.3 Lipoplexes for transport of combined DNA vaccines

In the human body, two main types of T-cells with different functions exist. The $CD8^+$ cells, so-called cytotoxic T-cells, recognise infected cells after protein presentation of DCs and eliminate these. The $CD4^+$ cells, so-called t-helper cells, release cytokines that affects the cellular, but also the humoral immune response. To investigate the effect of both cell types separately,

transgenic OTI ($CD8^+$) and OTII ($CD4^+$) mice were used. Since $CD8^+$ cells are most important for the antitumour response, differentiation between proliferations of both types is necessary.

Data is shown in Fig. 44. Comparing the different lipoplexes in OTI-cells, soluble OVA-protein together with the DNA of IκB kinase-β (IKK) showed higher efficiency than LPS with DNA coding for OVA. Two explanations are possible. Either IKK is a better activator than LPS or the intracellular production of OVA out of the DNA limit the effect of presentation followed by a lower immune response. Signal was highest for the combined application of the soluble forms of OVA and LPS. Since proteins do not have to localise in the nucleus for transcription and afterwards be translated, this result is not surprising. In OTII-cells, the highest signal was higher than any signal for OTI-cells. In general, $CD4^+$ cells show a more unspecific presentation of proteins, which explains this phenomenon. Again, the combined application of OVA-protein and LPS showed a higher efficiency compared to OVA encoding DNA in lipoplex with LPS. Furthermore, LPS had nearly no influence on the efficiency of OVA in lipoplexes. Surprisingly, the best effect could be seen for the lipoplex with IKK in combination with soluble OVA. For $CD4^+$ cells, IKK seemed to be a better DC-activator than LPS, even though it had to be transcripted and translated in DCs. Application of only IKK showed a low immune response for OTI- and OTII-cells, since there was no protein available for presentation on the cell surface.

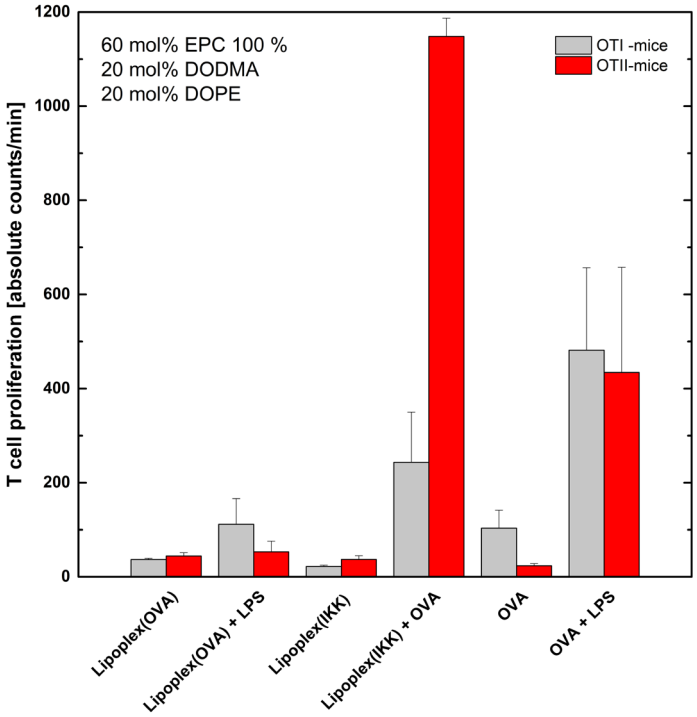

Figure 44: T-cell proliferation after transfection of DCs with different proteins and DNA in lipoplexes composed of 60 mol% EPC 100 %, 20 mol% DODMA and 20 mol% DOPE

5 Discussion

Cancer is one of the most common cause of death worldwide. The current first-line therapies often entail adverse side effects and in addition, the high diversity of tumour cells lowers the therapeutic success. Within the research on alternative and more personalised therapeutic options, nucleic acids such as mRNA or DNA have gained much interest in the last years. The nuclei acids encode for proteins that target structures which are specifically expressed on tumour cells. Thus, the healthy cells are less effected and severe side effects can be lowered. Using tumour vaccination as a therapeutic option, the immune system is trained to find and combat against tumour cells on its own. Thus, even small metastases which are difficult to localise with the current methods can be accessible.

Although the application of naked mRNA or DNA is currently applied successfully, drug delivery systems offer several benefits. Depending on the properties of the vehicle, the nucleic acids can be encapsulated for protection and selective transport to various targets in the body. A huge number of different particles, mostly in the nanosized range, are available and investigated intensively. Lipid-based nanocarriers constitute one option. Beside LNPs or micelles, lipoplexes show a great advance in the delivery of e.g. mRNA for therapeutic approaches. Lipoplexes normally consist of a zwitterionic base lipid and a cationic lipid which complex the anionic nucleic acid. A cationic charge is also necessary to facilitate a binding to the negatively charged cell membrane [169] so that particles are uptaken via endocytosis. [90,170] Unfortunately, just small amounts of the uptaken mRNA show a therapeutic effect because large amounts are trapped in the endosome. After uptake into the cell, nanoparticles are transported via endosome which gets more acidic during time due to the uptake of protons like H^+ via an energy-dependent proton pump. With the stage of late endosome or lysosome, nanoparticles will be destroyed. Hence, an endosomal release of the mRNA is crucial for a successful delivery. Cationic lipids have shown to favour this endosomal release by destabilisation of the endosomal membrane. [171–173]

As part of a drug delivery system, cationic lipids have three different functions which improve the transport and therapeutic effect of nucleic acids. In order to find the appropriate composition for the respective application, a detailed characterisation of formulations composed of cationic lipids and nucleic acids is required. In addition, a better understanding of the behaviour after application into the human body as well as at the point of action is needed.

5.1 mRNA-lipoplexes with cationic lipids

Partial results of the presented work have been published in: Ziller, A.; Nogueira, S. S.; Huehn, E.; Funari, S. S.; Brezesinski, G.; Hartmann, H.; Sahin, U.; Haas, H.; Langguth, P. Incorporation of mRNA in Lamellar Lipid Matrices for Parenteral Administration. Mol. Pharm. ***2017****, acs.molpharmaceut.7b01022.* [150]

For these studies, mRNA was incorporated into high concentrated lipid-based membrane systems for local administration. As zwitterionic base lipid, DOPC was chosen. For complexation of the negatively charged mRNA, cationic DOTAP as a commonly known transfection reagent was used. As mentioned earlier, DOPC forms only lamellar bilayers so that dissociation of the lipoplexes does not happen. [100] Furthermore, it does not fuse with the endosomal membrane. [90] Hence, it was possible to investigate solely the influence of DOTAP on the uptake of the mRNA. Several different compositions were assembled to gain detailed information on the molecular structure. Formulations were prepared with an excess of either cationic lipid or negatively charged mRNA to widen the portfolio of lipoplexes with different characteristics for various applications.

5.1.1. Development of a structural model

The aim of these experiments was the controlled insertion of mRNA into highly-concentrated lipid matrices as well as a controlled release of mRNA at the point of action. For the insertion of the mRNA, the lipid film method was used. Afterwards, the insertion was proven with several experimental techniques. The amount of free mRNA was determined to investigate to which extend the mRNA is bound to the cationic lipid surface. The zeta potential was measured to define the overall charge. In addition, it can be used as an indicator for the stability of the formulation. SAXS was applied to obtain information on the structural assembly of the lipid layers. Using DSC, the phase transition temperature was measured to determine in which way the DOTAP is inserted in the DOPC matrix. As an indicator for the stability, it can be used to evaluate if the inserted mRNA disturbs the bond of the lipid membrane. For one composition, cryo-TEM pictures were taken to support the findings. The release of mRNA out of lipoplexes and hence, the functionality of the systems was demonstrated in cell culture experiments. Summary of all data led to the development of a concise model which explains the insertion of mRNA in the lipid bilayers (Fig. 45). As already mentioned earlier, the exact

position of the mRNA could just be assumed and not proven with the named methods. Therefore, SANS experiments were performed additionally.

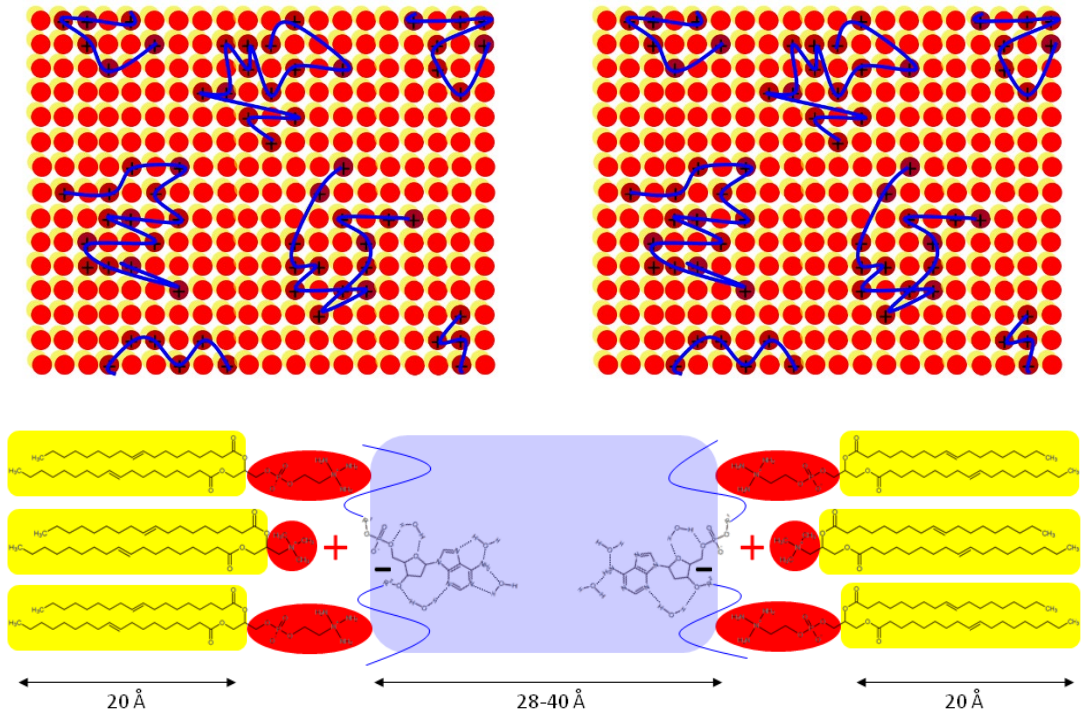

Figure 45: Lattice model (top view) of lipid layers illustrating the tentative organisation of mRNA at the lipid layer [top] and side view of a lipid bilayer illustrating the insertion of a DOTAP molecule and a nucleotide into the lipid membrane [bottom] (drawn after [150])

Structural changes between the individual samples could be observed by attractive or repulsive effects due to electrostatic interactions between the components. First of all, it could be shown that DOTAP was inserted homogenously into the DOPC matric. This is indicated by the monotonous increase of the phase transition temperature with higher fractions of DOTAP (Ch. 4.1.3). If there had been a phase separation, phase transition would have taken place at the temperature of pure DOPC. Phase separation is an often observed phenomenon when mixing two different lipids [174,175], which can be induced by e.g. polycationic ions [176] or peptides or proteins. [177] In contrast, mRNA does not induce such a phase separation between DOPC and DOTAP.

Furthermore, the influence of the electrostatic interactions on the structure is indicated by the enormous increase of the d-spacing, which led to a loss of correlation between the bilayers. Repulsive forces between the positive charges in the membranes after incorporation of

DOTAP can be named as a reason for that. In addition, the zeta potential changed from negative for pure DOPC to positive for the DOPC/DOTAP matrix (Ch. 4.1.2).

If mRNA is present, systems with pure DOPC remain unchanged as it could be indicated by the d-spacing in the SAXS experiments (Ch. 4.1.1). This phenomenon could be explained by electrostatic interactions occurring between the charged moieties in the membranes. Lipids are amphiphilic molecules and self-assemble to bilayers while they are in contact with water. Although EPC 80 % and DOPC have cationic headgroups, they do not interact with the negatively charged mRNA because of their zwitterionic character. Consequently, there is no structural change in liposomes of these pure neutral lipids with or without mRNA. After incorporation of DOTAP, the presence of positively charged headgroup results in repulsion between the membranes and leads to a strongly extended d-spacing. In the presence of mRNA, the negative charge in the aqueous space between the membranes compensates the positive charge of DOTAP and shield the electrostatic repulsion. Consequently, d-spacing decrease and the lamellar structure is recovered.

In case of the mixed lipid membranes, DOTAP acts as an anchor for the mRNA. 1/1 to 2/1 was figured out to be the stoichiometric ratio between the positive DOTAP and the negative mRNA. Furthermore, the N/P ratio of DOTAP to mRNA was significant for the properties of the different formulations. On the one hand, there are lipoplexes with an excess of DOTAP and a N/P ratio higher than 1/1. These lipoplexes showed lamellar structures which are comparable to the lipoplexes of pure DOPC. The incorporation of mRNA into the lipid membranes lead to a strong decrease in the d-spacing compared to formulations with DOPC and DOTAP. Hence, the negative mRNA is possible to compensate the repulsive interactions due to DOTAP in opposing membranes even in the presence of an excess of DOTAP with respect to mRNA. For these lipoplexes, the mRNA is completely inserted into the lipid membranes and bound to the DOTAP molecules. As shown in Ch. 4.1.2, the zeta potential is positive for all of these formulations which prove as well that the mRNA is inserted completely without any contact to the outer surface of the lipoplexes. In addition, no free mRNA could be detected. Hence, the mRNA can be encapsulated without any influence on the distance between the bilayers.

In contrast, some lipoplexes were prepared with an excess of mRNA and a resulting N/P ratio lower than 1/1. First, the amount of free mRNA increased which shows that not all of the mRNA is bound to the DOTAP molecules. In addition, zeta potential switched to negative values which means that mRNA is also located in the surrounding medium. Nevertheless, at

least a part of the excess mRNA seems to be inserted between the bilayer since the d-spacing increased with higher amounts of mRNA (Fig. 15). Nevertheless, as it can be derived from the following calculation, the mRNA can only account for a small fraction of the hydrophilic slab between the lipid bilayers:

For all systems containing DOPC and DOTAP, the d-spacing is between 70 and 80 Å. Pure, dehydrated DOPC-MLV have a d-spacing of 40 Å, so that the water layer between the lamellae is 20 Å. The highest fraction of DOTAP was 10 mol%. With an estimated area per lipid of around 75 $Å^2$ [178], the hydrophilic volume of DOTAP can be calculated as:

$$75\ Å^2 * 10 * \frac{40\ Å}{2} = 15000\ Å^3$$

Equation 10: Available volume for a nucleotide when binding to one DOTAP molecule

using 75 $Å^2$ as the area per lipid, 40 Å as the d-spacing of dehydrated DOPC and the factor 2 since two bilayers always share one hydrophilic slab. Factor 10 is used because one DOTAP molecule corresponds to nine DOPC molecules. A mRNA nucleotide binds just to DOTAP headgroups whereby the area of the DOTAP and the DOPC molecules can be occupied by one nucleotide. The results for different fractions of DOTAP are listed in Table 24.

Table 24: Calculated volume fraction of the mRNA in the aqueous slab for different amounts of DOTAP (taken from [150])

Fraction DOTAP [mol%]	Area per DOTAP [$Å^2$]	Water slab volume / DOTAP (20 Å)	Volume fraction of nucleotide [%] *
2.5	3000	60000	2.5
5	1500	30000	5
10	750	15000	10

*(available volume per nucleotide about 15000 $Å^3$)

In addition, the volume of a nucleotide can be calculated as:

$$\frac{330\ \frac{g}{mol}}{1{,}5\ \frac{g}{cm^3}} * 10^{24}\ \frac{Å^3}{cm^3} \Big/ 6 * 10^{23}\ \frac{1}{mol} = \frac{367\ Å^3}{Molecule}$$

Equation 11: Required volume of one nucleotide

330 g/mol is the molar mass of one average nucleotide and 1.5 g/cm^3 the density of the mRNA. 10^{24} presents the conversion factor from cm^3 to Å^3 since 1 cm^3 is equal to 10^{24} Å^3. Finally, division with the Avogadro constant leads to the volume which is needed per molecule.

When comparing both values, the volume of one nucleotide is less than 10 % of the total available volume. Consequently, the mRNA in the bilayer is surrounded by a large excess of water. The mRNA is probably oriented flat on the surface of one bilayer forming clusters of negative charge which interacts with the positive charge of the DOTAP molecules. Furthermore, there seems to be no connection of two bilayers via the mRNA strand since the hydrophilic slab in between is about 20 Å and one nucleotide is just about 5 Å.

SANS was applied to prove the developed structural model. Unfortunately, the performed measurements are not sufficient to clarify the exact position of the mRNA (Ch. 4.1.6). The high content of trehalose, needed to stabilise the samples, hinders a complete evaluation of the current data. Nevertheless, first conclusions can be drawn. Differences in the peak distribution between the samples with low (2.5 mol%) and high (10 mol%) mRNA can be seen (Fig. 22). Nevertheless, evaluation seems to be easier for the sample with 10 mol% mRNA since data is more reasonable. In addition, the membrane span of the lipoplexes is larger in comparison to pure DOPC/DOTAP membranes (Table 16), so that the expected position of the mRNA on top of each bilayer side seems to be likely.

Apart from that, SANS measurements revealed another interesting result. With the addition of the high content of trehalose, the d-spacing of the membranes changed depending on the composition of the sample. While pure DOPC led to smaller d-spacings, samples composed of DOTAP and mRNA showed larger d-spacings with existing trehalose (Fig. 26). Such an increase in the d-spacing after addition of trehalose was also recently shown by Al-Ayoubi et al.[179] using lipid bilayers composed of dimyristoyl-phosphatidylcholine (DMPC). Trehalose concentrations up to 0.7 M increased the d-spacing. [179] A decrease of van der Waals attraction

forces between the lipid bilayers are named as a reason for that. [180] Al-Ayoubi et al. [179] applied trehalose concentrations (0.15 to 1.4 M) comparable to the ones used in this thesis (0.27 and 1.31 M) and, among other things, SAXS pattern was investigated. A low amount of trehalose (0.15 M) showed a broadening of the Bragg peaks indicating a loss of the multilamellar structure while high contents of trehalose (1.1 to 1.4 M) led to a peak splitting in the gel phase. In addition, an inhomogeneous distribution of trehalose in the intermembrane water space which leads to the formation of coexistence regions is discussed. Regions with trehalose clusters having a high concentration result in a larger d-spacing in comparison to regions with a lower trehalose content. [179] Although the study of Al-Ayoubi et al. [179] is not completely comparable to the experiments performed in this thesis, the shown influence of trehalose on the properties of the lipid bilayers underlines the importance of a deeper investigation on trehalose-containing lipoplexes.

As in many pharmaceutical applications, trehalose was added as a cryoprotector if lyophilisation is necessary to achieve a long-term sample stability. Due to this property, several studies were performed to understand the mechanism. With the addition of trehalose to a vesicular formulation, an osmotic pressure appears. In addition, simulations revealed a stabilisation due to a replacement of water in the region of the lipid headgroup. Concentration was higher at the bilayer surface than in the bulk of the water phase. [181–183] A study performed in 2014 by Kent et al.[184] led to contrary results. Using SANS, a Gaussian distribution of trehalose with a higher concentration in the centre was found. The interaction of trehalose with the lipid headgroups was low. In contrast to earlier studies, these experiments were performed in a dehydrated state with multiple membranes instead. Earlier studies [181–183] were mainly performed with highly hydrated single layers of SUV and LUV while the study from 2014 [184] used dehydrated multiple layers which is more comparable to the actual system of highly viscous lipoplexes. The distribution of trehalose is dependent on the concentration. At low concentrations, sugars interact more with the lipid headgroups while at higher concentrations, some molecules are located in the centre of the water gap. [185]

Taking all these facts into consideration, the shown phenomenon of the trehalose has to be investigated more deeply since the influence of trehalose on the lipoplexes was not completely clear. In some of the experiments, differences between 0.27 and 1.31 M were visible and in others not. In addition, mRNA interacts with the lipid headgroups and hence, can act as a competitor of trehalose. Hence, also the presence of mRNA with different concentrations needs to be taken into consideration. Further experiments have to be performed to clarify the

insertion of the mRNA in the lipid bilayers and to model the different effects on the membrane structure indicated by the d-spacing below and above the charge equilibrium. In addition, the effect of trehalose on the lipid membranes has to be investigated more deeply at pharmaceutically realistic high concentration. Therefore, small-angle neutron scattering with its possibility for contrast variation is a suitable method.

5.1.2. Comparison with lipoplexes for transport of other nucleic acids

mRNA is one type of nucleic acids which can be incorporated in lipoplexes. In the past, more focus was on DNA and several methods were used for characterisation like SAXS [113,114,186] or freeze fraction electron microscopy. [187–189] The lamellar organisation is often found, which is, in accordance with a mathematical model applied by Dan et al.[190], also the most probable structure due to its high stability. [190] Nevertheless, the hexagonal H_{II} phase could be found as well. Some lipids like DOPE prefer this structure due to their shape so that the stability can even be higher than with the lamellar organisation. [191] In hexagonal systems, one DNA strand is surrounded by a monolayer of lipids which lead to the formation of cylindrical micelles. A monolayer of coated DNA cannot exist in solution, so by the interaction of the lipid layer with adjacent lipid layers, the structures connect among each other building a hexagonal lattice ("honeycomb"). [58,192] The void in such a micelle has a diameter of around 28 Å, which is again sufficient for embedding a DNA strand with two hydration shells. [112] Spaghetti-like structures were formed out of supercoiled DNA coated with a lipid bilayer and a total diameter of around 130 Å. This structure was just visible with monovalent cationic lipids and also dependent on the ratio of DC-Chol:DOPE (1/4 to 3/2), while higher amounts of DOPE formed non-bilayer structures like the honeycomb. [188,193] Furthermore, these structures seemed to be just marginally stable and always attached to larger liposomal aggregates. [191] Ewert et al.[194] described another structure in 2006. Polycationic lipids with 3 to 5 charges alone normally form micelles due to the size of the headgroup whereas they form lamellae in presence of DNA. Here, a formulation with 20 mol% of a synthesised lipid with a highly charged and hyperbranched headgroup led to a lamellar phase which was in coexistence with tubular micelles arranged in a hexagonal lattice. The interaxial distance of the micelles was about 81.5 Å. DNA rods were embedded in the interstices of the micelles. Since the diameter of micelles is about 41 Å, there was enough space for the DNA (25 to 30 Å) in between. [194] A comparable structure was already found in 1992 by Ghirlando et al.[195] whereby the micelles were formed out of surfactants instead of lipids. [195]

siRNA is another often used nucleic acid. Bouxsein et al.[196] prepared lipoplexes with DOTAP, DOPE and DOPC similar as described earlier for the DNA-lipoplexes. Combination of DOTAP and DOPE led to lamellar structures with low amounts of DOPE and to hexagonal structures with higher amounts of DOPE. Lipoplexes composed of DOTAP and DOPC showed lamellar structures with a membrane spacing of around 55 Å for a large proportion of DOTAP. With increasing amounts of DOPC, spacing increased first continuously and then rapidly for high proportions. This phenomenon was explained as a "pinched" lamellar phase. Locally enriched regions of DOTAP are formed and build an anchor for the siRNA. Domains rich in DOPC containing large pockets of water are located between domains rich in DOTAP which are pinched electrostatically by the siRNA. [196] Such pinched lamellar phases were also observed for complexes composed of the anionic polypeptide poly-L-glutamic acid (PGA), the neutral lipid dilauroyl-sn-glycero-phosphocholine (DLPC) mixed with the cationic lipid didodecyl dimethylammonium bromide (DDAB). [197]

Obviously, several structural organisations occur depending on the composition of the formulation. For a proper comparison, it is necessary to compare the mRNA-lipoplexes to DNA or siRNA-lipoplexes with the same lipid composition. Several studies performed similar structural investigations on DNA-lipoplexes with DOPC and DOTAP. [112–114] In general, SAXS data revealed multilayer structures with intercalated DNA in between the lipid membranes for these compositions. Lipoplexes showed the same peak distribution applied concentrated and diluted. First of these measurements were presented by Rädler et al.[113] in 1997. Lipoplexes were prepared by mixing a liposomal suspension (25 mg/ml) with a DNA solution (5 mg/ml). Different L/D ratios (L=DOPC+DOTAP (1/1), D=DNA) were tested. For low DNA concentrations (L/D=50), globules around 1 μm were visible. With the increase of the DNA concentration, first chainlike structure (L/D=10) and larger aggregates (L/D=5) appeared. For L/D=2 with an excess of DNA, size of the complexes decreased again due to repulsion. Zeta potential showed a positive charge for L/D higher than 5 and a negative value for L/D lower than 5. D-spacing remained stable for different lipid to DNA (L/D) ratios around 65.1 ± 2 Å. With 39 Å for the thickness of the lipid bilayer, the water gap was determined to be 26.1 ± 2.5 Å. A monolayer of DNA including the hydration layer is said to have a diameter of 20 Å so that the water gab is just sufficient for one DNA layer. In addition to the Bragg peaks, an intermediate peak caused by the DNA-interaxial spacing appeared (d_{DNA}). While the spacing caused by the lipid membrane remained constant, the d_{DNA} was around 35 Å for L/D lower than 5 and 46 Å for L/D higher than 5. An excess of either liposomes (L/D>5) or DNA (L/D<5) is a possible explanation for this phenomenon. [113] Based on this work,

Koltover et al.[112] showed a similar d-spacing of 66.84 Å for the same formulations. [112] Instead of changing the DNA concentration, Salditt et al.[114] varied the ratio of DOPC to DOTAP while keeping the ratio of DOTAP:DNA = 2.2 to ensure charge neutrality of all tested samples. With the increase of DOPC from a lipid mass ratio of 0 to 3, lamellar spacing increased from 57.8 to 70.3 Å while the interhelical spacing of the DNA increased from 26 to 54 Å. Lipid dilution led to an increase of both spacings due to an excess of lipids. [114]

DNA-lipoplexes are studied much more extensively [112–114,118,168,198], but similarities to mRNA-lipoplexes studied in this thesis can already be seen. Both systems form lamellar structures which were affected by the composition. With higher amounts of DOPC, d-spacing of mRNA-lipoplexes increased. A possible explanation is lower electrostatic interactions between the cationic DOTAP and the anionic nucleic acids. This dilution effect occurred for lipoplexes with siRNA as well. In accordance with the developed structural model, the phenomenon of a pinched lamellar phase seems not to be likely because it was assumed that there is no connection between opposing membranes. Furthermore, Schiessel et al.[199] explained the pinching effect for rigid polyanions which would not be applicable for mRNA. [199] Nevertheless, it cannot be excluded completely.

However, distinct differences have to be considered for the design of dedicated delivery systems for mRNA. Like DNA, mRNA phases were organised lamellar with the mRNA sandwiched in the hydrophobic slab in between adjacent lipid bilayers. Differences can be seen in the detailed internal organisation of the mRNA in between the bilayers. Since mRNA is single-stranded, it has a much lower secondary order than the double-stranded DNA which makes it more like a classical polyelectrolyte binding to a lipid membrane. [200] This higher secondary order of DNA caused the interhelical spacing and led to intermediate peaks in the scattering curves, which did not occur for mRNA or siRNA. Increasing amounts of DNA led to larger d-spacings while d-spacing of DNA-lipoplexes remained constant over a range of DNA concentrations. Instead, the interhelical spacing of the DNA rods decreased with more DNA which seemed to be logical due to higher packing because of less available space between the lipid bilayers. In mRNA-lipoplexes with DOPC and DOTAP, d-spacing increases with more mRNA as soon as there is an excess of mRNA (Fig. 15). A lack of available space is not likely to be the reason for that since d-spacing of pure DOPC-lipoplexes remained stable even with high amounts of mRNA. With pure DOPC, mRNA just floats in between the lipid membranes and is not attached to it because a cationic anchor is missing. With the introduction of DOTAP

as an anchor, mRNA is attached to one side of the membrane. The cationic charge is compensated by the corresponding amount of mRNA while the excess of anionic charge of the mRNA strand led to electrostatic repulsion between the lipid bilayers. In contrast, an excess of DOTAP over mRNA led to the same d-spacing as for pure DOPC. A small amount of mRNA is necessary to shield the cationic charge of DOTAP.

In contrast to many earlier studies using DNA or siRNA, only low fractions of mRNA were inserted into the hydrophilic slabs in a controlled manner since the used lipid matrix was highly concentrated. With the help of formulation parameters like N/P ratio or molar fraction of the cationic lipid, this insertion can be adjusted precisely. For DNA, it was possible to achieve an extensive insight into coherencies between the molecular organisation and formulation parameters could be obtained over the last years. [201–204] Further studies on the systems comprising mRNA are needed to clarify these correlations in comparison to the earlier studied systems. The insight and ability for accurate assembly of these delivery vehicles will be helpful for the rational development of novel mRNA nanomedicines.

5.2 mRNA-lipoplexes with ionizable lipids

Cationic lipids are associated with toxic effects which is due to different reasons. After application into the bloodstream, positive charge can lead to aggregation due to attachment of components like proteins on the surface of the particles forming a protein corona.[205] The surface properties are modified which lead to a prolonged blood circulation combined with the inhibition of the selective transport. At worst, huge aggregates can cause thrombosis since size can increase dramatically. The focus of this works was a local administration so that this problem could be neglected. Degradation of the lipids represents another drawback. Depending on their structure, some lipids like DOTMA are not biodegradable due to their ether as linker structure which can lead to an accumulation. In contrast, some structures like DOTAP with an esther as linkage structure are not stable enough so that a premature degradation is possible. [65] Despite all these drawbacks, cationic charged lipids are requisite for a cellular uptake and endosomal release. [173,206–208] Ionizable lipids offer a possibility to overcome this hurdle. Depending on the pH, such lipids can be both neutral or positively charged. At a pH around 7.4, the lipid is mainly neutral while it becomes cationic with an acidic pH. Consequently, the problem of aggregation could be avoided while the positive charge necessary for the endosomal release is still available. For evaluation of the potency of ionizable lipids, the ionizable lipid

DODMA and the corresponding permanently charged lipid DOTMA was formulated in lipoplexes and the investigated concerning their molecular organisation.

5.2.1 pH-dependent structural changes

First SAXS experiments (Ch. 4.1.1-I) were performed to evaluate whether there are differences in the molecular structure of lipoplexes upon incorporating a permanently charged or an ionizable lipid. Pure EPC 80 % was tested to ensure a pH-independent behaviour of the base lipid which could have been proven. Just a slight decrease of the d-spacing of one lamellar system occurred which is likely due to the composition of EPC 80 %. Besides 80 to 85 % of PC, there are around 7 to 9.5% of phosphatidylethanolamine (PE) and 2 to 3 % sphingomyelins in this lipid mixture. The remaining 5 to 10 % consist of other phospholipids, triglycerides and minor components like cholesterol. Due to its natural origin, the composition can vary within different batches. This variation is also a possible explanation for the different peak appearance. When testing the ionizable lipids, pure EPC 80 % formed double peaks in SAXS (Ch. 8.1-I), whereas for the measurement of DOTAP as cationic lipid, EPC 80 % just showed single peaks (Fig. 14 [top left]). These double peaks appeared not only for pure EPC 80 % but also for the formulations with DOTMA or DODMA. Two lamellar systems which to some extent just varied slightly in their properties existed in parallel.

Interestingly, EPC 80 % membrane behaviour differed after incorporation of DOTMA in comparison to DOTAP. A mixed membrane of EPC 80 % and DOTAP led to a loss of structure indicated by individual bilayer scattering (form factor) (Fig. 14 [top left]). With the incorporation of DOTMA, the lamellar system remained although the scattering peaks were less distinct as with pure EPC 80 % (Ch. 8.1-I with 0 mol% mRNA). An explanation for this phenomenon has to be found. DOTMA and DOTAP just differ in the linkage structure. The formulation of pure EPC 80 % with mRNA and either DOTAP or DOTMA demonstrated comparable bilayer properties. d-spacing was in the same range and showed the same dependency. With an increase of cationic lipid, the distance between the bilayers decreased and with a higher content of mRNA, the d-spacing increased. Therefore, the varied structure of the linkage should not cause the above-mentioned variation. A possible explanation is the buffer. The samples with DOTAP were prepared in trehalose buffer and contained no salts which would otherwise compensate the charge of the cationic headgroups. Consequently, the strong membrane repulsion led to this loss of structure. The lipoplexes for the experiments with the ionizable lipids were prepared in a buffer containing EDTA and HEPES. The emerging ions

could operate as counterions to the cationic headgroups and hence, weaken the electrostatic repulsion between the lipid bilayers. After incorporation of mRNA, the effect of the buffer is negligible due to a higher charge of the nucleic acids.

With higher content of cationic lipid, the systems achieved a more distinct order as indicated by four single peaks (Ch. 8.1-I). For DOTMA, this distinct order was visible for both pH values due to the permanent charge. Lipoplexes with DODMA just formed such a distinct order at pH 5. Despite, formulations with DODMA did not behave like pure EPC 80 % membranes. It can be assumed, that DODMA is not completely uncharged at pH 7.5 so that low electrostatic interactions changed the scattering pattern in comparison to pure EPC 80 %. As expected, ionisation of DODMA changed dramatically at pH 5 leading to a similar scattering profile compared to samples with DOTMA. Nevertheless, slight differences like less orders of the DODMA systems compared to DOTMA are obvious. An incomplete ionisation of the headgroups at pH 5 seems logical if the expected pK_a of DODMA incorporated into a lipid membrane is between 6 and 7. Hence, the protonation of DODMA is not completely comparable to DOTMA at pH 5. The values for the d-spacing confirm this assumption. Formulations with DOTMA showed always slightly larger spacings in comparison to the same composition with DODMA, which can be explained with stronger repulsive forces due to a higher degree of protonation.

Until now, only few studies focused either on the structural organisation of lipoplexes containing ionizable lipids or their pH dependent behaviour. In 2004, Li et al.[209] investigated the influence of DODMA on the structure of dipalmitoleoylphosphatidylethanolamine (DPOPE) membranes. Already 2 mol% of DODMA induced the transition from L_α to H_{II} phase which happens due to interactions between the positive charge of the amino group of DODMA and the negative charge of the phosphate group of DPOPE. [209] Such a transition was not visible for the lipoplexes composed of DODMA, DOTMA or even DOTAP. This can be due to the different base lipids since PC and PE membranes differ in their lipid shape and hence, in their preferred structure. In comparison to DOPE, DOPC hinders cationic lipids to induce a non-bilayer structure. [96]

5.2.2 Determination of pK_a

For the application of ionizable lipids, a detailed investigation of this pH-dependent behaviour is necessary. The pK_a value is defined as the point where half of the molecules are charged and hence, represents a suitable parameter for the transition from mostly neutral to cationic.

The study of Jayaraman et al.[148] mentioned earlier in 1.4.5, shows that the pK_a is an essential parameter for the efficiency of formulations with ionizable lipids like DODMA. Hence, determination seems reasonable to achieve a predictive indicator for the *in vitro* and *in vivo* activity. Jeffs et al.[101] reported a pK_a of 6.8 for DODMA incorporated into a lipid bilayer composed of Chol/DSPC/DODMA/PEG-S-DSG (55/20/5/10 mol%) [101] while Heyes et al.[147] measured a surface pK_a of 7.0 for stabilised nucleic acid lipid particles (SNALP) composed of DSPC/Chol/PEG-C-DMA/DODMA (20/48/2/30 mol%). [147]

pK_a determination of the pure ionizable lipid makes only limited sense since it is normally applied in combination with other lipids. This raises the question whether the properties of the ionizable lipid remain or change under the influence of other components. Additionally, mRNA bound to the ionizable lipid must be taken into consideration as well. These questions were answered already by Pierrat and Lebeau [149] in 2015. Several ionizable compounds with varying headgroups were synthesised and tested. A formulation with DOPC and 10 mol% of an ionizable compound resulted in a pK_a of 7.01 [149], whereas the same percentage of this ionizable lipid led to a pK_a of 6.58 in combination with EggPC and cholesterol. [210] In addition, a complexation of DNA (N/P=3) caused a left shift with a decrease of the pK_a from 8.25 for the pure liposomes composed of DOPC and 10 mol% of another synthesised ionizable lipid to 7.44 for the lipoplexes. This could be due to changes in the lipid arrangement or a less easily protonation of the ionizable lipid due to the electrostatic interactions with the DNA. [149]

The suitability of the TNS assay was proven by Pierrat and Lebeau [149] who showed an influence of the composition and the encapsulation on the pK_a of the ionizable lipid as mentioned already above. Moreover, the ionisation was dependent on the concentration. An increase of the ionizable lipid from 10 mol% to 90 mol% led to a decrease of the pK_a from 7 to 4.88 what can be explained with stronger repulsive forces due to shorter distances between the ionizable headgroups. This is also a suitable explanation for the drop of the pK_a from 6.84 to 5.67 after exchanging DOPC with DPPC. For DOPC, the surface per molecule is larger (0.57 nm^2) in comparison to DPPC (0.41 nm^2) which leads to a shorter mean distance between to ionizable

headgroups and results in stronger repulsion. In contrast, the addition of NaCl to the test medium just led to negligible changes in the pK_a. [149]

The mentioned studies proofed, that the composition of the lipid bilayer, as well as the complexation with nucleic acids, has an influence on the ionisation of the ionizable lipid. Hence, the pK_a needs to be evaluated for the different compositions.

At the moment, there are no available studies on the pK_a determination of mRNA-lipoplexes with DODMA as ionizable lipid, so the actual data can just be compared with formulations containing siRNA or DNA. The measured pK_a value of the present study had several dependencies as it was mentioned in earlier studies before. [101,147,149] Higher amounts of DODMA led to a shift of the pK_a to lower values as is was also shown by Pierrat and Lebeau. [149] The more ionizable headgroups are incorporated into the lipid membrane, the more difficult it gets to ionise each headgroup and a higher hydrogen ion concentration is needed. Changing the base lipid from EPC 80 % to DOPC decreased the pK_a from 8.791 to 8.336.

Comparable to DNA, the complexation of mRNA in this thesis caused a left shift of the pK_a as long if there is an excess of ionizable lipid (Table 22). Possibly, protonation of the free remaining headgroups of DODMA is impeded due to the local attachment of mRNA to the lipid membrane. Surprisingly, equal or higher amounts of mRNA led to a higher pK_a. This would mean that TNS is able to replace mRNA out of the electrostatic interaction with DODMA. The left shift of the pK_a for samples with an excess of ionizable lipid does not necessarily indicate this replacement. Mutual impairment or structural changes like higher d-spacing due to a higher content of mRNA could lead to a more easy excess of TNS to the membrane surface. Nevetherless, this phenomenon was just tested with lower amounts of DODMA where higher standard deviations were observed. Hence, these experiments need to be repeated with higher amounts of ionizable lipids to achieve better certainty of results.

Finally, test conditions may not be neglected but their influence is not completely clear until now. 10 % DODMA with 5 % mRNA led to similar pK_a values when tested with 250 µM of ionizable lipid per well (8.502) and with 22 µM of ionizable lipid with the addition of 150 mM NaCl (8.791). In contrast to 50 % DODMA, the pK_a value changed intensively from 5.754 when testing 11.8 µM to 6.729 after application of 250 µM of ionizable lipid per well.

In addition to the TNS assay, SAXS measurements were used to determine the pK_a as well (Table 18). The previous experiments revealed structural differences of formulations containing DODMA at pH 7.5 and 5. The change is caused by a higher grade of protonation.

The pK_a can be interpreted as a point of structural transition since 50 % of the headgroups are charged when reaching this pH.

SAXS data underlined a dependency on the composition of the lipoplexes. For the samples with EPC 80 % as base lipid, a distinct transition was justed visible for 10 % DODMA and 10 % mRNA. At pH 6, peaks got lost and two lamellar systems fused together forming one new lamellar system as indicated by the d-spacing and the peak area. Lower amounts of DODMA and/or mRNA showed a gradual transition where structures disappear in the acidic pH between 5.5. and 4.5. Using the TNS assay, the formulation with 10 % DODMA and 5 % mRNA revealed a pK_a of 8.5. This pH was not tested with SAXS but it is unlikely, that there would be structural changes at an alkaline pH.

Previous studies discovered that a higher content of DODMA is necessary to achieve a highly ordered system (Ch. 8.1-I). The same applies to the pH-dependent transition. Although lamellae can also be formed solely by base lipids like EPC 80 % or DOPC, charges are necessary to achieve a pH-dependent response. In addition to the content of the ionizable lipid, the mRNA concentration may not be neglected as there were also differences of samples between 5 and 10 % mRNA. Finally, the interplay between the anionic and cationic charges constitutes the driving forces for the structural changes of the membranes due to pH variations.

The replacement of EPC 80 % (Ch. 4.2.1.-I) by DOPC (Ch. 4.2.1.-II) led to lipoplexes with a higher order of structure. Furthermore, the data underline the contribution of the mRNA to the formation of the lamellar system. The formulation without mRNA shows broad SAXS peaks at acidic pH due to electrostatic repulsion between the bilayers whereas this phenomenon does not occur if mRNA was present. The transition of these systems was characterised by a peak fusion which occurred at higher pH values in comparison to samples with EPC 80 % (Table 22). The formulation with 10 % DODMA showed fusion at pH 7 while peaks of the sample with 20 % DODMA fused slightly earlier. Using the TNS assay, the determined pK_a values of the identical samples were a bit higher but showed the same tendency. 20 % DODMA had a pK_a of 8.839 and both samples with 10 % DODMA a pK_a around 8.3. to 8.4. These results are in contrast to the TNS data of lipoplexes with EPC 80 %, where higher content of DODMA led to lower pK_a values.

Summing up, the molecular structure of the lipoplexes differed with a varied pH while this change was dependent on composition or test conditions. The expected pK_a of DODMA containing formulations is between 6 and 7 which was also proven in earlier studies. [101,147] The

TNS assay revealed pK_a values between up to 8.9 which seem to be way too high. A pK_a higher than 7 would result in a stronger protonation of DODMA after application in the bloodstream so that there will not be any advantages over DOTMA. The same can be applied for the high pK_a values for the formulations with DOPC determined by SAXS. Nevertheless, the scattering data of the EPC 80 %-containing lipoplexes showed that the transition of the lamellar system can also take place in the desired pH range.

In addition to the TNS assay, other methods like the incorporation of a pH-responsive membrane label can also be used to determine the pK_a. First experiments with the fluorescent lipid 1,2-dioleoyl-sn-glycero-3-phosphoethanolamine-N-(carboxyfluorescein) (PE-CF) were performed. Since the dye is covalently bound to a lipid, correct location is assured. Carboxyfluorescein is a hydrophilic molecule so that it will not interact with the lipophilic part of the membrane but reflect only the changes in the hydrophilic area close to the bilayer [211,212]. PE-CF was incorporated into the lipid film with a concentration of 0.1 % of total lipid concentration. Samples were treated the same way as with the TNS assay and fluorescence intensity was measured afterwards. Due to protonation, fluorescence differs depending on the pH. Unfortunately, the signal was too low for an analysis so that the concentration needs to be higher to obtain the desired results.

5.2.3 Release dependent structural changes

For further characterisation of the lipoplex formulations, it is important to evaluate the pH dependeny of the ionizable lipids. Moreover, it is necessary to understand their behaviour after cellular contact. In conventional cell experiments, structural properties cannot be determined. Therefore, cellular contact has to be mimicked within the experiments allowing a suitable characterisation. For these studies, SAXS was used again and the cellular contact was mimicked with the addition of heparin as depicted in Figs. 36 to 39. [95,213] Samples mixed with the appropriate amount of heparin were measured time-dependent in pH 7.5 and pH 5 to investigate their behaviour at cellular contact and in the endosome.

In additional experiments, the release of mRNA after mixing with an acidic pH buffer and heparin was tested (Fig. 40). DOPG was tested in comparison since anionic lipids or liposomes are also used for mimicking cellular contact. Although the test conditions were slightly changed in comparison with the scattering experiments, the outcome can be used for first orientation. An increase of free mRNA was visible over time but, with a maximum of 18 % of the added

mRNA, it was lower than expected. However, mRNA was released and, probably, the low amounts of mRNA are enough to induce endosomal release and effective translation. The starting point was determined at neutral pH, so mRNA release could also be triggered by the acidic pH. Therefore, it has to be evaluated if the acidic pH, heparin or the combination of both is needed. Nevertheless, lowering the pH leads to protonation of DODMA which would cause an electrostatic interaction with the mRNA. Hence, stronger binding to the lipid membrane is more likely than a release of the mRNA. In addition, release could also be shown for the DOTMA-containing formulation. The pH should not have a large influence on permanently charged lipids. Presumably, the pH buffer alone cannot cause a release of mRNA out of the lipoplexes.

Some findings from the previous studies could be confirmed. Higher amounts of cationic or ionizable lipid, as well as mRNA, are necessary to achieve a highly structured lamellar system. This was characterised by a lower amount of coexisting lamellar systems and more single and pronounced SAXS peaks. Furthermore, evaluation of broader peaks, which arise for formulations with a low amount of cationic lipid, can affect the analysis and have to treated with caution. Structural changes were characterised by the loss of lamellar systems and varying SAXS peak areas which indicate expansion or reduction of one system. Interestingly, membrane d-spacing only changed slightly over time. A sufficient amount of cationic lipid was also necessary for a response to the addition of heparin. Samples with 2.5 % DOTMA or DODMA showed nearly no change over time.

The data showed that the lipoplexes containing DOTMA behaved similarly when mixed at pH 7.5 and 5. The present lamellar systems remained over time and just changed in their proportion as indicated by the SAXS peak areas. Slight differences in the peak pattern occurred only for the formulation with 10 % DOTMA and 2.5 % mRNA. It was to be expected, that DOTMA-containing formulations behave similarly since the pH is supposed to have no influence on the protonation of the headgroup. Nevertheless, slight differences arose and indicated more stable lipoplexes at pH 5. Probably, the higher amount of free protons interact as well with the anionic nucleotides connected to the lipid membrane and hence, stabilise the whole system by changing the electrostatic interactions between the lipid bilayers. Furthermore, interactions between the free protons and the negatively charged heparin, leading to lower impact of heparin, cannot be excluded.

The formulations with DODMA showed more variations between neutral and acidic pH which can be seen for 5 % DODMA and 5 % mRNA. Whereas just one lamellar system

remained over the whole time for pH 7.5, three systems occurred for pH 5. The SAXS peak pattern at pH 5 was comparable to the pattern of the same sample with DOTMA at neutral and acidic pH. This was to be expected since the headgroup of DODMA is protonated at pH 5 and DODMA should act like DOTMA. At pH 7.5, DODMA is nearly uncharged and is supposed to act more like a pure EPC 80 % membrane. However, the present lamellar systems with additional d-spacings around 80 to 90 Å do not occur for pure EPC 80 % membranes as shown earlier (Fig. 27). Hence, DODMA has also an influence at neutral pH which can be due to some already protonated headgroups. Nevertheless, the described phenomenon is not clearly visible for all compositions. Moreover, the samples with 10 % DODMA have smaller peak areas for both pH values which indicate lower amounts of ordered structures in comparison to DOTMA-containing lipoplexes. Consequently, the properties of DODMA at pH 5 cannot be compared completely with the properties of DOTMA. The same results were also found earlier in these studies.

After cellular uptake of lipoplexes, cationic lipids mix with the anionic lipids of the endosomal membrane, form ion pairs and hence, mRNA is released (Fig. 6). The formation of the ion pairs is accompanied by the formation of inverse hexagonal structures. [96] Unfortunately, such lipid structures could not be found in the experiments. The addition of heparin led to changed d-spacings and loss of lamellar structures but not to an inversion to other lipid structures. Heparin mimics cellular contact due to its high negative charge. Nevertheless, negatively charged lipids for the formation of ion pairs were not present. This can be a reason for the lack of inversion. Hence, the addition of negatively charged lipids through membrane mimicking liposomes (MML: PC/PE/PS/cholesterol of 45/20/20/15 w/w) [214] or pure DOPG would be a possibility to test if the inversion takes place if negative lipids are present. First release tests with DOPG have already been performed, but further experiments with SAXS and SANS are reasonable.

Summing up, heparin induced changes in the molecular organisation of the samples, but these changes were different than expected. Presumably, an anionic trigger and the acidic buffer is necessary to induce a release. Despite, the impact of both factors has to be investigated separately as well.

5.3 DNA-lipoplexes

The herein applied lipoplexes are aimed as drug delivery system for a personalised immunotherapy. However, most of the presented studies focused on the characterisation of the lipoplexes instead of the biological functionality. In this context, lipoplexes with similar compositions incorporating DNA were prepared to investigate their vaccination potential. Instead of the lipid film method, samples were prepared with the DAC as a new technique. Since APCs play a major role for the antigen-specific primary immune response [215], DCs were used instead of C2C12 murine myoblasts.

DAC facilitates RNase- and DNase-free conditions together with very small batch sizes in a simple and fast manner. [216] Hence, it supports the suitability of lipoplexes for individual immunotherapy. EPC 100 % was used together with different cationic lipids. Lipoplexes had a defined size and zeta potential (Fig. 41 and 42) and showed transfection in DCs depending on their composition (Fig. 43). The compositions with DODMA led to larger vesicles. One possible explanation can be the absence of electrostatic interactions due to low protonation of DODMA at neutral pH, although this is conflicting with the high zeta potential values for these compositions. A similar behaviour occurred for lipoplex with DC-Chol. Because it is a tertiary amine like DODMA, a lower potential due to less protonation would have been expected. Zuidam and Barenholz [217] found out, that DC-Chol in a 1:1 with DOPE is just protonated 50 %. [218] This is also reflected by the decrease of zeta potential after addition of DOPE. Large particles are said to have higher transfection efficiency as shown by several studies [133–135,137,138,219,220], although the highest transfection was not caused by the largest particles in the present study. Probably, the combination of size and composition resulted in the better transfection.

DOPE is said to be necessary for a successful transfection and hence, investigated intensively to find the most effective composition. [95,98,100] For lipoplexes composed of DC-Chol and DOPE, effective ratios were 3/2 and 1/1 while 1/2 worked even better. [221,222] In the present study, the addition of DOPE just led to minor changes in characteristic as well as transfection efficiency (Figs. 41 to 43), although the ratio of 1/1 was applied. Probably, the absolute amount of cationic lipid and DOPE was too low since both components represented just 40 mol% of the entire formulation. In the above named studies with the tested ratios of 3/2 to 1/2, DOPE and DC-Chol were used without the addition of a base lipid. [221,222] At least the combination of DODMA and DOPE resulted in higher activity which can be explained through an interplay

between the fusogenic properties of DOPE, the lower toxicity of DODMA due to lower protonation and the larger size of the vesicles. For a better estimation of the transfection activity, lipofectamine can be used as a positive control since jetPEI® as a polyethylenimine derivative cannot be completely compared to lipid-based formulations. Finally, it was shown that lipoplexes increase the uptake of DNA into cells, while the choice of cationic lipid as well as the addition of DOPE influences this uptake.

Transfecting APCs is a prerequisite for a successful therapy, but it is even more important that transfection leads to presentation of the antigen on the cells surface followed by an activation of T-cells which starts the immune reaction. Besides presentation of only the tumour protein, additional application of a DC-activating molecule is said to achieve a higher transfection efficiency and to overcome the problem of tolerance development. [223] Lipoplexes composed of EPC 100 %, DODMA and DOPE incorporating DNA of either the model antigen OVA or the activator IKK were applied in different combinations with the protein itself. Higher immune response is accessible with the application of a DC-activating molecule (Fig. 44). Above all, for $CD4^+$ cells, IKK seems to be an alternative to the conventional LPS. Since $CD8^+$ cells are more important for the antitumour response, the influence of IKK has to be investigated precisely. One possibility is the formulation of OVA and IKK as DNA encapsulated in the same lipoplex while it is also possible to use LPS in such a delivery system.

6 Conclusion

The formulation and structural characterisation of mRNA-lipoplexes for tumour vaccination as a new strategy for cancer therapy was the main objective of this thesis. Personalised therapies offer a chance to overcome low response rates of the current first-line. The mRNA encodes for proteins that are specifically expressed on tumour cells. A delivery system is beneficial to ensure a targeted transport and to mediated cellular uptake and endosomal release. Lipid-based systems were chosen as drug delivery particles due to their high biocompatibility together with a low immunogenicity and toxicity. In order to find a suitable formulation for each application, a detailed investigation on the molecular structure of the lipid systems after insertion of the mRNA as well as the evaluation of the formulations' behaviour after administration into the human body is necessary.

The majority of the studies performed on structural elucidation of lipid-based systems focused only on lipoplexes with DNA. Several advantages of mRNA over DNA justify the use of mRNA and also a detailed structural investigation of these lipoplexes. 1,2-Dioleoyl-3-trimethylammonium-propane (DOTAP) was chosen as a classical and well-known transfection reagent. Embedded in a highly concentrated matrix of neutral lipids like Egg-Phosphatidylcholine (EPC) or 1,2-Dioleoyl-sn-glycero-3-phosphocholine (DOPC), DOTAP served as an anchor for the mRNA.

The molecular assembly of the lipid membrane systems were characterised with small-angle X-ray scattering (SAXS). Zeta potential and the RiboGreen™ Assay was used to evaluate the overall charge and the localisation of the mRNA inside of the lipoplexes. The influence of the mRNA on the lipid membrane was evaluated with differential scanning calorimetry (DSC). The overall molecular organisation was found to be lamellar whereby the exact structure, reflected by the membrane distance of multilayer vesicles (d-spacing), was dependent on the ratio between DOTAP and mRNA (N/P ratio). Although there was always an excess of water in the hydrophilic space between the bilayers, the amount of mRNA affected the d-spacing in an analytical manner. In cell culture experiments, the release and the functionality of the mRNA was shown and transfection efficiency was dependent on the amount of DOTAP. A structural model could be developed where the mRNA forms cluster only on one side of the bilayer. The exact position of the mRNA has to be proven in further experiments.

Unfortunately, cationic lipids are associated with toxic effects, but the cationic charge is essential. Hence, ionizable lipids with a pH-dependent charge are used to reduce this toxicity and avoid aggregation after administration. At a neutral pH, lipids are expected to be nearly charged neutrally whereas at an acidic pH, the headgroups get protonated. For deeper investigation of the molecular organisation and its pH-dependent changes, 1,2-Dioleoyl-N,N-dimethyl-3-aminopropane (DODMA) was utilised as ionizable lipid together in comparison to the permanently charged lipid 1,2-Di-O-octadecenyl-3-trimethylammonium-propane (DOTMA). A highly concentrated matrix of EPC and DOPC was selected and various compositions were tested. As expected, the structure of DOTMA-containing lipoplexes was independent of the pH. Lipoplexes with DODMA changed in their appearance. At neutral pH, less ordered systems occurred. However, the structure was not completely comparable to pure EPC-containing lipoplexes. At acidic pH, the structure of lipoplexes was comparable but not identical to DOTMA-containing systems. Hence, DODMA has a slight charge, even at neutral pH but it is not completely charged at acidic pH. The pK_a as a characteristic parameter was measured with two different methods over a pH range of 3 to 10. With the TNS assay, explicit determination was just possible for 50 % DODMA. Using SAXS, samples showed a pH-dependent characteristic behaviour but a relatively accurate determination of pK_a was just possible for the lipoplexes with DOPC. Despite, clear structural changes occurred in the expected pH range of around 6. Cellular contact and endosomal release should be mimicked with the addition of heparin. Lamellar systems remained over the whole time and varied just in their number and proportion. A transformation into inverse hexagonal structures as it would be expected during the endosomal release, could not be observed.

The advantage of ionizable lipids as well as the positive influence of 1,2-Dioleoyl-sn-glycero-3-phosphoethanolamine (DOPE) on the transfection were proven in cell culture with encapsulated DNA. The immunological potential of lipoplexes was shown by the activation of immature dendritic cells (DCs). The dual asymmetric centrifuge (DAC) could be introduced as a new and feasible preparation method for the encapsulation of nucleic acids in liposomes.

Summing up, mRNA- as well as DNA-lipoplexes offer great possibilities for the individual approach of tumour vaccination. The obtained results for the structural characterisation have to be completed with more *in vitro* and *in vivo* data to get a better understanding of all the chances offered by this pharmaceutical product.

7 Outlook

The aim of this thesis was the detailed characterisation of lipoplexes for tumour vaccination. With all the performed experiments, a structural model of mRNA-lipoplexes composed of DOPC and DOTAP was developed. Nevertheless, further experiments are necessary to clarify open questions. SANS measurements have to be repeated to prove the exact position of the mRNA inside of the lipoplexes. In this context, the influence of the trehalose has to be evaluated at pharmaceutically realistic concentrations as well since sugars are often added due to their cryoprotectant properties. In addition to the scattering experiments, microscopy techniques are a good option to investigate the overall structure of the MLV. Cryo-TEM is more useful for a qualitative analysis, while techniques like SAXS or SANS provide more quantitative information. Despite, cryo-TEM implies direct imaging, so that the analysis is easier in comparison to indirect methods like SAXS which are more complicated in case the sample contains aggregates or has a broad size distribution. Therefore, cryo-TEM pictures for more than the one test composition are beneficial. In addition, freeze-fracture electron-microscopy is another suitable option to gain useful information on the appearance of the formulations.

In addition to a further characterisation, improvements of the composition of the lipoplexes are conceivable. Lipoplexes transfected C2C12 cells, but a higher transfection would be preferable. Hafez et al.[96] showed that DOPC, formulated with DOPS alone and together with DODAC, impeded the endosomal release by stabilisation of the bilayer structures. For a successful release of the mRNA, the formation of inverted hexagonal H_{II} lipid phases by the formed ion-pairs between cationic lipids of the delivery system and negative lipids of the endosome is necessary. The addition of DOPE to DOPC-containing lipoplexes resulted in a promotion of the H_{II} lipid phase. [96] Hence, the addition of DOPE to the tested lipoplexes would be an opportunity to induce higher transfection efficiency. Further lipids like cholesterol can also be used to increase the stability of the systems [224] or increase the circulation time by PEGylation [225] for a possible i.v.-injection.

The addition of DOPE would also be a feasible improvement for the lipoplexes containing DODMA as ionizable lipid. Mimicking cellular contact by addition of heparin and triggering an endosomal release by decreasing the pH of the buffer, the lamellar system of the lipoplexes vanished to a certain amount. Nevertheless, the hexagonal structures supporting the endoso-

mal release did not appear. Hence, the addition of DOPE could favour the formation of hexagonal structures. Furthermore, mimicking of cellular contact can also be performed with DOPG or MML instead of heparin to test if this results in a different structural arrangement of the lipoplexes. In addition, the release of mRNA has to be tested more detailed and results have to be linked to the scattering data. First tests where the free amount of mRNA was tested after addition of heparin and DOPG were performed. These tests have to be extended to lipoplexes with various N/P ratios to see possible differences between an excess of mRNA or ionizable lipid.

In later investigations concerning the pK_a of the lipoplexes, it has to be analysed if the determined pH is the actual pK_a or if it is the pH where the protonation of DODMA is sufficient to cause structural transitions. Perhaps, less than 50 % protonation is enough to induce modifications. Furthermore, it has to be clarified which level of protonation is really needed for cellular uptake as well as which grade forces an endosomal release.

To ensure a high encapsulation efficiency, the prepratation with ionizable lipids should be done under acidic conditions. Afterwards, a neutral pH for application can be adjusted by dialysis. For the present studies, this procedure was not possible due to the lipid film method. For further studies, such an improvement is possible by choosing another preparation method.

Most of the lipoplexes for this thesis were prepared by the lipid film method. For an industrial manufacturing, this method is not beneficial. Other techniques like ethanol injection [101] or DAC [216,226] with the possibility for a scale-up would be preferable. Due to that, the DNA-lipoplexes for this thesis were prepared with the DAC. It is a quite new technique which offers the possibility for a fast and sterile production of liposomes. Depending on the needs, very small amounts for research purposes but also larger amounts for commercial production can be prepared. Introducing new preparation methods, it is necessary to investigate the structure of samples prepared with these new techniques and evaluate if the structural model developed for this thesis apply also for these lipoplexes. In general, a comparison of the molecular structure of lipoplexes prepared with different methods would be instructive.

8 Appendix

8.1. pH dependent structural changes

I. Comparison of structures at pH 7.5 and 5 with EPC 80 %-lipoplexes using SAXS

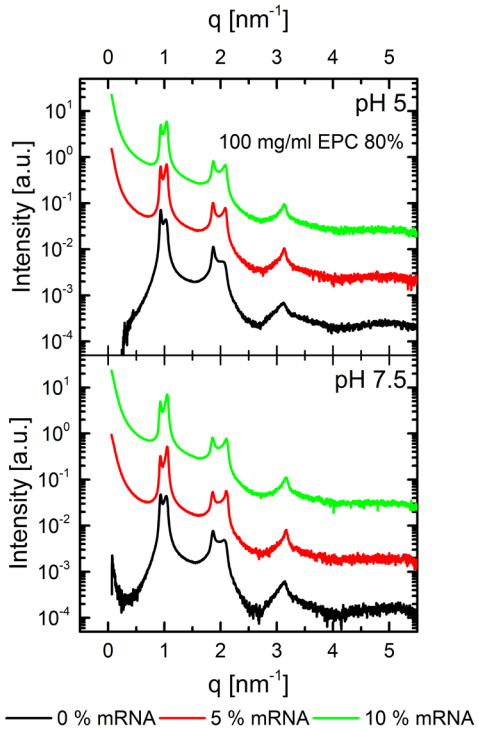

Figure (Appendix) 1: Peak pattern of lipoplexes with EPC 80 % and different amounts of mRNA, measured in pH 7.5 and 5 (cf. Fig 27)

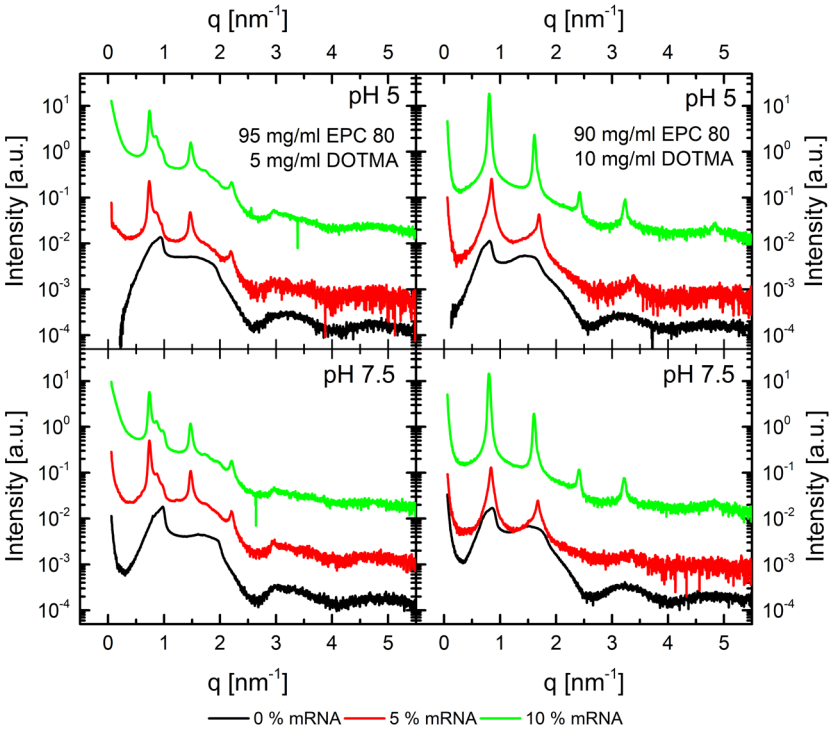

Figure (Appendix) 2: Peak pattern of lipoplexes with EPC 80 % and different amounts of DOTMA and mRNA, measured in pH 7.5 and 5 (cf. Fig. 28)

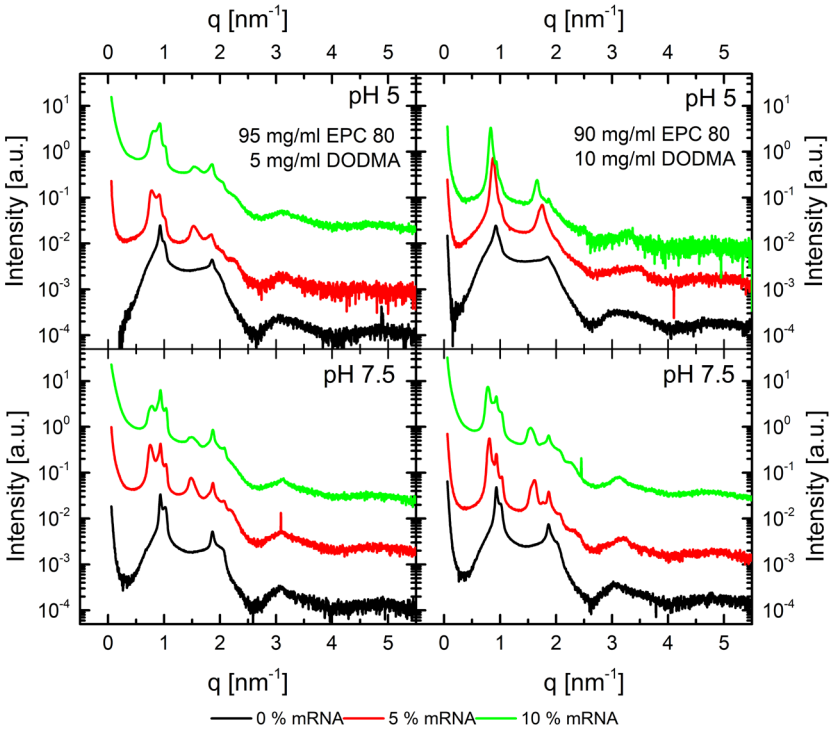

Figure (Appendix) 3: Peak pattern of lipoplexes with EPC 80 % and different amounts of DODMA and mRNA, measured in pH 7.5 and 5 (cf. Fig. 29)

II. Investigation of pH dependent structural transition with EPC 80 %-lipoplexes

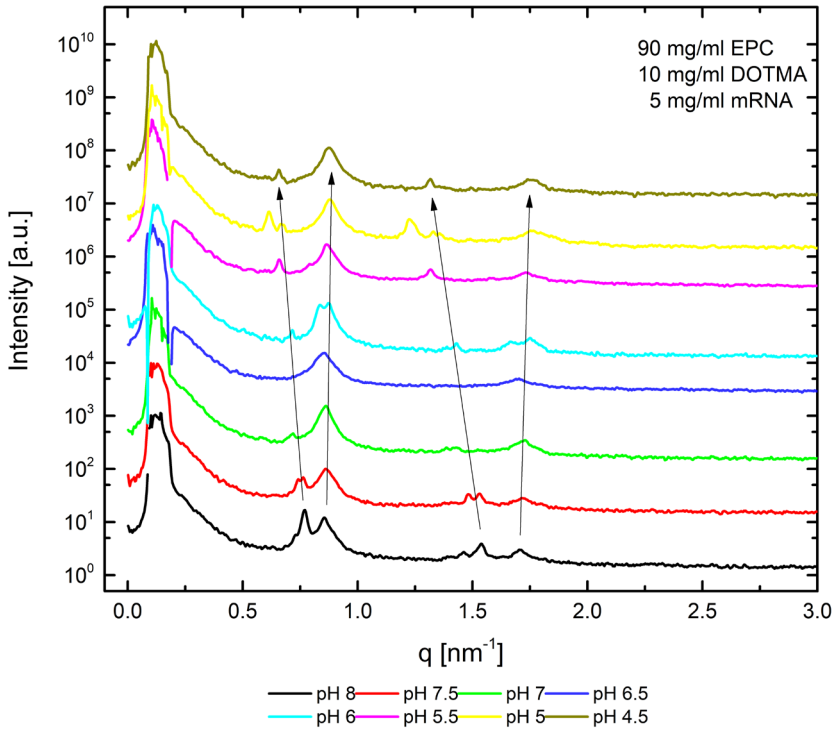

Figure (Appendix) 4: Peak pattern of lipoplexes with EPC 80 %, 10 mg/ml DOTMA and 5 mg/ml mRNA, measured from pH 8 to 4.5 (cf. Fig. 30)

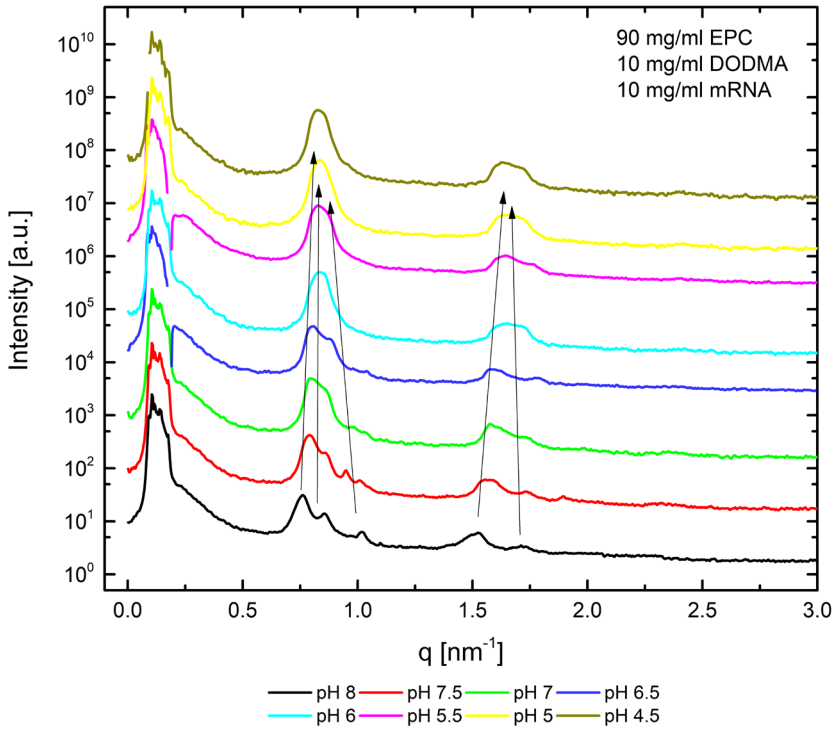

Figure (Appendix) 5: Peak pattern of lipoplexes with EPC 80 %, 10 mg/ml DODMA and 10 mg/ml mRNA, measured from pH 8 to 4.5 (cf. Fig. 31)

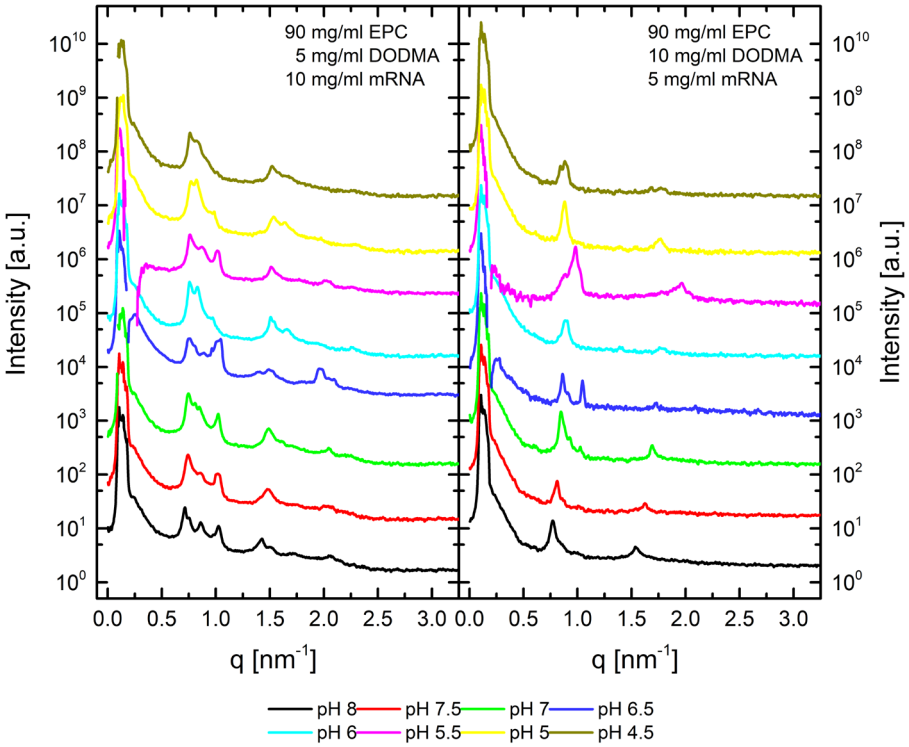

Figure (Appendix) 6: Peak pattern of lipoplexes with EPC 80 %, 5 and 10 mg/ml DODMA and 5 or 10 mg/ml mRNA, measured from pH 8 to 4.5 (cf. Figs. 30 and 31)

III. Investigation of pH dependent structural transition with DOPC-lipoplexes

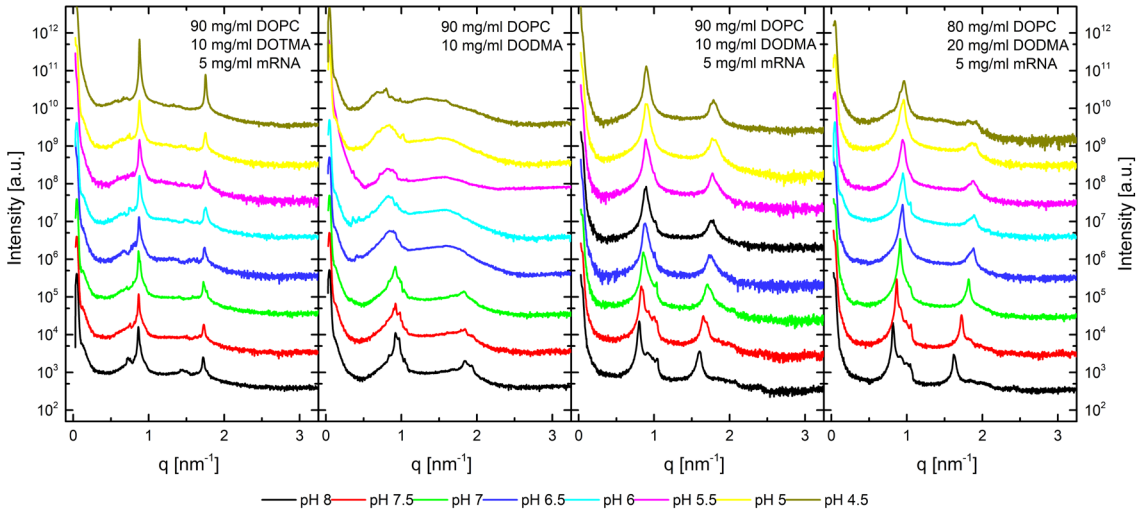

Figure (Appendix) 7: Peak pattern of lipoplexes with DOPC, different amounts of DOTMA or DODMA with or without 5 mg/ml mRNA, measured from pH 8 to 4.5 (cf. Fig. 32)

8.2. Release dependent structural changes

I. Investigation on structural changes with SAXS

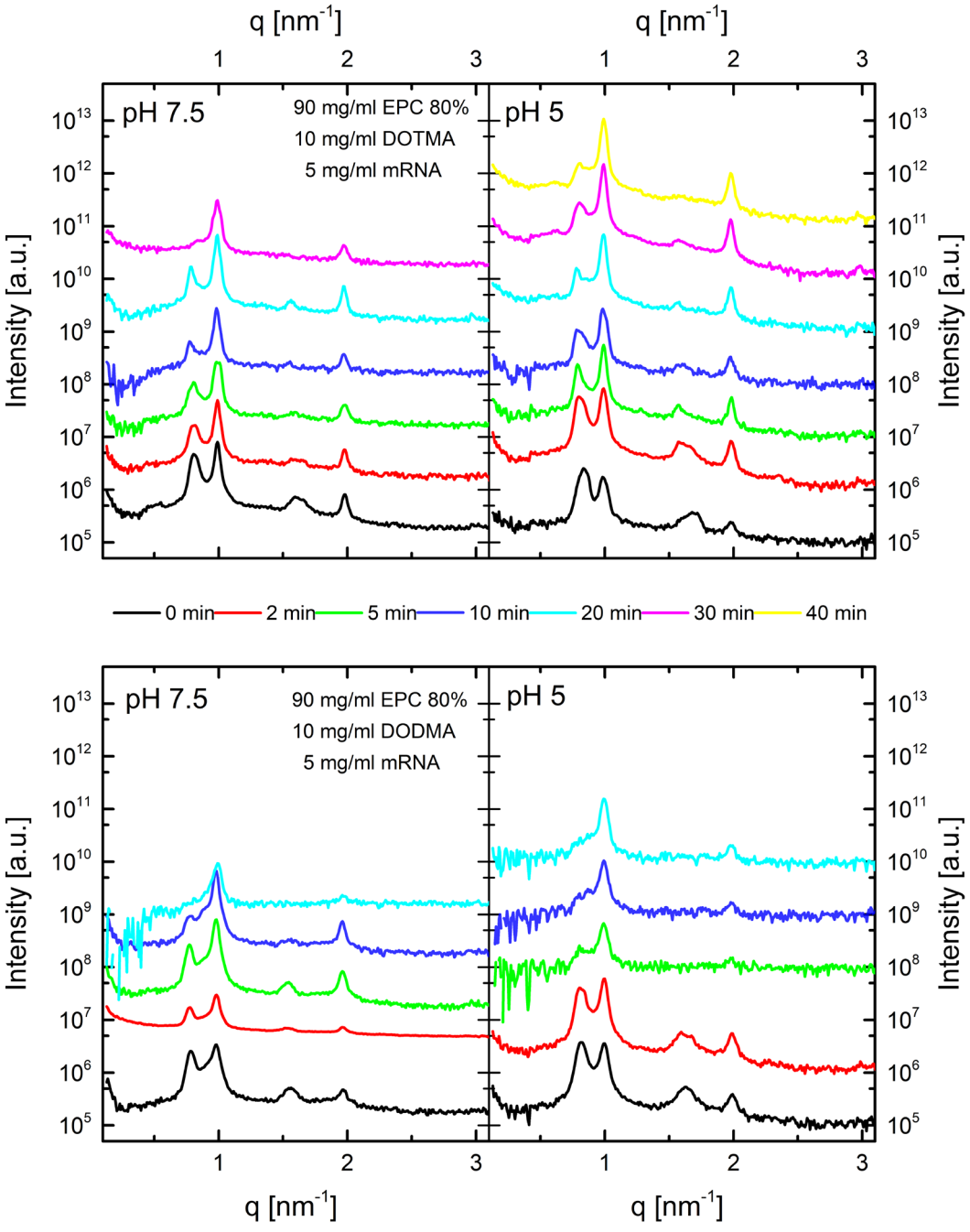

Figure (Appendix) 8: Peak pattern of lipoplexes with EPC 80 %, 10 mg/ml DOTMA or DODMA and 5 mg/ml mRNA after addition of heparin in pH 7.5 and 5 (cf. Fig. 36)

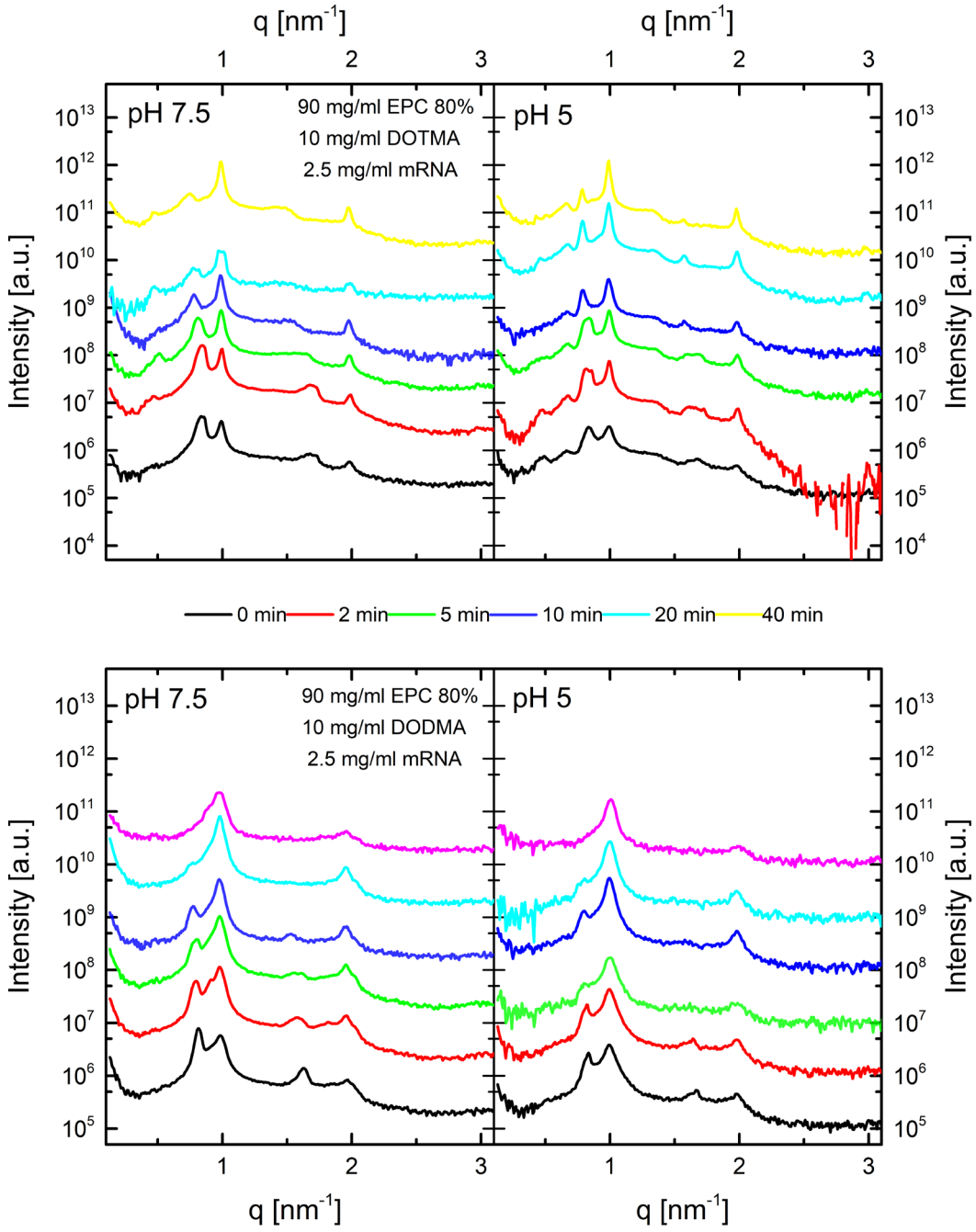

Figure (Appendix) 9: Peak pattern of lipoplexes with EPC 80 %, 10 mg/ml DOTMA or DODMA and 2.5 mg/ml mRNA after addition of heparin in pH 7.5 and 5 (cf. Fig. 37)

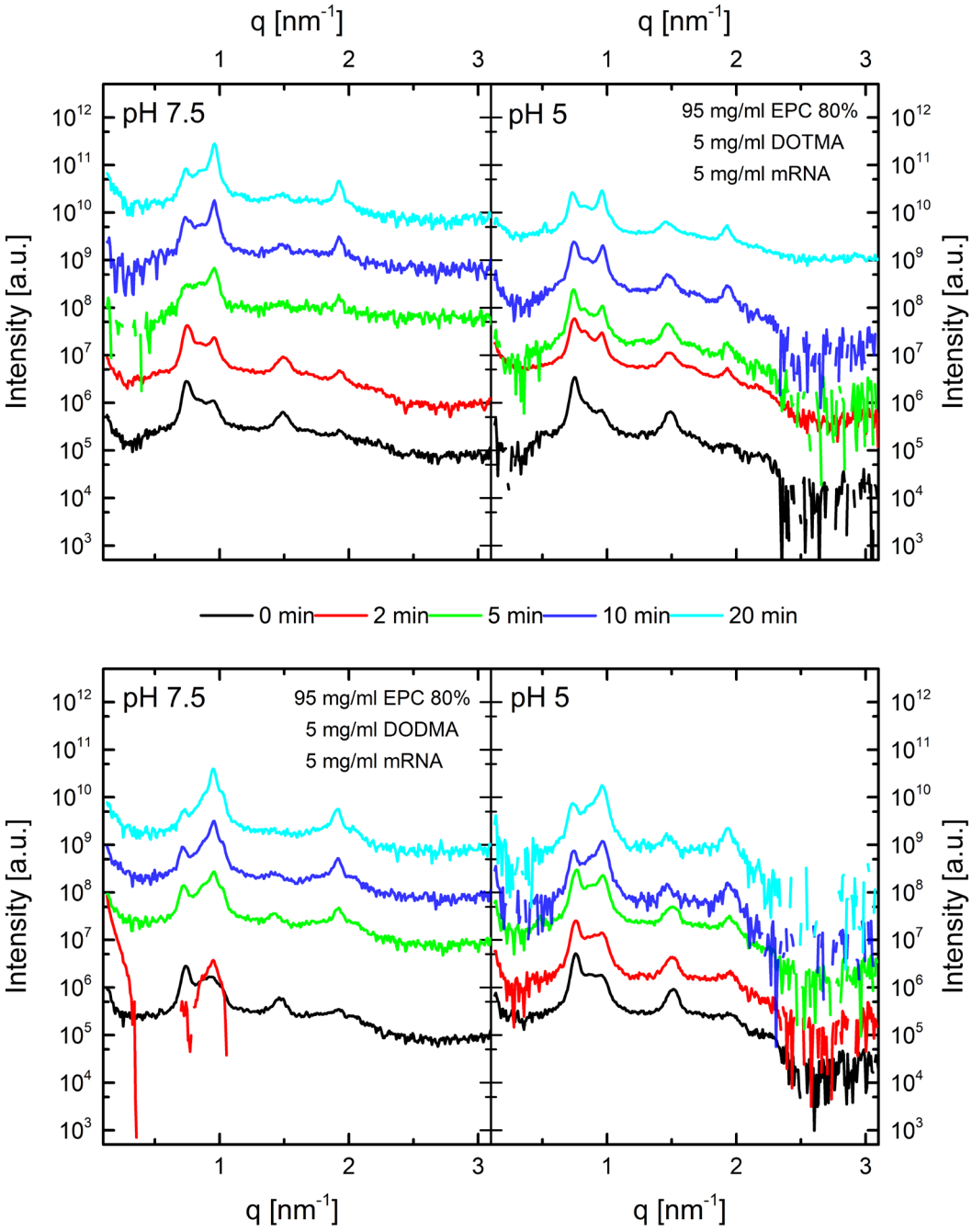

Figure (Appendix) 10: Peak pattern of lipoplexes with EPC 80 %, 5 mg/ml DOTMA or DODMA and 5 mg/ml mRNA after addition of heparin in pH 7.5 and 5 (cf. Fig. 38)

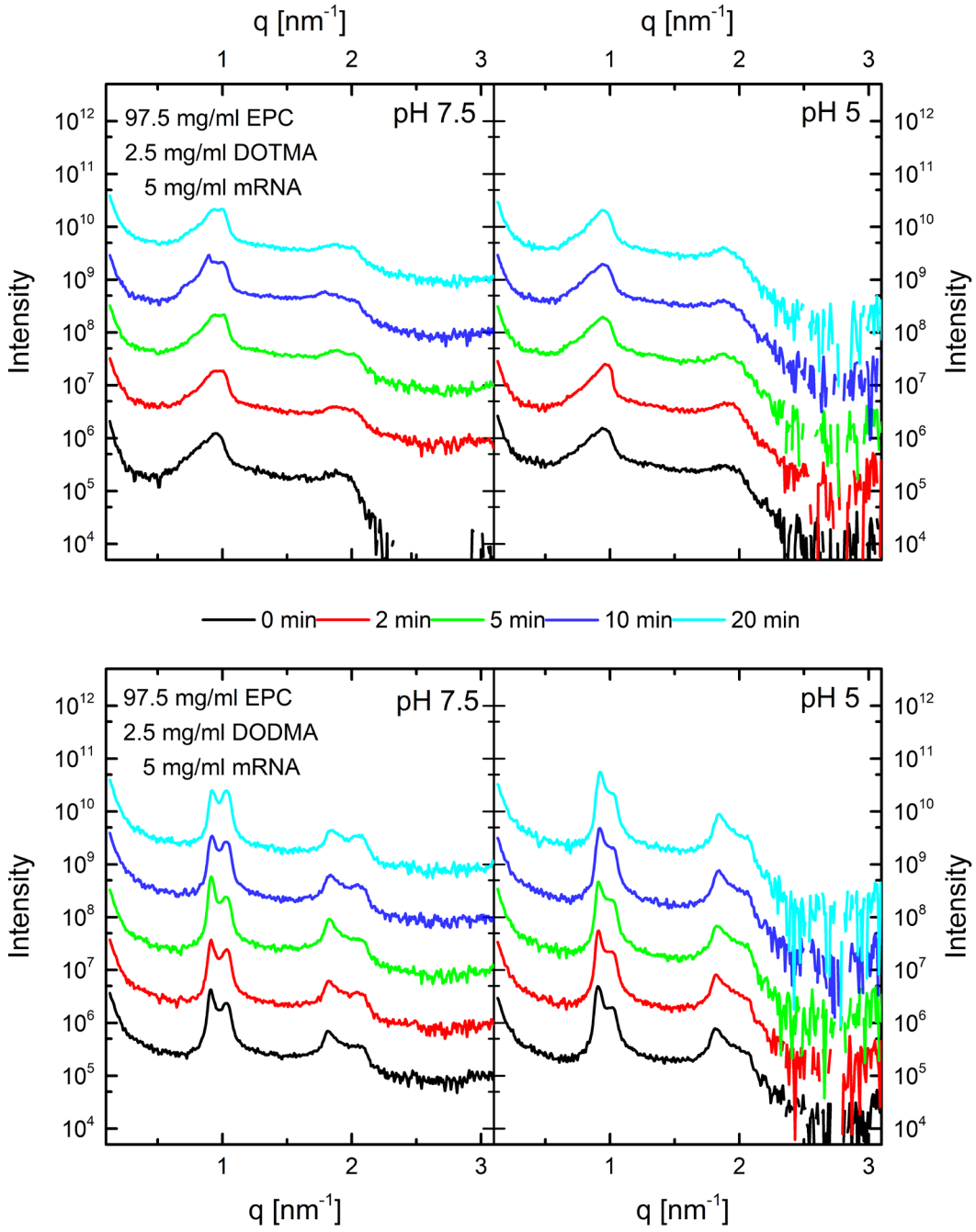

Figure (Appendix) 11: Peak pattern of lipoplexes with EPC 80 %, 2.5 mg/ml DOTMA or DODMA and 5 mg/ml mRNA after addition of heparin in pH 7.5 and 5 (cf. Fig. 39)

9 List of references

(1) Stewart, B. W.; Wild, C. P. *World Cancer Report 2014*.

(2) Coley, W. B. THE TREATMENT OF MALIGNAT TUMORS BY REPEATED INOCULATIONS OF ERYSIPELAS. *Am. J. Med. Sci.* **1893**, *105* (5), 487–510.

(3) Wolff, J. A.; Malone, R. W.; Williams, P.; Chong, W.; Acsadi, G.; Jani, A.; Felgner, P. L. Direct Gene Transfer into Mouse Muscle in Vivo. *Science* **1990**, *247* (4949 Pt 1), 1465–1468.

(4) Sahin, U.; Karikó, K.; Türeci, Ö. MRNA-Based Therapeutics — Developing a New Class of Drugs. *Nat. Rev. Drug Discov.* **2014**, *13* (10), 759–780.

(5) Conry, R. M.; LoBuglio, A. F.; Wright, M.; Sumerel, L.; Pike, M. J.; Johanning, F.; Benjamin, R.; Lu, D.; Curiel, D. T. Characterization of a Messenger RNA Polynucleotide Vaccine Vector. *Cancer Res.* **1995**, *55* (7), 1397–1400.

(6) Boczkowski, D.; Nair, S. K.; Snyder, D.; Gilboa, E. Dendritic Cells Pulsed with RNA Are Potent Antigen-Presenting Cells in Vitro and in Vivo. *J. Exp. Med.* **1996**, *184* (2), 465–472.

(7) Cullis, P. R.; Hope, M. J. Lipid Nanoparticle Systems for Enabling Gene Therapies. *Mol. Ther.* **2017**, *25* (7), 1467–1475.

(8) Pardi, N.; Hogan, M. J.; Pelc, R. S.; Muramatsu, H.; Andersen, H.; DeMaso, C. R.; Dowd, K. A.; Sutherland, L. L.; Scearce, R. M.; Parks, R.; Wagner, W.; Granados, A.; Greenhouse, J.; Walker, M.; Willis, E.; Yu, J.-S.; McGee, C. E.; Sempowski, G. D.; Mui, B. L.; Tam, Y. K.; Huang, Y.-J.; Vanlandingham, D.; Holmes, V. M.; Balachandran, H.; Sahu, S.; Lifton, M.; Higgs, S.; Hensley, S. E.; Madden, T. D.; Hope, M. J.; Karikó, K.; Santra, S.; Graham, B. S.; Lewis, M. G.; Pierson, T. C.; Haynes, B. F.; Weissman, D. Zika Virus Protection by a Single Low-Dose Nucleoside-Modified MRNA Vaccination. *Nature* **2017**, *543* (7644), 248–251.

(9) Kreiter, S.; Selmi, A.; Diken, M.; Koslowski, M.; Britten, C. M.; Huber, C.; Türeci, O.; Sahin, U. Intranodal Vaccination with Naked Antigen-Encoding RNA Elicits Potent Prophylactic and Therapeutic Antitumoral Immunity. *Cancer Res.* **2010**, *70* (22), 9031–9040.

(10) Kranz, L. M.; Diken, M.; Haas, H.; Kreiter, S.; Loquai, C.; Reuter, K. C.; Meng, M.; Fritz, D.; Vascotto, F.; Hefesha, H.; Grunwitz, C.; Vormehr, M.; Hüsemann, Y.; Selmi, A.; Kuhn, A. N.; Buck, J.; Derhovanessian, E.; Rae, R.; Attig, S.; Diekmann, J.; Jabulowsky, R. A.; Heesch, S.; Hassel, J.; Langguth, P.; Grabbe, S.; Huber, C.; Türeci, Ö.; Sahin, U. Systemic RNA Delivery to Dendritic Cells Exploits Antiviral Defence for Cancer Immunotherapy. *Nature* **2016**, *534* (7607), 396–401.

(11) Midoux, P.; Pichon, C. Lipid-Based MRNA Vaccine Delivery Systems. *Expert Rev. Vaccines* **2014**, *14* (2), 221–234.

(12) Scheel, B.; Aulwurm, S.; Probst, J.; Stitz, L.; Hoerr, I.; Rammensee, H. G.; Weller, M.; Pascolo, S. Therapeutic Anti-Tumor Immunity Triggered by Injections of Immunostimulating Single-Stranded RNA. *Eur. J. Immunol.* **2006**.

(13) Reynolds, A.; Leake, D.; Boese, Q.; Scaringe, S.; Marshall, W. S.; Khvorova, A.

Rational SiRNA Design for RNA Interference. *Nat. Biotechnol.* **2004**, *22* (3), 326–330.

(14) Bringmann, A.; Held, S. A. E.; Heine, A.; Brossart, P. RNA Vaccines in Cancer Treatment. *J. Biomed. Biotechnol.* **2010**, *2010*, 623687.

(15) Ulmer, J. B.; Mason, P. W.; Geall, A.; Mandl, C. W. RNA-Based Vaccines. *Vaccine* **2012**, *30* (30), 4414–4418.

(16) Schlake, T.; Thess, A.; Fotin-Mleczek, M.; Kallen, K.-J. Developing MRNA-Vaccine Technologies. *RNA Biol.* **2012**, *9* (11), 1319–1330.

(17) Pascolo, S. Vaccination with Messenger RNA. *Methods Mol. Med.* **2006**, *127*, 23–40.

(18) Eisenächer, K.; Steinberg, C.; Reindl, W.; Krug, A. The Role of Viral Nucleic Acid Recognition in Dendritic Cells for Innate and Adaptive Antiviral Immunity. *Immunobiology* **2008**, *212* (9–10), 701–714.

(19) Karikó, K.; Weissman, D. Naturally Occurring Nucleoside Modifications Suppress the Immunostimulatory Activity of RNA: Implication for Therapeutic RNA Development. *Curr. Opin. Drug Discov. Devel.* **2007**, *10* (5), 523–532.

(20) Weide, B.; Garbe, C.; Rammensee, H. G.; Pascolo, S. Plasmid DNA- and Messenger RNA-Based Anti-Cancer Vaccination. *Immunology Letters*. 2008.

(21) Alberer, M.; Gnad-Vogt, U.; Hong, H. S.; Mehr, K. T.; Backert, L.; Finak, G.; Gottardo, R.; Bica, M. A.; Garofano, A.; Koch, S. D.; Fotin-Mleczek, M.; Hoerr, I.; Clemens, R.; von Sonnenburg, F. Safety and Immunogenicity of a MRNA Rabies Vaccine in Healthy Adults: An Open-Label, Non-Randomised, Prospective, First-in-Human Phase 1 Clinical Trial. *Lancet* **2017**.

(22) Kloke, B.-P.; Kreiter, S.; Diken, M.; Sahin, U. Aktiv Personalisierte Tumorvakzine - Wege in Die Klinische Translation. *DPhG Pharmakon*. 2015, pp 304–308.

(23) Sharova, L. V.; Sharov, A. A.; Nedorezov, T.; Piao, Y.; Shaik, N.; Ko, M. S. H. Database for MRNA Half-Life of 19 977 Genes Obtained by DNA Microarray Analysis of Pluripotent and Differentiating Mouse Embryonic Stem Cells. *DNA Res.* **2009**.

(24) Yang, E.; van Nimwegen, E.; Zavolan, M.; Rajewsky, N.; Schroeder, M.; Magnasco, M.; Darnell, J. E.; Jr. Decay Rates of Human MRNAs: Correlation with Functional Characteristics and Sequence Attributes. *Genome Res.* **2003**, *13* (8), 1863–1872.

(25) Kaczmarek, J. C.; Patel, A. K.; Kauffman, K. J.; Fenton, O. S.; Webber, M. J.; Heartlein, M. W.; DeRosa, F.; Anderson, D. G. Polymer–Lipid Nanoparticles for Systemic Delivery of MRNA to the Lungs. *Angew. Chemie - Int. Ed.* **2016**.

(26) Fenton, O. S.; Kauffman, K. J.; McClellan, R. L.; Appel, E. A.; Dorkin, J. R.; Tibbitt, M. W.; Heartlein, M. W.; De Rosa, F.; Langer, R.; Anderson, D. G. Bioinspired Alkenyl Amino Alcohol Ionizable Lipid Materials for Highly Potent in Vivo MRNA Delivery. *Adv. Mater.* **2016**.

(27) Miller, J. B.; Zhang, S.; Kos, P.; Xiong, H.; Zhou, K.; Perelman, S. S.; Zhu, H.; Siegwart, D. J. Non-Viral CRISPR/Cas Gene Editing In Vitro and In Vivo Enabled by Synthetic Nanoparticle Co-Delivery of Cas9 MRNA and SgRNA. *Angew. Chemie - Int. Ed.* **2017**.

(28) Kreiter, S.; Diken, M.; Selmi, A.; Türeci, Ö.; Sahin, U. Tumor Vaccination Using Messenger RNA: Prospects of a Future Therapy. *Curr. Opin. Immunol.* **2011**, *23* (3), 399–406.

(29) Deering, R. P.; Kommareddy, S.; Ulmer, J. B.; Brito, L. A.; Geall, A. J. Nucleic Acid Vaccines: Prospects for Non-Viral Delivery of MRNA Vaccines. *Expert Opin. Drug Deliv.* **2014**, *11* (6), 885–899.

(30) Blain, J. C.; Szostak, J. W. Progress Toward Synthetic Cells. *Annu. Rev. Biochem.* **2014**, *83* (1), 615–640.

(31) Abe, K.; Fujiyoshi, Y. Cryo-Electron Microscopy for Structure Analyses of Membrane Proteins in the Lipid Bilayer. *Curr. Opin. Struct. Biol.* **2016**, *39*, 71–78.

(32) Grabbe, S.; Haas, H.; Diken, M.; Kranz, L. M.; Langguth, P.; Sahin, U. Translating Nanoparticulate-Personalized Cancer Vaccines into Clinical Applications: Case Study with RNA-Lipoplexes for the Treatment of Melanoma. *Nanomedicine (Lond).* **2016**, *11* (20), 2723–2734.

(33) Boczkowski, D.; Nair, S. RNA as Performance-Enhancers for Dendritic Cells. *Expert Opin. Biol. Ther.* **2010**, *10* (4), 563–574.

(34) Sullenger, B. A.; Gilboa, E. Emerging Clinical Applications of RNA. *Nature.* 2002.

(35) Hajj, K. A.; Whitehead, K. A. Tools for Translation: Non-Viral Materials for Therapeutic MRNA Delivery. *Nat. Rev. Mater.* **2017**, *2*, 17056.

(36) Weide, B.; Carralot, J. P.; Reese, A.; Scheel, B.; Eigentler, T. K.; Hoerr, I.; Rammensee, H. G.; Garbe, C.; Pascolowz, S. Results of the First Phase I/II Clinical Vaccination Trial with Direct Injection of MRNA. *J. Immunother.* **2008**.

(37) Rittig, S. M.; Haentschel, M.; Weimer, K. J.; Heine, A.; Muller, M. R.; Brugger, W.; Horger, M. S.; Maksimovic, O.; Stenzl, A.; Hoerr, I.; Rammensee, H. G.; Holderried, T. A. W.; Kanz, L.; Pascolo, S.; Brossart, P. Intradermal Vaccinations with RNA Coding for TAA Generate CD8 and CD4 Immune Responses and Induce Clinical Benefit in Vaccinated Patients. *Mol. Ther.* **2011**.

(38) Stenzl, A.; Feyerabend, S.; Kübler, H.; Retz, M.; Grüllich, C.; Hipp, M.; Klinkhardt, U.; Hong, H. S.; Doener, F.; Koch, S. D.; Scholl, M.; Brutlach, S.; Schroeder, A.; Seibel, T.; Halama, N.; Schönborn-Kellenberger, O.; Fotin-Mleczek, M.; Gnad-Vogt, U. Results of an Open Label Randomized Phase II Trial of CV9104, an MRNA-Based Multivalent Cancer Immunotherapy in Patients (Pts) with Intermediate or High Risk Localized Prostate Cancer (PC) Undergoing Radical Prostatectomy (RPE). *Ann. Oncol.* **2017**, *28* (suppl_5).

(39) Thomas, A.; Giaccone, G. Why Has Active Immunotherapy Not Worked in Lung Cancer? *Ann. Oncol. Off. J. Eur. Soc. Med. Oncol.* **2015**, *26* (11), 2213–2220.

(40) Butts, C.; Socinski, M. A.; Mitchell, P. L.; Thatcher, N.; Havel, L.; Krzakowski, M.; Nawrocki, S.; Ciuleanu, T. E.; Bosquée, L.; Trigo, J. M.; Spira, A.; Tremblay, L.; Nyman, J.; Ramlau, R.; Wickart-Johansson, G.; Ellis, P.; Gladkov, O.; Pereira, J. R.; Eberhardt, W. E. E.; Helwig, C.; Schröder, A.; Shepherd, F. A. Tecemotide (L-BLP25) versus Placebo after Chemoradiotherapy for Stage III Non-Small-Cell Lung Cancer (START): A Randomised, Double-Blind, Phase 3 Trial. *Lancet Oncol.* **2014**, *15* (1), 59–68.

(41) Vansteenkiste, J. F.; Cho, B. C.; Vanakesa, T.; De Pas, T.; Zielinski, M.; Kim, M. S.; Jassem, J.; Yoshimura, M.; Dahabreh, J.; Nakayama, H.; Havel, L.; Kondo, H.; Mitsudomi, T.; Zarogoulidis, K.; Gladkov, O. A.; Udud, K.; Tada, H.; Hoffman, H.; Bugge, A.; Taylor, P.; Gonzalez, E. E.; Liao, M. L.; He, J.; Pujol, J. L.; Louahed, J.; Debois, M.; Brichard, V.; Debruyne, C.; Therasse, P.; Altorki, N. Efficacy of the MAGE-A3 Cancer Immunotherapeutic as Adjuvant Therapy in Patients with Resected MAGE-A3-Positive Non-Small-Cell Lung Cancer (MAGRIT): A Randomised, Double-Blind, Placebo-Controlled, Phase 3 Trial. *Lancet Oncol.* **2016**, *17* (6), 822–835.

(42) Bahl, K.; Senn, J. J.; Yuzhakov, O.; Bulychev, A.; Brito, L. A.; Hassett, K. J.; Laska, M. E.; Smith, M.; Almarsson, Ö.; Thompson, J.; Ribeiro, A. (Mick); Watson, M.; Zaks, T.; Ciaramella, G. Preclinical and Clinical Demonstration of Immunogenicity by MRNA Vaccines against H10N8 and H7N9 Influenza Viruses. *Mol. Ther.* **2017**.

(43) Sahin, U.; Derhovanessian, E.; Miller, M.; Kloke, B.-P.; Simon, P.; Löwer, M.; Bukur, V.; Tadmor, A. D.; Luxemburger, U.; Schrörs, B.; Omokoko, T.; Vormehr, M.; Albrecht, C.; Paruzynski, A.; Kuhn, A. N.; Buck, J.; Heesch, S.; Schreeb, K. H.; Müller, F.; Ortseifer, I.; Vogler, I.; Godehardt, E.; Attig, S.; Rae, R.; Breitkreuz, A.; Tolliver, C.; Suchan, M.; Martic, G.; Hohberger, A.; Sorn, P.; Diekmann, J.; Ciesla, J.; Waksmann, O.; Brück, A.-K.; Witt, M.; Zillgen, M.; Rothermel, A.; Kasemann, B.; Langer, D.; Bolte, S.; Diken, M.; Kreiter, S.; Nemecek, R.; Gebhardt, C.; Grabbe, S.; Höller, C.; Utikal, J.; Huber, C.; Loquai, C.; Türeci, Ö.; Attig, S.; Loquai, C.; Vogler, I.; Diekmann, J.; Gebhardt, C.; Diken, M.; Buck, J.; Suchan, M.; Sorn, P.; Müller, F.; Schreeb, K. H.; Kasemann, B.; Höller, C.; Miller, M.; Brück, A.-K.; Breitkreuz, A.; Vormehr, M.; Bolte, S.; Zillgen, M.; Paruzynski, A.; Sahin, U.; Utikal, J.; Huber, C.; Kuhn, A. N.; Schrörs, B.; Hohberger, A.; Rothermel, A.; Grabbe, S.; Ortseifer, I.; Albrecht, C.; Martic, G.; Rae, R.; Kloke, B.-P.; Omokoko, T.; Witt, M.; Kreiter, S.; Tadmor, A. D.; Godehardt, E.; Löwer, M.; Türeci, Ö.; Derhovanessian, E.; Langer, D.; Luxemburger, U.; Ciesla, J.; Heesch, S.; Tolliver, C.; Simon, P.; Waksmann, O.; Bukur, V. Personalized RNA Mutanome Vaccines Mobilize Poly-Specific Therapeutic Immunity against Cancer. *Nature* **2017**, *547* (7662), 222.

(44) Slingluff, C. L.; Engelhard, V. H.; Ferrone, S. Peptide and Dendritic Cell Vaccines. *Clin. Cancer Res.* **2006**, *12* (7 Pt 2), 2342s–2345s.

(45) Romero, P.; Banchereau, J.; Bhardwaj, N.; Cockett, M.; Disis, M. L.; Dranoff, G.; Gilboa, E.; Hammond, S. A.; Hershberg, R.; Korman, A. J.; Kvistborg, P.; Melief, C.; Mellman, I.; Palucka, A. K.; Redchenko, I.; Robins, H.; Sallusto, F.; Schenkelberg, T.; Schoenberger, S.; Sosman, J.; Türeci, Ö.; Van den Eynde, B.; Koff, W.; Coukos, G. The Human Vaccines Project: A Roadmap for Cancer Vaccine Development. *Sci. Transl. Med.* **2016**, *8* (334), 334ps9.

(46) Vormehr, M.; Schrörs, B.; Boegel, S.; Löwer, M.; Türeci, Ö.; Sahin, U. Mutanome Engineered RNA Immunotherapy: Towards Patient-Centered Tumor Vaccination. *J. Immunol. Res.* **2015**, *2015*, 1–6.

(47) Melief, C. J. M.; van Hall, T.; Arens, R.; Ossendorp, F.; van der Burg, S. H. Therapeutic Cancer Vaccines. *J. Clin. Invest.* **2015**, *125* (9), 3401–3412.

(48) Kaczmarek, J. C.; Kowalski, P. S.; Anderson, D. G. Advances in the Delivery of RNA Therapeutics: From Concept to Clinical Reality. *Genome Med.* **2017**, *9* (1), 60.

(49) Bangham, A. D.; Standish, M. M.; Watkins, J. C. Diffusion of Univalent Ions across

the Lamellae of Swollen Phospholipids. *J. Mol. Biol.* **1965**, *13* (1), IN26-IN27.

(50) Allen, T. M.; Cullis, P. R. Liposomal Drug Delivery Systems: From Concept to Clinical Applications. *Advanced Drug Delivery Reviews*. Elsevier January 1, 2013, pp 36–48.

(51) Akbarzadeh, A.; Rezaei-Sadabady, R.; Davaran, S.; Joo, S. W.; Zarghami, N.; Hanifehpour, Y.; Samiei, M.; Kouhi, M.; Nejati-Koshki, K. Liposome: Classification, Preparation, and Applications. *Nanoscale Res. Lett.* **2013**, *8* (1), 102.

(52) Garg, T.; Goyal, A. K. Liposomes : Targeted and Controlled Delivery System. *Drug Deliv. Lett.* **2014**, No. 4, 62–71.

(53) Maruyama, K. Intracellular Targeting Delivery of Liposomal Drugs to Solid Tumors Based on EPR Effects. *Advanced Drug Delivery Reviews*. Elsevier March 18, 2011, pp 161–169.

(54) Sercombe, L.; Veerati, T.; Moheimani, F.; Wu, S. Y.; Sood, A. K.; Hua, S. Advances and Challenges of Liposome Assisted Drug Delivery. *Frontiers in Pharmacology*. 2015.

(55) Hafez, I. M.; Cullis, P. R. Roles of Lipid Polymorphism in Intracellular Delivery. *Adv. Drug Deliv. Rev.* **2001**, *47* (2–3), 139–148.

(56) Yeagle, P. L. Chapter 7 - Structures of Lipid Assemblies . In *The Membranes of Cells (Third Edition)* ; Yeagle, P. L., Ed.; Academic Press: Boston, 2016; pp 115–154.

(57) Shah, J. C.; Sadhale, Y.; Chilukuri, D. M. Cubic Phase Gels as Drug Delivery Systems. *Adv. Drug Deliv. Rev.* **2001**, *47* (2), 229–250.

(58) Seddon, J. M. Structure of the Inverted Hexagonal (HII) Phase, and Non-Lamellar Phase Transitions of Lipids. *BBA - Reviews on Biomembranes*. 1990.

(59) Jahn, R.; Grubmüller, H. Membrane Fusion. *Curr. Opin. Cell Biol.* **2002**, *14* (4), 488–495.

(60) Gruner, S. M.; Cullis, P. R.; Hope, M. J.; Tilcock, C. P. S. Lipid Polymorphism:The Molecular Basis of Nonbilayer Phases. *Annu. Rev. Biophys. Biophys. Chem.* **1985**, *14* (1), 211–238.

(61) Elouahabi, A.; Ruysschaert, J. M. Formation and Intracellular Trafficking of Lipoplexes and Polyplexes. *Molecular Therapy*. 2005.

(62) Lappalainen, K.; Jääskeläinen, I.; Syrjänen, K.; Urtti, A.; Syrjänen, S. Comparison of Cell Proliferation and Toxicity Assays Using Two Cationic Liposomes. *Pharm. Res.* **1994**, *11* (8), 1127–1131.

(63) Lv, H.; Zhang, S.; Wang, B.; Cui, S.; Yan, J. Toxicity of Cationic Lipids and Cationic Polymers in Gene Delivery. *Journal of Controlled Release*. Elsevier August 10, 2006, pp 100–109.

(64) Tros de Ilarduya, C.; Sun, Y.; Düzgüneş, N. Gene Delivery by Lipoplexes and Polyplexes. *Eur. J. Pharm. Sci.* **2010**, *40* (3), 159–170.

(65) Hirko, A.; Tang, F.; Hughes, J. Cationic Lipid Vectors for Plasmid DNA Delivery. *Curr. Med. Chem.* **2003**, *10* (14), 1185–1193.

(66) Horobin, R. W.; Weissig, V. A QSAR-Modeling Perspective on Cationic Transfection

Lipids. 1. Predicting Efficiency and Understanding Mechanisms. *J. Gene Med.* **2005**, *7* (8), 1023–1034.

(67) Christensen, D.; Korsholm, K. S.; Andersen, P.; Agger, E. M. Cationic Liposomes as Vaccine Adjuvants. *Expert Rev. Vaccines* **2011**, *10* (4), 513–521.

(68) Markov, O. V.; Mironova, N. L.; Shmendel, E. V.; Serikov, R. N.; Morozova, N. G.; Maslov, M. A.; Vlassov, V. V.; Zenkova, M. A. Multicomponent Mannose-Containing Liposomes Efficiently Deliver RNA in Murine Immature Dendritic Cells and Provide Productive Anti-Tumour Response in Murine Melanoma Model. *J. Control. Release* **2015**, *213*, 45–56.

(69) Tacken, P. J.; de Vries, I. J. M.; Torensma, R.; Figdor, C. G. Dendritic-Cell Immunotherapy: From Ex Vivo Loading to in Vivo Targeting. *Nat. Rev. Immunol.* **2007**, *7* (10), 790–802.

(70) Scheel, B.; Teufel, R.; Probst, J.; Carralot, J.-P.; Geginat, J.; Radsak, M.; Jarrossay, D.; Wagner, H.; Jung, G.; Rammensee, H.-G.; Hoerr, I.; Pascolo, S. Toll-like Receptor-Dependent Activation of Several Human Blood Cell Types by Protamine-Condensed MRNA. *Eur. J. Immunol.* **2005**, *35* (5), 1557–1566.

(71) Cu, Y.; Broderick, K.; Banerjee, K.; Hickman, J.; Otten, G.; Barnett, S.; Kichaev, G.; Sardesai, N.; Ulmer, J.; Geall, A. Enhanced Delivery and Potency of Self-Amplifying MRNA Vaccines by Electroporation in Situ. *Vaccines* **2013**.

(72) Hofmann, A. M.; Wurm, F.; Huhn, E.; Nawroth, T.; Langguth, P.; Frey, H. Hyperbranched Polyglycerol-Based Lipids via Oxyanionic Polymerization: Toward Multifunctional Stealth Liposomes. *Biomacromolecules* **2010**, *11* (3), 568–574.

(73) Danhier, F.; Feron, O.; Préat, V. To Exploit the Tumor Microenvironment: Passive and Active Tumor Targeting of Nanocarriers for Anti-Cancer Drug Delivery. *Journal of Controlled Release*. 2010.

(74) Maeda, H.; Sawa, T.; Konno, T. Mechanism of Tumor-Targeted Delivery of Macromolecular Drugs, Including the EPR Effect in Solid Tumor and Clinical Overview of the Prototype Polymeric Drug SMANCS. In *Journal of Controlled Release*; 2001.

(75) Maeda, H.; Bharate, G. Y.; Daruwalla, J. Polymeric Drugs for Efficient Tumor-Targeted Drug Delivery Based on EPR-Effect. *European Journal of Pharmaceutics and Biopharmaceutics*. 2009, pp 409–419.

(76) Bae, Y. H. Drug Targeting and Tumor Heterogeneity. *Journal of Controlled Release*. 2009, pp 2–3.

(77) Klinman, D. M.; Shirota, H.; Petrenko, L.; Hong, C. Contribute to DNA Vaccine Immunogenicity Potential of Transfected Muscle Cells to Potential of Transfected Muscle Cells to Contribute to DNA Vaccine Immunogenicity. *J Immunol Ref.* **2007**, *179*, 329–336.

(78) Davis, H.; Millan, C. B.; Watkins, S. Immune-Mediated Destruction of Transfected Muscle Fibers after Direct Gene Transfer with Antigen-Expressing Plasmid DNA. *Gene Ther.* **1997**, *4*, 181–188.

(79) Casares, S.; Inaba, K.; Brumeanu, T.-D.; Steinman, R. M.; Bona, C. A. Antigen Presentation by Dendritic Cells after Immunization with DNA Encoding a Major

Histocompatibility Complex Class II–restricted Viral Epitope. *J. Exp. Med* **1997**, *186* (9), 1481–1486.

(80) Lorenz, C.; Fotin-Mleczek, M.; Roth, G.; Becker, C.; Dam, T. C.; Verdurmen, W. P. R.; Brock, R.; Probst, J.; Schlake, T. Protein Expression from Exogenous MRNA: Uptake by Receptor-Mediated Endocytosis and Trafficking via the Lysosomal Pathway. *RNA Biol.* **2011**, *8* (4), 627–636.

(81) Simons, K.; Toomre, D. Lipid Rafts and Signal Transduction. *Nat. Rev. Mol. Cell Biol.* **2000**, *1*, 31.

(82) van der Goot, F. G.; Gruenberg, J. Intra-Endosomal Membrane Traffic. *Trends Cell Biol.* **2006**, *16* (10), 514–521.

(83) Luzio, J. P.; Bright, N. A.; Pryor, P. R. The Role of Calcium and Other Ions in Sorting and Delivery in the Late Endocytic Pathway: Figure 1. *Biochem. Soc. Trans.* **2007**, *35* (5), 1088–1091.

(84) Scott, C. C.; Gruenberg, J. Ion Flux and the Function of Endosomes and Lysosomes: PH Is Just the Start: The Flux of Ions across Endosomal Membranes Influences Endosome Function Not Only through Regulation of the Luminal PH. *BioEssays* **2011**, *33* (2), 103–110.

(85) Fong, L. G.; Le, D. The Processing of Ligands by the Class A Scavenger Receptor Is Dependent on Signal Information Located in the Cytoplasmic Domain. *J. Biol. Chem.* **1999**.

(86) Diken, M.; Kreiter, S.; Selmi, A.; Britten, C. M.; Huber, C.; Türeci, Ö.; Sahin, U. Selective Uptake of Naked Vaccine RNA by Dendritic Cells Is Driven by Macropinocytosis and Abrogated upon DC Maturation. *Gene Ther.* **2011**, *18* (7), 702–708.

(87) Pinnaduwage, P.; Schmitt, L.; Huang, L. Use of a Quaternary Ammonium Detergent in Liposome Mediated DNA Transfection of Mouse L-Cells. *BBA - Biomembr.* **1989**, *985* (1), 33–37.

(88) Felgner, P. L.; Gadek, T. R.; Holm, M.; Roman, R.; Chan, H. W.; Wenz, M.; Northrop, J. P.; Ringold, G. M.; Danielsen, M. Lipofection: A Highly Efficient, Lipid-Mediated DNA-Transfection Procedure. *Proc. Natl. Acad. Sci.* **1987**, *84* (21), 7413–7417.

(89) Bertling, W. M.; Gareis, M.; Paspaleeva, V.; Zimmer, A.; Kreuter, J.; Nurnberg, E.; Harrer, P. Use of Liposomes, Viral Capsids, and Nanoparticles as DNA Carriers. *Biotechnol. Appl. Biochem.* **1991**, *13* (3), 390–405.

(90) Wrobel, I.; Collins, D. Fusion of Cationic Liposomes with Mammalian Cells Occurs after Endocytosis. *BBA - Biomembr.* **1995**, *1235* (2), 296–304.

(91) Friend, D. S.; Papahadjopoulos, D.; Debs, R. J. Endocytosis and Intracellular Processing Accompanying Transfection Mediated by Cationic Liposomes. *Biochim. Biophys. Acta - Biomembr.* **1996**.

(92) Kang, J. H.; Jang, W. Y.; Ko, Y. T. The Effect of Surface Charges on the Cellular Uptake of Liposomes Investigated by Live Cell Imaging. *Pharm. Res.* **2017**.

(93) Juliano, R. L.; Ming, X.; Carver, K.; Laing, B. Cellular Uptake and Intracellular

Trafficking of Oligonucleotides: Implications for Oligonucleotide Pharmacology. *Nucleic Acid Ther.* **2014**, *24* (2), 101–113.

(94) Doherty, G. J.; McMahon, H. T. Mechanisms of Endocytosis. *Annu. Rev. Biochem.* **2009**.

(95) Xu, Y.; Szoka, F. C. Mechanism of DNA Release from Cationic Liposome/DNA Complexes Used in Cell Transfection. *Biochemistry* **1996**, *35* (18), 5616–5623.

(96) Hafez, I. M.; Maurer, N.; Cullis, P. R. On the Mechanism Whereby Cationic Lipids Promote Intracellular Delivery of Polynucleic Acids. *Gene Ther.* **2001**, *8* (15), 1188–1196.

(97) Mui, B.; Ahkong, Q. .; Chow, L.; Hope, M. . Membrane Perturbation and the Mechanism of Lipid-Mediated Transfer of DNA into Cells. *Biochim. Biophys. Acta - Biomembr.* **2000**, *1467* (2), 281–292.

(98) Stegmann, T.; Legendre, J.-Y. Gene Transfer Mediated by Cationic Lipids: Lack of a Correlation between Lipid Mixing and Transfection. *Biochim. Biophys. Acta - Biomembr.* **1997**, *1325* (1), 71–79.

(99) Benjaminsen, R. V; Mattebjerg, M. A.; Henriksen, J. R.; Moghimi, S. M.; Andresen, T. L. The Possible "Proton Sponge " Effect of Polyethylenimine (PEI) Does Not Include Change in Lysosomal PH. *Mol. Ther.* **2013**, *21* (1), 149–157.

(100) Zuhorn, I. S.; Bakowsky, U.; Polushkin, E.; Visser, W. H.; Stuart, M. C. A.; Engberts, J. B. F. N.; Hoekstra, D. Nonbilayer Phase of Lipoplex-Membrane Mixture Determines Endosomal Escape of Genetic Cargo and Transfection Efficiency. *Mol. Ther.* **2005**, *11* (5), 801–810.

(101) Jeffs, L. B.; Palmer, L. R.; Ambegia, E. G.; Giesbrecht, C.; Ewanick, S.; MacLachlan, I. A Scalable, Extrusion-Free Method for Efficient Liposomal Encapsulation of Plasmid DNA. *Pharm. Res.* **2005**, *22* (3), 362–372.

(102) Zelphati, O.; Szoka, F. C. CATIONIC LIPOSOMES AS AN OLIGONUCLEOTIDE CARRIER: MECHANISM OF ACTION. *J. Liposome Res.* **1997**, *7* (3), 1–49.

(103) Stevens, M. M.; George, J. H. Exploring and Engineering the Cell Surface Interface. *Science* **2005**, *310* (5751), 1135–1138.

(104) Caracciolo, G.; Callipo, L.; De Sanctis, S. C.; Cavaliere, C.; Pozzi, D.; Laganà, A. Surface Adsorption of Protein Corona Controls the Cell Internalization Mechanism of DC-Chol–DOPE/DNA Lipoplexes in Serum. *Biochim. Biophys. Acta - Biomembr.* **2010**, *1798* (3), 536–543.

(105) Betker, J. L.; Gomez, J.; Anchordoquy, T. J. The Effects of Lipoplex Formulation Variables on the Protein Corona and Comparisons with in Vitro Transfection Efficiency. *J. Control. Release* **2013**, *171* (3), 261–268.

(106) Busbridge, I. W. Coherent and Non-Coherent Scattering in the Theory of Line Formation. *Mon. Not. R. Astron. Soc.* **1953**, *113* (1), 52–66.

(107) Lin Wang, Z. *Elastic and Inelastic Scattering in Electron Diffraction and Imaging*; 1995.

(108) Atkinson, D.; Hauser, H.; Shipley, G. G.; Stubbs, J. M. Structure and Morphology of

Phosphatidylserine Dispersions. *BBA - Biomembr.* **1974**, *339* (1), 10–29.

(109) Pabst, G.; Kučerka, N.; Nieh, M.-P.; Rheinstädter, M. C.; Katsaras, J. Applications of Neutron and X-Ray Scattering to the Study of Biologically Relevant Model Membranes. *Chem. Phys. Lipids* **2010**, *163*, 460–479.

(110) Di Cola, E.; Grillo, I.; Ristori, S. Small Angle X-Ray and Neutron Scattering: Powerful Tools for Studying the Structure of Drug-Loaded Liposomes. *Pharmaceutics* **2016**, *8* (2), 1–16.

(111) Arleth, L.; Vermehren, C. An Analytical Model for the Small-Angle Scattering of Polyethylene Glycol-Modified Liposomes. *J. Appl. Cryst* **2010**, *43*, 1084–1091.

(112) Koltover, I.; Salditt, T.; Rädler, J. O.; Safinya, C. R. An Inverted Hexagonal Phase of Cationic Liposome-DNA Complexes Related to DNA Release and Delivery. *Science* **1998**, *281* (5373), 78–81.

(113) Rädler, J. O.; Koltover, I.; Salditt, T.; Safinya, C. R.; Radler, J. O. Structure of DNA-Cationic Liposome Complexes: DNA Intercalation in Multilamellar Membranes in Distinct Interhelical Packing Regimes. *Science* **1997**, *275* (5301), 810–814.

(114) Salditt, T.; Koltover, I.; Rädler, J. O.; Safinya, C. R. Self-Assembled DNA–cationic-Lipid Complexes: Two-Dimensional Smectic Ordering, Correlations, and Interactions. *Phys. Rev. E* **1998**, *58* (1), 889–904.

(115) Kratky, O. X-Ray Small Angle Scattering with Substances of Biological Interest in Diluted Solutions. *Prog. Biophys. Mol. Biol.* **1963**, *13*, 105–173.

(116) Jousma, H.; Talsma, H.; Spies, F.; Joosten, J. G. H.; Junginger, H. E.; Crommelin, D. J. A. Characterization of Liposomes. The Influence of Extrusion of Multilamellar Vesicles through Polycarbonate Membranes on Particle Size, Particle Size Distribution and Number of Bilayers. *Int. J. Pharm.* **1987**, *35* (3), 263–274.

(117) Lasic, D. D.; Strey, H.; Stuart, M. C. A.; Podgornik, R.; Frederik, P. M. The Structure of DNA - Liposome Complexes. *J. Am. Chem. Soc.* **1997**, *119* (4), 832–833.

(118) Salditt, T.; Koltover, I.; Rädler, J. O.; Safinya, C. R. Two-Dimensional Smectic Ordering of Linear DNA Chains in Self-Assembled DNA-Cationic Liposome Mixtures. *Phys. Rev. Lett.* **1997**, *79* (13), 2582–2585.

(119) Uhríková, D.; Hanulová, M.; Funari, S. S.; Khusainova, R. S.; Šeršeň, F.; Balgavý, P. The Structure of DNA–DOPC Aggregates Formed in Presence of Calcium and Magnesium Ions: A Small-Angle Synchrotron X-Ray Diffraction Study. *Biochim. Biophys. Acta - Biomembr.* **2005**, *1713* (1), 15–28.

(120) Caracciolo, G.; Amenitsch, H. Cationic Liposome/DNA Complexes: From Structure to Interactions with Cellular Membranes. *Eur. Biophys. J.* **2012**, *41* (10), 815–829.

(121) Mochizuki, S.; Kanegae, N.; Nishina, K.; Kamikawa, Y.; Koiwai, K.; Masunaga, H.; Sakurai, K. The Role of the Helper Lipid Dioleoylphosphatidylethanolamine (DOPE) for DNA Transfection Cooperating with a Cationic Lipid Bearing Ethylenediamine. *Biochim. Biophys. Acta* **2013**, *1828* (2), 412–418.

(122) Janich, C.; Taßler, S.; Meister, A.; Hause, G.; Schäfer, J.; Bakowsky, U.; Brezesinski, G.; Wölk, C. Structures of Malonic Acid Diamide/Phospholipid Composites and Their Lipoplexes. *Soft Matter* **2016**, *12* (27), 5854–5866.

(123) Nascimento, T. L.; Hillaireau, H.; Noiray, M.; Bourgaux, C.; Arpicco, S.; Pehau-Arnaudet, G.; Taverna, M.; Cosco, D.; Tsapis, N.; Fattal, E. Supramolecular Organization and SiRNA Binding of Hyaluronic Acid-Coated Lipoplexes for Targeted Delivery to the CD44 Receptor. *Langmuir* **2015**, *31* (41), 11186–11194.

(124) Tajik-Ahmadabad, B.; Mechler, A.; Muir, B. W.; McLean, K.; Hinton, T. M.; Separovic, F.; Polyzos, A. A QCM-D and SAXS Study of the Interaction of Functionalised Lyotropic Liquid Crystalline Lipid Nanoparticles with SiRNA. *ChemBioChem* **2017**, *18* (10), 921–930.

(125) Chen, Y.; Pollack, L. SAXS Studies of RNA: Structures, Dynamics, and Interactions with Partners. *Wiley Interdiscip. Rev. RNA* **2016**, *7* (4), 512–526.

(126) Menczel, J. D.; Judovits, L.; Prime, R. B.; Bair, H. E.; Reading, M.; Swier, S. Differential Scanning Calorimetry (DSC). In *Thermal Analysis of Polymers: Fundamentals and Applications*; John Wiley & Sons, Inc.: Hoboken, NJ, USA, 2008; pp 7–239.

(127) Biltonen, R. L.; Lichtenberg, D. The Use of Differential Scanning Calorimetry as a Tool to Characterize Liposome Preparations. *Chem. Phys. Lipids* **1993**, *64* (1–3), 129–142.

(128) Demetzos, C. Differential Scanning Calorimetry (DSC): A Tool to Study the Thermal Behavior of Lipid Bilayers and Liposomal Stability. *J. Liposome Res.* **2008**, *18* (3), 159–173.

(129) Zhang Yuan-Peng; and Reimer, D. L.; Guoyang, and Z.; H., and L. P.; B, and B. M. Self-Assembling DNA-Lipid Particles for Gene Transfer. *Pharm. Res.* **1997**, *14* (2), 190–196.

(130) Hassani, Z.; Lemkine, G. F.; Erbacher, P.; Palmier, K.; Alfama, G.; Giovannangeli, C.; Behr, J. P.; Demeneix, B. A. Lipid-Mediated SiRNA Delivery down-Regulates Exogenous Gene Expression in the Mouse Brain at Picomolar Levels. *J. Gene Med.* **2005**.

(131) Rakhmanova, V. A.; Pozharski, E. V.; MacDonald, R. C. Mechanisms of Lipoplex Formation: Dependence of the Biological Properties of Transfection Complexes on Formulation Procedures. *J. Membr. Biol.* **2004**, *200* (1), 35–45.

(132) REJMAN, J.; OBERLE, V.; ZUHORN, I. S.; HOEKSTRA, D. Size-Dependent Internalization of Particles via the Pathways of Clathrin- and Caveolae-Mediated Endocytosis. *Biochem. J.* **2004**, *377* (1), 159–169.

(133) Ross, P. C.; Hui, S. W. Lipoplex Size Is a Major Determinant of in Vitro Lipofection Efficiency. *Gene Ther.* **1999**, *6* (4), 651–659.

(134) Almofti, M. R.; Harashima, H.; Shinohara, Y.; Almofti, A.; Li, W.; Kiwada, H. Lipoplex Size Determines Lipofection Efficiency with or without Serum. *Mol. Membr. Biol.* **2003**, *20* (1), 35–43.

(135) Turek, J.; Dubertret, C.; Jaslin, G.; Antonakis, K.; Scherman, D.; Pitard, B. Formulations Which Increase the Size of Lipoplexes Prevent Serum-Associated Inhibition of Transfection. *J. Gene Med.* **2000**, *2* (1), 32–40.

(136) Zelphati, O.; Uyechi, L. S.; Barron, L. G.; Szoka, F. C. Effect of Serum Components on the Physico-Chemical Properties of Cationic Lipid/Oligonucleotide Complexes and on Their Interactions with Cells. *Biochim. Biophys. Acta - Lipids Lipid Metab.* **1998**,

1390 (2), 119–133.

(137) Escriou, V.; Ciolina, C.; Lacroix, F.; Byk, G.; Scherman, D.; Wils, P. Cationic Lipid-Mediated Gene Transfer: Effect of Serum on Cellular Uptake and Intracellular Fate of Lipopolyamine/DNA Complexes. *Biochim. Biophys. Acta - Biomembr.* **1998**, *1368* (2), 276–288.

(138) Ma, B.; Zhang, S.; Jiang, H.; Zhao, B.; Lv, H. Lipoplex Morphologies and Their Influences on Transfection Efficiency in Gene Delivery. *J. Control. Release* **2007**, *123* (3), 184–194.

(139) Jiang, W.; Kim, B. Y. S.; Rutka, J. T.; Chan, W. C. W. Nanoparticle-Mediated Cellular Response Is Size-Dependent. *Nat. Nanotechnol.* **2008**, *3* (3), 145–150.

(140) Kennedy, M. T.; Pozharski, E. V.; Rakhmanova, V. A.; MacDonald, R. C. Factors Governing the Assembly of Cationic Phospholipid-DNA Complexes. *Biophys. J.* **2000**, *78* (3), 1620–1633.

(141) Singh, R.; Lillard, J. W. Nanoparticle-Based Targeted Drug Delivery. *Exp. Mol. Pathol.* **2009**, *86* (3), 215–223.

(142) Dobrovolskaia, M. A.; Patri, A. K.; Zheng, J.; Clogston, J. D.; Ayub, N.; Aggarwal, P.; Neun, B. W.; Hall, J. B.; McNeil, S. E. Interaction of Colloidal Gold Nanoparticles with Human Blood: Effects on Particle Size and Analysis of Plasma Protein Binding Profiles. *Nanomedicine* **2009**, *5* (2), 106–117.

(143) Faraji, A. H.; Wipf, P. Nanoparticles in Cellular Drug Delivery. *Bioorganic Med. Chem.* **2009**, *17* (8), 2950–2962.

(144) Mozafari, M. R. Nanoliposomes: Preparation and Analysis; 2010; pp 29–50.

(145) Jones, L. J.; Yue, S. T.; Cheung, C.-Y.; Singer, V. L. RNA Quantitation by Fluorescence-Based Solution Assay: RiboGreen Reagent Characterization. *Anal. Biochem.* **1998**, *265* (2), 368–374.

(146) Eastman, S. J.; Hope, M. J.; Cullis, P. R. Transbilayer Transport of Phosphatidic Acid in Response to Transmembrane PH Gradients. *Biochemistry* **1991**.

(147) Heyes, J.; Palmer, L.; Bremner, K.; MacLachlan, I. Cationic Lipid Saturation Influences Intracellular Delivery of Encapsulated Nucleic Acids. *J. Control. Release* **2005**, *107* (2), 276–287.

(148) Jayaraman, M.; Ansell, S. M.; Mui, B. L.; Tam, Y. K.; Chen, J.; Du, X.; Butler, D.; Eltepu, L.; Matsuda, S.; Narayanannair, J. K.; Rajeev, K. G.; Hafez, I. M.; Akinc, A.; Maier, M. A.; Tracy, M. A.; Cullis, P. R.; Madden, T. D.; Manoharan, M.; Hope, M. J. Maximizing the Potency of SiRNA Lipid Nanoparticles for Hepatic Gene Silencing In Vivo. *Angew. Chemie Int. Ed.* **2012**, *51* (34), 8529–8533.

(149) Pierrat, P.; Lebeau, L. Characterization of Titratable Amphiphiles in Lipid Membranes by Fluorescence Spectroscopy. *Langmuir* **2015**, *31* (45), 12362–12371.

(150) Ziller, A.; Nogueira, S. S.; Hühn, E.; Funari, S. S.; Brezesinski, G.; Hartmann, H.; Sahin, U.; Haas, H.; Langguth, P. Incorporation of MRNA in Lamellar Lipid Matrices for Parenteral Administration. *Mol. Pharm.* **2018**, acs.molpharmaceut.7b01022.

(151) Kuhn, A. N.; Diken, M.; Kreiter, S.; Selmi, A.; Kowalska, J.; Jemielity, J.;

Darzynkiewicz, E.; Huber, C.; Türeci, Ö.; Sahin, U.; Türeci, O.; Sahin, U. Phosphorothioate Cap Analogs Increase Stability and Translational Efficiency of RNA Vaccines in Immature Dendritic Cells and Induce Superior Immune Responses in Vivo. *Gene Ther.* **2010**, *17* (8), 961–971.

(152) Gast, F. U.; Hagerman, P. J. Electrophoretic and Hydrodynamic Properties of Duplex Ribonucleic Acid Molecules Transcribed in Vitro: Evidence That A-Tracts Do Not Generate Curvature in RNA. *Biochemistry* **1991**, *30* (17), 4268–4277.

(153) Kebbekus, P.; Draper, D. E.; Hagerman, P. Persistence Length of RNA. *Biochemistry* **1995**, *34* (13), 4354–4357.

(154) Abels, J. A.; Moreno-Herrero, F.; Van Der Heijden, T.; Dekker, C.; Dekker, N. H. Single-Molecule Measurements of the Persistence Length of Double-Stranded RNA. *Biophys. J.* **2005**, *88* (4), 2737–2744.

(155) Crowe, L. M.; Reid, D. S.; Crowe, J. H. Is Trehalose Special for Preserving Dry Biomaterials? *Biophys. J.* **1996**, *71* (4), 2087–2093.

(156) Peters, R. Fiber Optic Device for Detecting the Scattered Light or Fluorescent Light from Suspension, 2000.

(157) Giatrellis, S.; Nounesis, G. Nucleic Acid-Lipid Membrane Interactions Studied by DSC. *J. Pharm. Bioallied Sci.* **2011**, *3* (1), 70.

(158) Yu, C.; Koh, S.; Leisch, J. E.; Toney, M. F.; Strasser, P. Size and Composition Distribution Dynamics of Alloy Nanoparticle Electrocatalysts Probed by Anomalous Small Angle X-Ray Scattering (ASAXS). *Faraday Discuss.* **2009**, *140* (0), 283–296.

(159) Harroun, T. A.; Wignall, G. D.; Katsaras, J. *Neutron Scattering in Biology*; Springer-Verlag: Berlin/Heidelberg, 2006.

(160) Brown, A.; Suit, H. The Centenary of the Discovery of the Bragg Peak. *Radiother. Oncol.* **2004**, *73* (3), 265–268.

(161) Zizak, I. MySpot: A Versatile Microfocussing Station for Scanning Methods at BESSY II. *J. large-scale Res. Facil. JLSRF* **2016**, *2*.

(162) Blanchet, C. E.; Spilotros, A.; Schwemmer, F.; Graewert, M. A.; Kikhney, A.; Jeffries, C. M.; Franke, D.; Mark, D.; Zengerle, R.; Cipriani, F.; Fiedler, S.; Roessle, M.; Svergun, D. I. Versatile Sample Environments and Automation for Biological Solution X-Ray Scattering Experiments at the P12 Beamline (PETRA III, DESY). *J. Appl. Crystallogr.* **2015**, *48*, 431–443.

(163) Stuhrmann, H. Contrast Variation Application in Small-Angle Neutron Scattering Experiments. *J. Phys. Conf. Ser.* **2012**, *351*.

(164) Nawroth, T.; Buch, P.; Buch, K.; Langguth, P.; Schweins, R. Liposome Formation from Bile Salt-Lipid Micelles in the Digestion and Drug Delivery Model FaSSIF Mod Estimated by Combined Time-Resolved Neutron and Dynamic Light Scattering. *Mol. Pharm.* **2011**, *8* (6), 2162–2172.

(165) Hühn, E. Rational Design of Sustained Release Liposomal MRNA Formulations for Parenteral Administration and Image-Guided Assessment of in Vivo Performance, 2013.

(166) Jain, M. K.; Wu, N. M. Effect of Small Molecules on the Dipalmitoyl Lecithin Liposomal Bilayer: III. Phase Transition in Lipid Bilayer. *J. Membr. Biol.* **1977**, *34* (1), 157–201.

(167) Lohner, K. Effects of Small Organic Molecules on Phospholipid Phase Transitions. *Chem. Phys. Lipids* **1991**, *57* (2–3), 341–362.

(168) Koltover, I.; Salditt, T.; Safinya, C. R. Phase Diagram, Stability, and Overcharging of Lamellar Cationic Lipid-DNA Self-Assembled Complexes. *Biophys. J.* **1999**, *77* (2), 915–924.

(169) Stamatatos, L.; Leventis, R.; Zuckermann, M. J.; Silvius, J. R. Interactions of Cationic Lipid Vesicles with Negatively Charged Phospholipid Vesicles and Biological Membranes. *Biochemistry* **1988**, *27* (11), 3917–3925.

(170) Zabner, J.; Fasbender, A. J.; Moninger, T.; Poellinger, K. A.; Welsh, M. J. Cellular and Molecular Barriers to Gene Transfer by a Cationic Lipid. *J. Biol. Chem.* **1995**.

(171) Zhou, X.; Huang, L. DNA Transfection Mediated by Cationic Liposomes Containing Lipopolylysine: Characterization and Mechanism of Action. *Biochim. Biophys. Acta* **1994**, *1189*, 195–203.

(172) El Ouahabi, A.; Thiry, M.; Pector, V.; Fuks, R.; Ruysschaert, J. M.; Vandenbranden, M. The Role of Endosome Destabilizing Activity in the Gene Transfer Process Mediated by Cationic Lipids. *FEBS Lett.* **1997**.

(173) Wattiaux, R.; Jadot, M.; Warnier-Pirotte, M. T.; Wattiaux-De Coninck, S. Cationic Lipids Destabilize Lysosomal Membrane in Vitro. *FEBS Lett.* **1997**.

(174) Brezesinski, G.; Möhwald, H. Langmuir Monolayers to Study Interactions at Model Membrane Surfaces. *Adv. Colloid Interface Sci.* **2003**.

(175) Estrela-Lopis, I.; Brezesinski, G.; Möhwald, H. Miscibility of DPPC and DPPA in Monolayers at the Air/Water Interface. *Chem. Phys. Lipids* **2004**.

(176) Jacobson, K.; Papahadjopoulos, D. Phase Transitions and Phase Separations in Phospholipid Membranes Induced by Changes in Temperature, PH, and Concentration of Bivalent Cations. *Biochemistry* **1975**, *14* (1), 152–161.

(177) Boggs, J. M.; Wood, D. D.; Moscarello, M. A.; Papahadjopoulos, D. Lipid Phase Separation Induced by a Hydrophobic Protein in Phosphatidylserine-Phosphatidylcholine Vesicles. *Biochemistry* **1977**, *16* (11), 2325–2329.

(178) Kučerka, N.; Tristram-Nagle, S.; Nagle, J. F. Structure of Fully Hydrated Fluid Phase Lipid Bilayers with Monounsaturated Chains. *J. Membr. Biol.* **2006**.

(179) Al-Ayoubi, S. R.; Schinkel, P. K. F.; Berghaus, M.; Herzog, M.; Winter, R. Combined Effects of Osmotic and Hydrostatic Pressure on Multilamellar Lipid Membranes in the Presence of PEG and Trehalose. *Soft Matter* **2018**, *14* (43), 8792–8802.

(180) Kiselev, M. A.; Zbytovska, J.; Matveev, D.; Wartewig, S.; Gapienko, I. V.; Perez, J.; Lesieur, P.; Hoell, A.; Neubert, R. Influence of Trehalose on the Structure of Unilamellar DMPC Vesicles. *Colloids Surfaces A Physicochem. Eng. Asp.* **2005**, *256* (1), 1–7.

(181) Sum, A. K.; Faller, R.; De Pablo, J. J.; Pablo, J. J. de. Molecular Simulation Study of

Phospholipid Bilayers and Insights of the Interactions with Disaccharides. *Biophys. J.* **2003**, *85* (5), 2830–2844.

(182) Pereira, C. S.; Hünenberger, P. H. Effect of Trehalose on a Phospholipid Membrane under Mechanical Stress. *Biophys. J.* **2008**, *95* (8), 3525–3534.

(183) Pereira, C. S.; Hünenberger, P. H. Interaction of the Sugars Trehalose, Maltose and Glucose with a Phospholipid Bilayer: A Comparative Molecular Dynamics Study. *J. Phys. Chem. B* **2006**, *110* (31), 15572–15581.

(184) Kent, B.; Hunt, T.; Darwish, T. A.; Hauss, T.; Garvey, C. J.; Bryant, G. Localization of Trehalose in Partially Hydrated DOPC Bilayers: Insights into Cryoprotective Mechanisms. *J. R. Soc. Interface* **2014**, *11* (95), 20140069–20140069.

(185) Andersen, H. D.; Wang, C.; Arleth, L.; Peters, G. H.; Westh, P. Reconciliation of Opposing Views on Membrane–sugar Interactions. *Proc. Natl. Acad. Sci.* **2011**.

(186) Angelov, B.; Angelova, A.; Drechsler, M.; Lesieur, S. Rapid Mixing Stopped-Flow Small-Angle X-Ray Scattering Study of Lipoplex Formation at Beamline ID02@ESRF. *J. Surf. Investig. X-ray, Synchrotron Neutron Tech.* **2015**, *9* (1), 105–110.

(187) Xu, Y.; Hui, S. W.; Frederik, P.; Szoka, F. C. Physicochemical Characterization and Purification of Cationic Lipoplexes. *Biophys. J.* **1999**, *77* (July), 341–353.

(188) Sternberg, B.; Sorgib, F. L.; Huangb, L. New Structures in Complex Formation between DNA and Cationic Liposomes Visualized by Freeze-Fracture Electron Microscopy. *FEBS Lett.* **1994**, *356*, 361–366.

(189) Eastman, S. .; Siegel, C.; Tousignant, J.; Smith, A. .; Cheng, S. .; Scheule, R. . Biophysical Characterization of Cationic Lipid:DNA Complexes. *Biochim. Biophys. Acta - Biomembr.* **1997**, *1325* (1), 41–62.

(190) Dan, N. The Structure of DNA Complexes with Cationic Liposomes-Cylindrical or Flat Bilayers? *Biochim. Biophys. Acta - Biomembr.* **1998**, *1369* (1), 34–38.

(191) May, S.; Ben-Shaul, A. DNA-Lipid Complexes: Stability of Honeycomb-like and Spaghetti-like Structures. *Biophys. J.* **1997**, *73* (5), 2427–2440.

(192) Tarahovsky, Y. S.; Khusainova, R. S.; Gorelov, A. V.; Nicolaeva, T. I.; Deev, A. A.; Dawson, A. K.; Ivanitsky, G. R. DNA Initiates Polymorphic Structural Transitions in Lecithin. *FEBS Lett.* **1996**.

(193) Sternberg, B. Morphology of Cationic Liposome/DNA Complexes in Relation to Their Chemical Composition. *J. Liposome Res.* **1996**, *6* (3), 515–533.

(194) Ewert, K. K.; Evans, H. M.; Zidovska, A.; Bouxsein, N. F.; Ahmad, A.; Safinya, C. R. A Columnar Phase of Dendritic Lipid-Based Cationic Liposome-DNA Complexes for Gene Delivery: Hexagonally Ordered Cylindrical Micelles Embedded in a DNA Honeycomb Lattice. *J. Am. Chem. Soc.* **2006**.

(195) Ghirlando, R.; Minsky, A.; Wachtel, E. J.; Arad, T. DNA Packaging Induced by Micellar Aggregates: A Novel in Vitro DNA Condensation System. *Biochemistry* **1992**.

(196) Bouxsein, N. F.; McAllister, C. S.; Ewert, K. K.; Samuel, C. E.; Safinya, C. R. Structure and Gene Silencing Activities of Monovalent and Pentavalent Cationic Lipid Vectors Complexed with SiRNA. *Biochemistry* **2007**.

(197) Subramanian, G.; Hjelm, R. P.; Deming, T. J.; Smith, G. S.; Li, Y.; Safinya, C. R. Structure of Complexes of Cationic Lipids and Poly(Glutamic Acid) Polypeptides: A Pinched Lamellar Phase. *J. Am. Chem. Soc.* **2000**, *122* (1), 26–34.

(198) Majzoub, R. N.; Ewert, K. K.; Safinya, C. R. Cationic Liposome-Nucleic Acid Nanoparticle Assemblies with Applications in Gene Delivery and Gene Silencing. *Philos. Trans. A. Math. Phys. Eng. Sci.* **2016**, *374* (2072), 20150129.

(199) Schiessel, H. Bending of Charged Flexible Membranes Due to the Presence of Macroions. *Eur. Phys. J. B* **1998**, *6* (3), 373–380.

(200) Yang, L.; Liang, H.; Angelini, T. E.; Butler, J.; Coridan, R.; Tang, J. X.; Wong, G. C. L. Self-Assembled Virus–membrane Complexes. *Nat. Mater.* **2004**, *3* (9), 615–619.

(201) Bruinsma, R. Electrostatics of DNA-Cationic Lipid Complexes: Isoelectric Instability. *Eur. Phys. J. B* **1998**, *4* (1), 75–88.

(202) Bruinsma, R.; Mashl, J. Long-Range Electrostatic Interaction in DNA-Cationic Lipid Complexes. *Europhys. Lett.* **1998**, *41* (2), 165–170.

(203) Golubović, L.; Golubović, M. Fluctuations of Quasi-Two-Dimensional Smectics Intercalated between Membranes in Multilamellar Phases of DNA-Cationic Lipid Complexes. *Phys. Rev. Lett.* **1998**, *80* (19), 4341–4344.

(204) OHern, C. S.; Lubensky, T. C. Sliding Columnar Phase of DNA Lipid Complexes. *Phys Rev Lett* **1998**, *80* (19), 4345–4348.

(205) Treuel, L.; Docter, D.; Maskos, M.; Stauber, R. H. Protein Corona - from Molecular Adsorption to Physiological Complexity. *Beilstein J. Nanotechnol.* **2015**, *6* (1), 857–873.

(206) Bennett, C. F.; Chiang, M. Y.; Chan, H.; Shoemaker, J. E.; Mirabelli, C. K. Cationic Lipids Enhance Cellular Uptake and Activity of Phosphorothioate Antisense Oligonucleotides. *Mol. Pharmacol.* **1992**, *41* (6), 1023–1033.

(207) Lappalainen, K.; Urtti, A.; Jääskeläinen, I.; Syrjänen, K.; Syrjänen, S. Cationic Liposomes Mediated Delivery of Antisense Oligonucleotides Targeted to HPV 16 E7 MRNA in CaSki Cells. *Antiviral Res.* **1994**, *23* (2), 119–130.

(208) Zelphati, O.; Szoka, F. C. Intracellular Distribution and Mechanism of Delivery of Oligonucleotides Mediated by Cationic Lipids. *Pharm. Res.* **1996**.

(209) Li, S. J.; Yamazaki, M. Low PH Stabilizes the Inverted Hexagonal II Phase in Dipalmitoleoylphosphatidylethanolamine Membrane. *J. Biol. Phys.* **2004**, *30* (4), 377–386.

(210) Fernández, M. A. S.; Fromherz, P. Lipoid PH Indicators as Probes of Electrical Potential and Polarity in Micelles. *J. Phys. Chem.* **1977**.

(211) Langner, M.; Pruchnik, H.; Kubica, K. The Effect of the Lipid Bilayer State on Fluorescence Intensity of Fluorescein-PE in a Saturated Lipid Bilayer. *Zeitschrift fur Naturforsch. - Sect. C J. Biosci.* **2000**, *55* (5–6), 418–424.

(212) Kubica, K.; Langner, M.; Gabrielska, J. The Dependence of Fluorescein-PE Fluorescence Intensity on Lipid Bilayer State. Evaluating the Interaction between the Probe and Lipid Molecules. *Cell Mol Biol Lett* **2003**, *8* (4), 943–954.

(213) Ramgopal, Y.; Mondal, D.; Venkatraman, S. S.; Godbey, W. T.; Yuen, G. Y.

Controlled Release of Complexed DNA from Polycaprolactone Film: Comparison of Lipoplex and Polyplex Release. *J. Biomed. Mater. Res. - Part B Appl. Biomater.* **2009**, *89* (2), 439–447.

(214) Koynova, R.; MacDonald, R. C. Natural Lipid Extracts and Biomembrane-Mimicking Lipid Compositions Are Disposed to Form Nonlamellar Phases, and They Release DNA from Lipoplexes Most Efficiently. *Biochim. Biophys. Acta* **2007**, *1768* (10), 2373–2382.

(215) Mellman, I.; Coukos, G.; Dranoff, G. Cancer Immunotherapy Comes of Age. *Nature.* 2011.

(216) Hirsch, M.; Ziroli, V.; Helm, M.; Massing, U. Preparation of Small Amounts of Sterile SiRNA-Liposomes with High Entrapping Efficiency by Dual Asymmetric Centrifugation (DAC). *J. Control. Release* **2009**, *135* (1), 80–88.

(217) Zuidam, N. J.; Barenholz, Y. Electrostatic and Structural Properties of Complexes Involving Plasmid DNA and Cationic Lipids Commonly Used for Gene Delivery. *Biochim. Biophys. Acta* **1998**, *1368* (1), 115–128.

(218) Zuidam, N. J.; Barenholz, Y. Electrostatic Parameters of Cationic Liposomes Commonly Used for Gene Delivery as Determined by 4-Heptadecyl-7-Hydroxycoumarin1A Preliminary Report of This Study Was Presented at the 3rd Annual Conference: Artificial Self-Assembling Systems for Gene Deliv. *Biochim. Biophys. Acta - Biomembr.* **1997**, *1329* (2), 211–222.

(219) Felgner, J. H.; Kumar, R.; Sridhar, C. N.; Wheeler, C. J.; Tsai, Y. J.; Border, R.; Ramsey, P.; Martin, M.; Felgner, P. L. Enhanced Gene Delivery and Mechanism Studies with a Novel Series of Cationic Lipid Formulations. *J. Biol. Chem.* **1994**, *269* (4), 2550–2561.

(220) Hattori, Y.; Suzuki, S.; Kawakami, S.; Yamashita, F.; Hashida, M. The Role of Dioleoylphosphatidylethanolamine (DOPE) in Targeted Gene Delivery with Mannosylated Cationic Liposomes via Intravenous Route. *J. Control. Release* **2005**, *108* (2–3), 484–495.

(221) FARHOOD, H.; SERBINA, N.; HUANG, L. The Role of Dioleoyl Phosphatidylethanolamine in Cationic Liposome Mediated Gene Transfer. *Biochim. Biophys. Acta - Biomembr.* **1995**, *1235* (2), 289–295.

(222) Maitani, Y.; Igarashi, S.; Sato, M.; Hattori, Y. Cationic Liposome (DC-Chol/DOPE=1:2) and a Modified Ethanol Injection Method to Prepare Liposomes, Increased Gene Expression. *Int. J. Pharm.* **2007**, *342* (1–2), 33–39.

(223) Darwech, I.; Otero, J. E.; Alhawagri, M. A.; Abu-Amer, Y. Tyrosine Phosphorylation Is Required for IκB Kinase-β (IKKβ) Activation and Function in Osteoclastogenesis. *J. Biol. Chem.* **2010**.

(224) Kirby, C.; Clarke, J.; Gregoriadis, G. Effect of the Cholesterol Content of Small Unilamellar Liposomes on Their Stability in Vivo and in Vitro. *Biochem. J.* **1980**, *186* (2), 591–598.

(225) Papahadjopoulos, D.; Allen, T. M.; Gabizon, A.; Mayhew, E.; Matthay, K.; Huang, S. K.; Lee, K. D.; Woodle, M. C.; Lasic, D. D.; Redemann, C. Sterically Stabilized Liposomes: Improvements in Pharmacokinetics and Antitumor Therapeutic Efficacy.

Proc. Natl. Acad. Sci. **1991**, *88* (24), 11460–11464.

(226) Massing, U.; Cicko, S.; Ziroli, V. Dual Asymmetric Centrifugation (DAC)--a New Technique for Liposome Preparation. *J. Control. Release* **2008**, *125* (1), 16–24.

List of publications

Articles

1. Ziller, A.; Nogueira, S. S.; Huehn, E.; Funari, S. S.; Brezesinski, G.; Hartmann, H.; Sahin, U.; Haas, H.; Langguth, P. Incorporation of mRNA in Lamellar Lipid Matrices for Parenteral Administration. *Mol. Pharm.* **2017**, acs.molpharmaceut.7b01022.

2. Siewert, C.; Haas, H.; Nawroth, T.; Ziller, A.; Nogueira, S. S.; Schroer, M. A.; Blanchet, C. E.; Svergun, D. I.; Radulescu, A.; Bates, F.; Huesemann, Y.; Radsak, M. P.; Sahin, U.; Langguth, P. Investigation of Charge Ratio Variation in MRNA – DEAE-Dextran Polyplex Delivery Systems. *Biomaterials* **2019**, *192*, 612–620.

Poster presentations

1. Ziller A., Uebbing L., Hühn E., Funari S. S., Hartmann, H.; Sahin, U.; Haas, H.; Langguth, P. mRNA-lipoplexes for controlled delivery in personalized cancer vaccines. Poster presentation at the "14th Zsigmondy Colloquium of the German Colloid Society" 2018, Mainz.

2. Siewert C., Nawroth T., Ziller A., Langguth P., Nogueira S. S., Haas H., Radulescu A., Sahin U. mRNA Nanoparticles for parenteral Therapy. Poster presentation at the "MLZ conference – Neutrons for Health" 2017, Bad Reichenhall.

3. Ziller A., Nogueira, S. S., Haas, H., Funari, S. S., Brezesinski, G.; Hartmann, H.; Sahin, U.; Haas, H.; Langguth, P. mRNA incorporated into lipid matrices as controlled release systems. Poster presentation and short talk at the "Clinical Nanomedicine and Targeted Medicine Enabling Technologies for Personalized Medicine" 2016, Basel.

4. Ziller A., Hobernik D., Bros M., Langguth P. Lipoplexes for transport of combined DNA vaccines. Poster presentation at the "10th World Meeting on Pharmaceutics, Biopharmaceutics and Pharmaceutical Technology" 2016, Glasgow.

5. Ziller A., Hobernik D., Bros M., Langguth P. Influence of different cationic lipids and DOPE on the cell uptake of DNA formulated in lipoplexes. Poster presentation at the DPhG annual meeting 2015, Düsseldorf.

6. Fritz T., Voigt M., Ziller A., Worm M., Müller S. S. Aufnahme und intrazelluläre Verteilung von RNA Formulierungen in neuartigen Stealth Liposomen. Poster presentation at the summer school of the CRC 1066 2014, Stromberg.

Acknowledgement

Ohne die Unterstützung zahlreicher Personen und Institutionen hätte ich meine Dissertation in dieser Form nicht realisieren können. Für die vielfältige Hilfe möchte ich mich an dieser Stelle sehr herzlich bedanken.

Affidavit

Ich erkläre hiermit, dass ich diese Dissertation selbstständig ohne Hilfe Dritter und ohne Benutzung anderer als der angegebenen Quellen und Hilfsmittel verfasst habe. Alle den benutzten Quellen wörtlich oder sinngemäß entnommenen Stellen sind als solche einzeln kenntlich gemacht.

Diese Arbeit ist bislang keiner anderen Prüfungsbehörde vorgelegt worden und auch nicht veröffentlicht worden.

Ich bin mir bewusst, dass eine falsche Erklärung rechtliche Folgen haben wird.

_____

Ort, Datum, Unterschrift

Curriculum vitae